SMALL MOLECULES FOR ACTIVE TARGETING AND DEVELOPMENT OF PROTACS

A Dissertation

by

BOSHENG ZHAO

Submitted to the Office of Graduate and Professional Studies of
Texas A&M University
in partial fulfillment of the requirements for the degree of

DOCTOR OF PHILOSOPHY

Chair of Committee,	Kevin Burgess
Committee Members,	Tadhg P. Begley
	Jean-Philippe Pellois
	Richard Gomer
Head of Department,	Simon W. North

May 2020

Major Subject: Chemistry

ABSTRACT

Targeted therapy for cancer is a hot topic in recent years. Small molecule pharmaceuticals have advantages relative to antibodies with respect to cell penetration and affordability. This dissertation focuses on the application of small molecules targeting cancer. The binding of a small molecule ligand (IY-IY) to the tropomyosin receptor kinase C (TrkC), which is overexpressed on cancer cells, was validated by photoaffinity labeling (PAL) and used to deliver a kinase inhibitor (KI) into cancer cells. Further, IY-IY and two CDK4/6 inhibitors were modified to proteolysis targeting chimeras (PROTACs) which were capable of inducing degradation of their targets, providing an alternative approach of regulating protein functions.

In the first study, a PAL cassette was designed to contain an alkyne, a trifluoromethyl phenyl diazirine, and a free piperidine-NH for facile conjugation to protein binding ligands. This PAL cassette was synthesized via a relatively direct route involving routine steps. In the proof-of-concept study, a sulfonamide ligand for carbonic anhydrase IX (CAIX) and IY-IY for TrkC were conjugated to the cassette. Photoaffinity labeling experiments were performed using purified extracellular domains of both these protein-receptors, and using cells that express these receptors, labeling of the protein was observed in all experiments.

In the second study, IY-IY was used to deliver the promiscuous KI dasatinib into breast cancer cells. Conjugates with non-cleavable and cleavable linkers were compared in cellular assays and shown to have more impact on the cell viabilities of $TrkC^+$ breast

cancer cells over TrkC$^-$ epithelial cells. The IY-IY fragment was also used to recruit the E3 ligase cereblon, giving a potent PROTAC for TrkC degradation in metastatic breast cancer cells.

In the third study, PROTACs based on two selective, FDA-approved CDK4/6 inhibitors were formed. One of them, based on palbociclib, potently initiates degradation of these CDK proteins, suppresses the downstream phosphorylation of retinoblastoma protein (Rb) and leads to cell cycle arrest. These PROTACs are active at nanomolar concentrations, and appear to act catalytically in the cells.

DEDICATION

To my family and friends

ACKNOWLEDGEMENTS

I would first like to thank my advisor, Professor Kevin Burgess, for his guidance, motivation, support and patience during my research in Texas A&M University. I learned tremendous knowledge in organic synthesis from him. His introduction for medicinal chemistry raised my interest and brought me closer to this area of research. Besides, I received many helpful resources from him, through which I have learnt useful chemical and biological techniques. His passion and dedication on research also have a great impact on me, and fosters a wonderful environment in the group.

I would like to thank my committee members, Prof. Tadhg P. Begley, Prof. Jean-Philippe Pellois and Prof. Richard Gomer for their guidance, support and valuable advice throughout the course of this research.

I would like to thank Dr. Larry Dangott for his helpful advice and insightful discussions on protein-based assays in the photoaffinity labeling project. Thanks Dr. Gloria Conover for her mentorship on protein expression and purification. Thanks Dr. Erik Knudsen for his collaboration and useful discussion on CDK project.

I would also like to thank Dr. Anyanee Kamkaew, Dr. Dongyue Xin for their guidance during my first two years. Thanks also go to my colleagues Dr. Chen-ming Lin, Dr. Zhe Gao, Dr. Zhengyang Jiang and Dr. Syed M. Usama for collaborations and useful communications. I would appreciate all the past and current Burgess group members for the great lab environment they created and help they gave.

Finally, thanks to my girlfriend Yi Meng for her understanding, love and patience.

Thanks to my family and friends for their encouragement and support.

CONTRIBUTORS AND FUNDING SOURCES

Contributors

This work was supervised by a dissertation committee at Texas A&M consisting of Prof. Kevin Burgess (advisor) of the Department of Chemistry; Prof. Tadhg P. Begley (committee member) of the Department of Chemistry; Prof. Jean-Philippe Pellois (committee member) of the Departments of Chemistry, and Biochemistry and Biophysics; Prof. Richard Gomer (committee member) of the Department of Biology.

The photoaffinity labeling experiments in Chapter II were performed with the help of Dr. Larry Dangott of Protein Chemistry Laboratory in Texas A&M University. Some intermediate compounds in Chapter III were prepared with help of Dr. Syed M. Usama of Department of Chemistry. Preliminary data indicating the significance of CDK2 in pancreatic ductal adenocarcinoma (PDAC) model were obtained by Dr. Erik Knudsen of Roswell Park Comprehensive Cancer Center. Appendix A was completed with the contribution of Dr. Syed M. Usama of Department of Chemistry. Appendix B was completed in collaboration with Dr. Erik Knudsen from Roswell Park Comprehensive Cancer Center.

All other work conducted for the dissertation was completed by the student independently.

Funding Sources

The work in Chapter II was supported by the Department of Defense BCRP Breakthrough Award (BC141561), the Cancer Prevention and Research Institute of Texas (RP150559 and RP170144), and the Robert A. Welch Foundation (A-1121). The NMR instrumentation at Texas A&M University was supported by a grant from the National Science Foundation (DBI-9970232) and the Texas A&M University System.

The work in Chapter III, IV and Appendix A was supported by the Department of Defense BCRP Breakthrough Award (BC141561), the Cancer Prevention and Research Institute of Texas (RP150559 and RP180875), and the National Institutes of Health (R01EY029645). The NMR instrumentation at Texas A&M University was supported by a grant from the National Science Foundation (DBI-9970232) and the Texas A&M University System.

The contents are solely the responsibility of the authors and do not necessarily represent the official views of the Department of Defense, the Cancer Prevention and Research Institute of Texas, the Welch Foundation, the National Institutes of Health, the National Science Foundation, or Texas A&M University.

NOMENCLATURE

Ab	Antibody
ADC	Antibody drug conjugate
ANOVA	Analysis of Variance
ATCC	American Type Culture Collection
BCA	Bicinchoninic acid
Boc	*tert*-Butyloxycarbonyl
CAIX	Carbonic Anhydrase IX
CBB	Coomassie Brilliant Blue
$CDCl_3$	Deuterated chloroform
CDK	Cyclin Dependent Kinase
CML	Chronic Myeloid Leukemia
CRBN	Cereblon
das	Dasatinib
DC_{50}	Half maximal degrading concentration
DIPEA	*N*,*N*-Diisopropylethylamine
DM4	Maytansinoid DM4
DMEM	Dulbecco's Modified Eagle Media
DMF	Dimethyl formaldehyde
DMSO	Dimethyl Sulfoxide
DMSO-d_6	Deuterated dimethyl sulfoxide

DTT	Dithiothreitol
ECL	Enhanced chemiluminescence
Em	Emission
ESI	Electrospray ionization
Et_3N	Triethyl amine
Ex	Excitation
FBS	Fetal bovine serum
FDA	Food and Drug Administration
fluor	fluorophore
HATU	Hexafluorophosphate Azabenzotriazole Tetramethyl Uronium
HEPES	4-(2-hydroxyethyl)-1-piperazineethanesulfonic acid
HPLC	High Performance Liquid Chromatography
HRMS	High Resolution Mass Spectrometry
HRP	Horseradish peroxidase
IC_{50}	Half maximal inhibitory concentration
IgG	Immunoglobulin G
IY	Isoleucine tyrosine mimic
K_d	Dissociation constant
KI	Kinase Inhibitor
LED	Light-emitting diode
LRMS	Low Resolution Mass Spectrometry
mAb	monoclonal Antibody

MALDI	Matrix Assisted Laser Desorption/Ionization
MeCN	Acetonitrile
MeOD	Deuterated methanol
NMR	Nuclear magnetic resonance euterated chloroform
OD	Optical Density
pal	Palbociclib
PAL	Photoaffinity Labeling
PBS	Phosphate-buffered saline
PCR	Polymerase Chain Reaction
PDAC	Pancreatic Ductal Adenocarcinoma
PDB	Protein Data Bank
PDT	Photodynamic Therapy
PEG	Polyethylene Glycol
PFHM-II	Protein Free Hybridoma Medium II
POI	Protein of Interest
pom	Pomalidomide
PROTAC	Proteolysis Targeting Chimera
pTyr	Phosphorylated tyrosine
PVDF	Polyvinylidene difluoride
Rb	Retinoblastoma protein
rib	Ribociclib
RIPA	Radioimmunoprecipitation assay

SDS-PAGE	Sodium Dodecyl Sulfate-Polyacrylamide Gel Electrophoresis
TBS	Tris-buffered saline
TBS-T	Tris-buffered saline with Tween 20
TBTA	Tris((1-benzyl-4-triazolyl)methyl)amine
TCEP	Tris(2-carboxyethyl)phosphine
TEG	Triethylene glycol
THF	Tetrahydrofuran
TLC	Thin layer chromatography
TrkC	Tropomyosin receptor kinase C
UV	Ultraviolet
WT	Wild Type
YI	Tyrosine isoleucine mimic

TABLE OF CONTENTS

Page

LIST OF FIGURES

Page

LIST OF TABLES

Page

1. INTRODUCTION

Targeted therapy is one of the most promising methods for the treatment of cancer. It is a type of chemotherapy which is more specific to cancer cells over normal cells by targeting some specific genes, proteins or tumor microenvironment. Targeted therapy may involve: small molecules that selectively inhibit proteins overexpressed in cancer, and "active targeting", involving antibody drug conjugates (ADCs) and small molecule drug conjugates that target cell surface receptors overexpressed in cancer. While small molecules act on genes or proteins that are overexpressed in cancer cells, they are not guided to tumor via an extracellular interaction, therefore are referred as "passive targeting".[1] ADCs and small molecule drug conjugates, instead, can bind to macromolecules overexpressed on the surface of cancer cells and be internalized into those cells upon binding, followed by the intracellular drug release. This is described as "active targeting".[1-2] Active targeting is most commonly achieved via ADCs,[3] but small molecule drug conjugates have been used, and offer the significant advantage of deeper permeation into solid tumors.[4-5] Therapeutic indices are commonly used to assess relative safety of drug, by comparing the amount of drug needed for therapeutic effect to the amount that causes toxicity. Therapeutic indices of anticancer drugs can be improved by selective delivery into cancer cells via active targeting, which leads to greater accumulation of drug in tumor tissues.

Kinase inhibitors (KIs) are the main class of small molecules therapeutics for cancer. Protein kinases are enzymes that catalyze the transfer of phosphate groups from

ATP to residues of protein, named phosphorylation. Around 50% of all proteins undergo phosphorylation to affect cell signaling,[6] hence kinases and phosphatases regulate many cellular activities, such as cell division, proliferation and apoptosis.[7] There are more than 518 kinases in human kinome,[8] most having homologous sequences in their nucleotide binding pockets.[9] Overexpression of kinases or elevated kinase activities are frequently observed in cancer cells, either as a driver or direct consequence of cancer,[10] and, because of this, KIs have ascended to a prominent position in cancer therapy. KIs are designed to target specific mechanisms in tumor over healthy tissue, to slow down cancer cell propagation (senescence) and metastatic spread, usually with far less side-effects than broadly cytotoxic chemotherapeutic drugs. Since the first FDA-approval of a KI, imatinib (for the treatment of chronic myeloid leukemia; CML) in 2001, at least 54 more have been approved by Jan 2020, and it is almost certain that more will be approved, and off-label applications will be found. However, as of 2016, only 36% of approved KIs have one or two main targets, while 25% of them bind to no less than ten kinases.[11] Poor selectivity of KIs can be attributed to the high structural similarity of ATP-binding pockets among different kinases. Administration of KIs with poor selectivity can cause unwanted interruption of kinases in normal cells and limit their application in cancer therapy. Consequently, efforts are made to improve KI selectivities and expand their therapeutic windows.

Dasatinib (Sprycel), a tyrosine KI that approved for Philadelphia chromosome-positive (Ph+) chronic myeloid leukemia (CML) in 2006, has since featured in over 160 clinical trials. Unfortunately, treatment with dasatinib has side effects that can be severe

for some patients,[12-13] and this restricts dose levels. At least some of those side effects can be attributed to poor selectivity within the kinome. Consequently, it seems logical to use active targeting for selective delivery of KIs into cancer cells.

Only a few cell surface receptors have been explored for small molecule active targeting, for example, folate receptor.[14] Our work featured another receptor named tropomyosin receptor kinase C (TrkC).[15] Trk's are a family of receptor tyrosine kinases that bind neurotrophin growth hormones.[16] There are 3 most common types of Trk receptors: TrkA, TrkB and TrkC, each has different binding affinity to certain types of neurotrophins. Trk receptors dimerize in response to their neurotrophin partners, triggering auto-phosphorylation between dimers and enhancing their catalytic activities of kinase domains,[17] which will further phosphorylate a variety of intracellular proteins and activate signaling cascades that finally lead to cell proliferation and differentiation.[18-19] Among these receptors, overexpression of TrkC has been shown in association with several forms of cancer, including neuroblastoma,[20] glioblastoma,[21] metastatic breast cancer[22] and metastatic melanoma.[23] Previous work in our group led to a bivalent peptidomimetic, IY-IY, which binds selectively to cells that overexpress TrkC.[15, 24-25] The IY-IY motif binds to TrkC and can be internalized in the same way as the natural protein ligand of TrkC, neurotrophin-3 (NT-3).[1] Conjugation of a fluorescent dye to IY-IY gave a probe that could stain on metastatic breast cancer and metastatic melanoma tissue, and be internalized by TrkC-expressing cells[24, 26]. Moreover, a photodynamic therapy (PDT) agent linked to IY-IY almost ablated 4T1 primary tumors via one 10 mg/Kg dose, and metastasis was also inhibited.[26] We have also demonstrated a conjugate of IY-IY with a

cytotoxic cargo DM4 had a better therapeutic index than the parent drug in a murine model (Figure 1.1).[27] It seems IY-IY is a promising TrkC targeting agent, however, there is no direct evidence that proves its binding to TrkC.

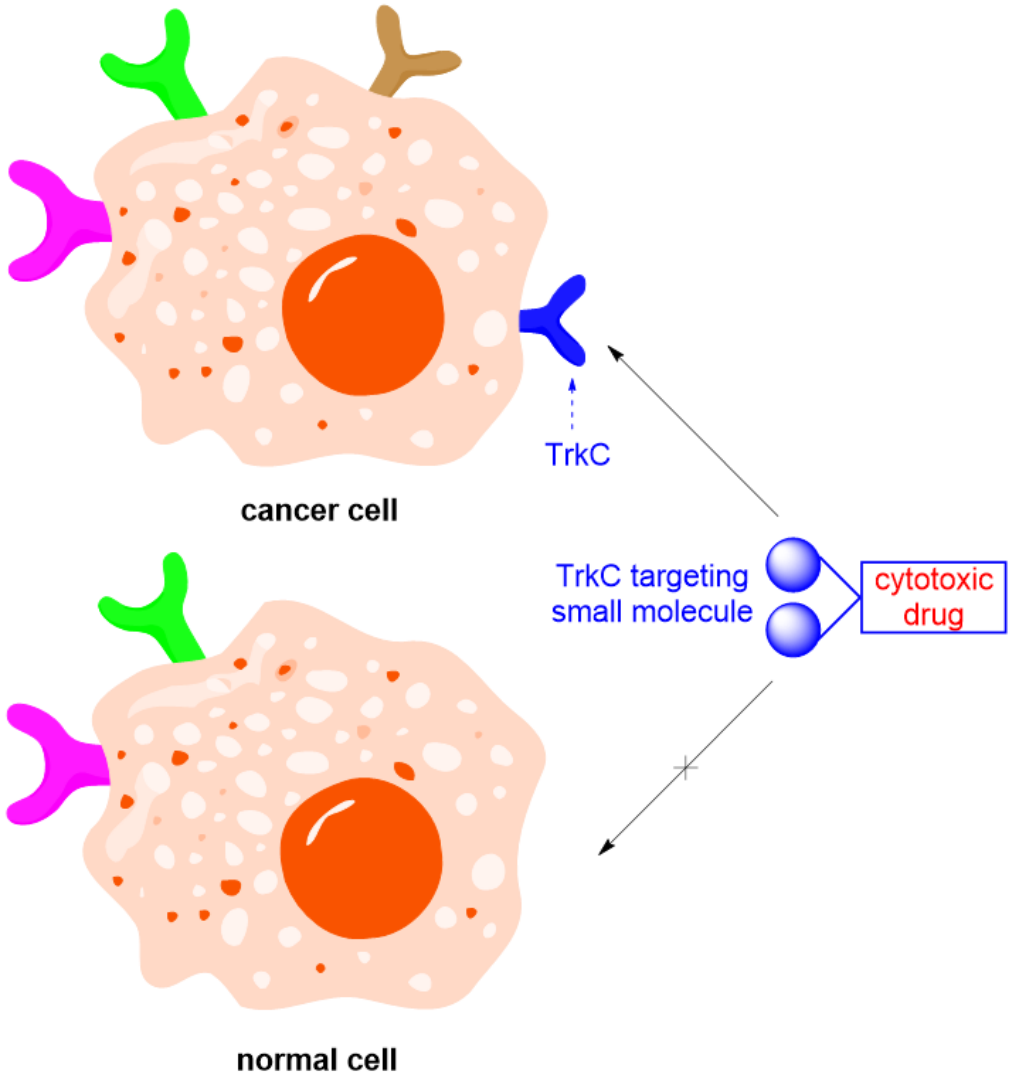

Figure 1.1 Illustration of targeting cancer by a representative small molecule that binds to tropomyosin receptor kinase (TrkC) that overexpressed in cancer cells. Upon binding, the small molecule drug conjugate can be preferentially delivered into cancer cells by receptor-mediated endocytosis.

This dissertation focuses on validation and application of a small molecule peptidomimetics IY-IY for active targeting cancer, and the development of Proteolysis Targeting Chimeras (PROTACs), one of which is also based on IY-IY. In Chapter II, a photoaffinity labeling (PAL) cassette was developed to confirm ligand-protein interactions. PAL is a powerful technique in drug discovery for identifying new drug targets and molecular interactions, and for probing the location and structure of binding sites.[28-29] PAL enables covalent binding of probes to macromolecular binding partners, which are then characterized via detection methodologies such as SDS-PAGE, biotin-streptavidin affinity purification and mass spectrometry. A typical PAL agent should contain three functionalities: targeting ligand, photoreactive group and reporter group.[30] In this study, trifluoromethyl phenyl diazirine is used as the photoreactive group, which can be activated under UV light (365 nm), forming a carbene intermediate that can insert into *C-H* bonds in any nearby amino acid side chain. Typically, to minimize the interference of the larger report group in ligand-protein interaction, a smaller acetylene moiety is used instead to incorporate the reporter group by click reaction after formation of covalent bond.

Two proteins were studied in the chapter II on a new cassette for PAL labeling: Carbonic Anhydrase IX (CAIX) as proof-of-concept study, and TrkC to confirm its interaction with the peptidomimetics IY-IY. The general procedure of PAL is as follows. First, ligand is allowed to interact with target protein to reach an equilibrium. The photoreactive group is then activated under UV light to generate a reactive species that covalently crosslinks the ligand to target protein. Finally, the reporter group is introduced

by a click reaction with the acetylene moiety; the detection method varies for different reporters. If a fluorophore is introduced, the sample can be visualized by in-gel fluorescence after SDS-PAGE separation. When biotin is used instead, target proteins can be identified via affinity purification based on streptavidin, followed by Western blot. Photolabeling experiments on these two proteins proved the effectiveness of the PAL cassette and provided the direct evidence of the interaction of IY-IY with TrkC.

In Chapter III, the IY-IY ligand was explored for selective delivery of a promiscuous KI dasatinib into $TrkC^+$ cancer cells over $TrkC^-$ normal cells, via the active targeting strategy. Two types of linkages between IY-IY and dasatinib were applied: a cleavable disulfide linker that can be decomposed by intracellular glutathione, and non-cleavable linker. The efficacy and selectivity of conjugates were tested and compared with dasatinib side-by-side. The conjugate with a disulfide linkage matched the activity of dasatinib in kinase inhibition and cell viability assays, and had a better performance compared to the non-cleavable conjugate, suggesting the importance of intracellular drug release. Most importantly, the cleavable conjugate could greatly improve the selectivity and the therapeutic index of dasatinib, validated by the comparison of cell viability between TrkC+ cancer cells (Hs578t) and TrkC- normal cells (MCF-10A). Furthermore, IY-IY was developed into a potent PROTAC of TrkC, by recruiting the E3 ligase cereblon, which could be served as a potential therapeutics in certain types of cancer where TrkC receptor is important[20-23].

PROTACs are heterobifunctional small molecules composed of two fragments: a ligand to bind protein of interest, and a E3 ligase ligand.[31-33] PROTACs can bring the

targeted protein and E3 ligase into proximity, and may potentially induce protein-protein interaction between target protein and E3 ligase to form a stable ternary complex when the linker length is optimal.[34-35] This can initiate ubiquitination and subsequent degradation of the target in the proteasome. PROTACs have several advantages over traditional inhibitors.[36] First, PROTACs have the potential to target proteins which are defined as "undruggable", because, unlike traditional inhibitors, they do not require active site binding. Second, in clinical trials, it is common that cancer cells gradually develop resistance to drugs over time, and sometimes this can be attributed to gene mutation. Deletion of mutated and non-mutated target proteins would definitely be desired in this case. Last but not least, some PROTACs act catalytically, hence can be even more effective than suicide inhibitors that permanently inactivate enzymes.[37]

Other than TrkC, application of PROTACs for cyclin dependent kinases (CDKs) 4/6 were developed in Chapter IV. CDKs are critical for cell cycle regulation, and are considered as potential targets for anticancer medication[38-41] because cancer cells proliferate faster than normal cells. Cell cycle arrest could suppress tumor growth and metastasis. First generation CDK inhibitors had poor selectivity among CDKs, and they were relatively unsuccessful in pharmaceutical development. For example, flavopiridol, a pan-CDK inhibitors with activity against CDK1, CDK2, CDK4, CDK6, CDK7 and CDK9, gave substantial *in vitro* activity, but low levels of clinical activity; its therapeutic window is narrow due to severe side effects.[42] Emergence of the first selective CDK4/6 inhibitors, changed the research landscape in this field.[43-45] In 2015, palbociclib (IBRANCE®) received accelerated approval from the US Federal Drug Administration

for use in a combination therapy with letrozole for estrogen receptor-positive, HER2-negative advanced breast cancer. Another two selective CDK4/6 inhibitors, ribociclib (KISQALI®) and abemaciclib (Verzenio®), were approved in 2017 for treatment of the same type of cancer. As of today, all three drugs feature in more than 20 clinical trials, and there is justifiable optimism surrounding their likely long-term clinical impacts. CDK4/6 are crucial in the regulation of G1-S phase in cell cycle, wherein they are activated as complexes with cyclins, leading to subsequent phosphorylation of retinoblastioma protein (Rb). Drugs that can inhibit the phosphorylation of Rb leads to cell cycle arrest that has been proven to be valuable in cancer therapy.[46] In this context, CDK4/6 PROTACs were designed as they may offer an alternative strategy to cell cycle arrest. Palbociclib and ribociclib were employed as the targeting ligand, and pomalidomide was used as the E3 ligase ligand. Conjugates with different linkers were prepared to screen the PROTACs with optimal degradation activity. As a result, the most potent PROTAC (DC_{50}: 20-50 nM) induced significant CDK4/6 degradation and inhibited cell proliferation in long term.

2. A CLICK-ADDRESSABLE CASSETTE FOR PHOTOAFFINITY LABELING*

2.1. Introduction

Photoaffinity labeling (PAL) is a valuable tool in target identification.[47] Preferred embodiments of this method include photolabile groups that decompose to carbenes or nitrenes, which undergo insertion reactions at reactive centers of proteins drawn into the environment by an attached ligand (Figure 2.1a). Difficulties with PAL tend to be encountered in detecting the proteins targeted by the reactive species; this usually requires labeling with a fluorophore or another entity to make the conjugates conspicuous.[48] However, fluorophores incorporated before the photodecomposition step can impact binding of the targeting ligand to the protein. Indeed, even without fluorophores, addition of PAL-groups to targeting ligands can impact how they bind proteins.[49] For these reasons, it is often advantageous to "click"[50-51] on a fluorophore after photodecomposition so that fluorophore-protein interactions have no impact on the coupling step, but after click the covalent conjugates can be readily detected. This letter describes a simple, conveniently accessible, "clickable cassette" **1** (Figure 2.1b) that may be readily conjugated to targeting ligands, and includes an alkyne for click-labeling with azides. Two applications of cassette **1** are also presented, *ie* labeling of carbonic anhydrase IX (CAIX) and of tropomyosin kinase receptor C (TrkC).

---

*Reprinted (adapted) with permission from "Click-addressable cassette for photoaffinity labeling" by Zhao, B.; Burgess, K. *ACS Med. Chem. Lett.* **2018**, *9*, 155-158. Copyright 2018 American Chemical Society.

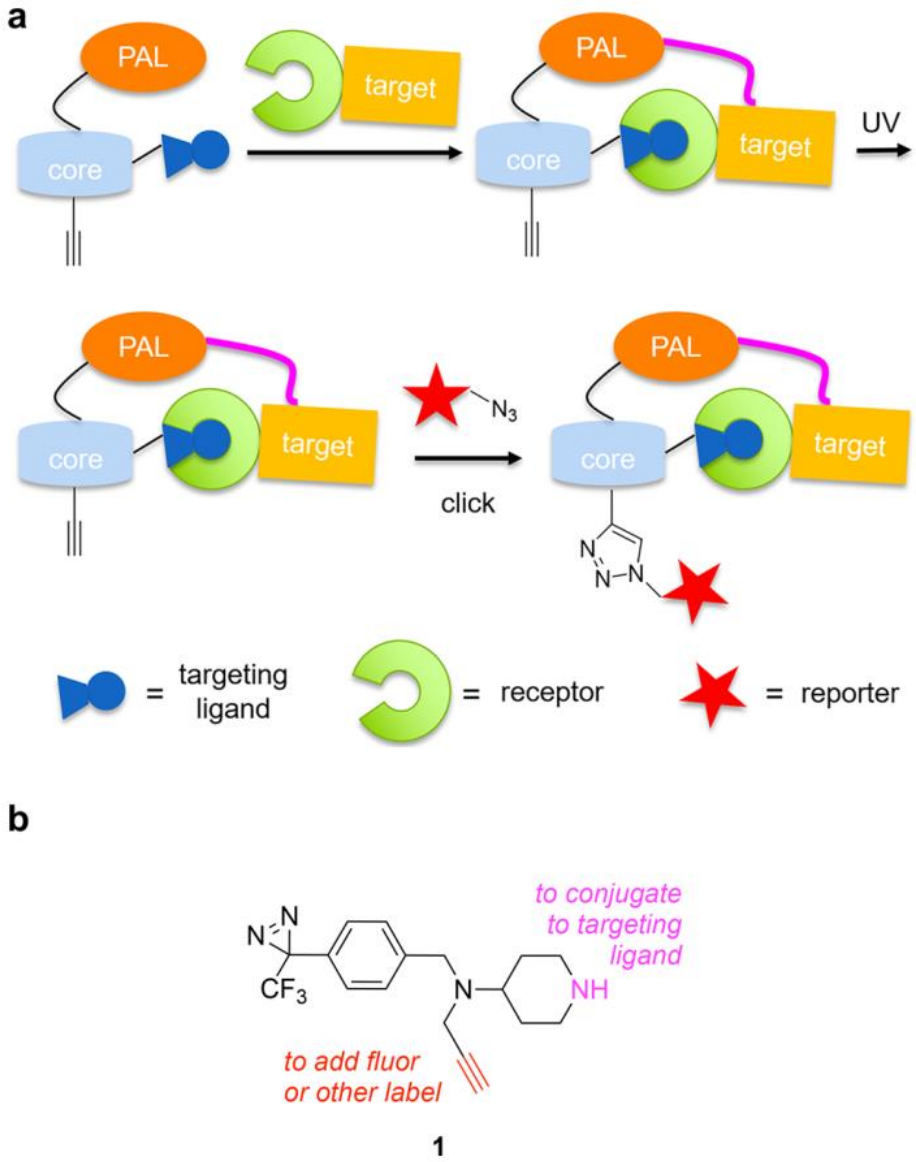

Figure 2.1 (a) Typical PAL strategy. (b) Cassette featured in this work.

Several criteria were prioritized in the design of PAL-cassette **1**, specifically: (i) ease of synthesis; (ii) a trifluoromethyl-substituted diazirine because that substituent is often preferred for PAL;[30] (iii) a highly nucleophilic secondary amine for coupling to

small molecule ligands; (iv) an alkyne for click-capture; and, (v) small structure overall to minimize non-specific binding of the cassette fragment to proteins. The presence of a tertiary amine in this system also means that it could be protonated to increase water solubilities of ligand-conjugates.

2.2. Materials and Methods

2.2.1. Materials and Instrumentation

All reactions were carried out under an inert atmosphere (nitrogen or argon where stated) with dry solvents under anhydrous conditions. Glassware for anhydrous reactions was dried in an oven at 140 ºC for minimum 6 h prior to use. Dry solvents were obtained by passing the previously degassed solvents through activated alumina columns. Yields refer to chromatographically and spectroscopically (1H-NMR) homogeneous materials, unless otherwise stated. Reagents were purchased at a high commercial quality (typically 97 % or higher) and used without further purification, unless otherwise stated. Analytical thin layer chromatography (TLC) was carried out on Merck silica gel plates with QF-254 indicator and visualized by UV. Flash column chromatography was performed using silica gel 60 (Silicycle, 230-400 mesh). 1H and 13C spectra were recorded on a 400 MHz spectrometer and were calibrated using residual non-deuterated solvent as an internal reference. The following abbreviations or combinations thereof were used to explain the multiplicities: s = singlet, d = doublet, t = triplet, q = quartet, m = multiplet, dd = doublet of doublet, ddd = doublet of doublet of doublets.

Human Carbonic Anhydrase IX was purchased from Sino Biological Inc. (10107-H08H) as a lyophilized powder. Human TrkC was purchased from Sino Biological Inc. (10048-H08H-20) as a lyophilized powder. MDA-MB-231 cells (from American Type Culture Collection) were cultured on 75 cm^2 culture flasks in Dulbecco's Modified Eagle Medium/nutrient mixture F-12 (DMEM/F12, Sigma Chemical, St. Louis, MO) supplemented with 10 % FBS. NIH3T3-TrkC cells were obtained and cultured according to previous procedures.[24] Cells were cultured in a humidified incubator at 37 °C with 5 % CO_2 and 95 % air. Carbonic anhydrase IX polyclonal antibody and goat anti-rabbit (H+L) secondary antibody (HRP conjugated) were obtained from Thermo Fisher Scientific. ECL western blotting substrate was obtained from Pierce, Thermo Scientific.

2.2.2. Experimental Procedures

Synthesis of *tert*-butyl 4-oxopiperidine-1-carboxylate (16)

At 0 ^oC, Et_3N (70 mmol) was added dropwise to a stirred solution of 4-piperidone (10 mmol) in 20 mL DCM and 4 mL MeOH. Then $(Boc)_2O$ (12 mmol) was added dropwise at 0 ^oC. The reaction mixture was then stirred at room temperature overnight followed by the addition of 30 mL H_2O. The reaction mixture was extracted with DCM (3 x 60 mL). Organic phase was collected, dried over $MgSO_4$. The solvent was removed under vacuum, washed with hexane to give the product as off-white solid (1.93 g, 95 %).

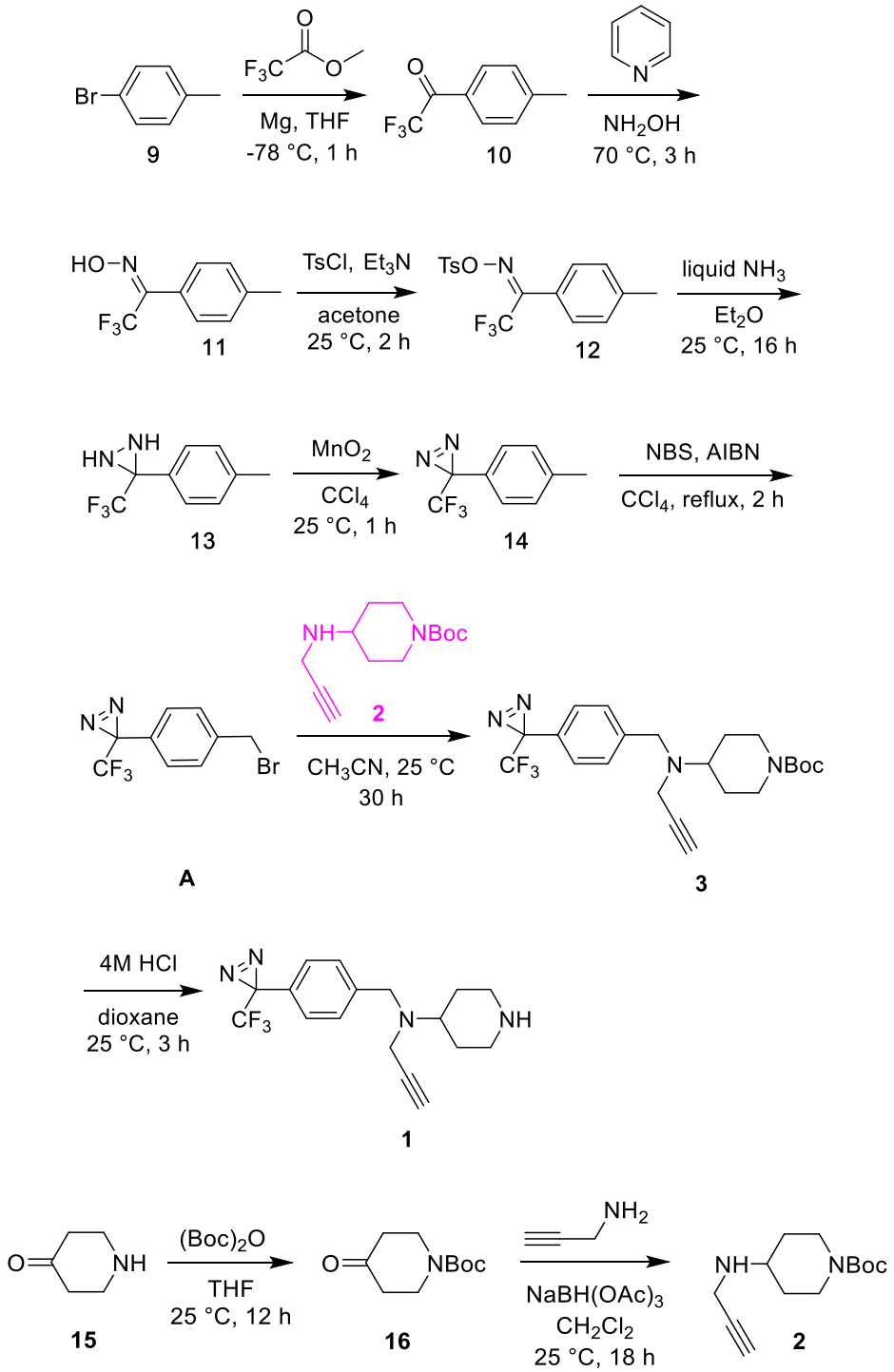

Figure 2.2 Synthetic scheme of PAL cassette **1**.

Synthesis of *tert*-butyl 4-(prop-2-yn-1-ylamino)piperidine-1-carboxylate (2)

Sodium triacetoxyborohydride (8.25 mmol) was added dropwise to a solution **16** (5.50 mmol) and propargylamine (6.25 mmol) in DCM and stirred at room temperature overnight. The reaction was quenched with 1 N HCl and basified with sat. Na_2CO_3 solution. The mixture was then extracted with DCM twice. Organic phase was collected, washed with Brine, dried over $MgSO_4$. The solvent was removed under vacuum to give the product as a yellow oil (1.09 g, 79 %). The crude material was used in the next step without further purification. ^{1}H-NMR (400 MHz, $CDCl_3$) δ 4.01 (d, *J* = 12.5 Hz, 2H), 3.47 (d, *J* = 2.4 Hz, 2H), 2.86 (ddd, *J* = 12.7, 6.3, 3.1 Hz, 3H), 2.21 (t, *J* = 2.4 Hz, 1H), 1.85 – 1.76 (m, 2H), 1.46 (s, 9H), 1.28 (m, 2H). ^{13}C-NMR (101 MHz, $CDCl_3$) δ 154.8, 82.1, 79.4, 71.3, 53.0, 42.3, 35.0, 32.0, 28.4.

Synthesis of *tert*-butyl 4-(prop-2-yn-1-yl(4-(3-(trifluoromethyl)-3H-diazirin-3-yl) benzyl)amino)piperidine-1-carboxylate (3)

Intermediate **A** was synthesized as reported.[52] Compound **2** (6 mmol) was added to a solution of **A** (3 mmol) in 15 mL MeCN and stirred at room temperature for 30 h. Solvent was removed under vacuum. The crude product was purified with flash chromatography (ethyl acetate: hexane = 1: 5) to give compound **3** as light-yellow oil (0.86 g, 64 %). ^{1}H-NMR (400 MHz, $CDCl_3$) δ 7.40 (d, *J* = 8.1 Hz, 2H), 7.16 (d, *J* = 8.0 Hz, 2H), 4.11 (s, 2H), 3.77 (s, 2H), 3.31 (d, *J* = 1.8 Hz, 2H), 2.78 (d, *J* = 14.2 Hz, 3H), 2.23 (s, 1H), 1.94 (d, *J* = 13.1 Hz, 2H), 1.56 (s, 2H), 1.49 (s, 9H). ^{13}C-NMR (101 MHz, $CDCl_3$) δ 154.7, 141.5, 129.0, 127.9, 127.0, 126.5, 79.7, 79.5, 77.2, 73.0, 58.7, 53.0, 43.0,

38.7, 29.7, 28.4. ^{19}F-NMR (376 MHz, $CDCl_3$) δ -65.33 (s). LRMS (ESI+) m/z calcd for $C_{22}H_{27}F_3N_4NaO_2^+$ $(M+Na)^+$ 459.2; found 459.0.

Synthesis of N-(prop-2-yn-1-yl)-N-(4-(3-(trifluoromethyl)-3H-diazirin-3-yl)benzyl) piperidin-4-amine (1) (Figure 2.2)

2.5 mL HCl (4M in dioxane) was added to **3** (0.5 mmol) and stirred at room temperature for 3 h. The solvent was removed under vacuum to give **1** as light-yellow oil (quantitative yield). ^{1}H-NMR (400 MHz, $CDCl_3$) δ 7.40 (d, *J* = 8.4 Hz, 2H), 7.16 (d, *J* = 8.0 Hz, 2H), 3.78 (s, 2H), 3.31 (d, *J* = 2.3 Hz, 2H), 3.25 (d, *J* = 11.8 Hz, 2H), 2.79 – 2.68 (m, 3H), 2.40 (dd, *J* = 11.0, 3.9 Hz, 1H), 2.23 (d, *J* = 2.3 Hz, 1H), 2.03 (d, *J* = 12.3 Hz, 2H), 1.65 – 1.57 (m, 2H). ^{13}C NMR (101 MHz, $CDCl_3$) δ 132.2, 131.2, 130.2, 127.1, 123.2, 82.2, 71.1, 60.0, 50.5, 43.3, 39.0, 29.7, 28.0. ^{19}F-NMR (376 MHz, $CDCl_3$) δ -65.09 (s). LRMS (ESI+) m/z calcd for $C_{17}H_{20}F_3N_4^+$ $(M+H)^+$ 337.2; found 336.9.

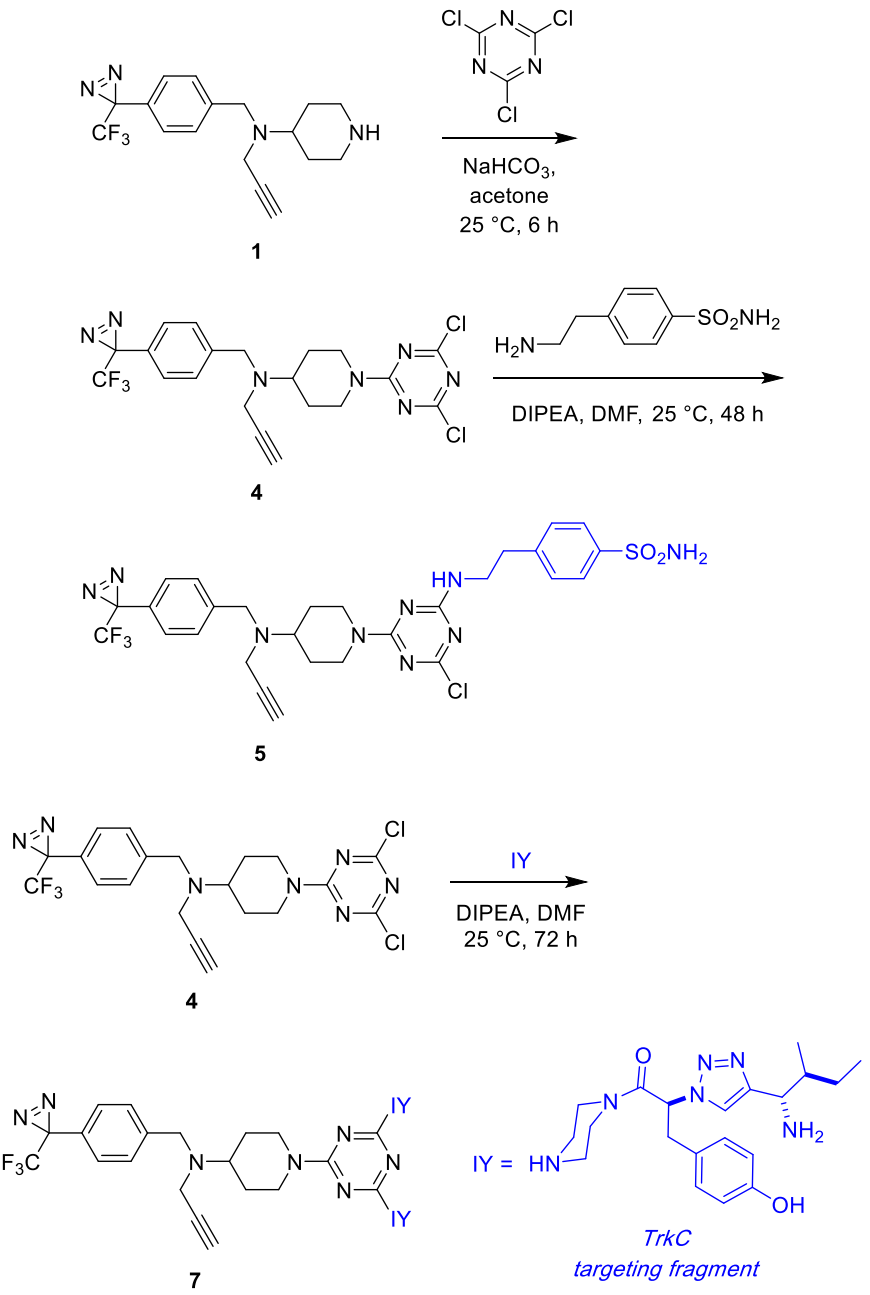

Figure 2.3 Synthetic scheme of PAL ligand for CAIX (**5**) and TrkC (**7**).

Synthesis of 1-(4,6-dichloro-1,3,5-triazin-2-yl)-N-(prop-2-yn-1-yl)-N-(4-(3-(trifluoro-methyl)-3H-diazirin-3-yl)benzyl)piperidin-4-amine (4)

Compound **1** (0.15 mmol) was dissolved in 2 mL acetone. $NaHCO_3$ (0.60 mmol) was added and stirred for 10 min. Afterwards, cyanuric chloride (0.15 mmol) was added and stirred at room temperature for another 6 h. The solvent was removed under vacuum. The mixture was partitioned between DCM and H_2O. The organic phase was collected, washed with H_2O and Brine, dried over $MgSO_4$. The solvent was removed under vacuum to give a light-yellow oil. The crude material was used in next step without further purification.

Synthesis of 4-(2-((4-chloro-6-(4-(prop-2-yn-1-yl(4-(3-(trifluoromethyl)-3H-diazirin-3-yl)benzyl)amino)piperidin-1-yl)-1,3,5-triazin-2-yl)amino)ethyl)benzenesulfonamide (5) (Figure 2.3)

Compound **4** (0.2 mmol) and 4-(2-aminoethyl)benzenesulfonamide (0.2 mmol) was dissolved in 4 mL DMF. DIPEA (1.0 mmol) was added to the mixture and stirred at room temperature for 48 h. The reaction mixture was diluted with 10 mL H_2O, then extracted with ethyl acetate (3 x 10 mL). Organic phase was collected, washed with 10% w/v aqueous LiCl (10 mL) and Brine (10 mL), dried over $MgSO_4$. The solvent was removed under vacuum. The crude product was purified with flash chromatography (ethyl acetate: hexane = 1: 1) to give **5** as white solid (68 mg, 50 %). ^{1}H NMR (400 MHz, acetone-d_6) δ 7.83 (d, *J* = 8.2 Hz, 2H), 7.53 (d, *J* = 8.1 Hz, 2H), 7.46 (d, *J* = 8.2 Hz, 2H), 7.26 (d, *J* = 8.0 Hz, 2H), 6.86 (s, 1H), 6.47 (s, 2H), 4.76 (d, *J* = 12.6 Hz, 1H), 4.63 (d, *J* = 12.5 Hz, 1H), 3.87 (d, *J* = 7.4 Hz, 2H), 3.70 (d, *J* = 6.8 Hz, 2H), 3.37 (d, *J* = 2.0 Hz, 2H), 3.03 (d, *J* = 7.2 Hz, 5H), 2.71 (s, 1H), 2.07 (s, 2H), 1.57 (d, *J* = 12.9 Hz, 2H). ^{13}C NMR

(101 MHz, acetone-d_6) δ 169.0, 166.0, 164.3, 144.1, 142.7, 142.3, 129.3 , 127.0, 126.4, 126.2, 121.0, 116.7, 79.8, 73.7, 58.6, 52.7, 42.5, 41.8, 38.5, 35.2, 35.0, 31.4. ^{19}F NMR (376 MHz, acetone-d_6) δ -66.32 (s). HRMS (ESI+) m/z calcd for $C_{28}H_{30}ClF_3N_9O_2S$ $(M+H)^+$ 648.1878; found 648.1872.

Synthesis of (2S,2'S)-1,1'-((6-(4-(prop-2-yn-1-yl(4-(3-(trifluoromethyl)-3H-diazirin-3-yl)benzyl)amino)piperidin-1-yl)-1,3,5-triazine-2,4-diyl)bis(piperazine-4,1-diyl))bis(2-(4-((1S,2S)-1-amino-2-methylbutyl)-1H-1,2,3-triazol-1-yl)-3-(4-hydroxyphenyl)propan-1-one) (7)

To a solution of compound **4** (0.106 mmol) in DMF was added DIPEA (1.06 mmol) and IY[15] (0.212 mmol) in THF. The mixture was stirred at room temperature for 72 h. DMF was then removed via lyophilizer. The crude product was purified via prep-HPLC to give **7** as white solid (28 mg, 22 %). ^{1}H NMR (400 MHz, DMSO-d_6) δ 9.25 (s, 2H), 8.21 (d, *J* = 9.1 Hz, 2H), 7.45 (d, *J* = 8.3 Hz, 2H), 7.25 (d, *J* = 7.9 Hz, 2H), 6.99 (d, *J* = 8.4 Hz, 4H), 6.61 (d, *J* = 8.3 Hz, 4H), 6.14 – 6.04 (m, 2H), 4.59 (d, *J* = 12.2 Hz, 2H), 4.16 (dd, *J* = 23.4, 5.6 Hz, 2H), 3.75 (s, 2H), 3.65 – 3.23 (m, 26H), 3.13 (s, 2H), 2.81 (t, *J* = 11.3 Hz, 3H), 1.94 – 1.78 (m, 5H), 1.35 (dd, *J* = 12.7, 7.4 Hz, 4H), 1.05 – 0.96 (m, 2H), 0.90 – 0.82 (m, 6H), 0.76 (d, *J* = 6.7 Hz, 4H). ^{13}C NMR (101 MHz, DMSO-d_6) δ 166.4, 165.1, 164.7, 156.7, 143.0, 130.7, 129.6 , 126.8, 126.5, 126.1, 123.3, 115.5, 80.8, 76.0, 60.7, 59.0, 52.9, 51.8, 45.4, 43.1, 42.7, 42.4, 38.8, 37.6, 29.5, 25.4, 21.5, 15.0, 14.6, 11.7, 11.6. ^{19}F NMR (376 MHz, DMSO-d_6) δ -64.65 (s). HRMS (MALDI+) m/z calcd for $C_{60}H_{77}F_3N_{19}O_4$ $(M+H)^+$ 1184.6353; found 1184.6298.

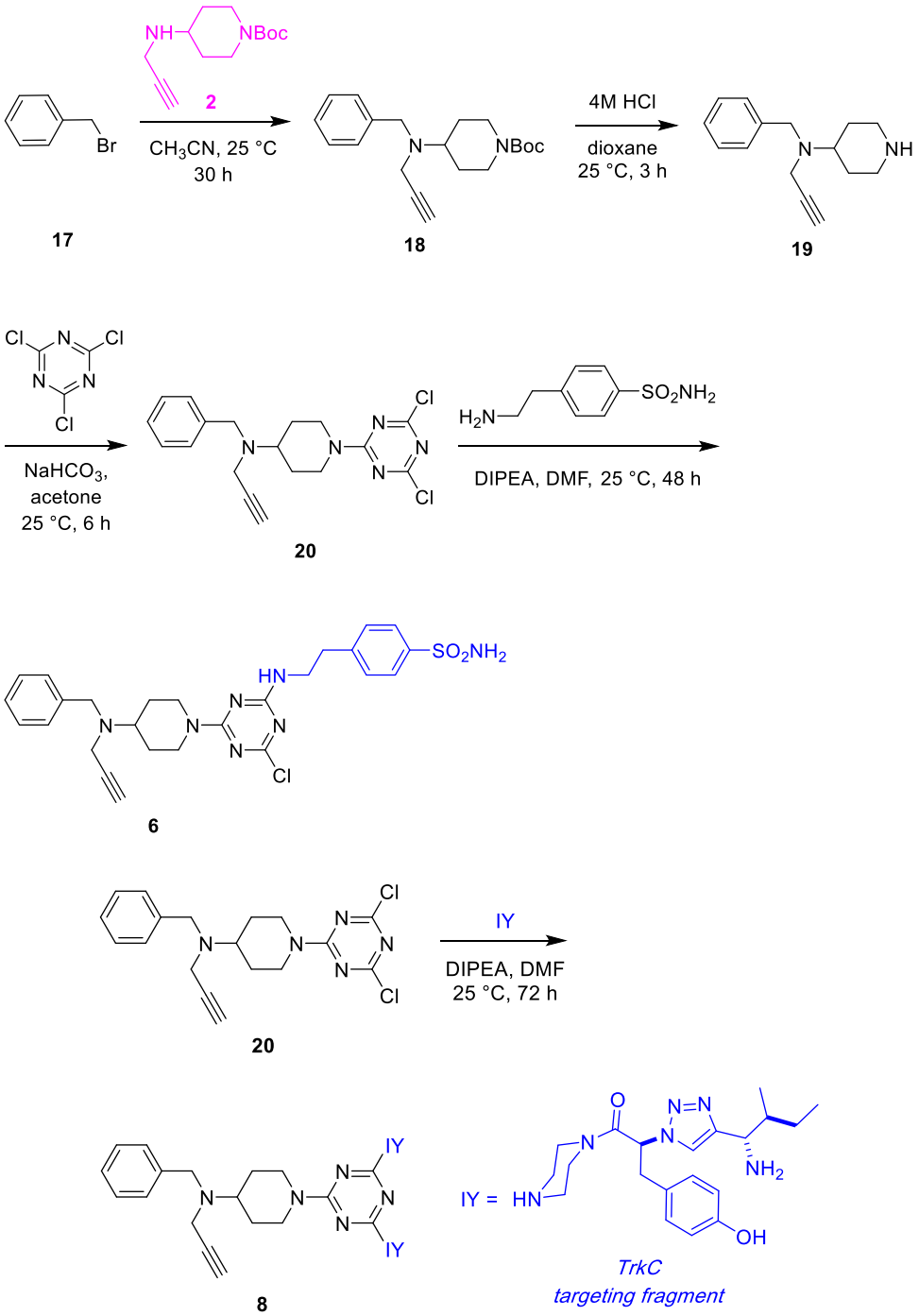

Figure 2.4 Synthetic scheme of PAL negative ligand **6** and **8**.

Synthesis of PAL negative ligand (6 and 8) (Figure 2.4)

Synthesis of ligand **6** and **8** are similar to **5** and **7**, respectively, starting from benzyl bromide instead of compound **A**.

4-(2-((4-(4-(benzyl(prop-2-yn-1-yl)amino)piperidin-1-yl)-6-chloro-1,3,5-triazin-2-yl)amino)ethyl)benzenesulfonamide (**6**): ^{1}H NMR (400 MHz, acetone-d_6) δ 8.01 (s, 1H), 7.83 (d, *J* = 8.2 Hz, 2H), 7.46 (d, *J* = 8.3 Hz, 2H), 7.38 (t, *J* = 6.5 Hz, 2H), 7.33 (t, *J* = 7.4 Hz, 2H), 7.25 (t, *J* = 7.2 Hz, 1H), 6.88 (d, *J* = 5.6 Hz, 1H), 6.50 (s, 2H), 4.76 (d, *J* = 13.0 Hz, 1H), 4.63 (d, *J* = 12.3 Hz, 1H), 3.81 (d, *J* = 7.9 Hz, 2H), 3.70 (dd, *J* = 13.5, 6.7 Hz, 2H), 3.36 (dd, *J* = 7.6, 2.0 Hz, 2H), 3.12 – 2.94 (m, 6H), 2.70 (s, 1H), 1.59 (d, *J* = 12.4 Hz, 2H). ^{13}C NMR (101 MHz, acetone-d_6) δ 169.0, 166.0, 164.3, 144.1, 142.3, 139.8, 129.3, 128.6 (d, *J* = 4.6 Hz), 128.2, 126.9, 126.2, 80.0, 73.5, 58.3, 53.3, 42.5, 41.9, 38.2, 35.0. LRMS (ESI+) m/z calcd for $C_{26}H_{31}ClN_7O_2S$ $(M+H)^+$ 540.2; found 540.2.

(2S,2'S)-1,1'-((6-(4-(benzyl(prop-2-yn-1-yl)amino)piperidin-1-yl)-1,3,5-triazine-2,4-diyl)bis(piperazine-4,1-diyl))bis(2-(4-((1S,2S)-1-amino-2-methylbutyl)-1H-1,2,3-triazol-1-yl)-3-(4-hydroxyphenyl)propan-1-one) (**8**): ^{1}H NMR (400 MHz, DMSO-d_6) δ 9.26 (s, 2H), 8.21 (d, *J* = 6.2 Hz, 2H), 7.32 (d, *J* = 5.8 Hz, 4H), 7.27 – 7.22 (m, 1H), 6.98 (d, *J* = 8.4 Hz, 4H), 6.61 (d, *J* = 8.4 Hz, 4H), 6.13 – 6.05 (m, 2H), 4.59 (d, *J* = 12.7 Hz, 2H), 4.15 (dd, *J* = 23.7, 5.6 Hz, 2H), 3.71 (s, 2H), 3.60 – 3.45 (m, 14H), 3.41 (s, 4H), 3.32 – 3.22 (m, 8H), 3.12 (s, 1H), 2.83 (t, *J* = 11.5 Hz, 3H), 1.92 (d, *J* = 6.2 Hz, 2H), 1.84 (d, *J* = 6.0 Hz, 2H), 1.44 – 1.29 (m, 4H), 1.16 – 1.08 (m, 1H), 1.05 – 0.95 (m, 2H), 0.90 – 0.83 (m, 7H), 0.76 (d, *J* = 6.7 Hz, 4H). ^{13}C NMR (101 MHz, DMSO-d_6) δ 166.4, 165.2, 164.7, 156.7, 140.0, 130.7, 128.9, 128.7, 127.3, 126.1, 123.3, 115.5, 80.9, 75.9, 60.7, 58.8, 53.4,

51.8, 45.5, 43.1, 42.4, 37.6, 29.6, 25.4, 21.5, 15.0, 14.56, 11.8, 11.6. LRMS (MALDI+) m/z calcd for $C_{58}H_{78}N_{17}O_4$ $(M+H)^+$ 1076.6; found 1076.9.

Fluorescent photoaffinity labeling of recombinant CAIX and TrkC

Recombinant CAIX or TrkC protein (2 μg) was dissolved in 25 mM HEPES buffer (20 μL) and kept on ice. For competition experiments, PAL- ligand **6** or **8** was allowed to incubate with CAIX or TrkC recombinant protein at 4 °C for 1 h. Then, PAL+ ligand **5** or **7** was added to all protein samples and incubated in dark at 4 °C for 2 h. All samples except UV negative ones were transferred to a 96-well plate and irradiated by a LED UV flashlight (365 nm) at 4 °C for 30 min. 19.5 μL of each sample were transferred into new Eppendorf tubes. 2.5 μL 10% SDS solution in water was added to each tube and mixed by vortexing. Then 0.5 μL 5 mM azide-fluor-488 (Sigma-Aldrich) was added, followed by 2.5 μL of click reaction catalyst cocktail (prepared immediately before use: mix 1.5 volumes of 1.7 mM TBTA in 80% tert-butanol/20% DMSO, 0.5 volumes of 50 mM $CuSO_4$ and 0.5 volumes of 50 mM TCEP by vortexing). Samples were mixed by vortexing and incubated in dark at room temperature for 3 h. Click reaction was quenched by adding 5 μL of 6 x SDS sample buffer, then was boiled at 95 °C for 5-10 min. SDS-PAGE was performed by using a handcast 10% polyacrylamide gel. The gel was run for an additional 5 minutes after the dye font reached the end of the gel to ensure all of the excess unreacted dyes had completely exited the gel. The gel was then washed with distilled water (3 x 10 min) and scanned on a Typhoon FLA 9500 fluorescent gel scanner (Alexa-488).

Biotin photoaffinity labeling of target proteins (CAIX and TrkC) in cell lysates

Cells (MDA-MB-231 or NIH3T3-TrkC) were lysed by RIPA buffer (Pierce) according to manufacturer's instructions. The total protein concentration was ~ 2 mg/mL, determined by BCA protein assay (Pierce). 200 μL cell lysate was incubated with or without PAL+ ligand **5** or **7** in dark at 4 ℃ for 3 h. For competition experiments, cell lysate was pre-inhibited with 200-fold PAL- ligand **6** or **8** at 4 °C for 1 h. Samples were then transferred to a 96-well plate and irradiated by a LED UV flashlight (365nm) at 4 ℃ for 30 min. All samples were transferred into new Eppendorf tubes. 1 μL biotin azide (20 mM in DMSO) was added to each reaction, followed by 25 μL click reaction catalyst cocktail (prepare immediately before use: mix 1.5 volumes of 1.7 mM TBTA in 80% tert-butanol/20% DMSO, 0.5 volumes of 50 mM $CuSO_4$, and 0.5 mM volumes of 50 mM TCEP by vortexing). Samples were mixed by vortexing and incubated for 5 h at room temperature with constant shaking.

40 μL NeutrAvidin resin (Pierce) prewashed with 1x PBS was then added to the reaction mixture, incubated for 2.5 h with constant shaking at room temperature and then placed at 4 ℃ overnight. Samples were warmed up to room temperature on the next day and centrifuged to pellet beads. Supernatants were discarded and beads were washed with 400 μL PBS-T (PBS + 0.1% Tween 20) 5 x 5 min followed by PBS 1 x 5 min with shaking. The remaining liquid was completely removed. 40 μL 1 x SDS-buffer was added and boiled at 100 ℃ for 10 min to elute proteins on bead. SDS-PAGE gel was performed by using a handcast 10% polyacrylamide gel. The gel was washed with distilled water 3 x 5 min. Proteins were visualized either directly by CBB-G250 staining or by

immunoblotting. For immunoblotting, proteins were transferred to PVDF membrane by Pierce Power Station according to manufacturer's instructions. Blots were detected using iBind Western Device according to manufacturer's instructions [polyclonal anti-CAIX antibody (1:1000), HRP-conjugated anti-rabbit IgG (H+L) (1:2000)]. Afterwards, blots were treated with ECL Western Blotting Substrate (Pierce) and scanned by ChemiDoc XRS (BioRad) imaging system.

2.3. Results and Discussion

Figure 2.5a describes the synthesis of cassette **1** from the known diazirine precursor **A**.[52] Nucleophilic displacement with the amine **2** (prepared via a reductive amination of propargyl amine with the corresponding ketone, see supporting) gave the Boc-protected cassette **3**; the deprotected cassette **1** was obtained through treatment with acid.

As a test application of PAL-**1**, this material was coupled with cyanuric chloride to give the pivotal intermediate **4** (Figure 2.5). A second S_NAr displacement on the triazine enabled incorporation of a carbonic anhydrase IX ligand in the conjugate **5**.

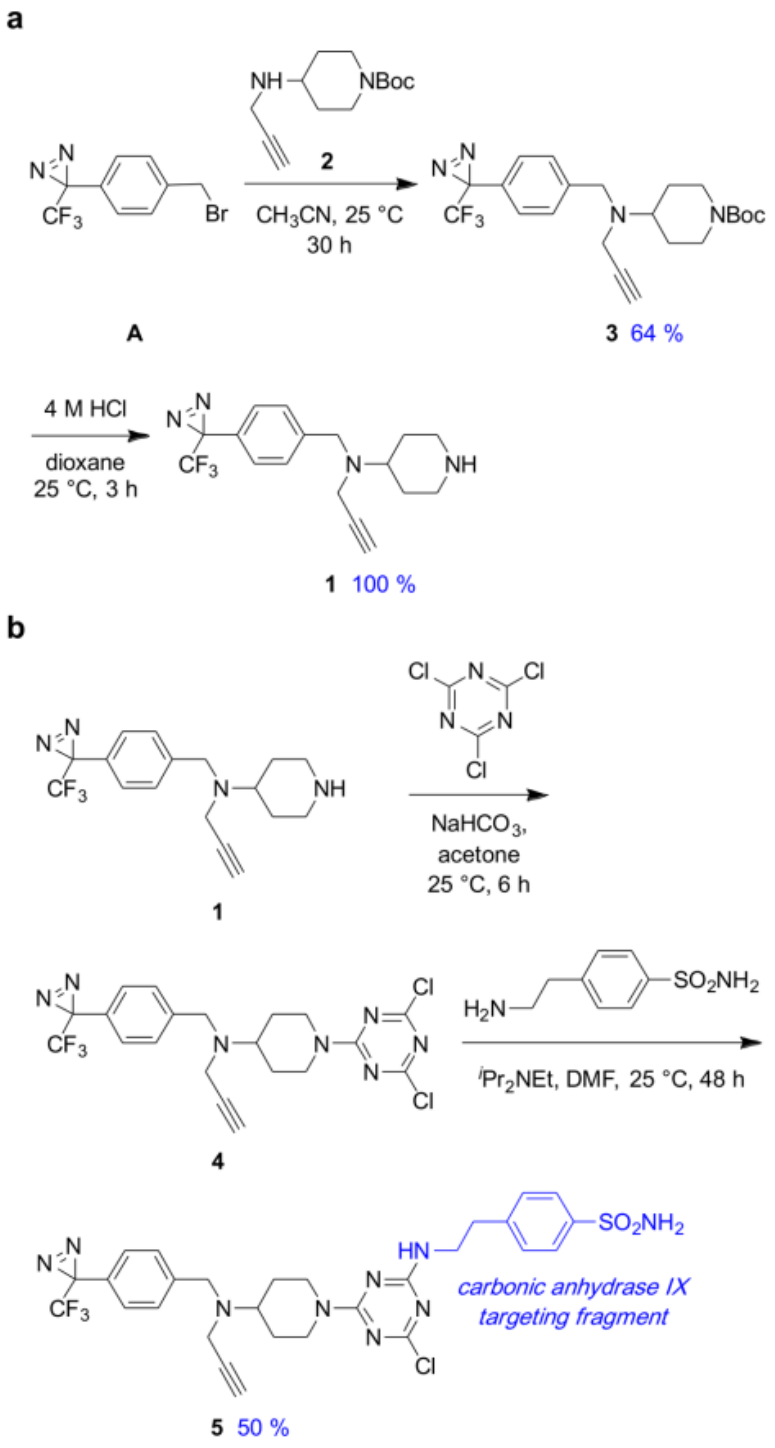

Figure 2.5 Synthesis of (**a**) cassette **1** and (**b**) **5**, comprising **1** conjugated with a CAIX ligand.

Carbonic anhydrase (CA) IX is a transmembrane protein, one of a family of enzymes that mediate reversible hydration of CO_2.[53] This enzyme tends to be overexpressed in hypoxic tumors but not significantly expressed in most normal tissues.[54] Small molecules that putatively bind CAIX are interesting in tumor targeting.[55-57]

In a photoaffinity labeling experiment, the conjugate **5** with recombinant CAIX in pH 7.4 HEPES buffer was illuminated at 365 nm (light emitting diode) for 30 min. Fifty-fold excesses of azide-fluor-488 (compared to ligand **5**), copper (2+) salts, and a reducing agent (tris(2-carboxyethyl)phosphine, TCEP) were added and the reaction mixture was held at 25 °C for 3 – 4 h in the dark to allow the click cycloaddition to proceed. Constituents of the sample were separated on an SDS-PAGE gel (Figure 2.6a); after fluorescence imaging, a band at 55 kDa was observed corresponding to labeled CAIX. Staining all proteins on the same gel with a Coomassie blue dye revealed the protein is present in all lanes, but comparison with the in-gel fluorescent image showed that 50-fold excess of the conjugate without a diazirine **6** blocked the photoaffinity labeling (lanes 2 and 4). When the sample was not illuminated (lane 5), no photoaffinity labeling occurred.

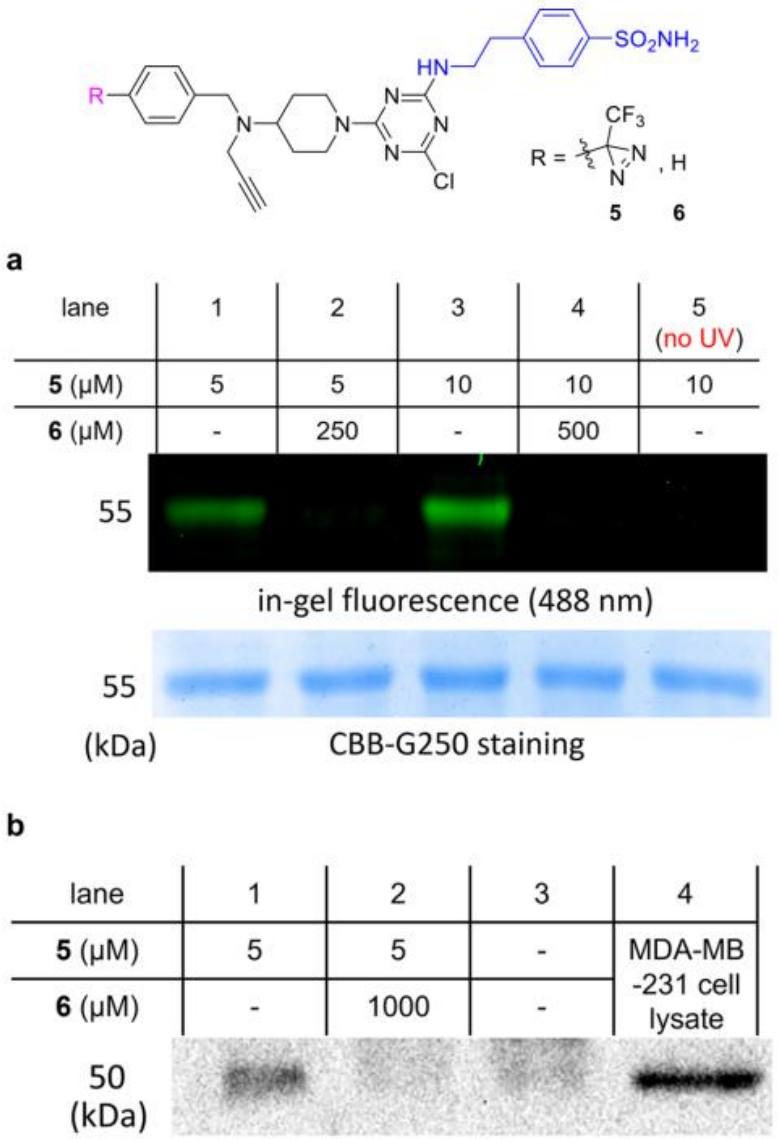

Figure 2.6 (**a**) Experiments with isolated protein. Photoaffinity labeling of recombinant CAIX after 30 min illumination with excess ligand **5** and click with azide-fluor-488; the top gel (black background) shows the fluorescence at 488 nm, and the one below depicts protein staining with Coomassie Brilliant Blue (CBB) G250. Competition with **6**, which lacks a diazirine, suppresses labeling with **5** (lanes 2 and 4). (**b**) Experiments with MDA-MB-231 cell lysates. MDA-MB-231 cell lysate was treated with PAL probe 5 under 365 nm illumination for 30 min, then clicked with biotin-azide. NeutrAvidin agarose was used to pull down the biotinylated proteins, and the material captured was run on SDS-PAGE gel. Lane 1 shows staining of CAIX on the Western blot image with a CAIX Ab, lane 2 shows sample pretreated with blocking ligand **6**. Lane 3 shows no ligands and lane 4 depicts the lysate without PAL.

The next set of experiments were undertaken to confirm that the cassette could be used on cell lysates, rather than purified recombinant protein, and that the conjugate could be observed via biotin-labeling and a pull-down procedure (Figure 2.6b). "Triple negative" breast cancer cells, MDA-MB-231 were used since these are known to express CAIX.[58] Thus, the overall procedure was photoaffinity labeling, click with biotin azide, pull-down on streptavidin coated beads, then SDS-PAGE gel and Western blot. This sequence revealed the presence of CAIX (lane 1), but not when excess blocking ligand **6** was present (lane 2) or when no photoaffinity label at all was used (lane 3). Lane 4 is a positive control showing that CAIX was present in the cell lysate before pull-down.

Several studies from these laboratories have featured a bivalent system with dipeptide fragments (Figure 2.7, blue in structures **7** and **8**) that putatively bind the cell surface receptor TrkC.[1, 15, 24, 26, 59-60] Thus conjugates **7** and **8** were formed to test this hypothesis via photoaffinity labeling.

Figure 2.7a shows in-gel fluorescence after a photoaffinity labeling, click, and SDS-PAGE sequence for solubilized TrkC receptor and the conjugate **7**. A band at around 100 kDa was observed (lanes 1 and 3) but not when 80x of the blocking ligand **8** was added (lanes 2 and 4), or if the illumination step was excluded (lane 5). Figure 2.7b shows a Western blot after illumination of **7** with NIH3T3 cells stably transfected with TrkC, "click" with biotin azide, capture onto NeutrAvidin agarose beads, then SDS-PAGE. Two TrkC bands were observed (whereas the parent NIH3T3 cells give none, Figure 2.8, lane 3); these are at similar, but not the same, molecular mass as the solubilized extracellular domain of the TrkC receptor in Figure 2.7a.

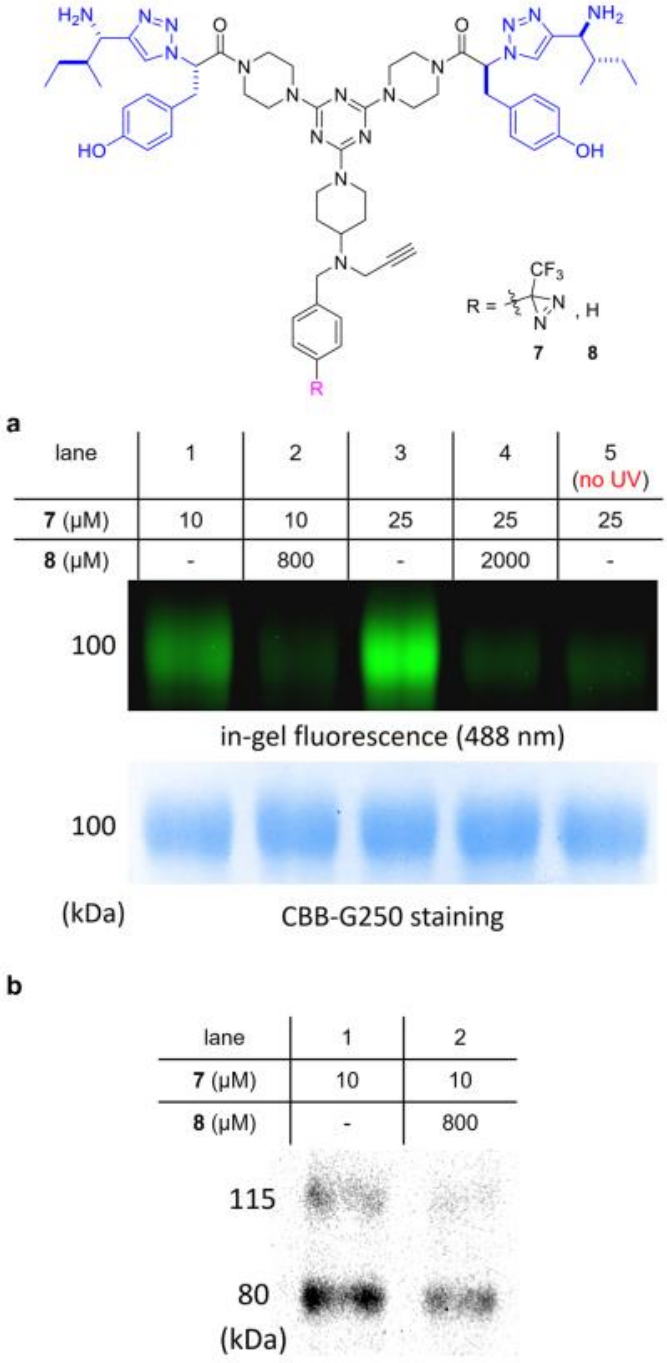

Figure 2.7 (**a**) Experiments with solubilized TrkC extracellular domain. Solubilized TrkC extracellular domain was incubated with **7** for 1 h, illuminated for 30 min at 365 nm, clicked with azide-fluor-488, then subjected to SDS-PAGE. Top gel: fluorescence at 488 nm. Bottom gel: protein staining with CBB G250. Competition with **8**, which lacks a diazirine, suppresses labeling with **7** (lanes 2 and 4). (**b**) Experiments with NIH3T3 TrkC^{+}

cell lysates. Cell lysate was treated with PAL probe **7** under 365 nm illumination for 30 min, then clicked with biotin azide. NeutrAvidin agarose was used to pull down the biotinylated proteins, and the material captured was run on SDS-PAGE gel. Lane 1 shows staining of TrkC on the Western blot image with anti-TrkC mAb, lane 2 shows sample pretreated with blocking ligand **8**.

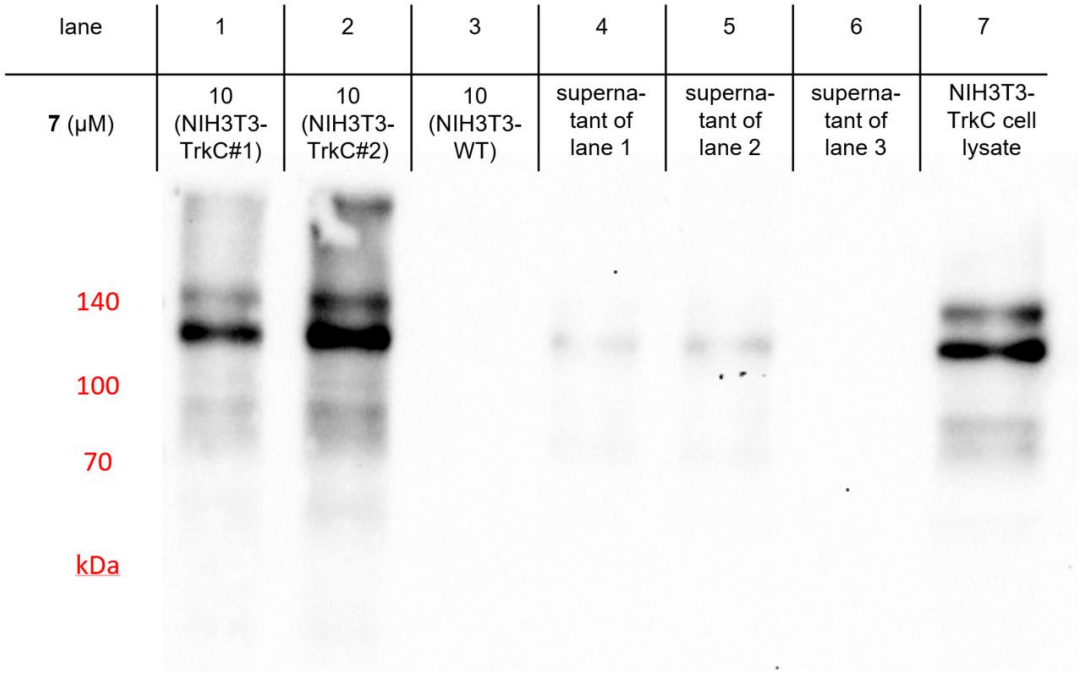

Figure 2.8 Biotin photoaffinity labeling of TrkC in NIH3T3-TrkC or NIH3T3-WT cell lysate followed by affinity pull-down assay. Eluted proteins (lane 1 - 2: NIH3T3-TrkC cell, and lane 3: NIH3T3-WT), corresponding supernatants (lane 4 - 6) and NIH3T3-TrkC whole cell lysate (lane 7) were subjected to SDS-PAGE gel and subsequent Western blotting using anti-TrkC mAb.

2.4. Conclusions

Other PAL ligands functionalized with alkynes have been reported prior to our work,[61-62] but the synthesis of cassette **1** appears to be more convenient than most and provides another type of system. This is because, unlike some other probes, synthesis of cassette **1** does not require reactive organometallics, except in the first step wherein the starting material was made on scale. Cassette **1** has a secondary amine that can be easily coupled to activated carboxylic acids; this feature makes the probe more portable. Both the small-molecule conjugates prepared in this work labeled their anticipated targets with sufficient efficiencies for observation in SDS-PAGE experiments.

3. TRKC-TARGETED KINASE INHIBITORS AND PROTACS*

3.1. Introduction

Therapeutic indices of chemotherapeutics can be improved by delivering them into cancer cells via "active targeting",[2] *ie* by conjugation with molecular fragments that bind cell surface receptors overexpressed in cancer cells. This approach leads to greater accumulation of drug in tumor over normal tissues, opening the therapeutic window. Active targeting is most commonly achieved via antibody-drug conjugates,[63] but small molecule approaches have significant advantage of deeper permeation into solid tumors.[4-5] Consequently, it seems logical to overlap active targeting of kinase inhibitors (KIs) with our interest in small molecule that binds TrkC.[1, 15, 24, 26-27, 64-66] TrkC is overexpressed on several metastatic cancer types, including neuroblastoma,[20] glioblastoma,[21] breast cancer[22] and melanoma.[23] Activation of TrkC promotes cell growth and metastasis in some forms of tumorigenesis.[67] We developed a small molecule fragment (IY-IY) that binds TrkC (K_d = 112 nM)[27] and can be internalized into cells;[15] recently we demonstrated a conjugate of this with a cytotoxic cargo (DM4) had a better therapeutic index than the parent drug in a murine model.[27]

There are a few examples of active targeting being used for less cytotoxic chemotherapeutics. Small molecule targeting fragments are probably better suited than

* Reprinted (adapted) with permission from "TrkC-Targeted Kinase Inhibitos And PROTACs" by Zhao, B.; Burgess, K. *Mol.Pharmaceutics* **2019**, *16*, 4313-4318. Copyright 2019 American Chemical Society.

antibodies for this strategy because they can be made on larger molar scales. The less cytotoxic chemotherapeutic featured in this study is the kinase inhibitor dasatinib.

Dasatinib (Sprycel®) was an approved drug for Philadelphia chromosome-positive (Ph+) chronic myeloid leukemia (CML) in 2006. Since then it has featured in over 150 clinical trials (clinicaltrials.gov) including an active Phase II study for breast cancer (NCT01471106). Treatment with dasatinib has side effects that can be severe for some patients,[12-13] and this restricts dose levels. At least some of those side effects can be attributed to poor selectivity within the kinome. In general, poor selectivity between kinases is a common problem with KIs because off-target interactions may lead to undesirable consequences; as of 2016, around 25% of FDA-approved KIs were known to bind ten or more targets.[68] Ultimately, active targeting may be a way to alleviate some of these off-target effects.

Recently we demonstrated active targeting of kinase inhibitors via conjugation with cyanine dyes that apparently bind all solid tumors.[69] Described here is uptake mediated by binding the IY-IY fragment of TrkC receptors applied to a KI (dasatinib).

PROTACs are a form of active targeting wherein a small molecule binds a target protein and delivers an E3-ligase ligand. In PROTACs, small molecule targeting groups are invulnerable to E3-ligase mediated degradation before binding the target protein and facilitate catalysis; this would not be so for PROTACs based on antibodies. Thus, here we use the IY-IY fragment to deliver a kinase inhibitor via TrkC, and also investigate how this same fragment could be used in PROTACs to degrade TrkC. Specifically, we report IY-IY-dasatinib conjugates (**2**) for actively targeting TrkC+ cancer cell to deliver the KI,

and a potent TrkC degrader (**4**) designed using the PROTACs concept. Consequently, we also report potentially the first TrkC PROTACs.[32, 70]

3.2. Materials and Methods

3.2.1. Materials and Instrumentation

All reactions were carried out under an inert atmosphere (nitrogen or argon where stated) with dry solvents under anhydrous conditions. Glassware for anhydrous reactions was dried in an oven at 140 ºC for minimum 6 h prior to use. Dry solvents were obtained by passing the previously degassed solvents through activated alumina columns. Yields refer to chromatographically and spectroscopically (^{1}H-NMR) homogeneous materials, unless otherwise stated. Reagents were purchased at a high commercial quality (typically 97 % or higher) and used without further purification, unless otherwise stated. Analytical thin layer chromatography (TLC) was carried out on Merck silica gel plates with QF-254 indicator and visualized by UV. Flash column chromatography was performed using silica gel 60 (Silicycle, 230-400 mesh). ^{1}H and ^{13}C spectra were recorded on a 400 MHz spectrometer and were calibrated using residual non-deuterated solvent as an internal reference. The following abbreviations or combinations thereof were used to explain the multiplicities: s = singlet, d = doublet, t = triplet, q = quartet, m = multiplet, dd = doublet of doublet, ddd = doublet of doublet of doublets.

Dasatinib was purchased from AK Scientific, Inc. Hs578t and MDA-MB-231 (from American Type Culture Collection, ATCC) were cultured on 75 cm^2 culture flasks in Dulbecco's Modified Eagle Medium/nutrient mixture F-12 (DMEM/F12, Sigma

Chemical, St. Louis, MO) supplemented with 10 % FBS. MCF-10A (from ATCC) was cultured in Mammary Epithelial Cell Growth Medium Kit (MEGM, catalog No. CC-3150 excluding GA-1000, Lonza/Clonetics Corporation) with 100 ng/mL cholera toxin (Sigma Aldrich). HUVEC (from ATCC) was cultured in F-12K Medium (ATCC) supplemented with 10 % FBS. NIH3T3-TrkC and NIH3T3 wild-type cells were cultured according to previous method.[24] Culture-Inserts for wound healing assay were purchased from Ibidi GmbH. Phospho-Src family (Tyr416), Src, TrkC and β-actin mAb were purchased from Cell Signaling Technology. Goat anti-rabbit (H+L) secondary antibody (HRP conjugated) were purchased from ThermoFisher Scientific. SuperSignal West Dura Substrate (ThermoFisher Scientific) was used as Western blot substrate.

3.2.2. Experimental Procedures

IY-IY-TEG, IY-IY-NH_2, YI-YI-NH_2 and **7** were made according to previous procedures. [15, 66, 71] **Das-N_3** was made according to literature.[72]

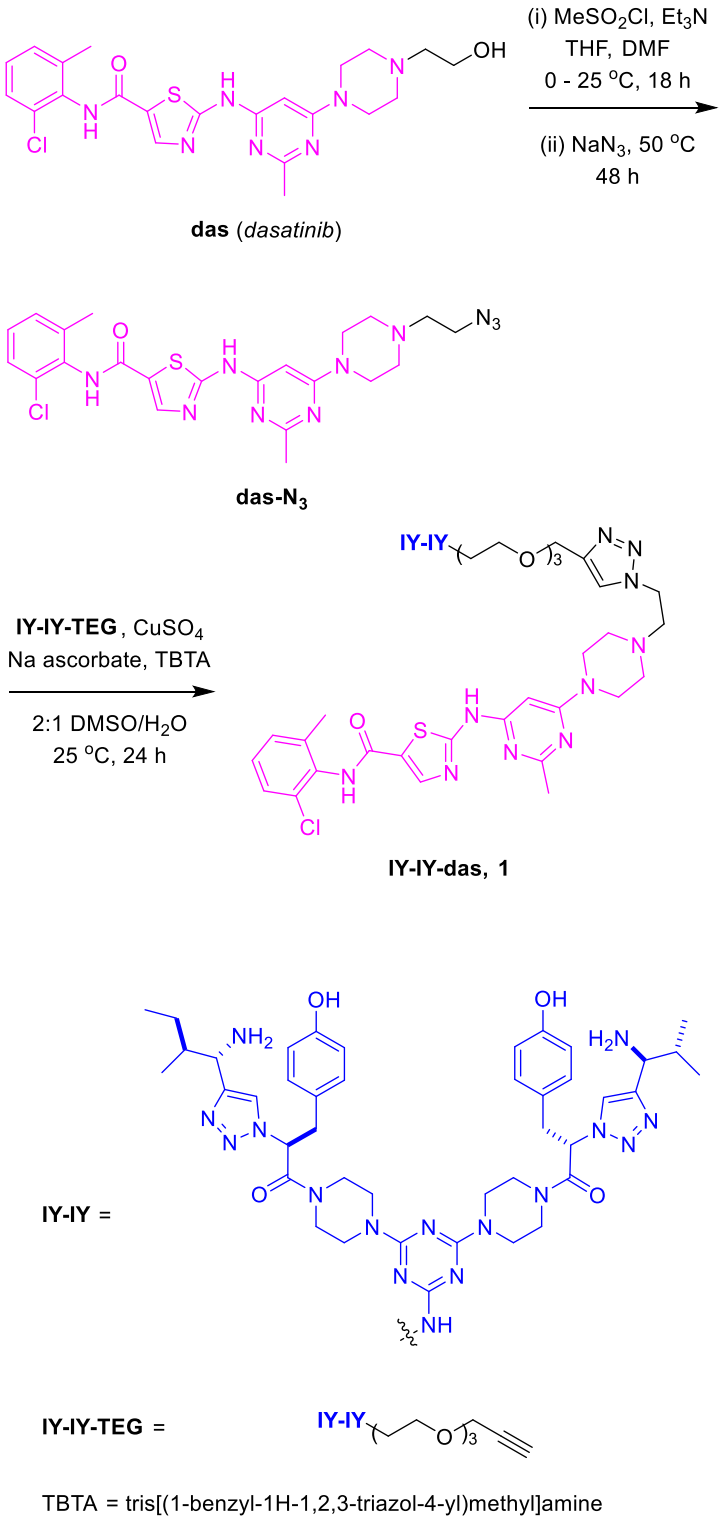

Figure 3.1 Synthesis of **IY-IY-das** (**1**) with a robust linker.

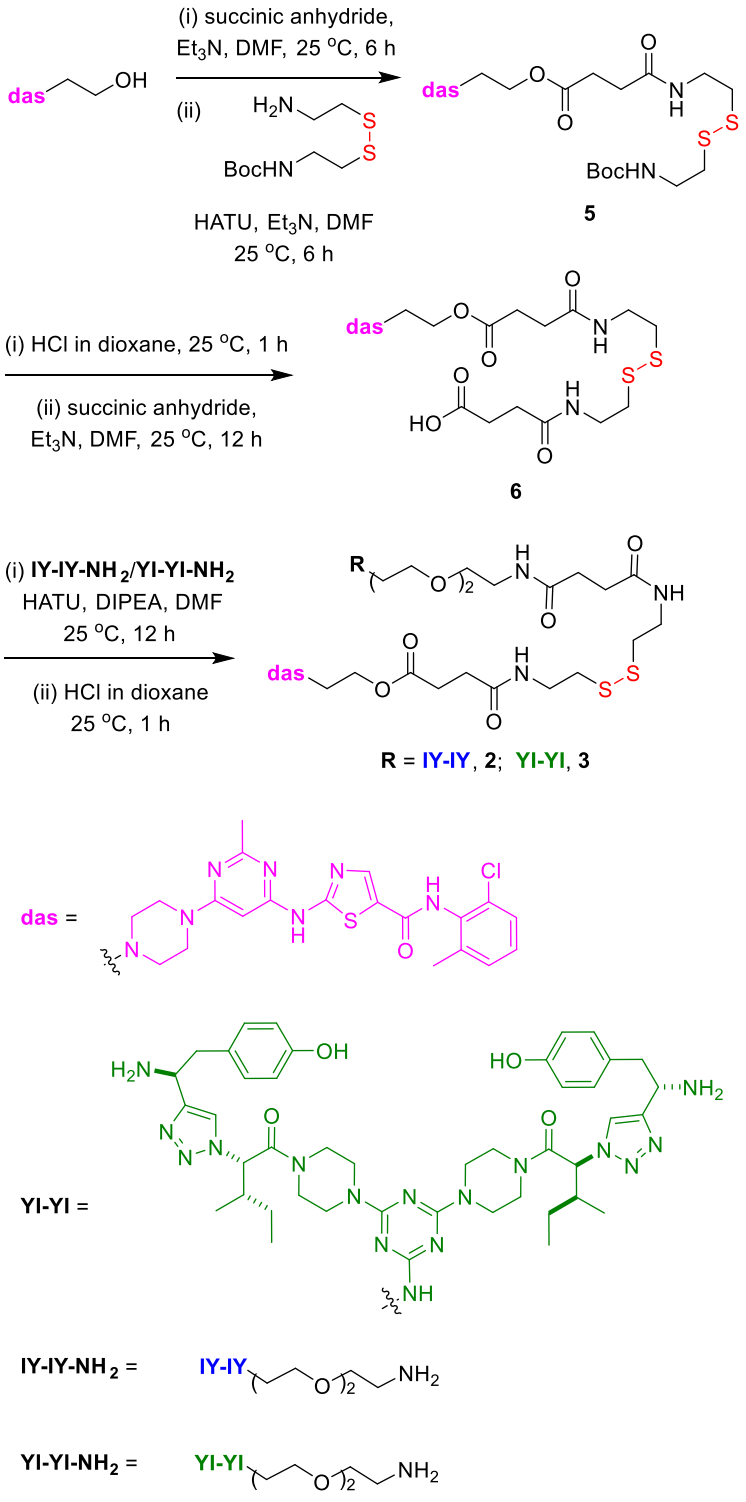

Figure 3.2 Synthesis of **IY-IY-SS-das** (**2**) and **YI-YI-SS-das** (**3**), having thiol-labile linkers.

Synthesis of 2-(4-(6-((5-((2-chloro-6-methylphenyl)carbamoyl)thiazol-2-yl)amino)-2-methylpyrimidin-4-yl)piperazin-1-yl)ethyl 2,2-dimethyl-4,13-dioxo-3-oxa-8,9-dithia-5,12-diazahexadecan-16-oate (5)

The product of step (i) in making compound **5, das-COOH**, was made according to literature.[73] For step (ii), to a solution of tert-butyl (2-((2-aminoethyl)disulfaneyl)-ethyl)carbamate (0.98 mmol) and **das-COOH** (1.07 mmol) in 10 mL DMF were added triethylamine (1.96 mmol) and HATU (1.17 mmol). The mixture was stirred for 6 h at room temperature. Solvent was removed in vacuo. The crude product was purified via column chromatography by eluting with 10% MeOH in DCM to obtain **5** as light yellow solid (680 mg, 84 %). ^{1}H NMR (400 MHz, MeOD) δ 8.18 (s, 1H), 7.35 (dd, *J* = 7.1, 2.0 Hz, 1H), 7.24 (t, *J* = 7.2 Hz, 2H), 6.32 (s, 1H), 4.54 (dd, *J* = 5.8, 3.9 Hz, 2H), 4.05 (s, 3H), 3.61 – 3.45 (m, 8H), 3.32 – 3.28 (m, 3H), 2.80 (t, *J* = 6.7 Hz, 2H), 2.74 (t, *J* = 6.9 Hz, 2H), 2.62 (s, 4H), 2.53 (s, 3H), 2.32 (s, 3H), 1.41 (s, 9H). ^{13}C NMR (101 MHz, MeOD) δ 173.3, 172.7, 165.0, 163.8, 162.2, 161.3, 156.9, 156.5, 138.9, 132.8, 128.8, 128.3, 126.9, 125.7, 117.6, 114.7, 83.5, 78.8, 57.2, 55.6, 51.5, 41.1, 39.4, 38.3, 37.7, 37.2, 30.1, 29.2, 27.4, 23.5, 17.3. HRMS (ESI+) m/z calcd for $C_{35}H_{49}ClN_9O_6S_3^+$ $(M+H)^+$ 822.2651; found 822.2597.

Synthesis of 1-(4-(6-((5-((2-chloro-6-methylphenyl)carbamoyl)thiazol-2-yl)amino)-2-methylpyrimidin-4-yl)piperazin-1-yl)-4,7,16-trioxo-3-oxa-11,12-dithia-8,15-diazanonadecan-19-oic acid (6)

4M HCl in dioxane was added to **5** (0.4 mmol) and stirred for 1 h at room temperature. Solvent was removed in vacuo. The residue was re-dissolved in 5 mL DMF. Triethylamine (6 mmol) and succinic anhydride (0.52 mmol) were added to the solution and stirred for another 12 h at room temperature. Solvent was removed and the crude product was purified via prep-HPLC to obtain **6** as white solid (214 mg, 65 %). ^{1}H NMR (400 MHz, MeOD) δ 8.18 (s, 1H), 7.35 (dd, *J* = 7.1, 2.0 Hz, 1H), 7.24 (t, *J* = 7.2 Hz, 2H), 6.29 (s, 1H), 4.55 (dd, *J* = 5.8, 4.0 Hz, 2H), 4.18 (dd, *J* = 38.9, 34.1 Hz, 4H), 3.63 – 3.40 (m, 11H), 2.78 (dt, *J* = 15.0, 6.7 Hz, 5H), 2.66 – 2.42 (m, 14H), 2.31 (s, 3H).
^{13}C NMR (101 MHz, MeOD) δ 174.9, 173.4, 173.3, 172.8, 163.9, 162.2, 161.3, 160.1, 159.7, 138.9, 132.8, 128.8, 128.3, 127.0, 117.3, 114.4, 83.5, 71.0, 57.1, 55.6, 51.6, 41.1, 38.4, 38.3, 37.3, 37.1, 30.2, 30.1, 29.2, 28.9, 28.3, 17.3. HRMS (ESI+) m/z calcd for $C_{34}H_{45}ClN_9O_7S_3^+$ $(M+H)^+$ 822.2287; found 822.2244.

Synthesis of 2-((6-(4-(2-(4-((2-(2-(2-((4,6-bis(4-((S)-2-(4-((1S,2S)-1-amino-2-methylbutyl)-1H-1,2,3-triazol-1-yl)-3-(4-hydroxyphenyl)propanoyl)piperazin-1-yl)-1,3,5-triazin-2-yl)amino)ethoxy)ethoxy)ethoxy)methyl)-1H-1,2,3-triazol-1-yl)ethyl)piperazin-1-yl)-2-methylpyrimidin-4-yl)amino)-N-(2-chloro-6-methylphenyl)thiazole-5-carboxamide (IY-IY-das, 1) (Figure 3.1)

$CuSO_4$ (3 μmol), Na ascorbate (12 μmol) and TBTA (3 μmol) were added to a mixture of **IY-IY-TEG** (10 μmol) and **das-N_3** (11 μmol) in 0.2 mL DMSO and 0.1 mL H_2O. The reaction mixture was stirred for 24 h at room temperature. Solvent was removed and the crude product was purified by prep-HPLC to obtain **1** as white solid (5.4 mg, 35 %). ^{1}H NMR (400 MHz, DMSO-d_6) δ 9.89 (s, 1H), 8.40 (s, 5H), 8.22 (dd, *J* = 39.5, 12.5 Hz, 4H), 7.40 (dd, *J* = 7.4, 1.7 Hz, 1H), 7.32 – 7.23 (m, 2H), 6.99 (d, *J* = 8.5 Hz, 4H), 6.61 (d, *J* = 8.4 Hz, 4H), 6.18 (s, 3H), 4.82 (t, *J* = 6.4 Hz, 3H), 4.58 – 4.49 (m, 4H), 4.41 – 4.36 (m, 2H), 3.68 – 3.21 (m, 42H), 2.45 (s, 3H), 2.24 (s, 3H), 1.99 – 1.88 (m, 2H), 1.40 – 1.28 (m, 2H), 1.01 (dt, *J* = 21.9, 7.8 Hz, 2H), 0.88 (t, *J* = 7.3 Hz, 6H), 0.75 (d, *J* = 6.8 Hz, 6H). ^{13}C NMR (101 MHz, DMSO-d_6) δ 169.6, 166.4, 165.9, 162.4, 158.9, 158.6, 158.2, 157.7, 156.8, 144.8, 142.1, 130.8, 129.5, 128.5, 127.5, 126.5(2C), 126.2, 125.9, 125.7, 125.0, 124.0, 122.7, 115.6, 70.2(2C), 70.0, 69.6, 69.4, 69.2, 51.3, 51.2, 45.4, 43.2, 43.0, 42.8, 41.4, 41.1, 37.7, 37.2, 35.7, 31.1, 26.0, 25.6, 18.7, 14.1, 11.6 HRMS (ESI+) m/z calcd for $C_{74}H_{100}ClN_{26}O_8S^+$ $(M+H)^+$ 1547.7621; found 1547.7593.

Synthesis of 2-(4-(6-((5-((2-chloro-6-methylphenyl)carbamoyl)thiazol-2-yl)amino)-2-methylpyrimidin-4-yl)piperazin-1-yl)ethyl 1-((4,6-bis(4-((R)-2-(4-((1R,2R)-1-amino-2-methylbutyl)-1H-1,2,3-triazol-1-yl)-3-(4-hydroxyphenyl)propanoyl) piperazin-1-yl)-1,3,5-triazin-2-yl)amino)-10,13,22-trioxo-3,6-dioxa-17,18-dithia-9,14,21-triazapentacosan-25-oate (IY-IY-SS-das, 2) (Figure 3.2)

To a solution of **6** (67 μmol) and **IY-IY-NH_2** (52 μmol) in 2.5 mL DMF were added triethylamine (130 μmol) and HATU (77 μmol). The mixture was stirred for 12 h

at room temperature. Solvent was removed and the crude product was purified by prep-HPLC. Solvent was removed via lyophilizer. 4M HCl in dioxane was added to the remaining solid and stirred for 1 h at room temperature. Dioxane was removed in vacuo. H_2O was added and removed via lyophilizer to obtain **2** as white solid (30 mg, 32 %). ^{1}H NMR (400 MHz, MeOD) δ 8.25 (dd, *J* = 25.5, 6.2 Hz, 4H), 7.35 (dd, *J* = 6.8, 2.2 Hz, 1H), 7.24 (d, *J* = 7.1 Hz, 2H), 7.05 (s, 5H), 6.69 (d, *J* = 8.0 Hz, 5H), 6.58 (s, 1H), 6.17 (s, 2H), 4.57 (s, 2H), 4.45 (d, *J* = 6.0 Hz, 2H), 3.76 – 3.34 (m, 52H), 2.88 – 2.76 (m, 5H), 2.71 – 2.55 (m, 12H), 2.31 (s, 3H), 2.03 (d, *J* = 6.0 Hz, 3H), 1.46 (d, *J* = 5.7 Hz, 2H), 1.19 – 1.07 (m, 2H), 0.98 (t, *J* = 7.3 Hz, 6H), 0.86 (d, *J* = 6.7 Hz, 6H). ^{13}C NMR (101 MHz, MeOD) δ 174.4, 174.2, 174.0, 173.3, 173.1, 172.6, 167.0, 164.4, 160.6, 159.7, 156.7, 155.7, 154.0, 142.9, 142.6, 141.7, 138.8, 132.7, 132.4, 130.3, 128.9, 127.0, 126.6, 125.7, 125.5, 123.7, 115.2, 72.2, 71.1, 70.2, 70.0, 68.9, 68.4, 60.8, 60.7, 57.5, 51.6, 51.3, 42.4, 40.5, 39.6, 38.6, 37.7, 37.6, 36.9, 30.5, 30.4, 30.2, 29.3, 28.8, 25.3, 21.2, 17.3(2C), 13.1, 10.1. HRMS (MALDI+) m/z calcd for $C_{83}H_{117}ClN_{26}O_{12}S_3^{2+}$ $(M+2H)^{2+}$ 900.4092; found 900.4090.

Synthesis of 2-(4-(6-((5-((2-chloro-6-methylphenyl)carbamoyl)thiazol-2-yl)amino)-2-methylpyrimidin-4-yl)piperazin-1-yl)ethyl 1-((4,6-bis(4-((2S,3S)-2-(4-((S)-1-amino-2-(4-hydroxyphenyl)ethyl)-1H-1,2,3-triazol-1-yl)-3-methylpentanoyl) piperazin-1-yl)-1,3,5-triazin-2-yl)amino)-10,13,22-trioxo-3,6-dioxa-17,18-dithia-9,14,21-triazapentacosan-25-oate (YI-YI-SS-das, 3)

3 was synthesized in a similar way as **2** by using **YI-YI-NH$_2$** instead of **IY-IY-NH$_2$**. White solid (36 mg, 35 %). ^{1}H NMR (400 MHz, DMSO-d_6) δ 10.33 (s, 1H), 8.80 (s,

7H), 8.51 (s, 3H), 8.15 (dd, *J* = 71.3, 51.1 Hz, 9H), 7.37 (d, *J* = 7.3 Hz, 1H), 7.26 (t, *J* = 8.3 Hz, 2H), 6.85 (d, *J* = 8.1 Hz, 4H), 6.57 (dd, *J* = 16.5, 9.1 Hz, 5H), 5.68 (d, *J* = 9.1 Hz, 2H), 4.51 (d, *J* = 46.8 Hz, 5H), 3.75 – 3.44 (m, 30H), 3.21 (dd, *J* = 56.5, 15.9 Hz, 13H), 2.76 (dd, *J* = 12.8, 6.3 Hz, 3H), 2.58 (s, 4H), 2.43 (t, *J* = 6.7 Hz, 2H), 2.31 (s, 3H), 2.24 (s, 3H), 0.97 – 0.72 (m, 18H). ^{13}C NMR (101 MHz, DMSO-d_6) δ 172.5, 172.0(2C), 171.4, 166.5, 166.3, 163.6, 161.2, 159.7, 157.0, 156.7, 156.5, 153.9, 144.0, 141.5, 139.2, 136.6, 133.8, 133.0, 130.7, 129.5, 128.7, 127.7, 127.5, 126.2, 123.8, 115.5, 72.6, 71.0, 70.1, 70.0, 69.5, 68.7, 63.1, 60.6, 58.7, 54.5, 50.9, 48.8, 44.1, 42.3, 42.0, 39.1, 38.5, 38.2, 37.7, 31.3, 31.2, 30.3, 29.6, 24.2, 23.9, 18.8, 15.6, 15.5, 11.1. HRMS (MALDI+) m/z calcd for $C_{83}H_{117}ClN_{26}O_{12}S_3^{2+}$ $(M+2H)^{2+}$ 900.4092; found 900.4086.

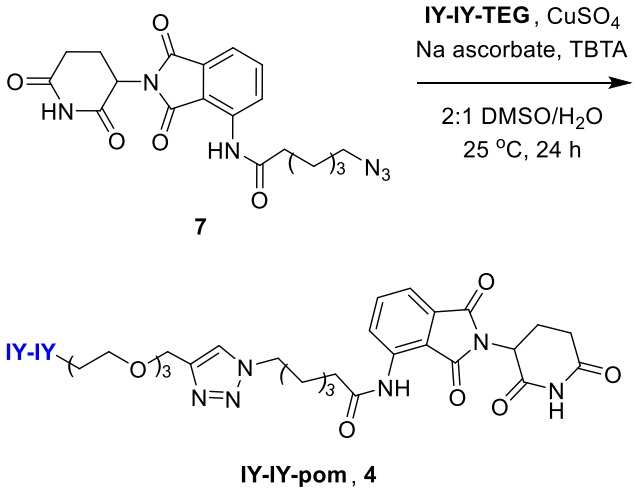

Figure 3.3 Synthesis of **IY-IY-pom** (**4**) as TrkC PROTAC.

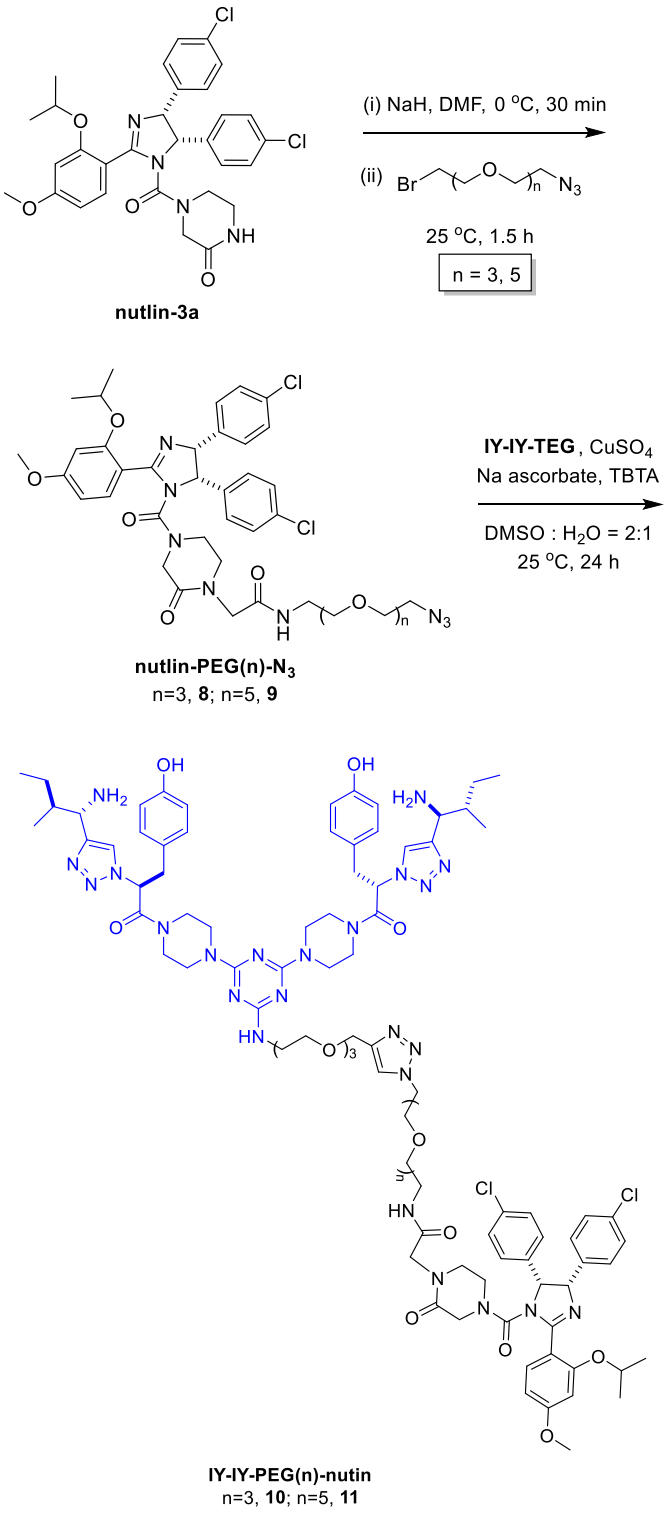

Figure 3.4 Synthesis of **IY-IY-PEG(n)-nutlin** (n=3, **10**; n=5, **11**) as TrkC PROTAC.

Synthesis of 6-(4-((2-(2-(2-((4,6-bis(4-((S)-2-(4-((1S,2S)-1-amino-2-methylbutyl)-1H-1,2,3-triazol-1-yl)-3-(4-hydroxyphenyl)propanoyl)piperazin-1-yl)-1,3,5-triazin-2-yl)amino)ethoxy)ethoxy)ethoxy)methyl)-1H-1,2,3-triazol-1-yl)-N-(2-(2,6-dioxopiperidin-3-yl)-1,3-dioxoisoindolin-4-yl)hexanamide (IY-IY-pom, 4) (Figure 3.3)

$CuSO_4$ (4 µmol), Na ascorbate (16 µmol) and TBTA (4 µmol) were added to a mixture of **IY-IY-TEG** (13.2 µmol) and **7** (14.6 µmol) in 0.3 mL DMSO and 0.15 mL H_2O. The reaction mixture was stirred for 24 h at room temperature. Solvent was removed and the crude product was purified by prep-HPLC to obtain **4** as white solid (7.3 mg, 32 %). ^{1}H NMR (400 MHz, DMSO-d_6) δ 11.11 (s, 1H), 9.67 (s, 1H), 8.48 – 8.40 (m, 6H), 8.29 (s, 2H), 8.07 (s, 1H), 7.84 – 7.79 (m, 1H), 7.60 (d, *J* = 7.0 Hz, 1H), 6.99 (d, *J* = 8.4 Hz, 4H), 6.61 (d, *J* = 8.4 Hz, 4H), 6.16 (s, 2H), 5.14 (dd, *J* = 12.8, 5.4 Hz, 1H), 4.50 (d, *J* = 3.7 Hz, 3H), 4.36 (dt, *J* = 14.2, 6.1 Hz, 4H), 3.63 – 3.38 (m, 30H), 3.27 (dd, *J* = 15.6, 7.5 Hz, 4H), 2.96 – 2.83 (m, 1H), 2.61 (d, *J* = 18.2 Hz, 1H), 2.54 (dd, *J* = 8.7, 4.6 Hz, 1H), 2.46 (t, *J* = 7.4 Hz, 2H), 2.07 (t, *J* = 5.2 Hz, 1H), 1.98 – 1.80 (m, 4H), 1.72 – 1.60 (m, 2H), 1.40 – 1.26 (m, 4H), 0.99 (dt, *J* = 21.9, 7.1 Hz, 2H), 0.88 (t, *J* = 7.3 Hz, 6H), 0.75 (d, *J* = 6.7 Hz, 6H). ^{13}C NMR (101 MHz, DMSO-d_6) δ 172.7, 171.8, 169.7, 167.7, 166.6, 165.9, 158.5, 158.2, 156.3, 143.8, 141.6, 136.5, 136.0, 131.4, 130.3, 126.3, 125.4, 123.7, 123.5, 118.3, 117.0, 115.1, 69.7(2C), 69.5(2C), 68.9, 68.8, 63.5, 50.7, 49.1, 48.9, 42.4, 37.2, 37.1, 36.2, 30.9(2C), 29.4, 25.3, 25.1, 24.1, 22.0, 13.7, 11.1. HRMS (MALDI+) m/z calcd for $C_{71}H_{95}N_{22}O_{12}^+$ $(M+H)^+$ 1447.7494; found 1447.7622.

Synthesis of N-(2-(2-(2-(2-(4-((2-(2-(2-((4,6-bis(4-((S)-2-(4-((1S,2S)-1-amino-2-methylbutyl)-1H-1,2,3-triazol-1-yl)-3-(4-hydroxyphenyl)propanoyl)piperazin-1-yl)-1,3,5-triazin-2-yl)amino)ethoxy)ethoxy)ethoxy)methyl)-1H-1,2,3-triazol-1-yl)ethoxy)ethoxy)ethoxy)ethyl)-2-(4-((4S,5R)-4,5-bis(4-chlorophenyl)-2-(2-isopropoxy-4-methoxyphenyl)-4,5-dihydro-1H-imidazole-1-carbonyl)-2-oxopiperazin-1-yl)acetamide (IY-IY-PEG3-nutlin, 10) (Figure 3.4)

$CuSO_4$ (2.6 µmol), Na ascorbate (10.4 µmol) and TBTA (2.6 µmol) were added to a mixture of **IY-IY-TEG** (8.6 µmol) and **8** (9.5 µmol) in 0.2 mL DMSO and 0.1 mL H_2O. The reaction mixture was stirred for 24 h at room temperature. Solvent was removed and the crude product was purified by prep-HPLC to obtain **10** as white solid (5.0 mg, 31 %). ^{1}H NMR (400 MHz, DMSO-d_6) δ 8.42 (s, 5H), 8.29 (s, 2H), 8.05 – 7.94 (m, 2H), 7.64 (d, *J* = 9.2 Hz, 1H), 7.24 (d, *J* = 8.5 Hz, 2H), 7.19 (d, *J* = 8.5 Hz, 2H), 7.12 (d, *J* = 8.5 Hz, 2H), 7.01 (dd, *J* = 13.1, 8.5 Hz, 6H), 6.74 (d, *J* = 5.5 Hz, 2H), 6.62 (d, *J* = 8.4 Hz, 4H), 6.21 – 6.12 (m, 2H), 5.96 (dd, *J* = 47.1, 9.8 Hz, 2H), 4.90 – 4.80 (m, 1H), 4.51 (dd, *J* = 7.5, 4.5 Hz, 5H), 4.39 (s, 2H), 3.89 (s, 3H), 3.83 – 3.73 (m, 8H), 3.56 – 3.18 (m, 49H), 1.98 – 1.89 (m, 2H), 1.33 (d, *J* = 6.0 Hz, 3H), 1.28 (d, *J* = 6.0 Hz, 3H), 1.09 – 0.93 (m, 2H), 0.88 (t, *J* = 7.3 Hz, 6H), 0.76 (d, *J* = 6.7 Hz, 6H).

HRMS (MALDI+) m/z calcd for $C_{92}H_{123}Cl_2N_{24}O_{15}^+$ $(M+H)^+$ 1873.8971; found 1873.8943.

Synthesis of N-(17-(4-((2-(2-(2-((4,6-bis(4-((S)-2-(4-((1S,2S)-1-amino-2-methylbutyl)-1H-1,2,3-triazol-1-yl)-3-(4-hydroxyphenyl)propanoyl)piperazin-1-yl)-1,3,5-triazin-2-yl)amino)ethoxy)ethoxy)ethoxy)methyl)-1H-1,2,3-triazol-1-yl)-3,6,9,12,15-pentaoxaheptadecyl)-2-(4-((4S,5R)-4,5-bis(4-chlorophenyl)-2-(2-isopropoxy-4-methoxyphenyl)-4,5-dihydro-1H-imidazole-1-carbonyl)-2-oxopiperazin-1-yl)acetamide (IY-IY-PEG5-nutlin, 11)

$CuSO_4$ (2.6 µmol), Na ascorbate (10.4 µmol) and TBTA (2.6 µmol) were added to a mixture of **IY-IY-TEG** (8.6 µmol) and **9** (9.5 µmol) in 0.2 mL DMSO and 0.1 mL H_2O. The reaction mixture was stirred for 24 h at room temperature. Solvent was removed and the crude product was purified by prep-HPLC to obtain **11** as white solid (5.9 mg, 35 %). ^{1}H NMR (400 MHz, DMSO-d_6) δ 8.45 – 8.27 (m, 8H), 8.03 (s, 1H), 7.92 (s, 1H), 7.65 (d, *J* = 8.3 Hz, 1H), 7.53 – 7.30 (m, 7H), 6.99 (d, *J* = 8.5 Hz, 4H), 6.78 – 6.68 (m, 3H), 6.61 (d, *J* = 8.4 Hz, 4H), 6.21 – 6.11 (m, 2H), 5.35 – 5.15 (m, 2H), 4.75 (dt, *J* = 12.2, 6.1 Hz, 1H), 4.50 (dd, *J* = 7.8, 4.5 Hz, 5H), 4.38 (s, 2H), 3.86 (s, 3H), 3.83 – 3.78 (m, 4H), 3.49 – 3.15 (m, 56H), 2.04 – 1.90 (m, 4H), 1.39 – 1.32 (m, 2H), 1.24 (d, *J* = 2.0 Hz, 6H), 1.04 – 0.95 (m, 2H), 0.88 (t, *J* = 7.3 Hz, 6H), 0.75 (d, *J* = 6.8 Hz, 6H). HRMS (MALDI+) m/z calcd for $C_{96}H_{132}Cl_2N_{24}O_{17}^{2+}$ $(M+2H)^{2+}$ 981.4784; found 981.4764.

Compound Stability in Serum

Conjugates (**1-3**, stock in DMSO) were added in mouse serum/PBS (1:1) at a concentration of 50 µM. The mixture was incubated at 37 °C and examined by analytical-HPLC at different time points up to 48 h.

Cytotoxicity Assay

Cells were seeded in 96-well plate (typically 5,000 cells/well, 3,000 cells/well for Hs578t cells) in 50 µL corresponding growth media and allowed to adhere overnight. Compounds were diluted in another 50 µL PFHM-II media (for MCF-10A cells use growth media MEGM instead) and added to each well. Cells were incubated for 72 h before AlamarBlue reagent (Invitrogen) was added. Cells were incubated for an additional 2 h and fluorescence intensity (Ex/Em 560/590 nm) was measured by a BioTek Synergy 4 Microplate Reader. Cell viabilities are calculated as: % live cells = $OD_{compound}/OD_{DMSO}$ × 100. Results are processed by GraphPad Prism 6.0 software.

Wound Healing Assay

Cells were seeded in 24-well plates using "culture-inserts 2 well" from Ibidi according to manufacturer's instruction (apply 70 µL/insert at density of: 3 x 10^5 cells/mL for Hs578t, 7 x 10^5 cells/mL for MDA-MB-231). Cells were allowed to adhere to plate overnight. Culture-inserts were removed and the culture media were replaced by fresh media with compounds (DMSO = 0.2%). Cells were imaged in brightfield every 30 min under EVOS Auto Fl 2 microscope. Images were processed and quantified via "Wound Healing ACAS Image Analysis" from Ibidi/MetaVÌ Labs online software.

Western blot

Cells were seeded in 24-well plate (50,000 cells/well for Hs578t, 80,000 cells/well for MDA-MB-231) and allowed to adhere overnight. Culturing media were replaced by

fresh media with compounds at desired concentrations (DMSO < 0.5%). Cells were incubated for 18 h before lysed by RIPA buffer (Pierce) according to manufacturer's instructions. Total protein concentrations were determined and calibrated by BCA protein assay (Pierce). Whole cell lysates were subjected to SDS-PAGE, transferred to PVDF membrane and proceeded to Western blot protocol: membrane was blocked with SuperBlock (TBS) Blocking Buffer (ThermoFisher Scientific) for 1 h at room temperature, incubated with primary antibodies overnight at 4 ºC, washed with TBS-T (TBS + 0.05% Tween 20) 3 times, incubated with secondary antibodies for 1 h at room temperature, washed with TBS-T 4-6 times. Afterwards, blots were treated with SuperSignal West Dura Substrate (ThermoFisher Scientific) and imaged by ChemiDoc XRS (BioRad) imaging system.

Dilution factor: anti-phospho-Src (Tyr 416) mAb (1:1000), anti-Src mAb (1:5000), anti-b-actin mAb (1:5000), HRP-conjugated anti-rabbit IgG (H+L) (1:75,000).

Protein Degradation Assay

Cells were seeded in 24-well plate (50,000 cells/well for Hs578t, 100,000 cells/well for NIH3T3-TrkC) and allowed to adhere overnight. Culturing media were replaced by fresh media with PROTACs (DMSO < 0.5%). Cells were incubated for certain time (varies in different experiments) before lysed by RIPA buffer (Pierce) according to manufacturer's instructions. Total protein concentrations were determined and calibrated by BCA protein assay (Pierce). Whole cell lysates were subjected to SDS-PAGE, transferred to PVDF membrane and proceeded to Western blot protocol: membrane was

blocked with SuperBlock (TBS) Blocking Buffer (ThermoFisher Scientific) for 1 h at room temperature, incubated with primary antibodies overnight at 4 ºC, washed with TBS-T (TBS + 0.05% Tween 20) 3 times, incubated with secondary antibodies for 1 h at room temperature, washed with TBS-T 4-6 times. Afterwards, blots were treated with SuperSignal West Dura Substrate (ThermoFisher Scientific) and imaged by ChemiDoc XRS (BioRad) imaging system. For time course study, cells were treated with PROTACs or DMSO for different time period before cell lysis.

Dilution factor: anti-TrkC mAb (1:1000), anti-b-actin mAb (1:5000), HRP-conjugated anti-rabbit IgG (H+L) (1:75,000).

3.3. Results and Discussion

3.3.1. Syntheses of IY-IY-Dasatinib Conjugates

Crystal structures of dasatinib in complex with kinases show the -OH group is exposed to solvent (*eg* c-Src and Lyn; Figure 3.5). These observations suggest that hydroxyl is an appropriate attachment point to couple targeting entities without interfering with binding of dasatinib to kinase targets.

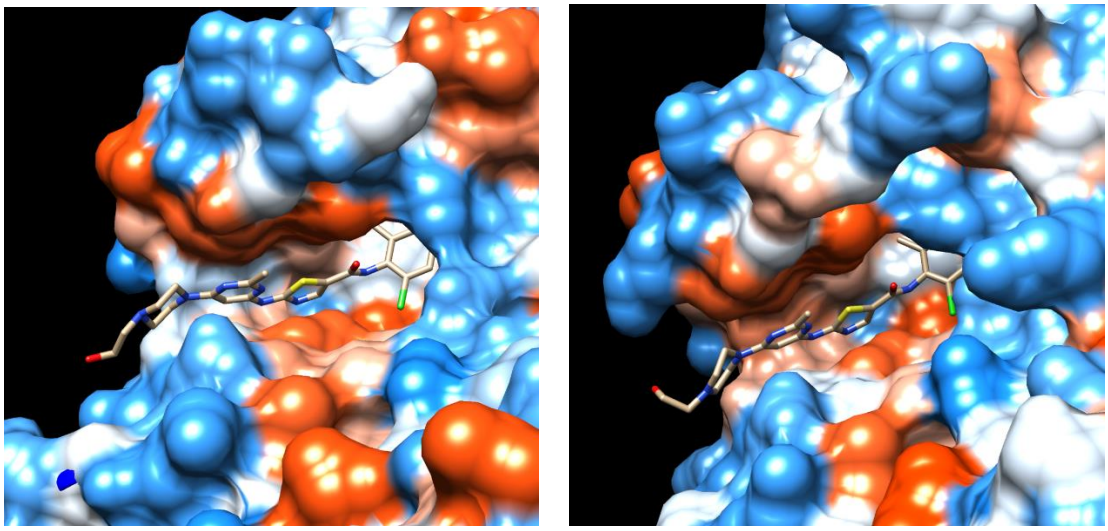

Figure 3.5 Crystal structure of dasatinib in complex with c-Src (left, PDB: 3G5D) and Lyn (right, PDB: 2ZVA).

Linker fragments to connect the IY-IY and KI fragments could be designed to be robust or labile in cells, and neither strategy is clearly superior. Pharmacokinetics of systems containing robust linkers is easier to assess and tune, but this approach requires the conjugates bind the target kinase. Conversely, if a cleavable linker is used then free KI (or KI derivative) may be released thereby circumventing any adverse effects the IY-IY fragment had on binding of the KI to the kinase, but unfavorable rates of cleavage are a possibility. For these reasons, this work features two IY-IY-dasatinib conjugates, one containing a non-cleavable linker (**1**), and the other comprising a cleavable one (**2**).

Figure 3.1 outlines the synthesis developed for the robust conjugate **1**. Highlights of this procedure include conversion of dasatinib to a known azide,[72] followed by copper-mediated Huisgen cycloaddition of that to an alkyne-functionalized IY-IY derivative, **IY-IY-TEG**, that was reported in other study.[1]

Figure 3.2 outlines preparation of the disulfide-linked, conjugate **2**. Intracellular glutathione and other thiols are anticipated to liberate the dasatinib fragment in this system once it is internalized into the cell. Thus, **2** was accessed from a carboxylic acid derivative of dasatinib[73] coupled to a commercially available amino disulfide; subsequent amine deprotection, coupling with succinic anhydride to give a carboxylic acid terminus, and amide coupling to an amino IY-IY derivative[66] led to the final product (Figure 3.2). Unlike IY-IY, the inverted sequence YI-YI does not bind TrkC.[24, 26-27] Consequently, a negative control with the inverted side chain sequence, *ie* **3**, was made in a similar fashion.

3.3.2. Stabilities, Kinase Inhibition, and Cellular Effects of Conjugates 1 - 3

Stabilities of conjugates **1 - 3** in 1:1 mouse serum/PBS were determined via reverse phase HPLC (Figure 3.6). All three conjugates were stable under these conditions after 48 h incubation at 37 °C. These experiments imply that even the disulfide conjugate **2** in blood would be relatively stable if delivered by *iv* injection.

Monitoring c-Src pTyr levels via Western blot required selection of an appropriate $TrkC^+$ cell line. MDA-MB-231 triple negative breast cancer cells have been reported to express TrkC[74] but confirmatory gels are not shown in this literature. However, two different batches of MDA-MB-231 cells (from American Type Culture Collection, ATCC) were tested with TrkC-mAbs from two different sources, and throughout we were unable to detect TrkC. TrkC was detected though, in another triple negative metastatic breast cancer line, Hs578t, which is consistent with previous reports.[27, 67]

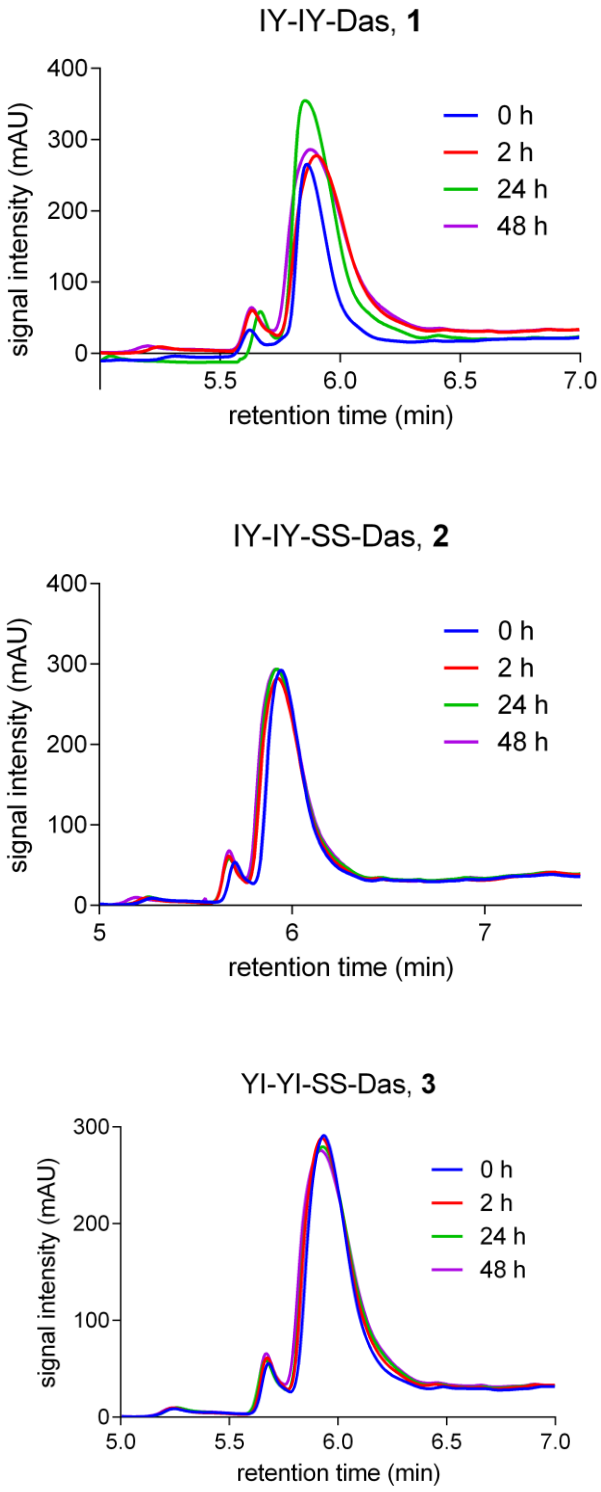

Figure 3.6 Stabilities of conjugates **1** – **3** in 1:1 mouse serum/PBS at 37 °C.

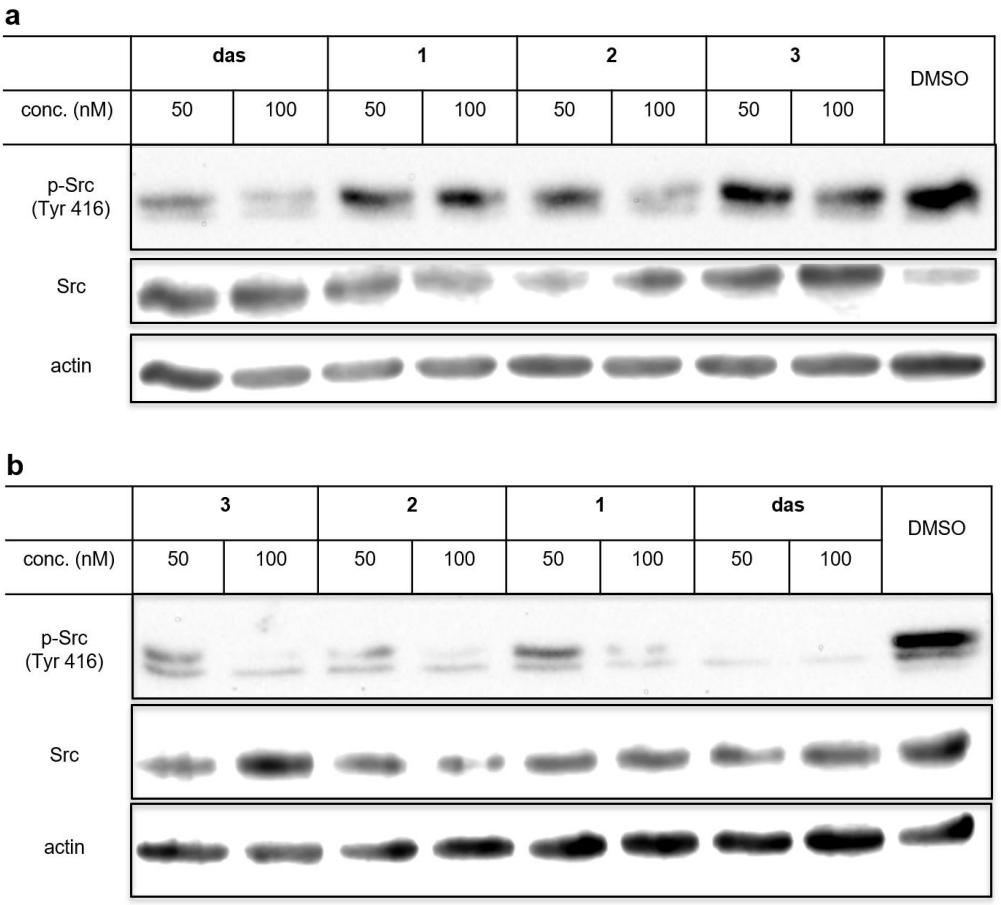

Figure 3.7 Western blot analyses of the inhibitory effect of p-Src treated with das and conjugates **1** – **3** in: (**a**) Hs578t; and, (**b**) MDA-MB-231, cells.

Figure 3.7a shows blotting to monitor the levels of c-Src in Hs578t when treated with conjugates **1** - **3**. Cells were incubated with the compounds for 18 h before lysis and analyses. Conjugate **2** exhibited inhibited production of p-Src as effectively as **das**, whereas **1** and **3** showed significantly less inhibition. Insignificant TrkC expression was observed in our MDA-MB-231 cells (see above), so these were used in negative control experiments. In these cells, all three compounds inhibited p-Src slightly (there appeared to be no difference for **1** – **3** when the probe was used at 100 nM, and only were minor

differences at 50 nM), but all were less effective than **das** (Figure 3.7b). These observations are consistent with internalization and delivery of the conjugates, particularly **2**, into the $TrkC^+$ Hs578t cells, but lesser into the MDA-MB-231 where TrkC levels are low, at most. Observation of more p-Src inhibition for the labile disulfide-containing conjugate **2** implies liberation of modified dasatinib is a superior strategy to use than the robust linker in **1**.

Wound healing assays were also performed on the two cell lines featured above further to test the functionality of conjugate **2**. Phosphorylation of Src is a positive regulator of cell migration,[75-76] so recovery rates are expected to be slower for cells treated with **das** and its conjugates compared to untreated groups. In the current study, cell suspensions were applied to 24-well plate with inner "culture-insert wells" (Ibidi) to create the artificial wound. Cells were allowed to attach overnight, followed by removal of inserts and addition of compounds. Wound recoveries were imaged by time lapse microscope and scratch closure speeds were measured. Hs578t cells treated with **2** exhibited the slowest closure speed among all conjugates, but faster than **das** (Figure 3.8). In contrast, treatment with **IY-IY-TEG** had no effect on cell migration compared to the DMSO control (Figure 3.8); thus this experiment showed no evidence that the IY-IY fragment activates TrkC to induce or suppress cell migration. However, treatment of MDA-MB-231 cells with all three conjugates gave similar recovery rates that are unambiguously slower than the DMSO control but faster than **das** (Figure 3.9). These results further confirm a delivery of IY-IY active targeting relies on TrkC overexpression and disulfide cleavage to observe the effect of the KI drug cargo.

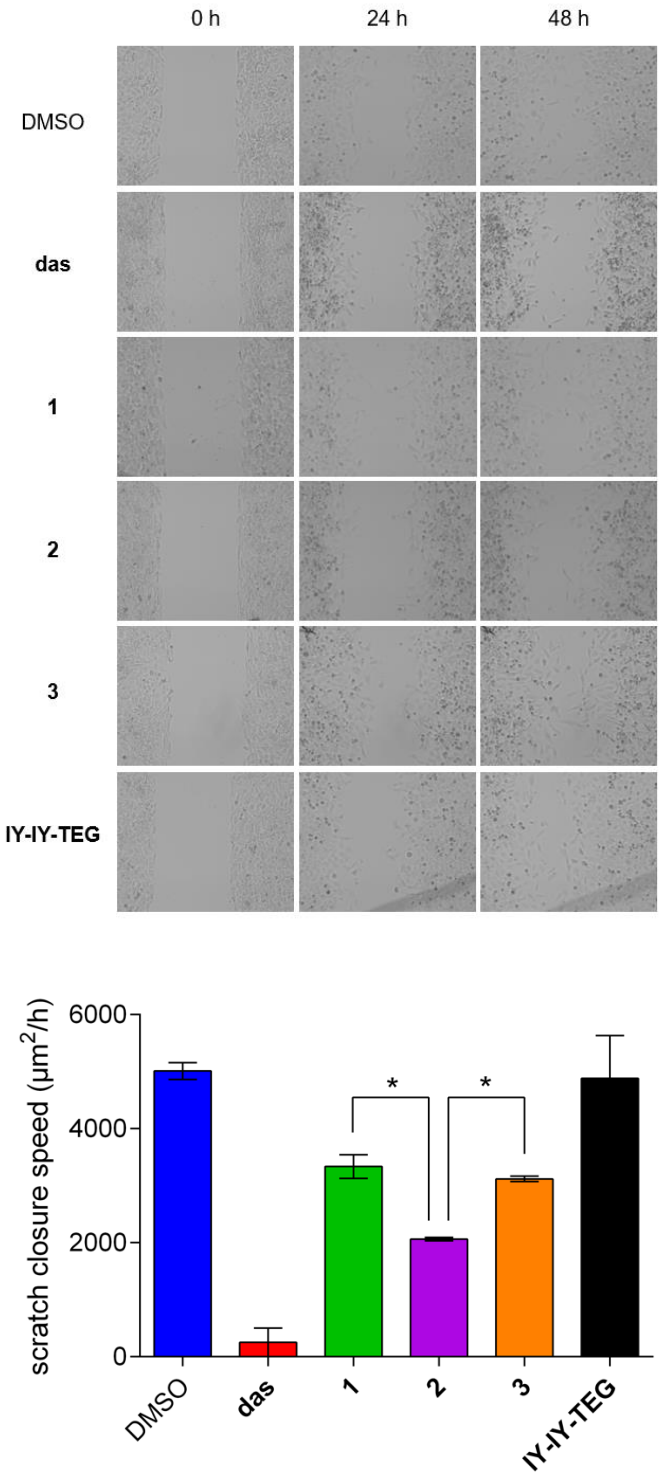

Figure 3.8 Wound healing for Hs578t cells treated with das and conjugates **1**, **2** and **3**. *, $p < 0.01$ using One-Way ANOVA.

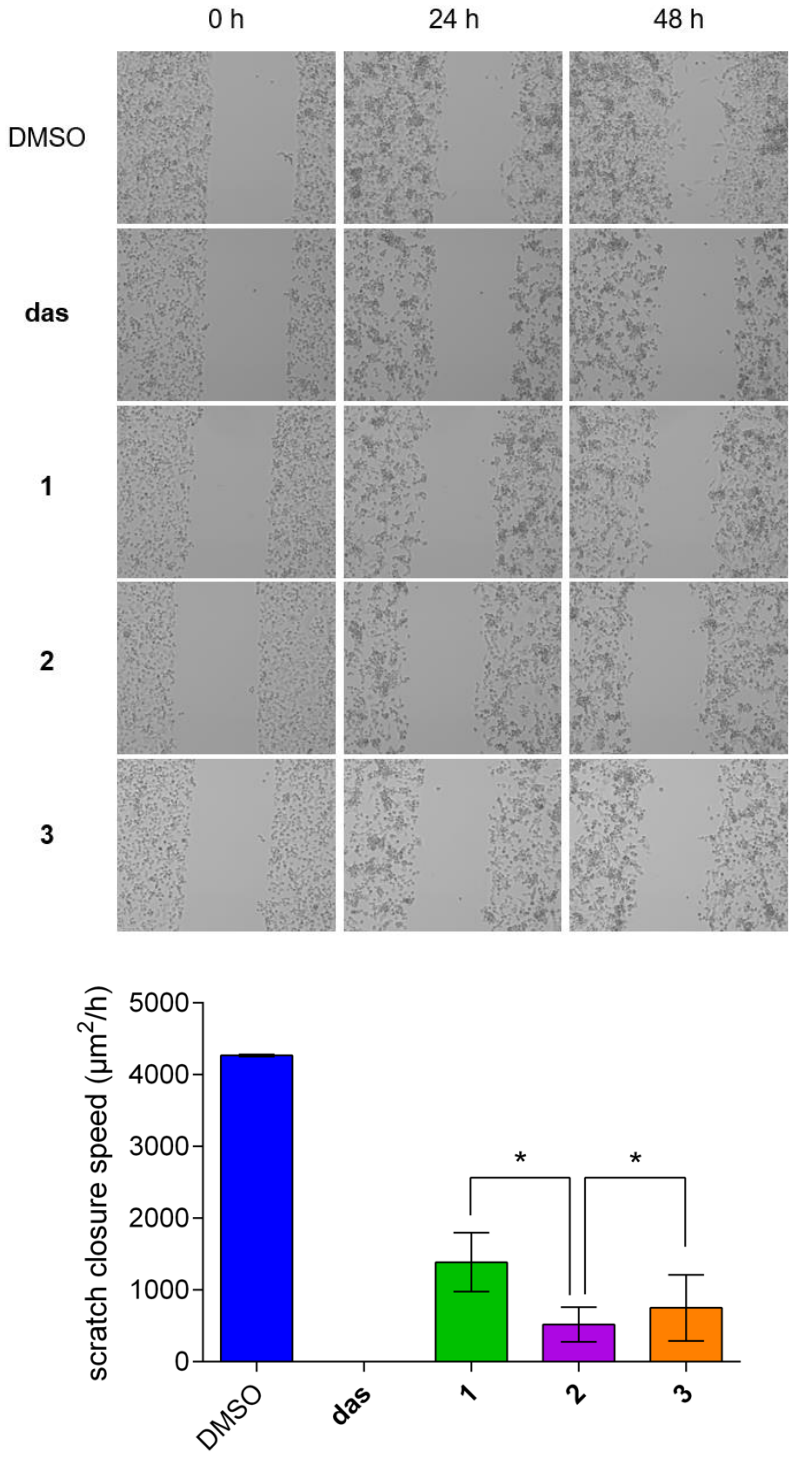

Figure 3.9 Wound healing assay for MDA-MB-231 treated with das and conjugates **1**, **2** and **3**. *, p : Not Significant (N. S.) using One-Way ANOVA.

Having confirmed the functionalities of conjugate **2**, we next examined whether our active targeting strategy can improve selectivity for $TrkC^+$ cancerous over $TrkC^-$ normal cells. Hs578t, a triple negative cell line, and MCF-10A, a non-tumorigenic breast epithelial cell line which does not overexpress TrkC, were selected for comparisons in a cytotoxicity assay. In the $TrkC^+$ cancer cell line Hs578t, conjugate **2** exhibited a similar cytotoxicity to **das**, whereas non-cleavable conjugate **1** and the non-targeting control with an inverted side chain sequence **3** were less toxic (Figure 3.10). This observation supports the previous assertion that, among the conjugates studied, IY-IY active targeting and a thiol-sensitive, disulfide linkage is crucial to suppress cell viability in $TrkC^+$ cells. In the non-cancerous cell line MCF-10A, however, **2** is the least toxic of **das** and **1** - **3** (Figure 3.10) indicating binding to the TrkC receptor is important. Cytotoxicity in MDA-MB-231 was also tested but no substantial difference is observed among all four compounds (Figure 3.11); this is in accord with lower TrkC expression levels for MDA-MB-231 compared with Hs578t. Overall, the cell viability for the compound **2** was less in the $TrkC^+$ Hs578t cells than the TrkC-deficient MDA-MB-231 line. When a normal vascular endothelial cell line, HUVEC, was tested (Figure 3.11) **2** proved to be less cytotoxic than **das**, and of similar potency to **1**. Overall, these results suggested IY-IY active targeting can improve the selectivity for $TrkC^+$ cancer cells over normal cells.

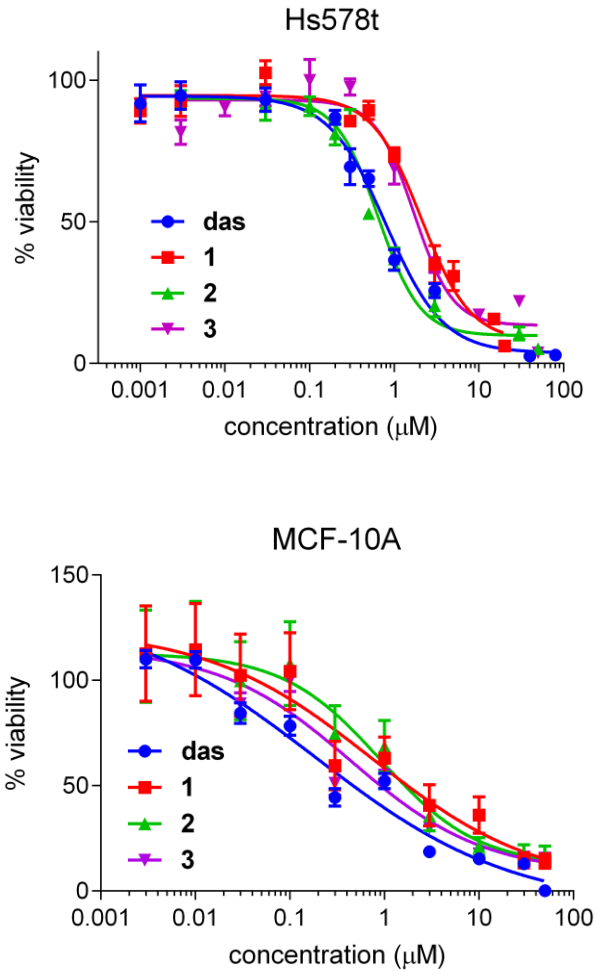

Figure 3.10 Cytotoxicity assay of dasatinib and conjugates **1** – **3** on Hs578t ($TrkC^+$) and MCF-10A ($TrkC^-$, non-cancerous) cells.

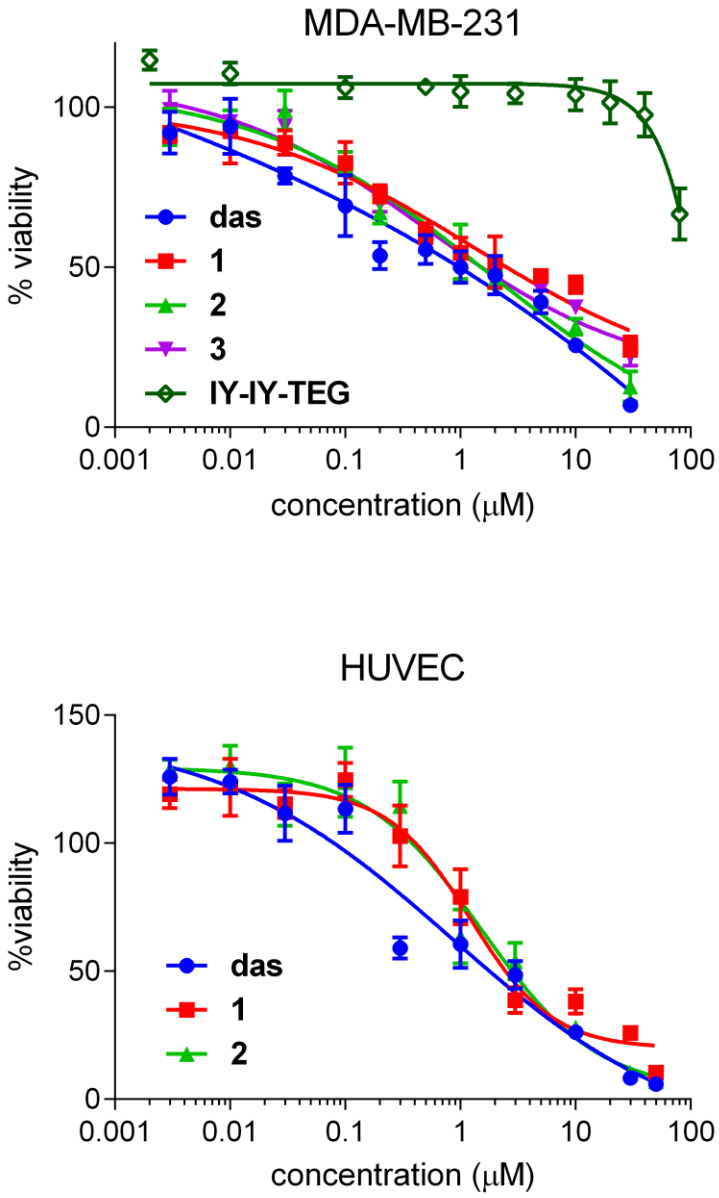

Figure 3.11 Cytotoxicity assay of dasatinib and conjugates **1** – **3** on MDA-MB-231 and HUVEC cells.

3.3.3. IY-IY Based PROTACs for TrkC

Several E3 ligand/ligase pairs have been reported for PROTACs, and two, nutlin-3a/MDM2 and pomalidomide (**pom**)/cereblon(CRBN), were tested here. Thus, **IY-IY-PEG(n)-nutlin** (n=3, **10**; n=5, **11**) and **IY-IY-pom** (**4**) were prepared by azide-alkyne cycloaddition of **IY-IY-TEG** to known pom-azide[77] or nutlin-azide[78] (Figure 3.3, 3.4).

When the nutlin-based PROTACs (**10** and **11**) incubated with a TrkC-transfected cell line, NIH3T3-TrkC, only **11** induced significant degradation at 40 μM (Figure 3.12) and this took 24 h (Figure 3.13) to be clearly observable. Incomplete degradation and long times might be a consequence of significantly higher TrkC expression levels in transfected cells over natural cell lines.

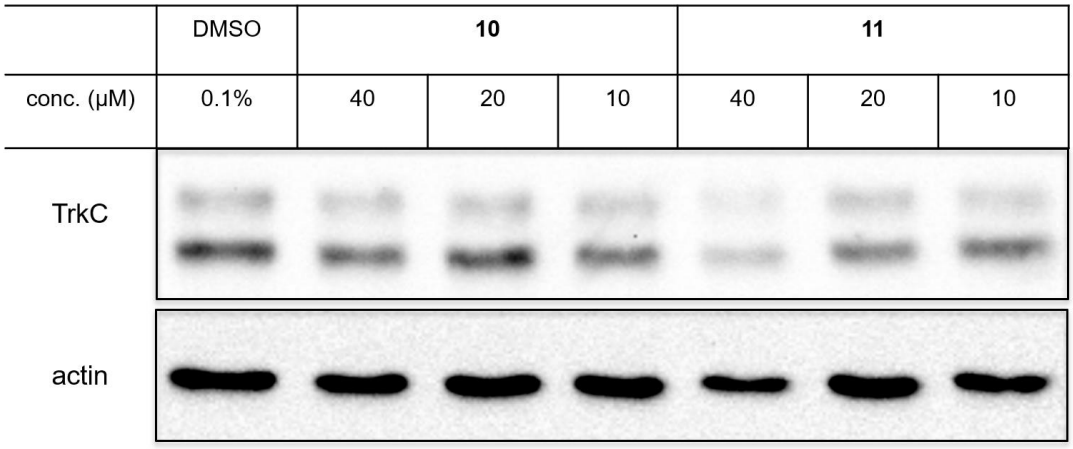

Figure 3.12 Degradation of TrkC in NIH3T3-TrkC cells by IY-IY-PEG(n)-nutlin (n=3, **10**; n=5, **11**) with 24 h incubation.

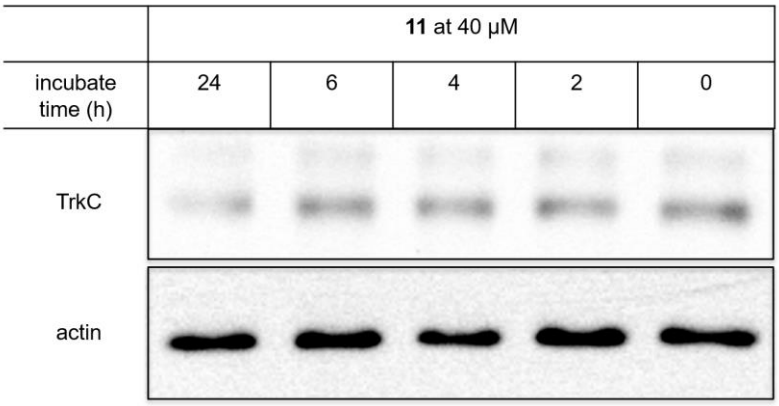

Figure 3.13 Time course TrkC degradation experiment with treatment of PROTACs (IY-IY-PEG5-nutlin, **11**) in NIH3T3-TrkC cells.

For the natural $TrkC^+$ cell line, Hs578t, almost no degradation was observed when incubated with **11** at up to 10 μM (Figure 3.14). However, the PROTAC based on pomalidomide, **4**, induced potent TrkC degradation at 1-10 μM, with an estimated DC_{50} (50% protein degradation conc.) of 0.1 - 1.0 μM (Figure 3.14). This observation is consistent with reports that imply nutlin-based PROTACs tend to be less effective than those comprising **pom**/CRBN pairs.[32]

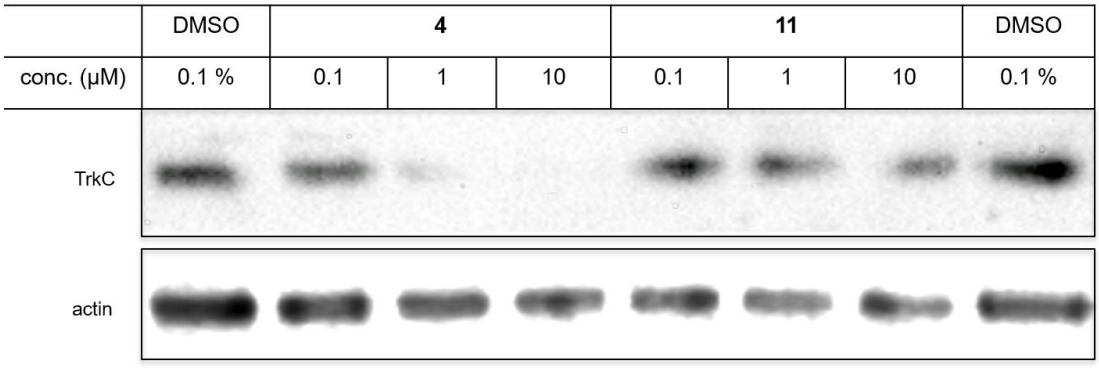

Figure 3.14 TrkC levels in Hs578t cell lysates after 24 h incubation with IY-IY-pom (**4**) and IY-IY-PEG5-nutlin (**11**).

3.4. Conclusions

In summary, the TrkC targeted conjugate **2** preferentially delivered dasatinib into $TrkC^+$ cancer cells over normal cells, and matched the activity of dasatinib in cell viability and pTyr blotting assays. The cleavable disulfide bond connecting dasatinib to the IY-IY targeting fragment was important to the activity of the conjugate in all the assays used (viability, pTyr, and wound healing). Conjugate **2** has the potential to improve the selectivity and therapeutic index of the promiscuous kinase inhibitor dasatinib.

The IY-IY fragment was also useful for development of the first potent TrkC degrader **4** comprising this ligand bound to pomalidomide to recruit CRBN for degradation. TrkC PROTACs may provide opportunities for alternative therapeutic strategies in diseases where that receptor is important.

4. PROTACS SUPPRESSION OF CDK4/6, CRUCIAL KINASES FOR CELL CYCLE REGULATION IN CANCER*

4.1. Introduction

Cyclin dependent kinases (CDKs) are critical for cell cycle regulation. Cell cycle arrest in cancer could suppress tumor growth and metastasis, so inhibition of the CDKs is an active research area.[38, 40] The first inhibitors had little or no selectivity between the various members of the series, and they were relatively unsuccessful in pharmaceutical development. Emergence of the first selective CDK4/6 inhibitors, however, changed the research landscape completely.[43-45] In 2015, palbociclib (IBRANCE®) received accelerated approval from the US Federal Drug Administration for use in a combination therapy for estrogen receptor-positive, HER2-negative advanced breast cancer; such approval is only granted when substances show exceptional efficacy in treatment of diseases for which there is an urgent unmet need. A second selective CDK inhibitor, ribociclib (KISQALI®), was approved in 2017 for treatment of the same cancer sub-type. As of today, palbociclib and ribociclib feature in at least 20 ongoing clinical trials for treatment of cancers of breast metastases, non-small cell lung, prostate, pancreas and brain (glioblastoma), so there is justifiable optimism surrounding the likely long-term clinical impact of these drugs.

---

* Reproduced from "PROTACs suppression of CDK4/6, crucial kinases for cell cycle regulation in cancer" by Zhao, B.; Burgess, K. *Chem. Commun.*, **2019**, *55*, 2704-2707. with permission from the Royal Society of Chemistry.

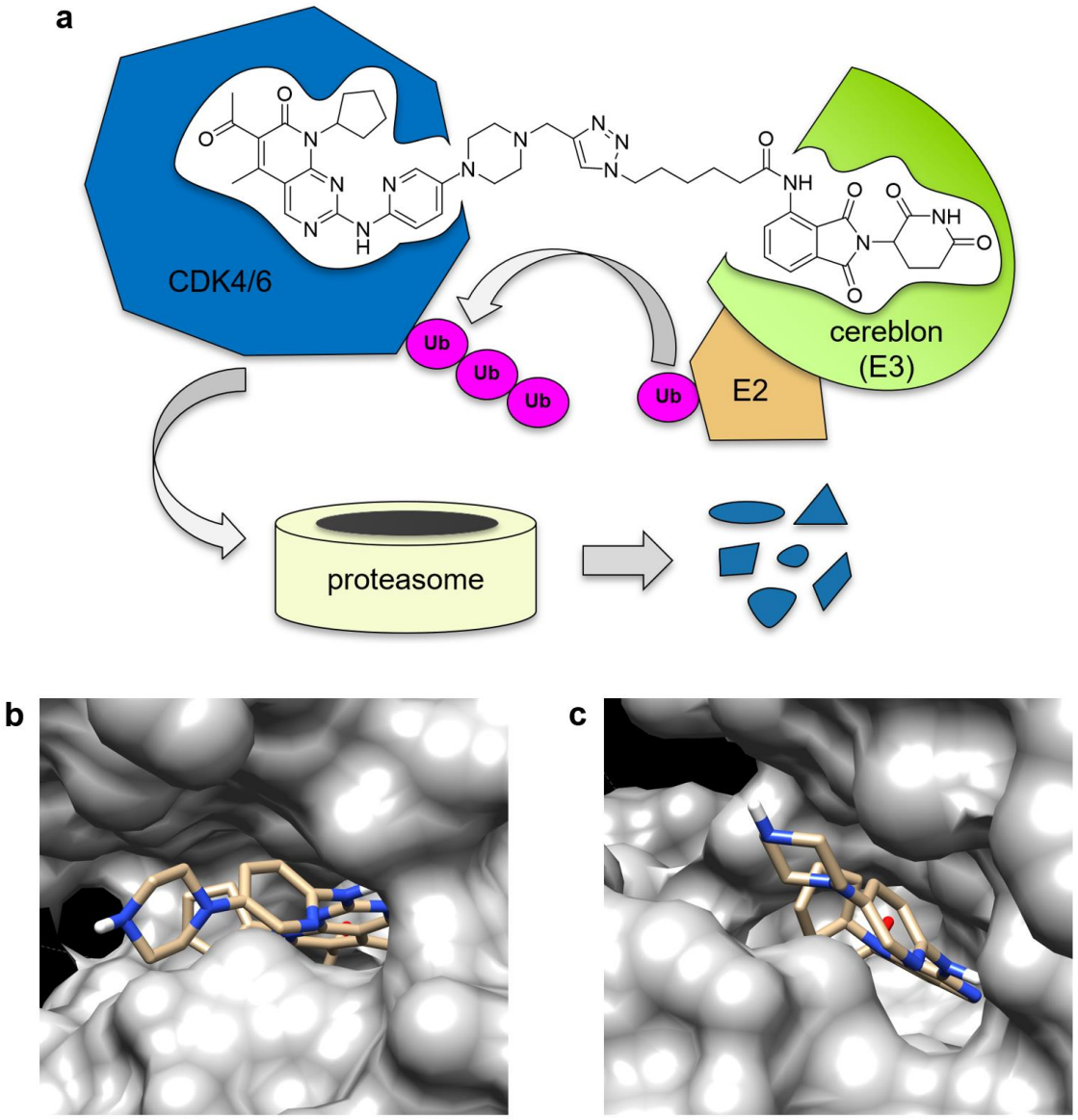

Figure 4.1 (**a**) Central hypothesis on depletion of CDK4/6 via PROTACs. X-ray structures of CDK6 co-crystallized with palbociclib (**b**, PDB: 5L2I) and ribociclib (**c**, PDB: 5L2T).

Both palbociclib and ribociclib selectively inhibit CDK 4 and 6 over others. CDK4/6 are important in the G1-S phase of cell cycling, wherein they trigger a sequence

of events leading to phosphorylation of retinoblastoma (Rb) protein. Failure to phosphorylate Rb leads to arrested cell development in ways that have been proven to be valuable in chemotherapy.[40, 79-80]

PROteolysis TArgeting Chimeras (PROTACs) are hybrids of two molecular fragments: one to bind a protein targeted for ubiquitination, and another to dock with an E3 ubiquitin ligase.[32-33, 37] These chimeras can force the targeted protein and E3 ligase to become proximal, this can initiate ubiquitination then proteolysis of the target in the proteasome. A compelling feature of PROTACs is their potential to act catalytically in the cell, hence they can be even more effective than suicide inhibitors that permanently inactivate enzymes with 1:1 inhibitor: protein stoichiometries.[81]

Approaches involving PROTACs are mechanistically distinct from others involving inhibition of kinases, because they instead involve its destruction. Recently, there have been reports of PROTACs applied to CDK9,[82] and some degraders of CDK8.[83] These reports prompted us to reveal our studies on PROTACs based on palbociclib and ribociclib (Figure 4.1a). Figure 4.1b and 4.1c show crystallographic data for palbociclib and ribociclib bound to CDK6. Both kinase inhibitors project a free piperazine-*N* into solvent, leading us to hypothesize that site could be conjugated to an E3 ligase ligand. Consequently, we set out to prepare conjugates of pomalidomide (**pom**, a E3 ligase ligand) to palbociclib and to ribociclib, and assay them for accelerated homeostasis of CDK4/6 and suppression of Rb-phosphorylation.

4.2. Materials and Methods

4.2.1. Materials and Instrumentation

All reactions were carried out under an inert atmosphere (nitrogen or argon where stated) with dry solvents under anhydrous conditions. Glassware for anhydrous reactions was dried in an oven at 140 ºC for minimum 6 h prior to use. Dry solvents were obtained by passing the previously degassed solvents through activated alumina columns. Yields refer to chromatographically and spectroscopically (^{1}H-NMR) homogeneous materials, unless otherwise stated. Reagents were purchased at a high commercial quality (typically 97 % or higher) and used without further purification, unless otherwise stated. Analytical thin layer chromatography (TLC) was carried out on Merck silica gel plates with QF-254 indicator and visualized by UV. Flash column chromatography was performed using silica gel 60 (Silicycle, 230-400 mesh). ^{1}H and ^{13}C spectra were recorded on a 400 MHz spectrometer and were calibrated using residual non-deuterated solvent as an internal reference. The following abbreviations or combinations thereof were used to explain the multiplicities: s = singlet, d = doublet, t = triplet, q = quartet, m = multiplet, dd = doublet of doublet, ddd = doublet of doublet of doublets.

Palbociclib and Ribociclib were purchased from LC Laboratories. MDA-MB-231, MCF-7 and U87-MG cells (from American Type Culture Collection) were cultured on 75 cm^2 culture flasks in Dulbecco's Modified Eagle Medium/nutrient mixture F-12 (DMEM/F12, Sigma Chemical, St. Louis, MO) supplemented with 10 % FBS. CDK4, CDK6 and Phospho-Rb (Ser780) mAb were purchased from Cell Signaling Technology. Goat anti-rabbit (H+L) secondary antibody (HRP conjugated) were purchased from

ThermoFisher Scientific. SuperSignal West Dura Substrate (ThermoFisher Scientific) was used as Western blot substrate.

4.2.2. Experimental Procedures

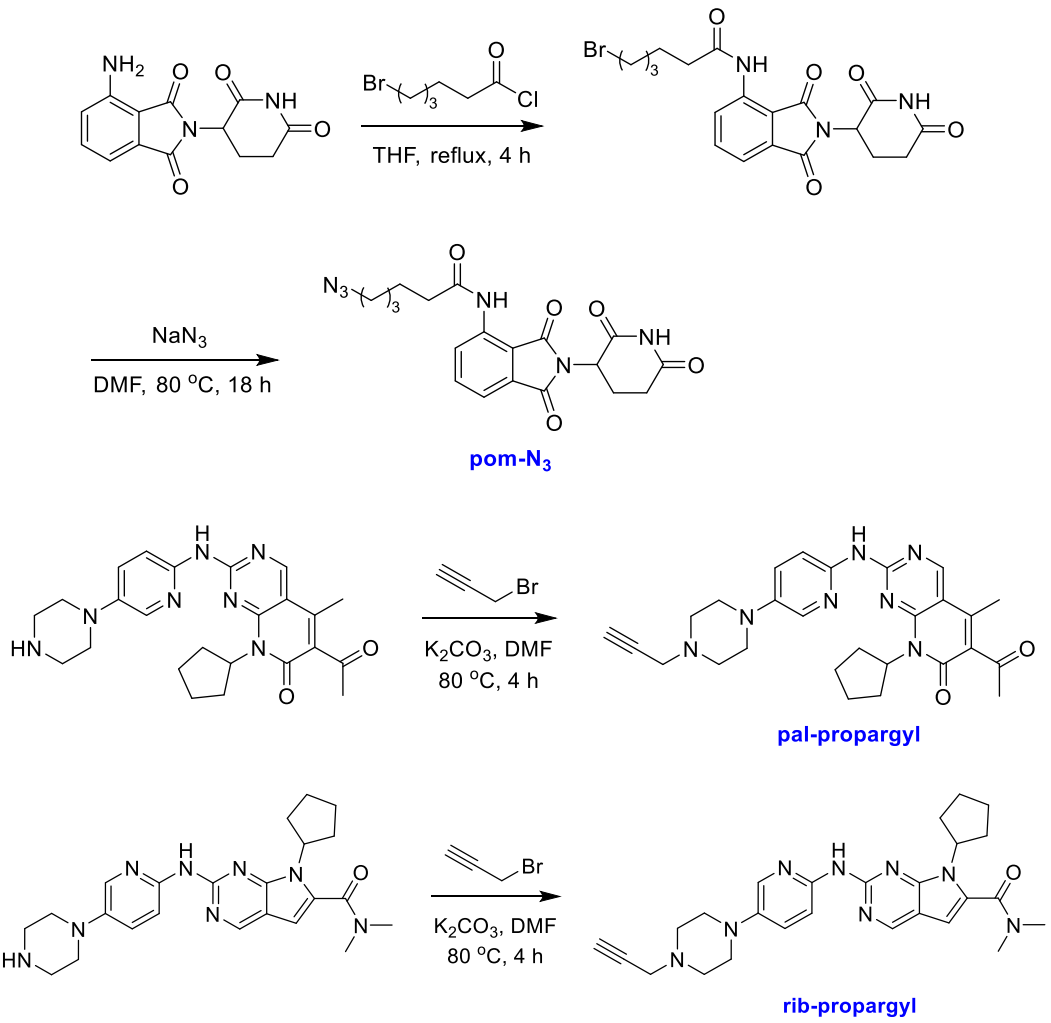

Figure 4.2 Syntheses of **pom-N3**, **pal-propargyl** and **rib-proprgyl**.

Pom-N3 was made according to literature[77].

Synthesis of 6-acetyl-8-cyclopentyl-5-methyl-2-((5-(4-(prop-2-yn-1-yl)piperazin-1-yl)pyridin-2-yl)amino)pyrido[2,3-d]pyrimidin-7(8H)-one (pal-propargyl) (Figure 4.2)

To a solution of palbociclib (0.25 mmol) and K_2CO_3 (0.50 mmol) in 2 mL DMF was added propargyl bromide (0.30 mmol). The mixture was heated to 80 ^oC and stirred for 4 h. Solvent was removed. H_2O was added to the mixture and the crude product was purified by prep-HPLC to obtain **pal-propargyl** as yellow solid (110 mg, 90 %). ^1H NMR (400 MHz, MeOD) δ 9.08 (d, *J* = 4.2 Hz, 1H), 8.15 – 7.99 (m, 2H), 7.81 – 7.67 (m, 1H), 6.06 – 5.97 (m, 1H), 4.69 (dd, *J* = 10.6, 2.4 Hz, 1H), 4.15 (d, *J* = 2.5 Hz, 1H), 4.07 – 3.85 (m, 2H), 3.72 (dd, *J* = 12.3, 7.2 Hz, 1H), 3.64 – 3.49 (m, 6H), 3.38 (t, *J* = 2.5 Hz, 1H), 2.52 (s, 3H), 2.44 (d, *J* = 1.3 Hz, 3H), 2.33 (dt, *J* = 15.2, 7.8 Hz, 2H), 2.10 (t, *J* = 6.7 Hz, 2H), 1.96 – 1.88 (m, 2H), 1.72 (dd, *J* = 10.5, 5.5 Hz, 2H). ^{13}C NMR (101 MHz, MeOD) δ 202.6, 161.2, 157.3, 155.8, 144.3, 142.1, 141.7, 132.2, 116.0, 115.8, 109.7, 92.3, 82.9, 79.2, 72.3, 54.1, 50.7, 46.2, 45.3, 30.0, 27.6, 25.3, 12.7. HRMS (ESI+) m/z calcd for $C_{27}H_{32}N_7O_2^+$ $(M+H)^+$ 486.2612; found 486.2604.

Synthesis of 7-cyclopentyl-N,N-dimethyl-2-((5-(4-(prop-2-yn-1-yl)piperazin-1-yl)pyridin-2-yl)amino)-7H-pyrrolo[2,3-d]pyrimidine-6-carboxamide (rib-propargyl)

Rib-propargyl was synthesized in a similar way as **pal-propargyl** using ribociclib instead of palbociclib. Light yellow solid (105 mg, 89 %). ^1H NMR (400 MHz, MeOD) δ 8.99 (d, *J* = 1.3 Hz, 1H), 8.11 – 7.96 (m, 2H), 7.47 (d, *J* = 9.4 Hz, 1H), 6.84 (s, 1H), 6.07 (d, *J* = 6.3 Hz, 1H), 4.69 (dd, *J* = 10.0, 2.4 Hz, 1H), 4.19 (d, *J* = 2.5 Hz, 1H),

3.95 (ddd, *J* = 45.4, 37.3, 13.2 Hz, 2H), 3.70 (dt, *J* = 4.9, 3.9 Hz, 1H), 3.64 – 3.45 (m, 6H), 3.40 (t, *J* = 2.5 Hz, 1H), 3.18 (d, *J* = 8.3 Hz, 6H), 2.48 (dd, *J* = 12.3, 8.4 Hz, 2H), 2.20 – 2.05 (m, 4H), 1.76 (d, *J* = 5.6 Hz, 2H). ^{13}C NMR (101 MHz, MeOD) δ 163.4, 152.4, 151.2, 145.9, 145.5, 141.3, 136.6, 134.1, 125.0, 115.1, 114.9, 101.1, 79.7, 71.8, 58.3, 50.7, 46.2, 38.2, 34.0, 30.1, 24.2. HRMS (ESI+) m/z calcd for $C_{26}H_{33}N_8O^+$ $(M+H)^+$ 473.2772; found 473.2775.

Synthesis of 6-(4-((4-(6-((6-acetyl-8-cyclopentyl-5-methyl-7-oxo-7,8-dihydropyrido [2,3-d]pyrimidin-2-yl)amino)pyridin-3-yl)piperazin-1-yl)methyl)-1H-1,2,3-triazol-1-yl)-N-(2-(2,6-dioxopiperidin-3-yl)-1,3-dioxoisoindolin-4-yl)hexanamide (pal-pom)

$CuSO_4$ (6 µmol), Na ascorbate (24 µmol) and TBTA (6 µmol) were added to a mixture of **pal-propargyl** (20 µmol) and **pom-N_3** (22 µmol) in 0.4 mL DMSO and 0.2 mL H_2O. The reaction mixure was stirred overnight at room temperature. Solvent was removed. H_2O was added to the mixture and the crude product was purified by prep-HPLC to obtain **pal-pom** as a yellow solid (8.6 mg, 48 %). ^{1}H NMR (400 MHz, MeOD) δ 9.04 (s, 1H), 8.59 (d, *J* = 8.4 Hz, 1H), 8.21 (s, 1H), 7.98 (d, *J* = 2.3 Hz, 1H), 7.92 (d, *J* = 9.3 Hz, 1H), 7.78 (dd, *J* = 12.6, 5.1 Hz, 2H), 7.57 (d, *J* = 7.3 Hz, 1H), 6.00 (p, *J* = 8.8 Hz, 1H), 5.15 (dd, *J* = 12.4, 5.5 Hz, 1H), 4.58 – 4.49 (m, 4H), 3.49 (s, 7H), 2.95 – 2.67 (m, 4H), 2.56 – 2.50 (m, 5H), 2.43 (s, 3H), 2.33 (dt, *J* = 15.7, 7.9 Hz, 3H), 2.23 – 2.01 (m, 6H), 1.97 – 1.66 (m, 7H), 1.45 (dq, *J* = 15.3, 7.7 Hz, 2H). ^{13}C NMR (101 MHz, MeOD) δ 202.5, 173.0, 172.8, 170.1, 168.4, 166.8, 161.2, 156.9, 155.8, 155.5, 144.1, 141.8, 141.6, 136.7, 136.0, 135.7, 134.3, 132.6, 131.6, 126.6, 125.6, 124.5, 118.1, 116.9, 116.2, 110.0,

54.2, 50.8, 50.3, 50.0, 49.2, 45.7, 36.4, 30.7, 30.0, 29.4, 27.6, 25.5, 25.3, 24.1, 22.2, 12.8. HRMS (MALDI+) m/z calcd for $C_{46}H_{52}N_{13}O_7^+$ $(M+H)^+$ 898.4107; found 898.4092.

Synthesis of 7-cyclopentyl-2-((5-(4-((1-(6-((2-(2,6-dioxopiperidin-3-yl)-1,3-dioxoisoindolin-4-yl)amino)-6-oxohexyl)-1H-1,2,3-triazol-4-yl)methyl)piperazin-1-yl)pyridin-2-yl)amino)-N,N-dimethyl-7H-pyrrolo[2,3-d]pyrimidine-6-carboxamide (rib-pom)

Rib-pom was synthesized in a similar way as **pal-pom** using **pal-propargyl** instead of **rib-propargyl**. Light yellow solid (6.7 mg, 38 %). ^{1}H NMR (400 MHz, MeOD) δ 8.96 (s, 1H), 8.57 (d, *J* = 8.4 Hz, 1H), 8.24 (s, 1H), 7.99 (dd, *J* = 9.5, 2.9 Hz, 1H), 7.93 (d, *J* = 2.8 Hz, 1H), 7.76 (dd, *J* = 8.4, 7.4 Hz, 1H), 7.54 (d, *J* = 7.2 Hz, 1H), 7.42 (d, *J* = 9.4 Hz, 1H), 6.83 (s, 1H), 5.15 (dd, *J* = 12.6, 5.5 Hz, 1H), 4.58 (s, 2H), 4.52 (t, *J* = 6.9 Hz, 2H), 3.54 (s, 8H), 3.18 (d, *J* = 7.8 Hz, 6H), 2.99 – 2.65 (m, 4H), 2.49 (dt, *J* = 12.4, 7.8 Hz, 4H), 2.22 – 1.93 (m, 9H), 1.77 (dt, *J* = 15.0, 7.4 Hz, 4H), 1.45 (dq, *J* = 15.5, 7.8 Hz, 2H). ^{13}C NMR (101 MHz, MeOD) δ 173.1, 172.8, 170.1, 168.4, 166.9, 163.4, 152.4, 151.1, 145.8, 145.4, 141.2, 136.7, 136.6, 135.9, 135.7, 134.0, 131.6, 126.6, 125.6, 125.0, 118.1, 116.9, 115.1, 114.9, 101.1, 58.3, 50.8, 50.3, 50.0, 49.2, 46.0, 36.4, 34.0, 30.7, 30.1, 29.4, 25.5, 24.2, 24.1, 22.2. HRMS (MALDI+) m/z calcd for $C_{45}H_{53}N_{14}O_6^+$ $(M+H)^+$ 885.4267; found 885.4245.

Synthesis of 5-(4-((4-(6-((6-acetyl-8-cyclopentyl-5-methyl-7-oxo-7,8-dihydropyrido [2,3-d]pyrimidin-2-yl)amino)pyridin-3-yl)piperazin-1-yl)methyl)-1H-1,2,3-triazol-1-yl)-N-(2-(2,6-dioxopiperidin-3-yl)-1,3-dioxoisoindolin-4-yl)pentanamide (pal-pom-2)

Pal-pom-2 was synthesized in a similar way as **pal-pom** using **pom-N$_3$** analog with one less -CH_2. Yellow solid (8.8 mg, 52 %). ^{1}H NMR (400 MHz, MeOD) δ 9.07 (s, 1H), 8.56 (d, *J* = 8.0 Hz, 1H), 8.27 (s, 1H), 8.07 – 7.95 (m, 2H), 7.77 (dd, *J* = 8.4, 7.4 Hz, 1H), 7.68 (d, *J* = 9.3 Hz, 1H), 7.58 (d, *J* = 6.8 Hz, 1H), 6.07 – 5.95 (m, 1H), 5.15 (dd, *J* = 12.5, 5.5 Hz, 1H), 4.62 – 4.51 (m, 4H), 3.56 (s, 7H), 2.96 – 2.66 (m, 3H), 2.57 (t, *J* = 7.2 Hz, 2H), 2.51 (d, *J* = 3.1 Hz, 3H), 2.45 – 2.27 (m, 6H), 2.22 – 2.00 (m, 7H), 1.97 – 1.62 (m, 7H). HRMS (MALDI+) m/z calcd for $C_{45}H_{50}N_{13}O_7^+$ $(M+H)^+$ 884.3951; found 884.3928.

Synthesis of 7-cyclopentyl-2-((5-(4-((1-(5-((2-(2,6-dioxopiperidin-3-yl)-1,3-dioxoisoindolin-4-yl)amino)-5-oxopentyl)-1H-1,2,3-triazol-4-yl)methyl)piperazin-1-yl)pyridin-2-yl)amino)-N,N-dimethyl-7H-pyrrolo[2,3-d]pyrimidine-6-carboxamide (rib-pom-2)

Rib-pom-2 was synthesized in a similar way as **rib-pom** using **pom-N$_3$** analog with one less -CH_2. Light yellow solid (6.9 mg, 42 %). ^{1}H NMR (400 MHz, MeOD) δ 8.97 (s, 1H), 8.56 (d, *J* = 8.4 Hz, 1H), 8.28 (s, 1H), 8.05 – 7.92 (m, 2H), 7.82 – 7.73 (m, 1H), 7.56 (d, *J* = 7.3 Hz, 1H), 7.42 (d, *J* = 9.4 Hz, 1H), 6.84 (s, 1H), 5.15 (dd, *J* = 12.6, 5.5 Hz, 1H), 4.58 (dd, *J* = 13.6, 6.8 Hz, 5H), 3.56 (s, 8H), 3.18 (d, *J* = 7.8 Hz, 7H), 2.97 –

2.42 (m, 8H), 2.23 – 2.03 (m, 8H), 1.80 – 1.70 (m, 4H). HRMS (MALDI+) m/z calcd for $C_{44}H_{51}N_{14}O_6^+$ $(M+H)^+$ 871.4111; found 871.4083.

Kinase Binding Affinity Assay

Kinase-tagged T7 phage strains were prepared in an E. coli host derived from the BL21 strain. E. coli were grown to log-phase and infected with T7 phage and incubated with shaking at 32°C until lysis. The lysates were centrifuged and filtered to remove cell debris. The remaining kinases were produced in HEK-293 cells and subsequently tagged with DNA for qPCR detection. Streptavidin-coated magnetic beads were treated with biotinylated small molecule ligands for 30 minutes at room temperature to generate affinity resins for kinase assays. The liganded beads were blocked with excess biotin and washed with blocking buffer (SeaBlock (Pierce), 1% BSA, 0.05% Tween 20, 1 mM DTT) to remove unbound ligand and to reduce nonspecific binding. Binding reactions were assembled by combining kinases, liganded affinity beads, and test compounds in 1x binding buffer (20% SeaBlock, 0.17x PBS, 0.05% Tween 20, 6 mM DTT). Test compounds were prepared as 111X stocks in 100% DMSO. K_ds were determined using an 11-point 3-fold compound dilution series with three DMSO control points. All compounds for K_d measurements are distributed by acoustic transfer (non-contact dispensing) in 100% DMSO. The compounds were then diluted directly into the assays such that the final concentration of DMSO was 0.9%. All reactions performed in polypropylene 384-well plate. Each was a final volume of 0.02 ml. The assay plates were incubated at room temperature with shaking for 1 hour and the affinity beads were washed with wash buffer

(1x PBS, 0.05% Tween 20). The beads were then re-suspended in elution buffer (1x PBS, 0.05% Tween 20, 0.5 μM non-biotinylated affinity ligand) and incubated at room temperature with shaking for 30 minutes. The kinase concentration in the eluates was measured by qPCR.

Protein Degradation (Western Blot)

Cells were seeded in 24-well plate (80,000 cells/well) and allowed to adhere overnight. Culturing media were replaced by fresh media with PROTACs (DMSO < 0.5%). Cells were incubated for certain time (varies according to different experiments, see below) before lysed by RIPA buffer (Pierce) according to manufacturer's instructions. Total protein concentrations were determined and calibrated by BCA protein assay (Pierce). Whole cell lysates were subjected to SDS-PAGE, transferred to PVDF membrane and proceeded to Western blot protocol: membrane was blocked with SuperBlock (TBS) Blocking Buffer (ThermoFisher Scientific) for 1 h at room temperature, incubated with primary antibodies overnight at 4 ºC, washed with TBS-T (TBS + 0.05% Tween 20) 3 times, incubated with secondary antibodies for 1 h at room temperature, washed with TBS-T 4-6 times. Afterwards, blots were treated with SuperSignal West Dura Substrate (ThermoFisher Scientific) and imaged by ChemiDoc XRS (BioRad) imaging system.

For time course study, MDA-MB-231 cells were treated with PROTACs or 0.3% DMSO for different time period before cell lysis. For washout experiment, cells were treated with PROTACs or 0.3% DMSO for 18 h and washed with warm PBS twice to

remove PROTACs residue. Afterwards, cells were incubated for different time period before cell lysis. For rescue experiment, cells were pretreated with palbociclib, pomalidomide, MLN4924, MG-132 or 0.1% DMSO for 2 h before treated with PROTACs or 0.3% DMSO for 18 h and cell lysis.

Dilution factor: anti-CDK4 mAb (1:1000), anti-CDK6 mAb (1:1000), anti-phospho-Rb (Ser 780) mAb (1:1000), anti-b-actin mAb (1:5000), HRP-conjugated anti-rabbit IgG (H+L) (1:50,000).

Cytotoxicity Assay

MDA-MB-231 or MCF-7 cells were seeded in 96-well plate (5,000 cells/well) in 50 μL DMEM/F12 media with 10% FBS and allowed to adhere overnight. Compounds were diluted in PFHM-II media and added to each well. Cells were incubated for 72 h before AlamarBlue reagent (Invitrogen) was added. Cells were incubated for an additional 2 h and fluorescence intensity (Ex/Em 560/590 nm) was measured by a BioTek Synergy 4 Microplate Reader. Cell viabilities are calculated as: % live cells = $OD_{compound}/OD_{DMSO}$ × 100. Results are processed by GraphPad Prism 6.0 software.

Cell proliferation Assay

MCF-7 cells were seeded in 24-well plate (20,000 cells/well) in 0.5 mL DMEM/F12 media with 10% FBS and allowed to adhere overnight. Compounds were diluted in the same media and added to each well. Media were refreshed every 2 days with the exact same components in each well. At day 2, 4 and 6, AlamarBlue reagent

(Invitrogen) was added. Cells were incubated for an additional 2 h and fluorescence intensity (Ex/Em 560/590 nm) was measured by a BioTek Synergy 4 Microplate Reader. Percentage cell proliferation was calculated as $OD_{compound}/OD_{DMSO\ at\ day\ 2} \times 100$. Results are processed by GraphPad Prism 6.0 software.

To clarify, the cytotoxicity assay was performed using a shorter incubation time than the proliferation assay, and with a range of drug concentrations to get a S-curve. In the proliferation assay, the drug dose was set at 3 μM (not cytotoxic) but the incubation was carried on for a longer time to monitor the long-term effects.

4.3. Results and Discussion

In actuality, the PROTACs for this study were prepared by cycloadding a known azide[77] derived from pomalidomide to *N*-propargyl derivatives of palbociclib or ribociclib as shown in Figure 4.3.

PROTACs of palbociclib and ribociclib were examined in MDA-MB-231, a triple negative (estrogen receptor, progesterone receptor and HER2 negative) breast cancer cell line. Figure 4.4a and 4.4b show **pal-pom** dose-dependently depleted CDK4 and CDK6 when incubated with MDA-MB-231 cells for 18 h, but the extent of depletion was not linear for **rib-pom**. Also, both **pal-pom** and **rib-pom** degraded CDK4 more efficiently than CDK6, with a DC_{50} (the concentration for 50% protein degradation) of ~15 and ~100 nM to CDK4, respectively (Figure 4.4c, 4.4d). Observant readers may notice in Figure 4.4a and 4.4b that treatment of the cells with **pal** or **rib** consistently gives an increased level of CDK4/6. The reasons for this reproducible finding are unclear, but it seems the

cells somehow compensate for the inhibition. PROTACs are sensitive to linker length; we investigated modification of **pal-pom** and **rib-pom** with a slightly shorter linker, but this had no significant effect (Figure 4.5). Since **pal-pom** induced degradation was more efficient than **rib-pom**, the rest of this study focused on only the palbociclib derivative with the linker shown in Figure 4.3.

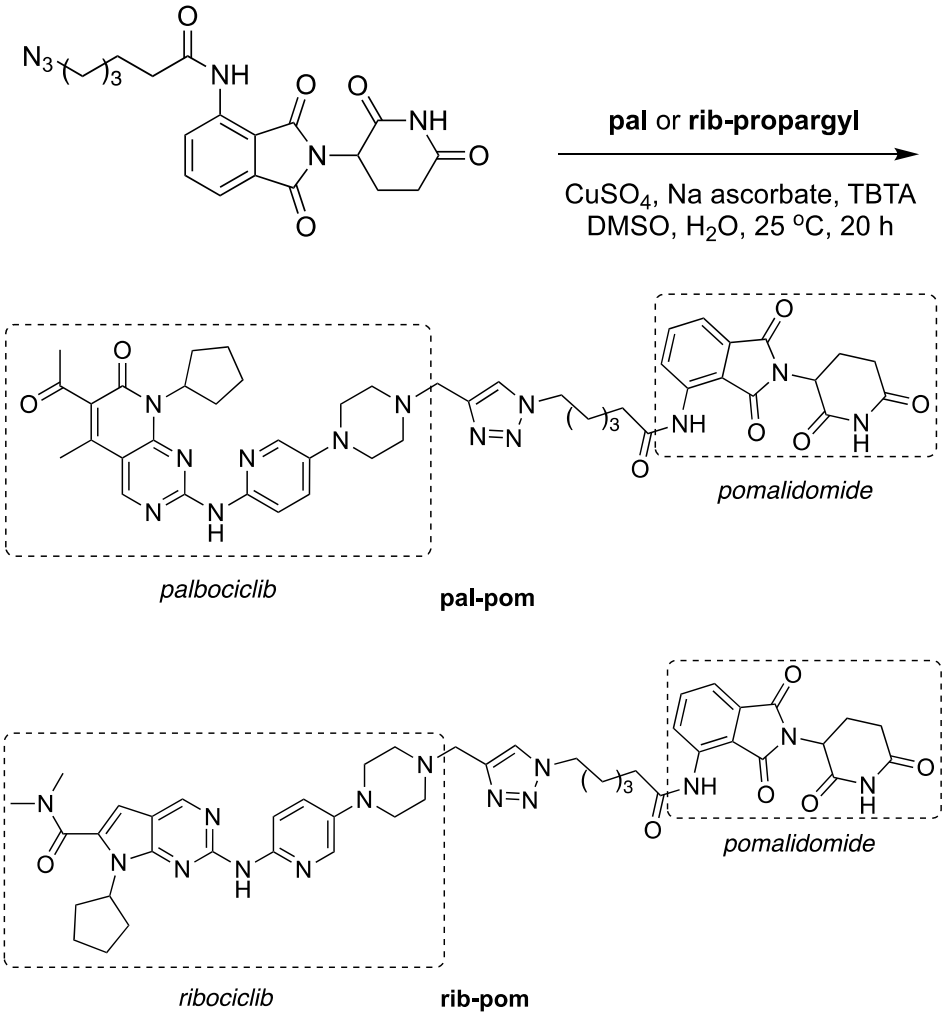

Figure 4.3 Syntheses of PROTACs for this study, **pal-pom** and **rib-pom.**

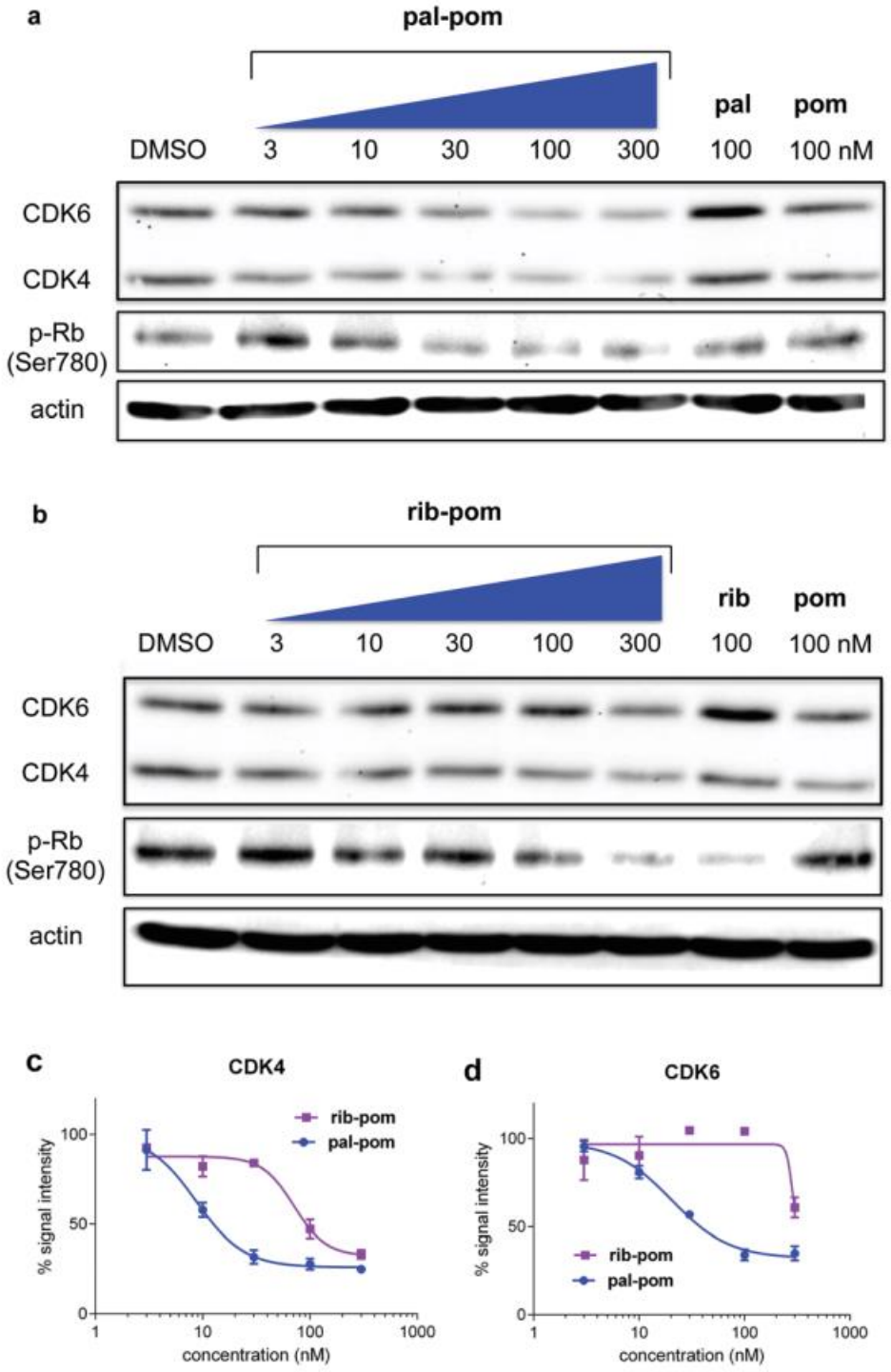

Figure 4.4 (**a**, **b**) Degradation of CDK4/6 on MDA-MB-231 cell line by **pal-pom** and **rib-pom**, respectively. (**c**, **d**) Quantified data for both PROTACs (normalized to DMSO control set as 100% protein concentration).

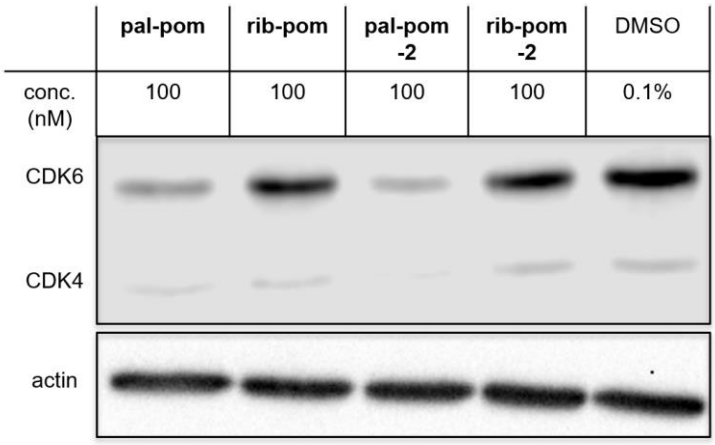

Figure 4.5 CDK4/6 degradation using different linkers on MDA-MB-231 cells. Similar results were observed when different length of linkers was applied.

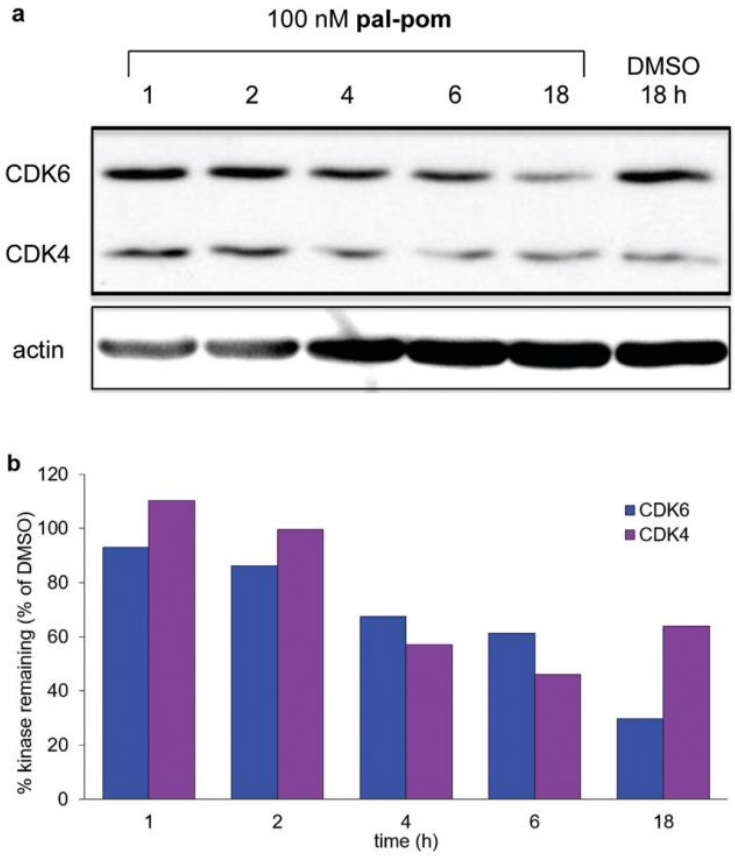

Figure 4.6 (**a**) Kinetics for depletion of CDK4 and CDK6 in response to 100 nM **pal-pom**. (**b**) Quantified data for (**a**), normalized to DMSO control set as 100%.

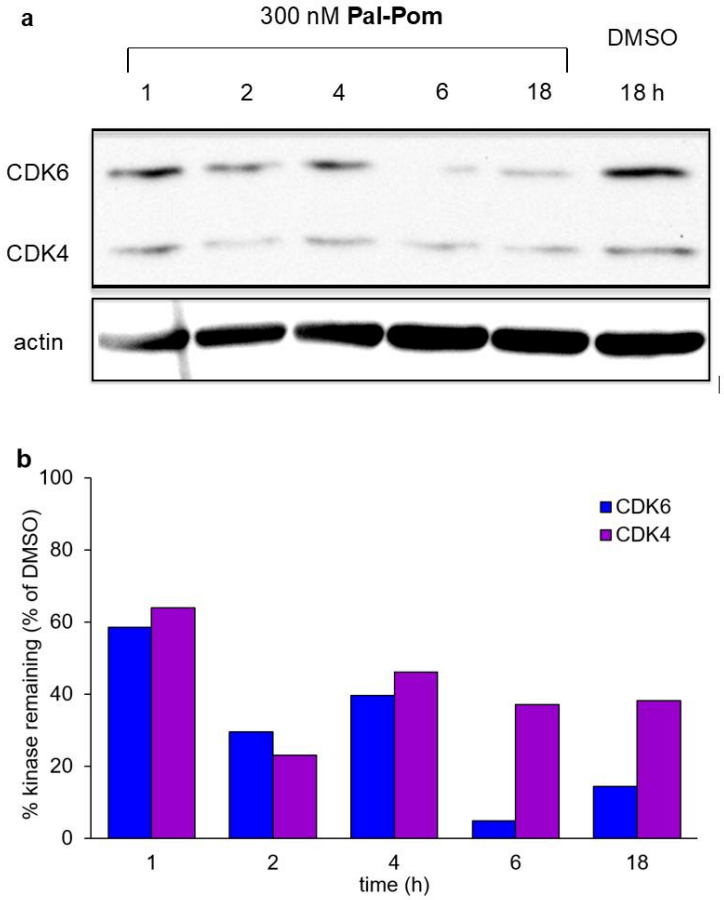

Figure 4.7 (**a**) Kinetics for depletion of CDK4 and CDK6 in response to 300 nM **pal-pom**. (**b**) Quantified data for (**a**), normalized to DMSO control set as 100%.

Phosphorylation of retinoblastoma protein (p-Rb) is regulated by CDK4 and CDK6. Consequently, depletion of these cyclin dependent kinases should reduce the level of the p-Rb. Blotting experiments in Figure 4.4a and 4.4b show that the PROTACs did indeed reduce the phosphorylation of Rb in a dose dependent way.

A time course study demonstrated that treatment of the same triple negative breast cell line with 100 nM **pal-pom** gave optimal CDK4 degradation after 4 h, whereas maximal decomposition of CDK6 took 6 h or more (Figure 4.6). Similar experiments but

with a higher PROTACs concentration (300 nM **pal-pom**) showed both CDK4 and CDK6 were degraded from the cell slightly faster (Figure 4.7).

Several "rescue" experiments were performed to confirm the mechanism of the observed CDK4/6 degradation by **pal-pom**, (Figure 4.8a). The first of these used palbociclib (10 μM) or pomalidomide (10 μM) to compete with **pal-pom** for the binding to CDK4/6 or to cereblon, respectively. Under these conditions, the kinase and ligase active sites should be blocked by the excess monovalent ligands, rendering the PROTACs impotent. Again, we observed that pretreatment with **pal** increased the levels of CDK4/6 (see above). Neddylation inhibitor MLN4924 (1 μM) was added in another experiment because it inhibits NEDD8-activating enzyme (NAE) and therefore prevents activation of cullin-RING ligases, which are critical for proteasome-mediated protein degradation.[84] Incidentally, pretreatment with MLN4924 caused an increased level of CDK4, similar to that caused by pretreatment with **pal**. The final experiment featured 20 μM of the proteasome inhibitor MG-132.[85] In the event, most CDK4/6 remained after 18 h PROTACs treatment as compared to a sample that was pretreated with 0.1% DMSO. This outcome suggests mechanism of PROTACs **pal-pom** involves binding to CDK4/6 and cereblon, and proteasome-mediated degradation.

Figure 4.8c shows data from "washout" experiments to see if CDK4/6 degradation is reversible wherein cells depleted in CDK4/6 by treatment with **pal-pom** were given 24 h in new media to facilitate efflux of the PROTACs. Concentrations of CDK4/6 were restored to at least their original levels.

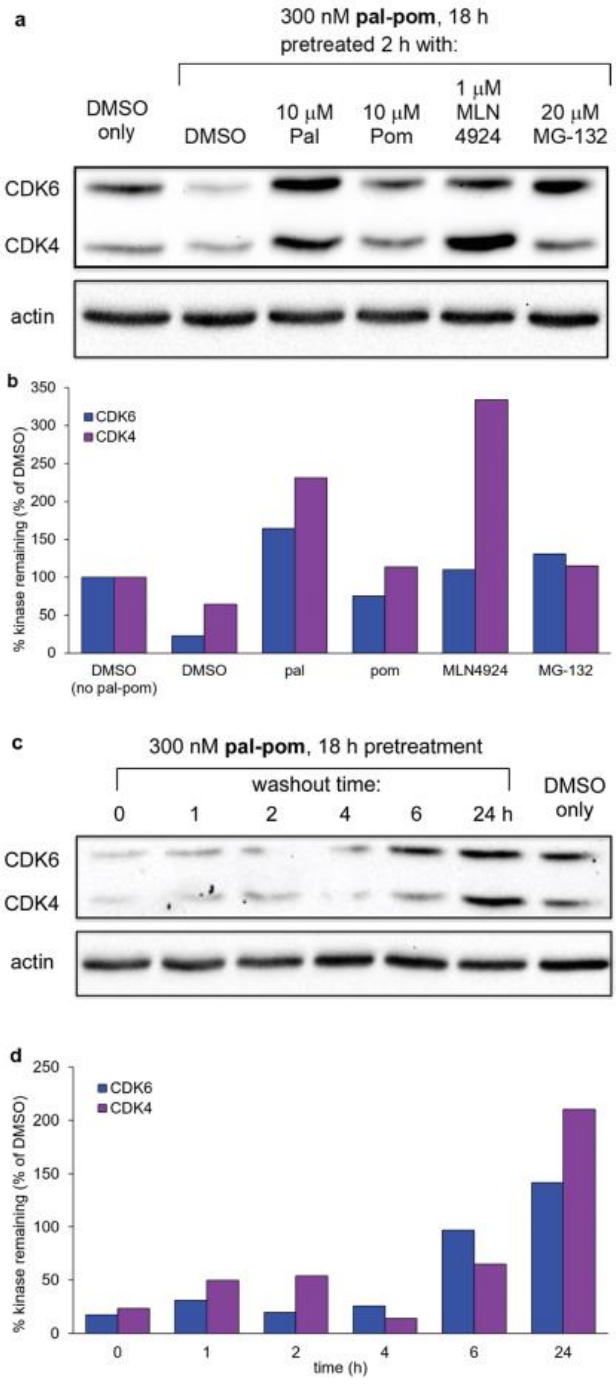

Figure 4.8 (**a**) Pre-treatment with 10 μM palbociclib or pomalidomide, 1 mM neddylation inhibitor MLN4924, 20 μM proteasome inhibitor MG-132 insulated the cells from CDK4/6 degradation by the PROTACs. (**b**) Quantified data for (**a**), normalized to DMSO control set as 100%. (**c**) Washout of the PROTACs from the cells

facilitates recovery of CDK4/6 levels after 24 h. (**d**) Quantified data for (**c**), normalized to DMSO control set as 100%.

Catalysis is the compelling reason to study PROTACs, but proving this occurs is difficult. One indicator is if the PROTACs DC_{50} in cell viability experiments is lower than the dissociation constant (K_d) of ligand that binds the parent protein. Consequently, K_d values were measured for **pal-pom** bound to CDK4 and CDK6 via KINOME*scan*™. KINOME*scan*™ is performed by combining DNA-tagged kinase, immobilized ligand, and test compounds; it is a competition binding assay featuring an immobilized, active-site directed ligand in which abilities of test samples to compete with immobilized ligand are measured via quantitative PCR of the DNA-tagged kinase (Table 4.1, Figure 4.9). DC_{50} values for CDK4/6 suppression (deduced from Figure 4.4) are indeed lower than the K_d values for kinase-bound **pal-pom** indicating the degradation is catalytic. Throughout, the K_d values for the inhibitor are less than those for the corresponding PROTACs, as anticipated because the PROTACs are significantly larger.

Kinase inhibitors such as palbociclib and ribociclib are intended to induce cell senescence rather than cytotoxicity.[86] Cytotoxicities of **pal-pom** and **rib-pom** on MDA-MB-231 cells were determined to be modest (IC_{50} estimated to be in the 10 – 50 μM range, Figure 4.10a), though definitive quantitation was limited by the solubilities of these compounds.

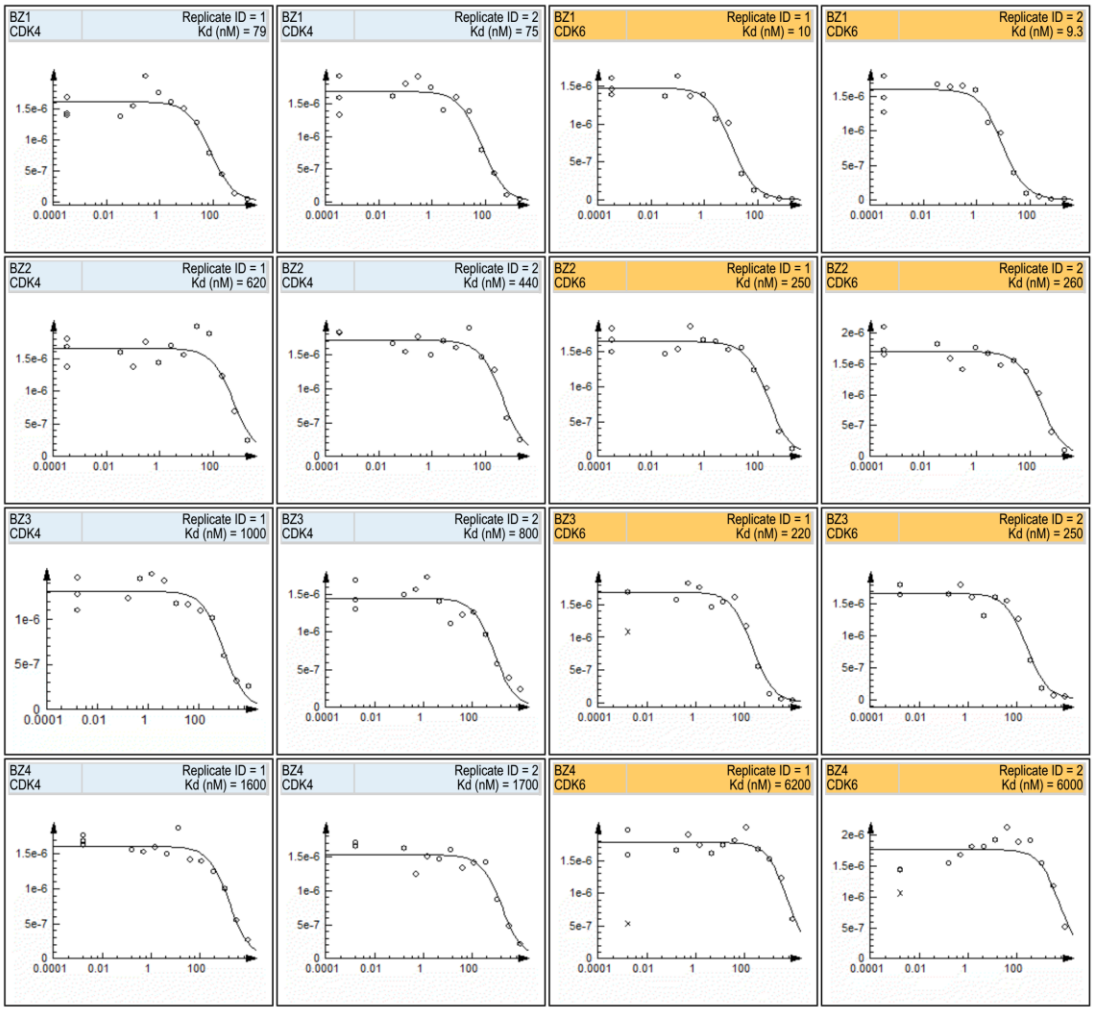

Figure 4.9 Kinase Binding Affinity Assay on CDK4/6, each K_d was determined in duplicate experiments. BZ1 = palbociclib, BZ2 = ribociclib, BZ3 = **pal-pom**, BZ4 = **rib-pom**.

Table 4.1 Comparison of kinase affinity (K_d) and DC_{50} for CDK4/6 depletion for the featured PROTACs.

kinase	pal	rib	pal-pom		rib-pom	
	K_d (nM)	K_d (nM)	K_d (nM)	DC_{50} (nM)	K_d (nM)	DC_{50} (nM)
CDK4	77±2	530±90	900±100	12.9±3.5	1.65±0.05	97±9.9
CDK6	9.7±0.4	255±5	235±15	34.1±7.3	6.1±0.1	~300

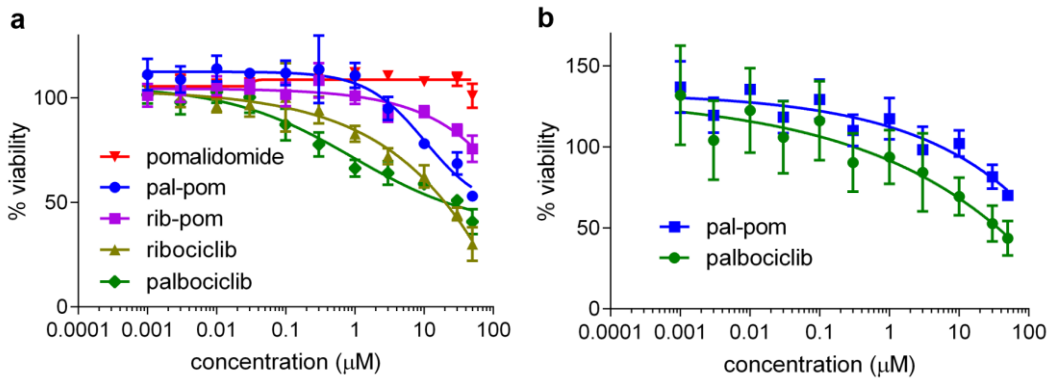

Figure 4.10 Cytotoxicity assay on (**a**) MDA-MB-231 cells and (**b**) MCF-7 cells (72 h incubation).

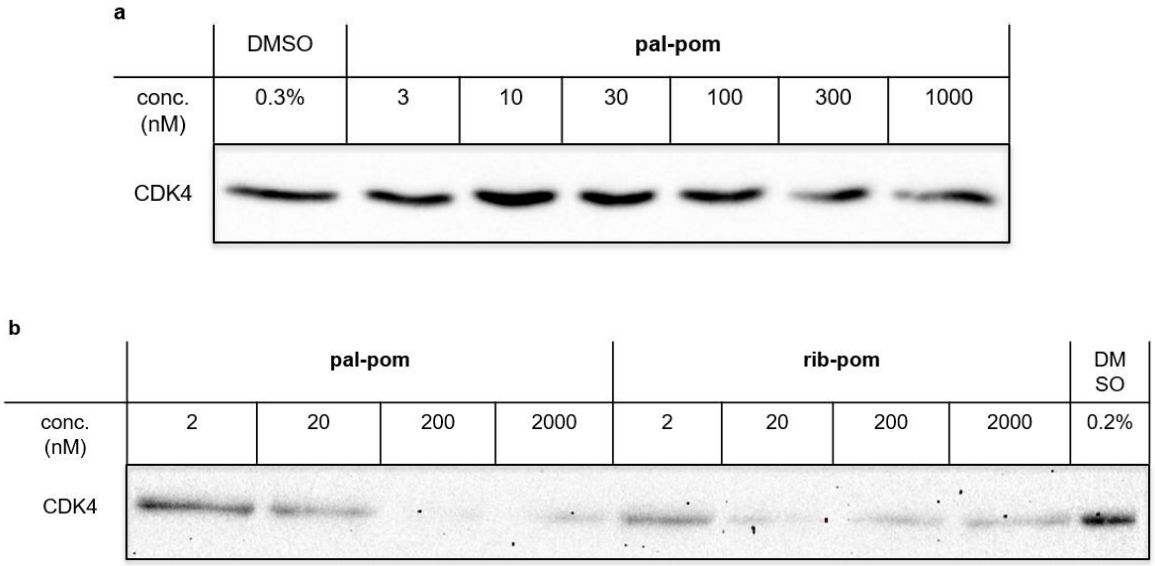

Figure 4.11 CDK4 depletion (Western blot) on (**a**) MCF-7 cells and (**b**) U87-MG cells with 18 h incubation of PROTACs. (CDK6 was not detected in these two cell lines by the same mAb used in MDA-MB-231 cell line)

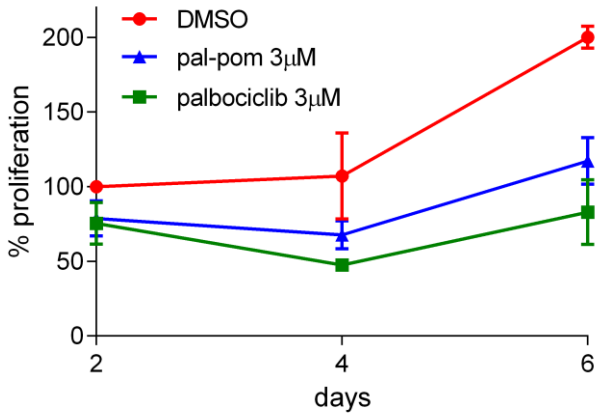

Figure 4.12 Cell proliferation assay on MCF-7 cell line. Culturing media were refreshed (with DMSO, pal-pom or palbociclib) every 2 days. Reading of DMSO control set at day 2 was used as 100% standard.

The work above features CDK4/6 PROTACs on a triple negative breast cancer cell line instead of the approved therapeutic end-point: estrogen receptor-positive, HER2-negative breast cancer. To further investigate the application of these PROTACs, similar experiments were performed on MCF-7 breast cancer cells, which are estrogen receptor-positive, HER2-negative; the PROTAC **pal-pom** worked, though, curiously, not as effectively as it did on MDA-MB-231 cells in protein degradation and cytotoxicity assay (Figure 4.10b and 4.11a). However, it did inhibit the MCF-7 cell proliferation over extended periods (up to 6 days, Figure 4.12). This observation motivated us to try a cell line for a completely different type of cancer: U87-MG cells corresponding to glioblastoma. In this case, both **pal-pom** and **rib-pom** at 20 - 200 nM gave significant depletion of CDK4 (Figure 4.11b).

4.4. Conclusions

In summary, as far as we are aware, this is the first report of a PROTACs that acts on CDK4/6. This finding is more significant than the closest work in the area, *ie* PROTACs suppression of CDK8/9, because only CDK4/6 are validated targets for cancer, and the PROTACs here feature FDA approved kinase inhibitors. Moreover, the potency of lead compound, **pal-pom** (DC_{50} 20 – 50 nM) are conspicuously higher than for the compounds reported to affect CDK8 and 9 (we estimate DC_{50}s of 1 – 10 μM from the data reported, Table 4.2). For further calibration, Table 4.2 also summarizes DC_{50}s of PROTACs on other completely different kinases and related proteins[77, 87-91], and this supports our assertion that the compounds reported here are relatively potent. Finally, observation of PROTACs activity for **pal-pom** and **rib-pom** on U87 glioblastoma cells bodes well for application of the same compounds to other cancer types.

Table 4.2 Summary of some reported PROTACs and their estimated DC_{50} value based on Western blots.

Protein	CDK8[83]	CDK9[82]	HDAC6[87]	BRD4[88]	BRD3[88]	BRD2[88]	ALK[89]	PI3K[77]	Sirt2[90]	BTK[91]
DC_{50}[a]	significant at 1 μM	~ 10 μM	100-300 nM	0.1-0.3 nM	30-100 nM	100-300 nM	30-60 nM	20-50 μM	0.2-1 μM	25-100 nM

[a] Estimated based on Western blots in corresponding papers.

5. CONCLUSIONS AND OUTLOOK FOR FUTURE WORK

5.1. Conclusions

This dissertation is focused on the validation and application of a ligand IY-IY for actively targeting some tumor types, and the development of PROTACs for TrkC and CDK4/6. A novel PAL cassette was developed to confirm the binding of IY-IY to TrkC receptor, as described in Chapter II. Ligand IY-IY was used to preferentially deliver a promiscuous KI (dasatinib) into $TrkC^+$ breast cancer cells over normal cells, as discussed in Chapter III. TrkC and CDK4/6 PROTACs were developed, as described in Chapters III and IV, respectively.

In Chapter II, a novel PAL cassette based on diazirine was designed and synthesized, in a more convenient route than traditional ones. The PAL cassette has three functional groups: a diazirine moiety for covalent bond linkage, a secondary amine to connect targeting ligand and an alkyne for introduction of a reporter group. Thus, two PAL-ligand conjugates were synthesized for CAIX and TrkC. The reported group, usually a bulky molecule, was incorporated after the photolabeling step to minimize the nonspecific binding of the cassette fragment to proteins. Fluorescent tagged protein can be scanned after SDS-PAGE separation, and biotin-labeled protein can be separated by a pull-down assay followed by Western blot detection. As a result, both conjugates labeled their anticipated targets with sufficient efficiencies and specificities. In a different case, a conjugate of the PAL cassette with a novel peptidomimetic that binds to PCSK9 was made, and photolabeling of recombinant PCSK9 was observed and confirmed to be

specific by blocking experiments.[29] In conclusion, the synthesis of this PAL cassette involves simple organic reactions, making it convenient for scale-up. The targeting ligand can be introduced by coupling with the secondary amine on the cassette, to afford the final PAL ligand. Moreover, this PAL cassette based on aromatic diazirine is smaller than most PAL ligands reported before, which is preferred to minimize the steric perturbation of the ligand-protein interaction. Some aliphatic diazirines which are even smaller than aromatic diazirine were also used for photoaffinity labeling, however, they are less stable and prone to generate carbocations that can react with the nucleophiles on the side chain of amino acids, causing nonspecific labeling.[92]

In Chapter III, active targeting strategy was applied to a promiscuous KI (dasatinib) improve its selectivity of cancer cells over normal cells. While dasatinib is an FDA-approved drug for Philadelphia chromosome-positive (Ph+) chronic myeloid leukemia (CML), some side effects were observed and some can be severe for some patients. Thus, targeting ligand IY-IY explored in Chapter II was conjugated with dasatinib, and two types of linkers were designed in this case: a non-cleavable linker and a cleavable disulfide linker. In cellular assays, the conjugate with cleavable linker preferentially delivered dasatinib into $TrkC^+$ cancer cells over normal cells and matched the activity of dasatinib in inhibiting p-Src, wound healing and cell viability assays, and the disulfide linker was proved to be important to the activity of the conjugate. This study demonstrates the potential to improve the selectivity and therapeutic index of the promiscuous kinase inhibitor by active targeting a surface receptor that overexpressed on cancer cells. Same active targeting strategies could be applied to other promiscuous

inhibitors, via different targeting ligands, in the case where undesired inhibition occurs in normal tissue. Indeed, in one of our recent papers, a tumor-seeking cyanine dye was used to deliver the same KI dasatinib into cancer cells, where the dye-KI conjugate limits cell proliferation more effectively than the parent kinase dasatinib.[69] Many drug candidates failed in clinical trials because of the potential toxicity to patients, some of which could be attributed to their poor selectivities. Active targeting strategy may offer an opportunity to improve the therapeutic window of these drugs.

In the last part of Chaptor III, IY-IY fragment was further exploited for development of the first potent TrkC PROTAC, by conjugation of pomalidomide to recruit CRBN for degradation. PROTACs have attracted attentions in recent years because of several advantages over traditional inhibitors, including the catalytic mechanism of action, the ability to act on undruggable protein and less vulnerability to mutations. Chapter IV described the development of the first CDK4/6 PROTACs. CDKs are critical for cell cycle regulation. Among these kinases, efforts have been made in the development of selective CDK4/6 inhibitors for treatment of cancer. In this study, conjugates of palbociclib or ribociclib with pomalidomide were designed and synthesized. Effects of linker length were investigated to optimize the efficacy of the PROTACs. The lead compound shows potent protein degradation with a DC_{50} of 12.9 and 34.1 nM to CDK4 and 6, respectively. The specificity of protein degradation was confirmed and mechanism of action were validated to be ubiquitin-related and proteasome-dependent. The lead PROTAC was also shown to inhibit cell proliferation in a similar way as palbociclib. In fact, there are several reports of palbociclib-based CDK PROTACs after our

publication,[93-95] and interestingly, some show selective degradation of CDK6 over CDK4, and this selectivity was exploited to dissect the role of CDK6 in coordinating signaling and gene control in CDK6-dependent acute myeloid leukemia (AML) cells.[96] Selective degradation by PROTACs could be achieved by using a non-selective inhibitor as the targeting ligand,[97] because the optimal linker length for the degradation of each protein of interest (POI) would be different, specifically, in favor of the cooperative binding and therefore the formation of the ternary complex (POI-PROTAC-E3).[98] Actually, some drug-resistant issues have emerged in some clinical trials of palbociclib in treatment of pancreatic cancer, and there are evidences showing that upregulated CDK2 activity plays a role in compensation of the loss of CDK4/6 activity. Thus, selective CDK2 inhibitor is highly desired, but unfortunately, has not been reported. Optimal linkage of current non-selective CDK2 inhibitors to E3 ligase may potentially lead to selective CDK2 degrader.

5.2. Future Work

Photoaffinity labeling is commonly used for the identification of unknown target proteins that small molecule ligands bind to, and for extrapolation of the binding pocket by studying the distribution of covalent linkage via MS-MS proteomic analysis. Nowadays, many small molecules binders are discovered by high-throughput screening, however, without the knowledge of the binding partners. PAL may serve as a convenient tool for the identification of the protein binders of small molecules following proteomic analysis, and may reveal hotspots. The PAL module reported in Chapter II is easy to make and ready to conjugate with small molecules, therefore have the potential applications in

the field of drug discovery. While the full structure of TrkC has not yet been reported, exploration of the mechanism of action on extracellular domain with small molecules is often desired. Therefore, it is of great interest to figure out the binding site of TrkC by PAL ligand, the potential mechanism of ligand-induced receptor homodimerization and the receptor-mediated endocytosis.

Active targeting strategy discussed in Chapter III may provide a perspective for drug delivery of promiscuous kinase inhibitors which failed in some clinical trials for certain cancer types, with an improved selectivity and therapeutic index. On the other hand, the development of TrkC PROTACs may provide opportunities for alternative therapeutic strategies in certain types of cancer including neuroblastoma, glioblastoma, breast cancer and melanoma where that receptor is important.

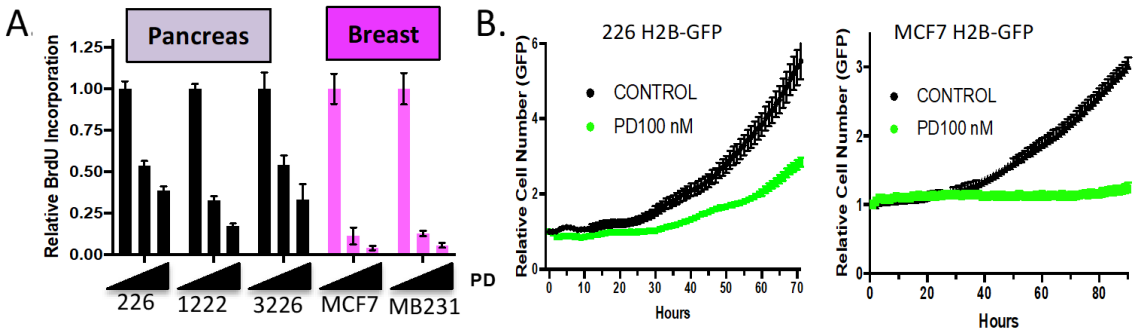

Figure 5.1 (**a**) Relative BrdU incorporation between PDAC and breast cancer cell lines treated with palbociclib (PD). The pancreatic cancer models are more resistant (PD-dose escalation 0, 100, 250 nM). (**b**) Live cell count of H2B-GFP labeled PDAC (left) or breast (right) cells treated with 100 nM palbociclib (PD). Breast cancer models are completely arrested, while data for the pancreatic cancer model 226 is representative of resistance present in most pancreatic models studied.

PROTACs can suppress protein expression, therefore provide an alternative method for regulating protein activities, as described in Chapter IV for CDK4/6. However, there are some drug-resistant issues emerging during the clinical trial of CDK4/6 inhibitors, and a key mechanism driving resistance is cell cycle plasticity. In cell cycle mechanism, retinoblastoma protein (Rb) potently suppresses many genes critical for cell cycle, whereas CDK4/6 regulates the phosphorylation of Rb, leading to the expression of Cyclin E. Cyclin E can active CDK2 by forming a complex with it and this can hyperphosphorylate Rb and lead to cell cycle progression. Comparison of some pancreatic ductal adenocarcinoma (PDAC) models with breast cancer models cultured in both 2D and 3D culture (Figure 5.1) shows these PDAC samples were far less perturbed by palbociclib treatment, compared to breast cancers. CDK2 activities were upregulated in these PDAC models, and most importantly, palbociclib became effective on PDAC cells if CDK2 was knocked down (Figure 5.2), indicating CDK2 activity was crucial for resistance. It is emerging that CDK4/6 and CDK2 inhibition have to be combined to potently inhibit the cell cycle.[38, 42, 99-100]

Selective inhibitors of CDKs are highly desired to minimize off-target effects. Unfortunately, there are no FDA-approved selective CDK2 inhibitors, and most of the experimental ones show sub-optimal selectivity, despite extensive efforts in this field. However, PROTACs derivatized from current CDK2 KIs can be made more selective for CDK2 over other CDKs than parent KIs by exploiting the fact that the effectiveness of PROTACs, and therefore its selectivity, are highly sensitive to linker structure, and E3

ligase ligand. Thus, PROTACs modifications provide opportunities for selectivity optimization that are not available to the parent KIs.

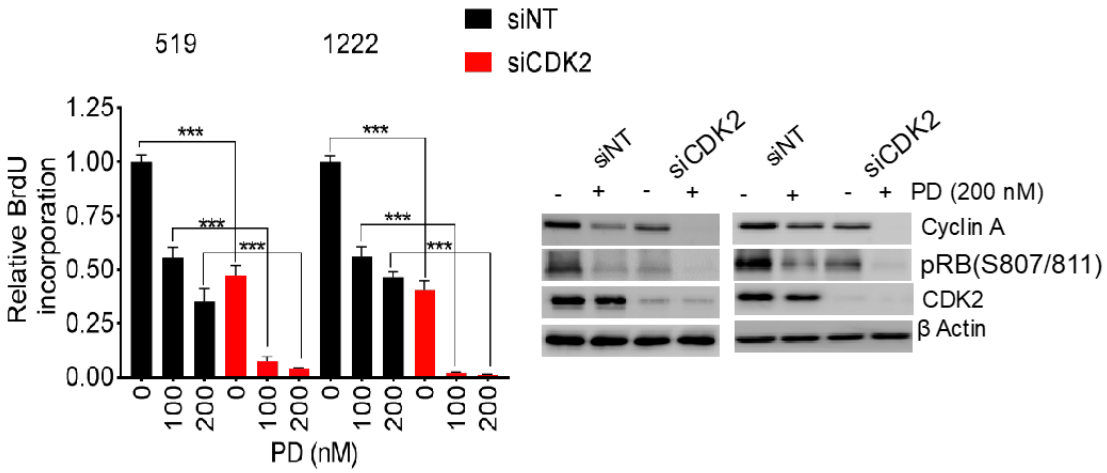

Figure 5.2 RNAi-mediated depletion of CDK2 was evaluated for its cooperative effects with palbociclib (PD). Representative immune blots and BrdU incorporation is shown (***p<0.001).

REFERENCES

1. Ko, E.; Kamkaew, A.; Burgess, K., Small Molecules Ligands for Active Targeting of TrkC-expressing Tumor Cells. *ACS Med. Chem. Lett.* **2012,** *3*, 1008-1012.

2. Minko, T.; Dharap, S. S.; Pakunlu, R. I.; Wang, Y., Molecular targeting of drug delivery systems to cancer. *Curr. Drug Targets* **2004,** *5* (4), 389-406.

3. Chari Ravi, V. J.; Miller Michael, L.; Widdison Wayne, C., Antibody-drug conjugates: an emerging concept in cancer therapy. *Angewandte Chemie (International ed. in English)* **2014,** *53*, 3796-3827.

4. Srinivasarao, M.; Low, P. S., Ligand-Targeted Drug Delivery. *Chem. Rev.* **2017,** *117*, 12133-12164.

5. Kue, C. S.; Kamkaew, A.; Burgess, K.; Kiew, L. V.; Chung, L. Y.; Lee, H. B., Small Molecules for Active Targeting in Cancer. *Med. Res. Rev.* **2016,** *36*, 494-575.

6. Wilhelm, M.; Schlegl, J.; Hahne, H.; Gholami, A. M.; Lieberenz, M.; Savitski, M. M.; Ziegler, E.; Butzmann, L.; Gessulat, S.; Marx, H.; Mathieson, T.; Lemeer, S.; Schnatbaum, K.; Reimer, U.; Wenschuh, H.; Mollenhauer, M.; Slotta-Huspenina, J.; Boese, J. H.; Bantscheff, M.; Gerstmair, A.; Faerber, F.; Kuster, B., Mass-spectrometry-based draft of the human proteome. *Nature* **2014,** *509* (7502), 582-+.

7. Adams, J. A., Kinetic and catalytic mechanisms of protein kinases. *Chemical reviews* **2001,** *101* (8), 2271-2290.

8. Wu, P.; Nielsen, T. E.; Clausen, M. H., FDA-approved small-molecule kinase inhibitors. *Trends Pharmacol. Sci.* **2015,** *36*, 422-439.

9. Wu, P.; Nielsen, T. E.; Clausen, M. H., Small-molecule kinase inhibitors: an analysis of FDA-approved drugs. *Drug Discov. Today* **2016,** *21* (1), 5-10.

10. Cohen, P., Protein kinases - the major drug targets of the twenty-first century? *Nature Reviews Drug Discovery* **2002,** *1* (4), 309-315.

11. Wu, P.; Nielsen, T. E.; Clausen, M. H., Small-molecule kinase inhibitors: an analysis of FDA-approved drugs. *Drug Discovery Today* **2016,** *21* (1), 5-10.

12. Wong, S.-F., New dosing schedules of dasatinib for CML and adverse event management. *Journal of Hematology & Oncology* **2009,** *2*, No pp given.

13. Conchon, M.; de Moura Freitas, C. M. B.; Rego, M. A. d. C.; Braga Junior, J. W. R., Dasatinib - clinical trials and management of adverse events in imatinib resistant/intolerant chronic myeloid leukemia. *Revista brasileira de hematologia e hemoterapia* **2011,** *33*, 131-9.

14. Low, P. S.; Henne, W. A.; Doorneweerd, D. D., Discovery and Development of Folic-Acid-Based Receptor Targeting for Imaging and Therapy of Cancer and Inflammatory Diseases. *Acc. Chem. Res.* **2008,** *41*, 120-129.

15. Chen, D.; Brahimi, F.; Angell, Y.; Li, Y.-C.; Moscowicz, J.; Saragovi, H. U.; Burgess, K., Bivalent Peptidomimetic Ligands of TrkC are Biased Agonists, Selectively Induce Neuritogenesis, or Potentiate Neurotrophin-3 Trophic Signals. *ACS Chem. Biol.* **2009,** *4* (9), 769-781.

16. Patapoutian, A.; Reichardt, L. F., Trk Receptors: Mediators of Neurotrophin Action. *Curr. Opin. Neurobiol.* **2001,** *11* (3), 272-280.

17. Segal, R. A., Selectivity in Neurotrophin Signaling: Theme and Variations. *Annu. Rev. Neurosci.* **2003,** *26,* 299-330.

18. Huang, E. J.; Reichardt, L. F., Trk receptors: roles in neuronal signal transduction. *Annu. Rev. Biochem.* **2003,** *72,* 609-642.

19. Chao, M. V., Neurotrophins and their receptors: A convergence point for many signalling pathways. *Nature Reviews Neuroscience* **2003,** *4* (4), 299-309.

20. Ryden, M.; Sehgal, R.; Dominici, C.; Schilling, F. H.; Ibanez, C. F.; Kogner, P., Expression of mRNA for the neurotrophin receptor trkC in neuroblastomas with favourable tumour stage and good prognosis. *Br. J. Cancer* **1996,** *74* (5), 773-779.

21. Wang, Y.; Hagel, C.; Hamel, W.; Muller, S.; Kluwe, L.; Westphal, M., Trk A, B, and C are commonly expressed in human astrocytes and astrocytic gliomas but not by human oligodendrocytes and oligodendroglioma. *Acta Neuropathol.* **1998,** *96*, 357-364.

22. Blasco-Gutierrez, M. J.; San Jose-Crespo, I. J.; Zozaya-Alvarez, E.; Ramos-Sanchez, R.; Garcia-Atares, N., TrkC: a new predictive marker in breast cancer? *Cancer Investigation* **2007,** *25* (6), 405-410.

23. Xu, X.; Tahan, S. R.; Pasha, T. L.; Zhang, P. J., Expression of neurotrophin receptor Trk-C in nevi and melanomas. *J. Cutan. Pathol.* **2003,** *30*, 318-322.

24. Kamkaew, A.; Burgess, K., Double-targeting Using a TrkC-Ligand Conjugated to Dipyrrometheneboron Difluoride (BODIPY) Based Photodynamic Therapy (PDT) Agent. *J. Med. Chem.* **2013,** *56*, 7608-7614.

25. Zhao, B.; Burgess, K., TrkC-Targeted Kinase Inhibitors and PROTACs. *Mol. Pharm.* **2019,** *16,* 4313 - 4318.

26. Kue, S. C., Anyanee Kamkaew, Hong Boon Lee, Lip Long Chung, Lik Voon Kiew, and Kevin Burgess, Targeted PDT Agent Eradicates TrkC Expressing Tumors Via Photodynamic Therapy (PDT). *Mol. Pharmacetics* **2015,** *12*, 212-222.

27. Jiang, Z.; Yang, Z.; Li, F.; Li, Z.; Fishkin, N.; Burgess, K., Targeted Maytansinoid Conjugate Improves Therapeutic Index for Metastatic Breast Cancer Cells. *Bioconjugate Chem.* **2018,** *29*, 2920-2926.

28. Smith, E.; Collins, I., Photoaffinity labeling in target- and binding-site identification. *Future Med. Chem.* **2015,** *7* (2), 159-183.

29. Taechalertpaisarn, J.; Zhao, B.; Liang, X.; Burgess, K., Small Molecule Inhibitors of the PCSK9-LDLR Interaction. *J. Am. Chem. Soc.* **2018,** *140*, 3242-3249.

30. Dubinsky, L.; Krom, B. P.; Meijler, M. M., Diazirine based photoaffinity labeling. *Bioorg. Med. Chem.* **2012,** *20* (2), 554-570.

31. Sakamoto, K. M.; Kim, K. B.; Kumagai, A.; Mercurio, F.; Crews, C. M.; Deshaies, R. J., Protacs: chimeric molecules that target proteins to the Skp1-Cullin-F box complex for ubiquitination and degradation. *Proc. Natl. Acad. Sci.* **2001,** *98* (15), 8554-8559.

32. Toure, M.; Crews, C. M., Small-Molecule PROTACS: New Approaches to Protein Degradation. *Angew. Chem., Int. Ed.* **2016,** *55*, 1966-1973.

33. Gu, S.; Cui, D.; Chen, X.; Xiong, X.; Zhao, Y., PROTACs: An Emerging Targeting Technique for Protein Degradation in Drug Discovery. *BioEssays* **2018,** *40*, 1-11.

34. Gadd, M. S.; Testa, A.; Lucas, X.; Chan, K.-H.; Chen, W.; Lamont, D. J.; Zengerle, M.; Ciulli, A., Structural basis of PROTAC cooperative recognition for selective protein degradation. *Nat. Chem. Biol.* **2017,** *13*, 514-521.

35. Zorba, A.; Zorba, A.; Nguyen, C.; Xu, Y.; Starr, J.; Borzilleri, K.; Smith, J.; Farley Kathleen, A.; Ding, W.; Schiemer, J.; Feng, X.; Chang Jeanne, S.; Uccello Daniel, P.; Young Jennifer, A.; Garcia-Irrizary Carmen, N.; Czabaniuk, L.; Schuff, B.; Oliver, R.; Montgomery, J.; Hayward Matthew, M.; Coe, J.; Chen, J.; Qiu, X.; West Graham, M.; Noe Mark, C.; Shanmugasundaram, V.; Gilbert Adam, M.; Brown Matthew, F.; Calabrese Matthew, F.; Zhu, H.; Niosi, M.; El-Kattan, A.; Luthra, S.; Shah Jaymin, C., Delineating the role of cooperativity in the design of potent PROTACs for BTK. *Proc. Natl. Acad. Sci. U. S. A.* **2018,** *115*, E7285-E7292.

36. Bondeson, D. P.; Mares, A.; Smith, I. E. D.; Ko, E.; Campos, S.; Miah, A. H.; Mulholland, K. E.; Routly, N.; Buckley, D. L.; Gustafson, J. L.; Zinn, N.; Grandi, P.; Shimamura, S.; Bergamini, G.; Faelth-Savitski, M.; Bantscheff, M.; Cox, C.; Gordon, D. A.; Willard, R. R.; Flanagan, J. J.; Casillas, L. N.; Votta, B. J.; den Besten, W.; Famm, K.; Kruidenier, L.; Carter, P. S.; Harling, J. D.; Churcher, I.; Crews, C. M., Catalytic in vivo protein knockdown by small-molecule PROTACs. *Nat. Chem. Biol.* **2015,** *11* (8), 611-617.

37. Burslem, G. M.; Smith, B. E.; Lai, A. C.; Jaime-Figueroa, S.; McQuaid, D. C.; Bondeson, D. P.; Toure, M.; Dong, H.; Qian, Y.; Wang, J.; Crew, A. P.; Hines, J.; Crews, C. M., The Advantages of Targeted Protein Degradation Over Inhibition: An RTK Case Study. *Cell Chemical Biology* **2018,** *25*, 67-77.

38. Goel, S.; DeCristo, M. J.; McAllister, S. S.; Zhao, J. J., CDK4/6 Inhibition in Cancer: Beyond Cell Cycle Arrest. *Trends Cell Biol.* **2018,** *28*, 911-925.

39. Sherr, C. J.; Beach, D.; Shapiro, G. I., Targeting CDK4 and CDK6: From Discovery to Therapy. *Cancer Discovery* **2016,** *6*, 353-367.

40. Pernas, S.; Tolaney Sara, M.; Winer Eric, P.; Goel, S., CDK4/6 inhibition in breast cancer: current practice and future directions. *Therapeutic advances in medical oncology* **2018,** *10*, 1758835918786451.

41. Alexander, L. T.; Mobitz, H.; Drueckes, P.; Savitsky, P.; Fedorov, O.; Elkins, J. M.; Deane, C. M.; Cowan-Jacob, S. W.; Knapp, S., Type II Inhibitors Targeting CDK2. *ACS Chem. Biol.* **2015,** *10*, 2116-2125.

42. Asghar, U.; Witkiewicz, A. K.; Turner, N. C.; Knudsen, E. S., The history and future of targeting cyclin-dependent kinases in cancer therapy. *Nature Reviews Drug Discovery* **2015,** *14*, 130-146.

43. Fry, D. W.; Harvey, P. J.; Keller, P. R.; Elliott, W. L.; Meade, M.; Trachet, E.; Albassam, M.; Zheng, X.; Leopold, W. R.; Pryer, N. K.; Toogood, P. L., Specific inhibition of cyclin-dependent kinase 4/6 by PD 0332991 and associated antitumor activity in human tumor xenografts. *Mol. Cancer Ther.* **2004,** *3*, 1427-1438.

44. O'Leary, B.; Finn, R. S.; Turner, N. C., Treating cancer with selective CDK4/6 inhibitors. *Nature Reviews Clinical Oncology* **2016,** *13*, 417-430.

45. Klein, M. E.; Kovatcheva, M.; Davis, L. E.; Tap, W. D.; Koff, A., CDK4/6 Inhibitors: The Mechanism of Action May Not Be as Simple as Once Thought. *Cancer Cell* **2018,** *34*, 9-20.

46. Xu, H. X.; Yu, S. N.; Liu, Q.; Yuan, X.; Mani, S.; Pestell, R. G.; Wu, K. M., Recent advances of highly selective CDK4/6 inhibitors in breast cancer. *Journal of Hematology & Oncology* **2017,** *10*.

47. Sumranjit, J.; Chung, S. J., Recent advances in target characterization and identification by photoaffinity probes. *Molecules* **2013,** *18* (9), 10425-10451.

48. Lapinsky, D. J., Tandem photoaffinity labeling-bioorthogonal conjugation in medicinal chemistry. *Bioorg. Med. Chem.* **2012,** *20*, 6237-6247.

49. Park, J.; Koh, M.; Koo, J. Y.; Lee, S.; Park, S. B., Investigation of Specific Binding Proteins to Photoaffinity Linkers for Efficient Deconvolution of Target Protein. *ACS Chem. Biol.* **2016,** *11* (1), 44-52.

50. Meldal, M.; Tornoe, C. W., Cu-Catalyzed Azide-Alkyne Cycloaddition. *Chem. Rev.* **2008,** *108*, 2952-3015.

51. Kolb, H. C.; Finn, M. G.; Sharpless, K. B., Click Chemistry: Diverse Chemical Function from a Few Good Reactions. *Angew. Chem. Int. Ed.* **2001,** *40*, 2004-21.

52. Stromgaard, K.; Saito, D. R.; Shindou, H.; Ishii, S.; Shimizu, T.; Nakanishi, K., Ginkgolide Derivatives for Photolabeling Studies: Preparation and Pharmacological Evaluation. *J. Med. Chem.* **2002,** *45*, 4038-4046.

53. Krishnamurthy, V. M.; Kaufman, G. K.; Urbach, A. R.; Gitlin, I.; Gudiksen, K. L.; Weibel, D. B.; Whitesides, G. M., Carbonic Anhydrase as a Model for Biophysical and Physical-Organic Studies of Proteins and Protein-Ligand Binding. *Chem. Rev.* **2008,** *108* (3), 946-1051.

54. Swietach, P.; Vaughan-Jones, R. D.; Harris, A. L., Regulation of tumor pH and the role of carbonic anhydrase 9. *Cancer and Metastasis Reviews* **2007,** *26*, 299-310.

55. Thiry, A.; Dogne, J.-M.; Masereel, B.; Supuran, C. T., Targeting tumor-associated carbonic anhydrase IX in cancer therapy. *Trends Pharmacol. Sci.* **2006,** *27* (11), 566-573.

56. Krall, N.; Pretto, F.; Neri, D., A bivalent small molecule-drug conjugate directed against carbonic anhydrase IX can elicit complete tumour regression in mice. *Chem. Sci.* **2014,** *5*, 3640-3644.

57. Krall, N.; Pretto, F.; Decurtins, W.; Bernardes, G. J. L.; Supuran, C. T.; Neri, D., A small-molecule drug conjugate for the treatment of carbonic anhydrase IX expressing tumors. *Angew. Chem., Int. Ed.* **2014,** *53* (16), 4231-4235.

58. Li, Y.; Wang, H.; Oosterwijk, E.; Tu, C.; Shiverick, K. T.; Silverman, D. N.; Frost, S. C., Expression and Activity of Carbonic Anhydrase IX Is Associated With Metabolic Dysfunction in MDA-MB-231 Breast Cancer Cells. *Cancer Investigation* **2009,** *27*, 613-623.

59. Brahimi, F.; Ko, E.; Malakhov, A.; Burgess, K.; Saragovi, H. U., Combinatorial assembly of small molecules into bivalent antagonists of TrkC or TrkA receptors. *PLoS One* **2014,** *9* (3), e89617/1-e89617/12.

60. Kamkaew, A.; Li, F.; Li, Z.; Burgess, K., An agent for optical imaging of TrkC-expressing, breast cancer. *MedChemComm* **2017,** *8*, 1946-1952.

61. Kumar, N. S.; Young, R. N., Design and synthesis of an all-in-one 3-(1,1-difluoroprop-2-ynyl)-3H-diazirin-3-yl functional group for photo-affinity labeling. *Bioorg. Med. Chem.* **2009,** *17* (15), 5388-5395.

62. Li, Z.; Hao, P.; Li, L.; Tan, C. Y. J.; Cheng, X.; Chen, G. Y. J.; Sze, S. K.; Shen, H.-M.; Yao, S. Q., Design and Synthesis of Minimalist Terminal Alkyne-Containing Diazirine Photo-Crosslinkers and Their Incorporation into Kinase Inhibitors for Cell- and Tissue-Based Proteome Profiling. *Angew. Chem., Int. Ed.* **2013,** *52* (33), 8551-8556.

63. Chari, R. V. J.; Miller, M. L.; Widdison, W. C., Antibody-Drug Conjugates: An Emerging Concept in Cancer Therapy. *Angew. Chem., Int. Ed.* **2014,** *53*, 3796-3827.

64. Kamkaew, A.; Li, F.; Li, Z.; Burgess, K., An Agent for Optical Imaging of TrkC-Expressing, Metastic Breast Cancer. *MedChemComm* **2017,** *8*, 1946-1952.

65. Zhao, B.; Burgess, K., Click-Addressable Cassette for Photoaffinity Labeling. *ACS Med. Chem. Lett.* **2018,** *9*, 155-158.

66. Yang, Z.; Usama, S. M.; Li, F.; Burgess, K.; Li, Z., A Zwitterionic Near-infrared Dye Linked TrkC Targeting Agent for Imaging Metastatic Breast Cancer. *MedChemComm* **2018,** *9*, 1754-1760.

67. Jin, W.; Kim, G.-M.; Kim, M.-S.; Lim, M.-H.; Yun, C.-H.; Jeong, J.; Nam, J.-S.; Kim, S.-J., TrkC plays an essential role in breast tumor growth and metastasis. *Carcinogenesis* **2010,** *31* (11), 1939-1947.

68. Wu, P.; Nielsen, T. E.; Clausen, M. H., Small-molecule kinase inhibitors: an analysis of FDA-approved drugs. *Drug Discov Today* **2016,** *21* (1), 5-10.

69. Usama, S. M.; Zhao, B.; Burgess, K., A Near-IR Fluorescent Dasatinib Derivative That Localizes in Cancer Cells. *Bioconjugate Chem.* **2019,** *30*, 1175-1181.

70. Bulatov, E.; Ciulli, A., Targeting Cullin-RING E3 ubiquitin ligases for drug discovery: structure, assembly and small-molecule modulation. *Biochem. J.* **2015,** *467* (3), 365-386.

71. Zhao, B.; Burgess, K., PROTACs Suppression Of CDK4/6, Crucial Kinases For Cell Cycle Regulation In Cancer. *Chem. Comm.* **2019,** *55*, 2704-2707.

72. Li, N.-S.; Gossai, N. P.; Naumann, J. A.; Gordon, P. M.; Piccirilli, J. A., Efficient Synthetic Approach to Linear Dasatinib-DNA Conjugates by Click Chemistry. *Bioconjugate Chem.* **2016,** *27*, 2575-2579.

73. Paunescu, E.; Clavel, C. M.; Nowak-Sliwinska, P.; Griffioen, A. W.; Dyson, P. J., Improved Angiostatic Activity of Dasatinib by Modulation with Hydrophobic Chains. *ACS Med. Chem. Lett.* **2015,** *6*, 313-317.

74. Kim, M. S.; Jeong, J.; Seo, J.; Kim, H.-S.; Kim, S.-J.; Jin, W., Dysregulated JAK2 expression by TrkC promotes metastasis potential, and EMT program of metastatic breast cancer. *Scientific Reports* **2016,** *6*, 33899.

75. Buettner, R.; Mesa, T.; Vultur, A.; Lee, F.; Jove, R., Inhibition of Src family kinases with dasatinib blocks migration and invasion of human melanoma cells. *Molecular Cancer Research* **2008,** *6*, 1766-1774.

76. Lewis-Tuffin, L. J.; Feathers, R.; Hari, P.; Durand, N.; Li, Z.; Rodriguez, F. J.; Bakken, K.; Carlson, B.; Schroeder, M.; Sarkaria, J. N.; Anastasiadis, P. Z., Src family

kinases differentially influence glioma growth and motility. *Molecular Oncology* **2015,** *9*, 1783-1798.

77. Li, W.; Gao, C.; Zhao, L.; Yuan, Z.; Chen, Y.; Jiang, Y., Phthalimide conjugations for the degradation of oncogenic PI3K. *Eur. J. Med. Chem.* **2018,** *151*, 237-247.

78. Schneekloth, A. R.; Pucheault, M.; Tae, H. S.; Crews, C. M., Targeted intracellular protein degradation induced by a small molecule: En route to chemical proteomics. *Bioorg. Med. Chem. Lett.* **2008,** *18* (22), 5904-5908.

79. Witkiewicz, A. K.; Chung, S.; Brough, R.; Vail, P.; Franco, J.; Lord, C. J.; Knudsen, E. S., Targeting the Vulnerability of RB Tumor Suppressor Loss in Triple-Negative Breast Cancer. *Cell Reports* **2018,** *22*, 1185-1199.

80. Xu, H.; Yu, S.; Liu, Q.; Yuan, X.; Mani, S.; Pestell, R. G.; Wu, K., Recent advances of highly selective CDK4/6 inhibitors in breast cancer. *J Hematol Oncol* **2017,** *10* (1), 97.

81. Bondeson, D. P.; Mares, A.; Smith, I. E.; Ko, E.; Campos, S.; Miah, A. H.; Mulholland, K. E.; Routly, N.; Buckley, D. L.; Gustafson, J. L.; Zinn, N.; Grandi, P.; Shimamura, S.; Bergamini, G.; Faelth-Savitski, M.; Bantscheff, M.; Cox, C.; Gordon, D. A.; Willard, R. R.; Flanagan, J. J.; Casillas, L. N.; Votta, B. J.; den Besten, W.; Famm, K.; Kruidenier, L.; Carter, P. S.; Harling, J. D.; Churcher, I.; Crews, C. M., Catalytic in vivo protein knockdown by small-molecule PROTACs. *Nat Chem Biol* **2015,** *11* (8), 611-7.

82. Robb, C. M.; Contreras, J. I.; Kour, S.; Taylor, M. A.; Abid, M.; Sonawane, Y. A.; Zahid, M.; Murry, D. J.; Natarajan, A.; Rana, S., Chemically induced degradation of CDK9 by a proteolysis targeting chimera (PROTAC). *Chem. Commun.* **2017,** *53*, 7577-7580.

83. Hatcher, J. M.; Wang, E. S.; Johannessen, L.; Kwiatkowski, N.; Sim, T.; Gray, N. S., Development of Highly Potent and Selective Steroidal Inhibitors and Degraders of CDK8. *ACS Med. Chem. Lett.* **2018,** *9*, 540-545.

84. Wolenski, F. S.; Fisher, C. D.; Sano, T.; Wyllie, S. D.; Cicia, L. A.; Gallacher, M. J.; Baker, R. A.; Kirby, P. J.; Senn, J. J., The NAE inhibitor pevonedistat (MLN4924) synergizes with TNF-alpha to activate apoptosis. *Cell Death Discov* **2015,** *1*, 15034.

85. Lee, D. H.; Goldberg, A. L., Proteasome inhibitors: valuable new tools for cell biologists. *Trends Cell Biol* **1998,** *8* (10), 397-403.

86. Yoshida, A.; Diehl, J. A., CDK4/6 inhibitor: from quiescence to senescence. *Oncoscience* **2015,** *2* (11), 896-7.

87. Yang, K.; Song, Y.; Xie, H.; Wu, H.; Wu, Y.-T.; Leisten, E. D.; Tang, W., Development of the first small molecule histone deacetylase 6 (HDAC6) degraders. *Bioorg. Med. Chem. Lett.* **2018,** *28*, 2493-2497.

88. Yu, Z.; Wu, L.; Yao, W. Heterocyclic compounds as immunomodulators and their preparation. 2017-US41899
2018013789, 20170713., 2018.

89. Zhang, C.; Han, X. R.; Yang, X.; Jiang, B.; Liu, J.; Xiong, Y.; Jin, J., Proteolysis Targeting Chimeras (PROTACs) of Anaplastic Lymphoma Kinase (ALK). *Eur J Med Chem* **2018,** *151*, 304-314.

90. Schiedel, M.; Herp, D.; Hammelmann, S.; Swyter, S.; Lehotzky, A.; Robaa, D.; Olah, J.; Ovadi, J.; Sippl, W.; Jung, M., Chemically Induced Degradation of Sirtuin 2 (Sirt2) by a Proteolysis Targeting Chimera (PROTAC) Based on Sirtuin Rearranging Ligands (SirReals). *J Med Chem* **2018,** *61* (2), 482-491.

91. Buhimschi, A. D.; Armstrong, H. A.; Toure, M.; Jaime-Figueroa, S.; Chen, T. L.; Lehman, A. M.; Woyach, J. A.; Johnson, A. J.; Byrd, J. C.; Crews, C. M., Targeting the C481S Ibrutinib-Resistance Mutation in Bruton's Tyrosine Kinase Using PROTAC-Mediated Degradation. *Biochemistry* **2018,** *57*, 3564-3575.

92. Das, J., Aliphatic Diazirines as Photoaffinity Probes for Proteins: Recent Developments. *Chem. Rev.* **2011,** *111*, 4405-4417.

93. Jiang, B. S.; Wang, E. S.; Donovan, K. A.; Liang, Y. K.; Fischer, E. S.; Zhang, T. H.; Gray, N. S., Development of Dual and Selective Degraders of Cyclin-Dependent Kinases 4 and 6. *Angew Chem Int Edit* **2019,** *58* (19), 6321-6326.

94. Rana, S.; Bendjennat, M.; Kour, S.; King, H. M.; Kizhake, S.; Zahid, M.; Natarajan, A., Selective Degradation of CDK6 by a palbociclib based PROTAC. *Bioorg. Med. Chem. Lett.* **2019,** *29*, 1375-1379.

95. Su, S.; Yang, Z. M.; Gao, H. Y.; Yang, H. Y.; Zhu, S. B.; An, Z. X.; Wang, J. J.; Li, Q.; Chandarlapaty, S.; Deng, H. T.; Wu, W.; Rao, Y., Potent and Preferential

Degradation of CDK6 via Proteolysis Targeting Chimera Degraders. *Journal of Medicinal Chemistry* **2019,** *62* (16), 7575-7582.

96. Brand, M.; Jiang, B.; Bauer, S.; Donovan, K. A.; Liang, Y.; Wang, E. S.; Nowak, R. P.; Yuan, J. C.; Zhang, T.; Kwiatkowski, N.; Mueller, A. C.; Fischer, E. S.; Gray, N. S.; Winter, G. E., Homolog-Selective Degradation as a Strategy to Probe the Function of CDK6 in AML. *Cell Chemical Biology* **2019,** *26* (2), 300-306 e9.

97. Mueller, M. P.; Rauh, D., Try Me: Promiscuous Inhibitors Still Allow for Selective Targeted Protein Degradation. *Cell Chemical Biology* **2018,** *25*, 4-6.

98. Bondeson, D. P.; Smith, B. E.; Burslem, G. M.; Buhimschi, A. D.; Hines, J.; Jaime-Figueroa, S.; Wang, J.; Hamman, B. D.; Ishchenko, A.; Crews, C. M., Lessons in PROTAC Design from Selective Degradation with a Promiscuous Warhead. *Cell Chemical Biology* **2018,** *25*, 78-87 e5.

99. Patel, P.; Tsiperson, V.; Gottesman, S. R. S.; Somma, J.; Blain, S. W., Dual Inhibition of CDK4 and CDK2 via Targeting p27 Tyrosine Phosphorylation Induces a Potent and Durable Response in Breast Cancer Cells. *Molecular Cancer Research* **2018,** *16*, 361-377.

100. Walter, D. M.; Yates, T. J.; Ruiz-Torres, M.; Kim-Kiselak, C.; Gudiel, A. A.; Deshpande, C.; Wang, W. Z.; Cicchini, M.; Stokes, K. L.; Tobias John, W.; Buza, E.; Feldser, D. M., RB constrains lineage fidelity and multiple stages of tumour progression and metastasis. *Nature* **2019,** *569*, 423-427.

101. Gonzalez-Vera, J. A., Probing the kinome in real time with fluorescent peptides. *Chem. Soc. Rev.* **2012,** *41*, 1652-1664.

102. Ethirajan, M.; Chen, Y.; Joshi, P.; Pandey, R. K., The Role of Porphyrin Chemistry in Tumor Imaging and Photodynamic Therapy. *Chem. Soc. Rev.* **2011,** *40*, 340-362.

103. Xu, C.; Webb, W. W., Measurement of two-photon excitation cross sections of molecular fluorophores with data from 690 to 1050 nm. *J. Opt. Soc. Am. B* **1996,** *13*, 481-491.

104. Sonnleitner, M.; Schutz, G. J.; Schmidt, T., Imaging individual molecules by two-photon excitation. *Chem. Phys. Lett.* **1999,** *300* (1,2), 221-226.

105. Deng, J.; Shao, J.; Markowitz, J. S.; An, G., ABC Transporters in Multi-Drug Resistance and ADME-Tox of Small Molecule Tyrosine Kinase Inhibitors. *Pharm. Res.* **2014,** *31*, 2237-2255.

106. Vetter, M. L.; Zhang, Z.; Liu, S.; Wang, J.; Cho, H.; Zhang, J.; Zhang, W.; Gray, N. S.; Yang, P. L., Fluorescent Visualization of Src by Using Dasatinib-BODIPY. *ChemBioChem* **2014,** *15*, 1317-1324.

107. Zhang, Z.; Kwiatkowski, N.; Zeng, H.; Lim, S. M.; Gray, N. S.; Zhang, W.; Yang, P. L., Leveraging kinase inhibitors to develop small molecule tools for imaging kinases by fluorescence microscopy. *Mol. BioSyst.* **2012,** *8*, 2523-2526.

108. Honigberg, L. A.; Smith, A. M.; Sirisawad, M.; Verner, E.; Loury, D.; Chang, B.; Li, S.; Pan, Z.; Thamm, D. H.; Miller, R. A.; Buggy, J. J., The Bruton tyrosine kinase inhibitor PCI-32765 blocks B-cell activation and is efficacious in models of autoimmune disease and B-cell malignancy. *Proc. Natl. Acad. Sci. U. S. A.* **2010,** *107*, 13075-13080, S13075/1-S13075/3.

109. Turetsky, A.; Kim, E.; Kohler, R. H.; Miller, M. A.; Weissleder, R., Single cell imaging of Bruton's Tyrosine Kinase using an irreversible inhibitor. *Scientific Reports* **2014,** *4*, 4782/1-4782/7.

110. Lee, S. Y.; Jang, C.; Lee, K. A., Polo-like kinases (plks), a key regulator of cell cycle and new potential target for cancer therapy. *Dev Reprod* **2014,** *18* (1), 65-71.

111. Shukla, S.; Skoumbourdis, A. P.; Walsh, M. J.; Hartz, A. M. S.; Fung, K. L.; Wu, C.-P.; Gottesman, M. M.; Bauer, B.; Thomas, C. J.; Ambudkar, S. V., Synthesis and Characterization of a BODIPY Conjugate of the BCR-ABL Kinase Inhibitor Tasigna (Nilotinib): Evidence for Transport of Tasigna and Its Fluorescent Derivative by ABC Drug Transporters. *Molecular Pharmaceutics* **2011,** *8*, 1292-1302.

112. Shukla, S.; Sauna, Z. E.; Ambudkar, S. V., Evidence for the interaction of imatinib at the transport-substrate site(s) of the multidrug-resistance-linked ABC drug transporters ABCB1 (P-glycoprotein) and ABCG2. *Leukemia* **2008,** *22* (2), 445-7.

113. Kwarcinski, F. E.; Brandvold, K. R.; Phadke, S.; Beleh, O. M.; Johnson, T. K.; Meagher, J. L.; Seeliger, M. A.; Stuckey, J. A.; Soellner, M. B., Conformation-Selective Analogues of Dasatinib Reveal Insight into Kinase Inhibitor Binding and Selectivity. *ACS Chem. Biol.* **2016,** *11*, 1296-1304.

114. Bhullar, K. S.; Lagaron, N. O.; McGowan, E. M.; Parmar, I.; Jha, A.; Hubbard, B. P.; Rupasinghe, H. P. V., Kinase-targeted cancer therapies: progress, challenges and future directions. *Molecular Cancer* **2018,** *17*, 48/1-48/20.

115. Ranjitkar, P.; Brock, A. M.; Maly, D. J., Affinity reagents that target a specific inactive form of protein kinases. *Chem. Biol.* **2010,** *17*, 195-206.

116. Okram, B.; Nagle, A.; Adrian, F. J.; Lee, C.; Ren, P.; Wang, X.; Sim, T.; Xie, Y.; Wang, X.; Xia, G.; Spraggon, G.; Warmuth, M.; Liu, Y.; Gray, N. S., A general strategy for creating "inactive-conformation" abl inhibitors. *Chem Biol* **2006,** *13* (7), 779-86.

117. Liu, Y.; Gray, N. S., Rational design of inhibitors that bind to inactive kinase conformations. *Nat Chem Biol* **2006,** *2* (7), 358-64.

118. Kim, D.; Jun, H.; Lee, H.; Hong, S.-S.; Hong, S., Development of new fluorescent xanthines as kinase inhibitors. *Org. Lett.* **2010,** *12*, 1212-1215.

119. Lee, J.-H.; Jung Kyung, H.; Lee, H.; Son Mi, K.; Yun, S.-M.; Hong, S.-S.; Ahn, S.-H.; Lee, K.-R.; Lee, S.; Kim, D.; Hong, S., HS-133, a novel fluorescent phosphatidylinositol 3-kinase inhibitor as a potential imaging and anticancer agent for targeted therapy. *Oncotarget* **2014,** *5*, 10180-97.

120. Kim, D.; Lee, H.; Jun, H.; Hong, S.-S.; Hong, S., Fluorescent phosphoinositide 3-kinase inhibitors suitable for monitoring of intracellular distribution. *Bioorg. Med. Chem.* **2011,** *19*, 2508-2516.

121. Sicard, R.; Dhuguru, J.; Liu, W.; Patel, N.; Landgraf, R.; Wilson James, N., A fluorescent reporter of ATP binding-competent receptor kinases. *Bioorganic & medicinal chemistry letters* **2012,** *22*, 5532-5535.

122. Dhuguru, J.; Liu, W.; Gonzalez, W. G.; Babinchak, W. M.; Miksovska, J.; Landgraf, R.; Wilson, J. N., Emission Tuning of Fluorescent Kinase Inhibitors: Conjugation Length and Substituent Effects. *J. Org. Chem.* **2014,** *79*, 4940-4947.

123. Lee, H.; Liu, W.; Brown, A. S.; Landgraf, R.; Wilson, J. N., Fluorescent Kinase Probes Enabling Identification and Dynamic Imaging of HER2(+) Cells. *Anal. Chem.* **2016,** *88*, 11310-11313.

124. Lee, H.; Landgraf, R.; Wilson, J. N., Synthesis and photophysical properties of a fluorescent cyanoquinoline probe for profiling ERBB2 kinase inhibitor response. *Bioorg. Med. Chem.* **2017,** *25*, 6016-6023.

125. Kim, E.; Yang, K. S.; Kohler, R. H.; Dubach, J. M.; Mikula, H.; Weissleder, R., Optimized Near-IR Fluorescent Agents for in Vivo Imaging of Btk Expression. *Bioconjugate Chem.* **2015,** *26*, 1513-1518.

126. Mikula, H.; Stapleton, S.; Kohler, R. H.; Vinegoni, C.; Weissleder, R., Design and development of fluorescent vemurafenib analogs for in vivo imaging. *Theranostics* **2017,** *7*, 1257-1265.

127. Zambon, A.; Niculescu-Duvaz, D.; Niculescu-Duvaz, I.; Marais, R.; Springer, C. J., BRAF as a therapeutic target: a patent review (2006 - 2012). *Expert Opin Ther Pat* **2013,** *23* (2), 155-64.

128. Miller, M. A.; Kim, E.; Cuccarese, M. F.; Plotkin, A. L.; Prytyskach, M.; Kohler, R. H.; Pittet, M. J.; Weissleder, R., Near infrared imaging of Mer tyrosine kinase (MERTK) using MERi-SiR reveals tumor associated macrophage uptake in metastatic disease. *Chem. Commun.* **2018,** *54*, 42-45.

129. Cummings, C. T.; Deryckere, D.; Earp, H. S.; Graham, D. K., Molecular pathways: MERTK signaling in cancer. *Clin Cancer Res* **2013,** *19* (19), 5275-80.

130. Liu, J.; Yang, C.; Simpson, C.; DeRyckere, D.; Van Deusen, A.; Miley, M. J.; Kireev, D.; Norris-Drouin, J.; Sather, S.; Hunter, D.; Korboukh, V. K.; Patel, H. S.; Janzen, W. P.; Machius, M.; Johnson, G. L.; Earp, H. S.; Graham, D. K.; Frye, S. V.; Wang, X., Discovery of Small Molecule Mer Kinase Inhibitors for the Treatment of Pediatric Acute Lymphoblastic Leukemia. *ACS Med. Chem. Lett.* **2012,** *3* (2), 129-134.

131. Song, X.; Han, X.; Yu, F.; Zhang, X.; Chen, L.; Lv, C., Polyamine-targeting gefitinib prodrug and its near-infrared fluorescent theranostic derivative for monitoring drug delivery and lung cancer therapy. *Theranostics* **2018,** *8,* 2217-2228.

132. Hoet, P. H.; Nemery, B., Polyamines in the lung: polyamine uptake and polyamine-linked pathological or toxicological conditions. *Am J Physiol Lung Cell Mol Physiol* **2000,** *278* (3), L417-33.

133. Gerner, E. W.; Meyskens, F. L., Jr., Polyamines and cancer: old molecules, new understanding. *Nat Rev Cancer* **2004,** *4* (10), 781-92.

134. Sos, M. L.; Koker, M.; Weir, B. A.; Heynck, S.; Rabinovsky, R.; Zander, T.; Seeger, J. M.; Weiss, J.; Fischer, F.; Frommolt, P.; Michel, K.; Peifer, M.; Mermel, C.; Girard, L.; Peyton, M.; Gazdar, A. F.; Minna, J. D.; Garraway, L. A.; Kashkar, H.; Pao, W.; Meyerson, M.; Thomas, R. K., PTEN Loss Contributes to Erlotinib Resistance in EGFR-Mutant Lung Cancer by Activation of Akt and EGFR. *Cancer Res.* **2009,** *69,* 3256-3261.

135. Yang, X.; Shi, C.; Tong, R.; Qian, W.; Zhau, H. E.; Wang, R.; Zhu, G.; Cheng, J.; Yang, V. W.; Cheng, T.; Henary, M.; Strekowski, L.; Chung, L. W. K., Near IR

Heptamethine Cyanine Dye-Mediated Cancer Imaging. *Clin. Cancer Res.* **2010,** *16*, 2833-2844.

136. Zang, C.; Long, L.; Shi, C., Mitochondria‐Targeting IR‐780 Dye and Its Derivatives: Synthesis, Mechanisms of Action, and Theranostic Applications. *Adv. Ther.* **2018,** *1*, 180069.1 - 180069.22.

137. Lin, C.-M.; Usama, S. M.; Burgess, K., Site-Specific Labeling of Proteins With Near-IR Dyes. *Molecules* **2018,** *23*, 2900.

138. Usama, S. M.; Lin, C.-M.; Burgess, K., On the Mechanisms of Update of Tumor-Seeking Cyanine Dyes. *Bioconjugate Chem.* **2018,** *29*, 3886-3895.

139. Canovas, C.; Bellaye, P.-S.; Moreau, M.; Romieu, A.; Denat, F.; Goncalves, V., Site-specific near-infrared fluorescent labelling of proteins on cysteine residues with meso-chloro-substituted heptamethine cyanine dyes. *Org. Biomol. Chem.* **2018,** *16*, 8831-8836.

140. Boobalan, R.; Liu, K.-K.; Chao, J.-I.; Chen, C., Synthesis and biological assay of erlotinib analogues and BSA-conjugated erlotinib analogue. *Bioorg. Med. Chem. Lett.* **2017,** *27*, 1784-1788.

141. Usama, S. M.; Park, G. K.; Nomura, S.; Baek, Y.; Choi, H.-S.; Burgess, K., Role Of Albumin Binding In Accumulation And Persistence Of Tumor-seeking Cyanine Dyes. *Bioconjug. Chem.* **2020**, preprint.

142. Liu, Z.; Chen, X., Simple bioconjugate chemistry serves great clinical advances: albumin as a versatile platform for diagnosis and precision therapy. *Chem. Soc. Rev.* **2016,** *45*, 1432-1456.

143. Stehle, G.; Sinn, H.; Wunder, A.; Schrenk, H. H.; Schutt, S.; Maier-Borst, W.; Heene, D. L., The loading rate determines tumor targeting properties of methotrexate-albumin conjugates in rats. *Anti-Cancer Drugs* **1997,** *8*, 677-685.

144. Noguchi, Y.; Wu, J.; Duncan, R.; Strohalm, J.; Ulbrich, K.; Akaike, T.; Maeda, H., Early phase tumor accumulation of macromolecules: a great difference in clearance rate between tumor and normal tissues. *Japanese Journal of Cancer Research* **1998,** *89* (3), 307-314.

145. Torchilin Vladimir, P., Passive and active drug targeting: drug delivery to tumors as an example. *Handbook of Experimental Pharmacology* **2010,** *197*, 3-53.

146. Heneweer, C.; Holland, J. P.; Divilov, V.; Carlin, S.; Lewis, J. S., Magnitude of enhanced permeability and retention effect in tumors with different phenotypes: 89Zr-albumin as a model system. *J. Nucl. Med.* **2011,** *52* (4), 625-633.

147. Lammers, T.; Kiessling, F.; Hennink, W. E.; Storm, G., Drug targeting to tumors: Principles, pitfalls and (pre-) clinical progress. *J. Controlled Release* **2012,** *161* (2), 175-187.

148. Levitt, D. G.; Levitt, M. D., Human serum albumin homeostasis: a new look at the roles of synthesis, catabolism, renal and gastrointestinal excretion, and the clinical value of serum albumin measurements. *International Journal of General Medicine* **2016,** *9*, 229-255.

149. Usama, S. M.; Jiang, Z.; Burgess, K., Conjugation Of Dasatinib With MHI-148 Has A Significant Advantageous Effect In Viability Assays For Glioblastoma Cells. *ChemMedChem* **2019,** *14*, 1575-1579.

150. Choi, P. J.; Denny, W. A.; Jose, J.; Cooper, E.; Schweder, P.; Mee, E.; Faull, R.; Dragunow, M.; Park, T. I. H., The synthesis of a novel Crizotinib heptamethine cyanine dye conjugate that potentiates the cytostatic and cytotoxic effects of Crizotinib in patient-derived glioblastoma cell lines. *Bioorg. Med. Chem. Lett.* **2019,** *29*, 2617-2621.

151. Jorge, S. E.; Schulman, S.; Freed, J. A.; Rangachari, D.; Kobayashi, S. S.; Huberman, M. S.; VanderLaan, P. A.; Costa, D. B., Responses to the multitargeted MET/ALK/ROS1 inhibitor crizotinib and co-occurring mutations in lung adenocarcinomas with MET amplification or MET exon 14 skipping mutation. *Lung cancer (Amsterdam, Netherlands)* **2015,** *90*, 369-74.

152. Nakada, M.; Kita, D.; Watanabe, T.; Hayashi, Y.; Teng, L.; Pyko, I. V.; Hamada, J.-i., Aberrant signaling pathways in glioma. *Cancers* **2011,** *3*, 3242-3278.

153. Liu, S.; Song, W.; Gao, X.; Su, Y.; Gao, E.; Gao, Q., Discovery of Nonpeptide, Reversible HER1/HER2 Dual-Targeting Small-Molecule Inhibitors as Near-Infrared Fluorescent Probes for Efficient Tumor Detection, Diagnostic Imaging, and Drug Screening. *Anal. Chem.* **2019,** *91*, 1507-1515.

154. Wang, M.; Tosi, U.; Wu Linda, Y.; Singh, R.; Kommidi, H.; Guo, H.; Law, B.; Ting, R.; Zhou, Z.; Schweitzer Melanie, E.; Souweidane Mark, M.; Hou, S., A Murine Model for Quantitative, Real-Time Evaluation of Convection-Enhanced Delivery (RT-CED) Using an (18)[F]-Positron Emitting, Fluorescent Derivative of Dasatinib. *Molecular Cancer Therapeutics* **2017,** *16*, 2902-2912.

155. Bobo, R. H.; Laske, D. W.; Akbasak, A.; Morrison, P. F.; Dedrick, R. L.; Oldfield, E. H., Convection-enhanced delivery of macromolecules in the brain. *Proc Natl Acad Sci U S A* **1994,** *91* (6), 2076-80.

156. Liu, Z.; Pourghiasian, M.; Radtke Mark, A.; Lau, J.; Pan, J.; Dias Gemma, M.; Yapp, D.; Lin, K.-S.; Benard, F.; Perrin David, M., An organotrifluoroborate for broadly applicable one-step (18) f-labeling. *Angew. Chem. Int. Ed.* **2014,** *53*, 11876-11880.

157. Perrin, D. M., [18F]-Organotrifluoroborates as Radioprosthetic Groups for PET Imaging: From Design Principles to Preclinical Applications. *Acc. Chem. Res.* **2016,** *49*, 1333-1343.

158. Tomas, A.; Futter, C. E.; Eden, E. R., EGF receptor trafficking: consequences for signaling and cancer. *Trends Cell Biol* **2014,** *24* (1), 26-34.

159. Yewale, C.; Baradia, D.; Vhora, I.; Patil, S.; Misra, A., Epidermal growth factor receptor targeting in cancer: a review of trends and strategies. *Biomaterials* **2013,** *34* (34), 8690-707.

160. Cheruku, R. R.; Cacaccio, J.; Durrani, F. A.; Tabaczynski, W. A.; Watson, R.; Marko, A.; Kumar, R.; El-Khouly, M. E.; Fukuzumi, S.; Missert, J. R.; Yao, R.; Sajjad, M.; Chandra, D.; Guru, K.; Pandey, R. K., Epidermal Growth Factor Receptor-Targeted Multifunctional Photosensitizers for Bladder Cancer Imaging and Photodynamic Therapy. *J. Med. Chem.* **2019,** *62*, 2598-2617.

161. Zhang, Y.; Tortorella, M. D.; Liao, J.; Qin, X.; Chen, T.; Luo, J.; Guan, J.; Talley, J. J.; Tu, Z., Synthesis and Evaluation of Novel Erlotinib-NSAID Conjugates as More Comprehensive Anticancer Agents. *ACS Med. Chem. Lett.* **2015,** *6*, 1086-1090.

162. Guiley, K. Z.; Stevenson, J. W.; Lou, K.; Barkovich, K. J.; Kumarasamy, V.; Wijeratne, T. U.; Bunch, K. L.; Tripathi, S.; Knudsen, E. S.; Witkiewicz, A. K.; Shokat, K. M.; Rubin, S. M., p27 allosterically activates cyclin-dependent kinase 4 and antagonizes palbociclib inhibition. *Science* **2019,** *366* (6471), eaaw2016, 1-12.

163. Hoet, P. H. M.; Nemery, B., Polyamines in the lung: polyamine uptake and polyamine-linked pathological or toxicological conditions. *Am. J. Physiol.* **2000,** *278*, L417-L433.

164. Gerner, E. W.; Meyskens, F. L., Jr., Polyamines and cancer: Old molecules, new understanding. *Nat. Rev. Cancer* **2004,** *4*, 781-792.

165. Jiang, Z.; Pflug, K.; Usama, S. M.; Kuai, D.; Yan, X.; Sitcheran, R.; Burgess, K., Cyanine-Gemcitabine Conjugates as Targeted Theranostic Agents for Glioblastoma Tumor Cells. *J. Med. Chem* **2019,** *62*, 9236-9245.

166. auf dem Keller, U.; Bellac, C. L.; Li, Y.; Lou, Y.; Lange, P. F.; Ting, R.; Harwig, C.; Kappelhoff, R.; Dedhar, S.; Adam, M. J.; Ruth, T. J.; Benard, F.; Perrin, D. M.; Overall, C. M., Novel Matrix Metalloproteinase Inhibitor [18F]Marimastat-Aryltrifluoroborate as a Probe for In vivo Positron Emission Tomography Imaging in Cancer. *Cancer Res.* **2010,** *70* (19), 7562-7569.

167. Li, Y.; Ting, R.; Harwig, C. W.; auf dem Keller, U.; Bellac, C. L.; Lange, P. F.; Inkster, J. A. H.; Schaffer, P.; Adam, M. J.; Ruth, T. J.; Overall, C. M.; Perrin, D. M., Towards kit-like 18F-labeling of marimastat, a noncovalent inhibitor drug for in vivo PET imaging cancer associated matrix metalloproteases. *MedChemComm* **2011,** *2*, 942-949.

168. Li, Y.; Liu, Z.; Harwig, C. W.; Pourghiasian, M.; Lau, J.; Lin, K.-S.; Schaffer, P.; Benard, F.; Perrin, D. M., 18F-click labeling of a bombesin antagonist with an alkyne-18F-ArBF3-: in vivo PET imaging of tumors expressing the GRP-receptor. *American Journal of Nuclear Medicine and Molecular Imaging* **2013,** *3*, 57-70.

169. Liu, Z.; Hundal-Jabal, N.; Wong, M.; Yapp, D.; Lin, K. S.; Benard, F.; Perrin, D. M., A new 18F-heteroaryltrifluoroborate radio-prosthetic with greatly enhanced stability that is labelled by 18F-19F-isotope exchange in good yield at high specific activity. *MedChemComm* **2014,** *5*, 171-179.

170. Liu, Z.; Lin, K.-S.; Benard, F.; Pourghiasian, M.; Kiesewetter, D. O.; Perrin, D. M.; Chen, X., One-step 18F labeling of biomolecules using organotrifluoroborates. *Nat. Protoc.* **2015,** *10* (9), 1423-1432.

171. Ametamey, S. M.; Honer, M.; Schubiger, P. A., Molecular Imaging with PET. *Chem. Rev.* **2008,** *108* (5), 1501-1516.

172. Pandey, S. K.; Gryshuk, A. L.; Sajjad, M.; Zheng, X.; Chen, Y.; Abouzeid, M. M.; Morgan, J.; Charamisinau, I.; Nabi, H. A.; Oseroff, A.; Pandey, R. K., Multimodality Agents for Tumor Imaging (PET, Fluorescence) and Photodynamic Therapy. A Possible "See and Treat" Approach. *J. Med. Chem.* **2005,** *48* (20), 6286-6295.

173. Abrahamse, H.; Hamblin, M. R., New photosensitizers for photodynamic therapy. *Biochem. J.* **2016,** *473*, 347-364.

174. Mehraban, N.; Freeman, H. S., Developments in PDT Sensitizers for Increased Selectivity and Singlet Oxygen Production. *Materials* **2015,** *8*, 4421-4456.

175. Knudsen, E. S.; O'Reilly, E. M.; Brody, J. R.; Witkiewicz, A. K., Genetic Diversity of Pancreatic Ductal Adenocarcinoma and Opportunities for Precision Medicine. *Gastroenterology* **2015**.

176. Vincent, A.; Herman, J.; Schulick, R.; Hruban, R. H.; Goggins, M., Pancreatic cancer. *Lancet* **2011,** *378* (9791), 607-20.

177. Paulson, A. S.; Tran Cao, H. S.; Tempero, M. A.; Lowy, A. M., Therapeutic advances in pancreatic cancer. *Gastroenterology* **2013,** *144* (6), 1316-26.

178. Kleger, A.; Perkhofer, L.; Seufferlein, T., Smarter drugs emerging in pancreatic cancer therapy. *Annals of oncology : official journal of the European Society for Medical Oncology / ESMO* **2014**.

179. Almhanna, K.; Philip, P. A., Defining new paradigms for the treatment of pancreatic cancer. *Curr Treat Options Oncol* **2011,** *12* (2), 111-25.

180. Philip, P. A.; Mooney, M.; Jaffe, D.; Eckhardt, G.; Moore, M.; Meropol, N.; Emens, L.; O'Reilly, E.; Korc, M.; Ellis, L.; Benedetti, J.; Rothenberg, M.; Willett, C.; Tempero, M.; Lowy, A.; Abbruzzese, J.; Simeone, D.; Hingorani, S.; Berlin, J.; Tepper, J., Consensus report of the national cancer institute clinical trials planning meeting on pancreas cancer treatment. *J Clin Oncol* **2009,** *27* (33), 5660-9.

181. Ottaiano, A.; Capozzi, M.; De Divitiis, C.; De Stefano, A.; Botti, G.; Avallone, A.; Tafuto, S., Gemcitabine mono-therapy versus gemcitabine plus targeted therapy in advanced pancreatic cancer: a meta-analysis of randomized phase III trials. *Acta Oncol* **2017,** *56* (3), 377-383.

182. Tadesse, S.; Caldon, E. C.; Tilley, W.; Wang, S., Cyclin-dependent kinase 2 inhibitors in cancer therapy: An update. *J. Med. Chem.* **2019,** *62*, 4233-4251.

183. Blain, S. W., Targeting p27 tyrosine phosphorylation as a modality to inhibit CDK4 and CDK2 and cause cell cycle arrest in breast cancer cells. *Oncoscience* **2018,** *5* (5-6), 144-145.

184. Alexander, L. T.; Mobitz, H.; Drueckes, P.; Savitsky, P.; Fedorov, O.; Elkins, J. M.; Deane, C. M.; Cowan-Jacob, S. W.; Knapp, S., Type II Inhibitors Targeting CDK2. *ACS Chem. Biol.* **2015,** *10* (9), 2116-2125.

185. Shen, W.; Tremblay, M. S.; Deshmukh, V. A.; Wang, W.; Filippi, C. M.; Harb, G.; Zhang, Y.-q.; Kamireddy, A.; Baaten, J. E.; Jin, Q.; Wu, T.; Swoboda, J. G.; Peters, E. C.; Cho, C. Y.; Li, J.; Laffitte, B. A.; McNamara, P.; Glynne, R.; Wu, X.; Herman, A. E.; Schultz, P. G., Small-Molecule Inducer of β Cell Proliferation Identified by High-Throughput Screening. *J. Am. Chem. Soc.* **2013,** *135* (5), 1669-1672.

186. Wang, Y.; Zhi, Y.; Jin, Q.; Lu, S.; Lin, G.; Yuan, H.; Yang, T.; Wang, Z.; Yao, C.; Ling, J.; Guo, H.; Li, T.; Jin, J.; Li, B.; Zhang, L.; Chen, Y.; Lu, T., Discovery of 4-((7H-Pyrrolo[2,3-d]pyrimidin-4-yl)amino)-N-(4-((4-methylpiperazin-1-yl)methyl)phenyl)-1H-pyrazole-3-carboxamide (FN-1501), an FLT3- and CDK-Kinase Inhibitor with Potentially High Efficiency against Acute Myelocytic Leukemia. *J. Med. Chem.* **2018,** *61*, 1499-1518.

187. Zhou, F.; Chen, L. Y.; Cao, C. G.; Yu, J.; Luo, X. J.; Zhou, P. T.; Zhao, L. F.; Du, W.; Cheng, J. J.; Xie, Y. M.; Chen, Y. W., Development of selective mono or dual

PROTAC degrader probe of CDK isoforms. *European Journal of Medicinal Chemistry* **2020,** *187*.

188. Zhang, C.; Liu, T.; Su, Y.; Luo, S.; Zhu, Y.; Tan, X.; Fan, S.; Zhang, L.; Zhou, Y.; Cheng, T.; Shi, C., A near-infrared fluorescent heptamethine indocyanine dye with preferential tumor accumulation for in vivo imaging. *Biomaterials* **2010,** *31*, 6612-6617.

189. Luo, S.; Yang, X.; Shi, C., Newly Emerging Theranostic Agents for Simultaneous Cancer targeted Imaging and Therapy. *Curr. Med. Chem.* **2016,** *23*, 483-497.

190. Gao, M.; Yu, F.; Lv, C.; Choo, J.; Chen, L., Fluorescent chemical probes for accurate tumor diagnosis and targeting therapy. *Chem. Soc. Rev.* **2017,** *46*, 2237-2271.

191. Tan, X.; Luo, S.; Wang, D.; Su, Y.; Cheng, T.; Shi, C., A NIR Heptamethine Dye With Intrinsic Cancer Targeting, Imaging and Photosensitizing Properties. *Biomaterials* **2012,** *33*, 2230-2239.

192. Thakkar, N.; Lockhart, A. C.; Lee, W., Role of Organic Anion-Transporting Polypeptides (OATPs) in Cancer Therapy. *AAPS Journal* **2015,** *17*, 535-545.

193. Kotsampasakou, E.; Ecker, G. F., Organic Anion Transporting Polypeptides as Drug Targets, in Transporters as Drug Targets. In *Transporters as Drug Targets*, Sitte, H. H.; Ecker, G. F.; Mannhold, R.; Buschmann, H.; Clausen, R. P., Eds. Wiley - VCH Verlag GmbH & Co. KGaA: 2017; pp 271 -324.

APPENDIX A

FLUORESCENT KINASE INHIBITORS AS PROBES

A.1 Introduction

There are more than 518 kinases in human kinome,[8] most having homologous kinase domains.[9] In cancer cells, various kinases are overexpressed or mutated to promote cell survival and propagation. Kinase inhibitors (KIs) are designed to selectively inhibit different kinases, hence they target specific mechanisms in tumor cells, over healthy tissue, to slow down cancer cell propagation and metastatic spread, often with less side-effects compared to broadly cytotoxic chemotherapeutic drugs. So far, 42 kinase inhibitors have been approved for various types of cancer (the following website can be used to keep track of progress in this regard www.brimr.org/PKI/PKIs and www.accessdata.fda.gov/ scripts/cder/daf/index.cfm). It is almost certain that more clinical candidates will be approved, and off-label applications will be found. Consequently, to facilitate these efforts, there is considerable interest in understanding aspects of the cell biology, pharmacokinetics (PK), and pharmacodynamics (PD) of KIs. Consequently, a field is emerging around fluorescently labelled KIs. In some cases, these probes can be used to study the biology of kinases, but in others conjugation of dyes can have unexpected, and potentially valuable effects. Fluorescently labelled KIs are the focus of this review. It excludes, however, peptidic chemosensors that, in many cases, change fluorescence on phosphorylation, without necessarily being kinase *inhibitors*. Those types of chemosensors, were reviewed in 2012[101] and are not covered here.

Optimal designs for tracking dye-labelled KIs are different for *in vitro*, cellular, and *in vivo* applications, so there is single KI-fluorophore probe type for all purposes (Figure A.1). Some studies prioritize minimal perturbation to the KI, and feature small fluorophores (sometimes abbreviated to "fluors" here). Small fluors, however, necessarily have short wavelength absorption and emission maxima, and that characteristic renders them inappropriate for *in vivo* studies, and sub-optimal for intracellular imaging. Other probes contain dyes that absorb and fluoresce beyond the range of intracellular autofluorescence (*ie* above 500 nm, and better >550 nm) that are suitable for confocal imaging. Even more extended near-IR fluorophores are favored for *in vivo* imaging where a key requirement is that light must permeation efficiently through tissue to excite the dye. Thus, absorption above approximately 750 nm wavelength is highly desirable for *in vivo* studies because, below that wavelength, dyes obscured by more than a few millimeters of tissue are hard to be excited even if powerful lasers are used. To calibrate, penetration of light of wavelength 800 nm is twice that of light of 630 nm.[102] *In vivo* imaging of fluorescent-KI probes requires larger dyes that tend to perturb the properties of the KI more than smaller fluorescent appendages, unless two-photon excitation[103-104] is used, and, as far as we are aware, no one has reported this for fluorescent-KI probes.

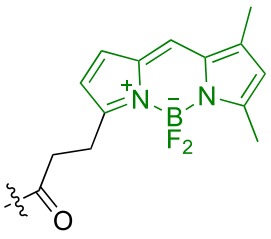

BODIPY

$\lambda_{max,abs}$ 503 nm, $\lambda_{max,em}$ 509 nm

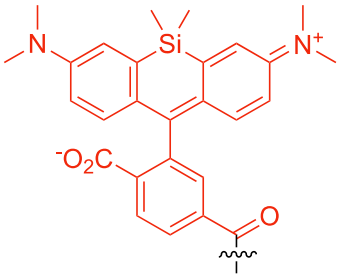

SiRh

$\lambda_{max,abs}$ 651 nm, $\lambda_{max,em}$ 671 nm

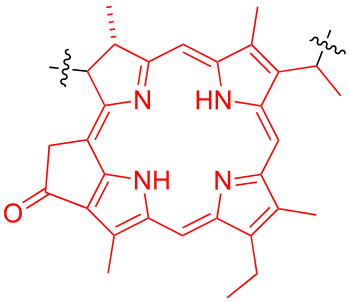

a porphyrin

$\lambda_{max,abs}$ ~665 nm, $\lambda_{max,em}$ ~670 nm

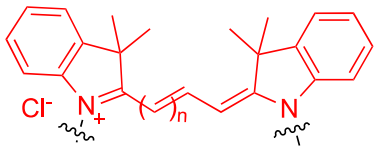

typical Cy3 and Cy5 cyanines

n = 1: Cy3, $\lambda_{max,abs}$ ~550 nm, $\lambda_{max,em}$ ~570 nm
n = 3: Cy5, $\lambda_{max,abs}$ ~650 nm, $\lambda_{max,em}$ ~675 nm

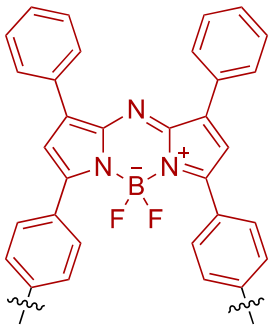

aza-BODIPY

$\lambda_{max,abs}$ 670 nm, $\lambda_{max,em}$ 730 nm

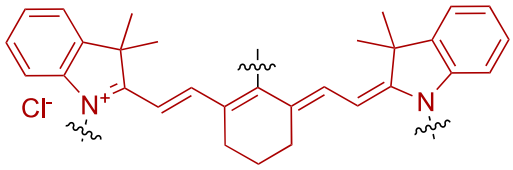

an extended heptamethine cyanine (Cy7)

$\lambda_{max,abs}$ ~780 nm, $\lambda_{max,em}$ ~800 nm

Figure A.1 Different types of fluorophores discussed in this review.

A.2 Probes for Cellular Uptake, Localization, and Efflux

A.2.1 Cellular Uptake and Localization

Small molecules can be endocytosed via various mechanisms, and pumped out of cells via pathways that may or may not be the same. For instance, KIs may passively diffuse into cells, and be effluxed via ATP-binding cassette (ABC) transporters.[105] This dynamic behavior means that observation of the amount of labeled substrate in a particular cell represents a snap-shot dynamic processes.

A.2.1.1 A Src Probe

Gray and Yang *et al* investigated dasatinib-BODIPY derivative **1** as a probe for intracellular imaging of its binding with Src.[106] As a prelude to those experiments, kinase binding and inhibition properties of **1** were validated via the Z'-Lyte kinase assay.[107] Z'-Lyte methodology is based on differential rates of proteolytic cleavage for peptides between the phosphorylated and non-phosphorylated states. Peptides modified to include donor-acceptor or donor-quencher FRET (Förster Resonance Energy Transfer) systems are cleaved rapidly in non-phosphorylated state, disrupting the energy transfer and giving a conspicuous spectroscopic change. Phosphorylation of the peptide impedes this process, hence the level of phosphorylation of the peptide can be quantitated.[107]

1

dasatinib (Sprycel®)

Src, BCR-Abl inhibitor

Formation of kinase-dye conjugates frequently results in reduced kinase inhibition and less potent effects on cell proliferation.[106] Z'-Lyte assays against ten known kinase targets of dasatinib showed **1** exhibited single-digit micromolar IC_{50}s against seven (including several Src family kinases); those values represent two- to ten-fold decreased activity compared to dasatinib. For instance, **1** exhibited a 40-fold decreased activity against Abl than dasatinib (Z'-Lyte), and it was 23x less active (IC_{50} = 47 nM) in a cell proliferation assay featuring BCR-Abl-transformed Ba/F3 cells than the parent KI (IC_{50} 2.1 nM). Conjugate **1** was not cytotoxic at concentrations <5 µM towards parental Ba/F3 cells that do not express BCR-Abl, excluding the possibility that cytotoxicity was unrelated to activation of BCR-Abl.

Next, net cellular uptake of **1** was determined using a hepatoma cell line Huh7, engineered to express a Src-mCherry fusion protein. Flow cytometry enabled counting of the cells showing fluorophores after treatment with **1**; high correlation of wavelengths corresponding to the mCherry(Src) and BODIPY channels were observed, suggesting the binding of probe to Src. That experiment alone does not report on selectivity of Src binding, because it does not exclude the possibility that **1** binds more than one intracellular protein; consequently, a control was necessary. Thus, the incubation and counting were

repeated using the parent inhibitor in a competitive experiment. That experiment showed fluorescence intensities declined significantly implying dasatinib and **1** compete for the same proteins, proving selective binding of the probe to the intended protein target (Figure A.2).

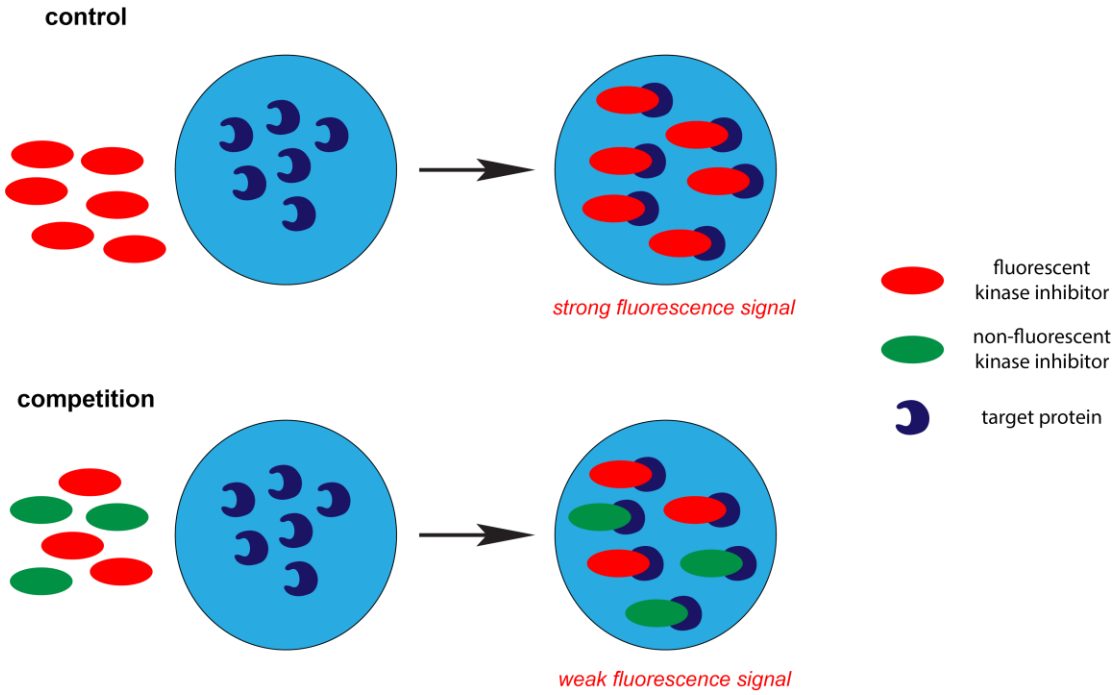

Figure A.2 Competitive binding of a dye-labeled kinase inhibitor to prove target selectivity.

A.2.1.2 Bruton's Tyrosine Kinase (Btk) Probes from Covalently Bound KIs

Rapid efflux from the cells is less likely for kinase inhibitors that covalently bind the target kinase. Consequently, probes based on irreversible kinase inhibitors resist wash out effects in cellular experiments, and have long residence times *in vivo*, making data

obtained from these easier to interpret than for non-covalent KI-dye probes that are necessarily more dynamic.

Ibrutinib (FDA approved for treatment of various forms of myeloma, leukemia and non-Hodgkin's lymphoma) inhibits Bruton's tyrosine kinase (Btk) by covalently binding a free Cys residue in that enzyme. Thus, Buggy's group made a fluorescent probe by attaching a linker between ibrutinib and BODIPY.[108] When the purified kinase, or a cell lysates containing it, were reacted with **2a**, fluorescent labeled Btk was observed via gel analyses. Btk-**2a** immunoprecipitation from the cell lysate was shown to deplete that protein.

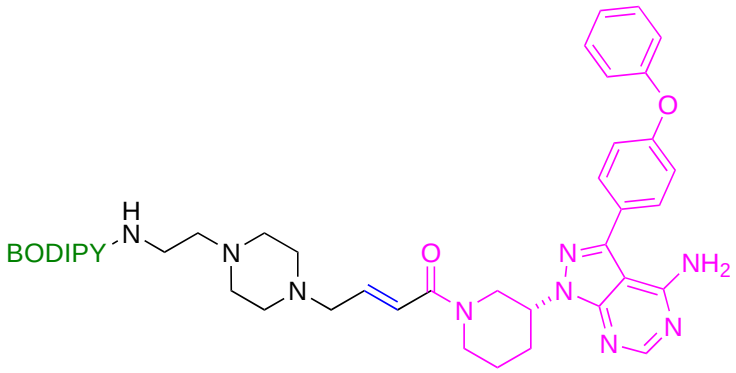

2a
ibrutinib (Imbruvica®)
Btk inhibitor

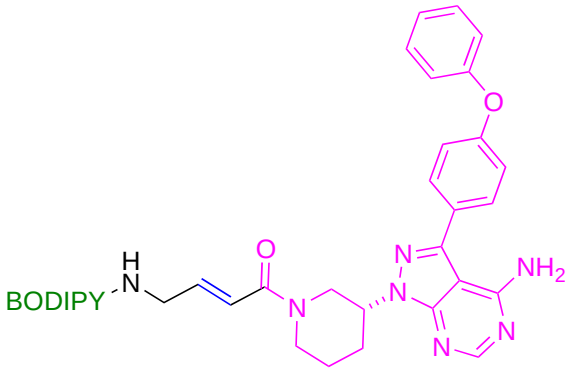

2b

companion diagnostic for flow cytometry in haematologic malignancies
imaging agent to localize and map Btk-positive tumors

After the work reported above, Weissleder's group prepared a labeled derivative **2b**, very similar to **2a**.[109] The IC_{50} of **2b** (~200 nM) was 100x inferior to that of the parent drug, but it still labeled Btk with high selectivity, presumably due to covalent binding. In flow cytometry to measure uptake, only cells that express this kinase were labeled, and that staining was blocked by the parent drug. Cells containing a Btk-mCherry fusion colocalized fluorescent protein and the BODIPY-fluorescence in flow analyses. Consequently, there is potential to use probe **2** as a diagnostic agent for hematologic malignancies via flow cytometry.

A.2.1.3 Probes for Polo-like kinases 1 - 3 (PLK1 - 3)

Polo-like kinases (PLK1 - 3) are thought to be concentrated in subcellular structures during mitosis. That location seems is consistent with the observation that phosphorylation of these kinases (on particular serine/threonine side-chains) regulates cell cycle progression.[110] Cyclin B is a mitotic marker and its concentration increases while

cell is going through mitosis. This motivated the combined groups of Gray and Yang to study inhibition of PLK1 - 3 using a BODIPY-functionalized derivative of BI2536 (inhibitor of PLK kinases),[107] *ie* probe **3**.

3
BI2536
PLK1-3 inhibitor
used to monitor localization of PLKs

Compound **3** was validated as a PLK probe by using the Z'-Lyte kinase assay to monitor enzyme activity, and detecting inhibition of the PLKs via Western blot. Probe **3** showed comparable binding and biochemical effects to the unlabeled inhibitor in these experiments. High and sustained cyclin B (mitotic marker) levels were observed when cell was treated with **3**, suggesting conjugating parent compound to dye can still induced a strong mitotic arrest and therefore does not significantly affect the cellular activity. In another experiment, the fluorescent KI was used to monitor localization of PLKs. Confocal microscopy experiments featuring probe **3** showed its localization in centrosomes (organelle involved in organizing microtubules), kinetochores (disc shaped protein assemblies where spindle fibers attach during cell division) and the mid-body of cells during telophase, and it overlapped with immunofluorescence staining of tubulin. In

a control competitive experiment, tubulin staining by probe **3** was disrupted in cells treated with excess BI2536, supporting the assertion that **3** selectively binds PLK kinases there.

A.2.2 Cellular Efflux

Labeled kinase probes facilitate monitoring of cell efflux, thus provide information on kinase inhibitor dynamics in and out of cells that would be difficult to obtain otherwise. ATP-binding cassette (ABC) transporters are ubiquitous in cellular efflux. Two well-known ABC transporters are P-glycoprotein (Pgp) and ABCG2.[105]

Ambudkar's group at National Institutes of Health made the BODIPY derivative **4** of the BCR-Abl inhibitor nilotinib. Nilotinib is FDA approved to treat drug-resistant chronic myelogenous leukemia (CML).[111] Compound **4** was validated as a probe by comparing its inhibition of BCR-Abl with the parent drug; it was less potent, but sufficiently active to inhibit BCR-Abl kinase activity in Western blotting. In flow cytometry, cells that express Pgp or ABCG2 retained significantly less of probe **4** than ones that have neither of these receptors. Moreover, cellular retention of **4** in Pgp^+ and $ABCG2^+$ cells was enhanced using inhibitors of these ABC transporters, implying **4** is pumped out via these pathways.

An *ex vivo* model was used to model efflux of **4** specifically at the blood brain barrier (BBB). Motivation for this experiment is that both Pgp^+ and $ABCG2^+$ limit movement of compounds across the membrane by efflux. In this model, freshly isolated rat brain capillaries incubated with **4** effluxed fluorescence of **4** via pathways that were inhibited by nilotinib. Efflux of **4** was inhibited by specific inhibitors of Pgp and ABCG2,

and it was shown that nilotinib and its fluorescent derivative bind at substrate binding site of Pgp and ABCG2.[112] Thus, nilotinib was shown to inhibit Pgp and ABCG2 but, surprisingly, not at the ATP-binding site of these transporter proteins.

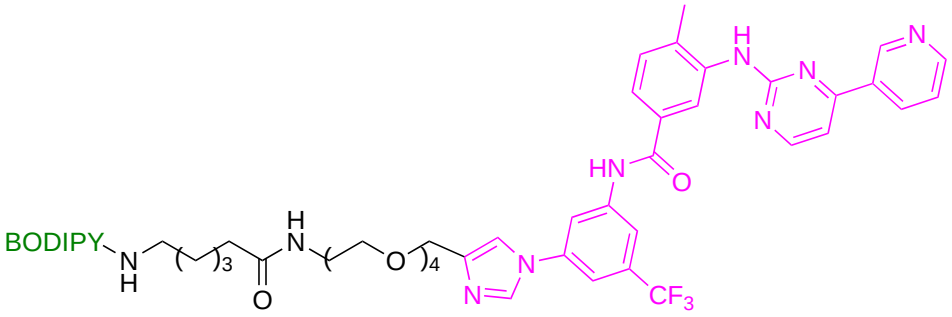

4
nilotinib (Tasigna®)
Bcr-Abl inhibitor
efflux of this probe observed from excised rat brain capiliaries

Incidentally, the authors of this study attempted to compare simulated physiochemical properties of their probes, but realized some computer programs used to do this are not parameterized for the *B-F* bonds of BODIPY dyes. Lack of parameterization is a trap that is relevant to simulations of physiochemical properties for other KI-BODIPY probes, and potentially for other containing molecular fragments not found in pharmaceuticals (*eg C – Si* bonds in SiRh dyes).

A.3 Probes of Kinase Conformations in Bound States

A.3.1 Some Essential Facets of Kinase Conformations

KIs can be classified in terms of conformations of kinases they bind to, or where and how they bind those enzymes. Type I inhibitors bind active kinase conformations in

the ATP pocket. Type II inhibitors bind various *inactive* conformations, including those classified as "DFG-out" and "αC-helix-out"). Type III inhibitors are non-ATP competitive inhibitors that bind sites adjacent the ATP binding pocket in ways that allow ATP and the KI to associate with the kinase simultaneously. Type IV inhibitors are allosteric ones that dock sites removed from the ATP binding site, and type V inhibitors bind covalently (Figure A.3a).[113-114]

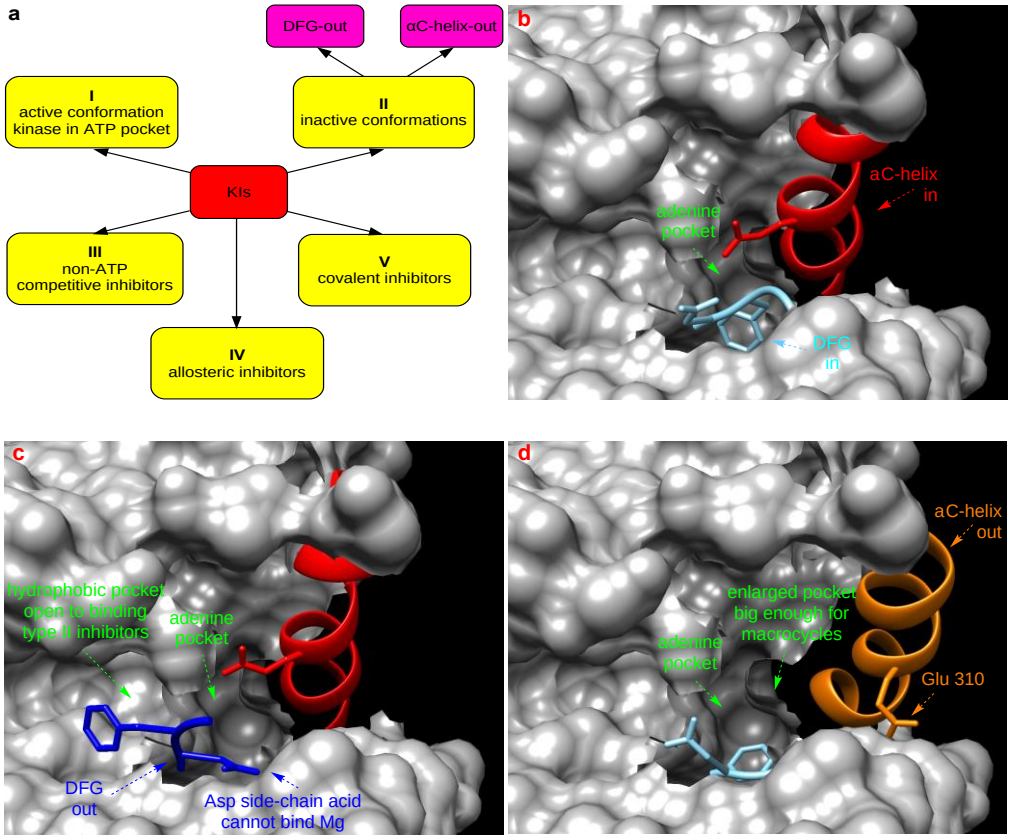

Figure A.3 (**a**) Different type of KIs. Structure of Src with kinase inhibitors in active (**b**, PDB: 3G5D), DFG-out (**c**, PDB: 4YBJ) and c-helix-out conformation (**d**, PDB: 4YBK). Type II inhibitors lead to DFG-out (dark blue) in contrast to DFG-in (light blue)

conformation. c-Helix-out inhibitors lead to αC-helix-out (orange) in contrast to αC-helix in (red) conformation. Small molecule ligands are excluded for simplicity.

Active conformations of kinases feature a DFG (Asp-Phe-Gly) motif pointing into the active site for Mg^{2+}/ATP coordination, and a salt bridge that is formed between the catalytic lysine and a glutamate in the αC-helix (Figure A.3b). Lack of selectivity for most type I inhibitors with respect to different kinases arises because of close similarities in the active conformations amongst all these enzymes. Conjugate **1** complexed with Src is an example of a type I inhibitor that features in this review.

Type II inhibitors bind inactive conformations that vary between kinases, and this variability tends to engender enhanced selectivities. Two inactive conformations that feature in this review are DFG-out (see Figure A.3c in dark blue) and αC-helix-out (Figure A.3d in orange).

DFG-out inactive conformations feature the DFG motif distal to the active site such that Mg^{2+} is prevented becoming coordinated with ATP and the nearby Asp of the kinase, thus suppressing capture and reactivity of ATP in the enzyme active site.[23,24] Transition of the DFG motif into this "out conformation" also exposes a hydrophobic pocket that then may be occupied by KI fragments. Enhanced selectivity of binding of type II KIs in many cases can be attributed to that hydrophobic pocket. Preclinical inhibitor **5**-H (based on the type I inhibitor dasatinib **1**, see above) exhibits this mode of binding to Src wherein the 3-trifluoromethylbenzamide fragment (colored blue above) occupies the newly exposed hydrophobic pocket.

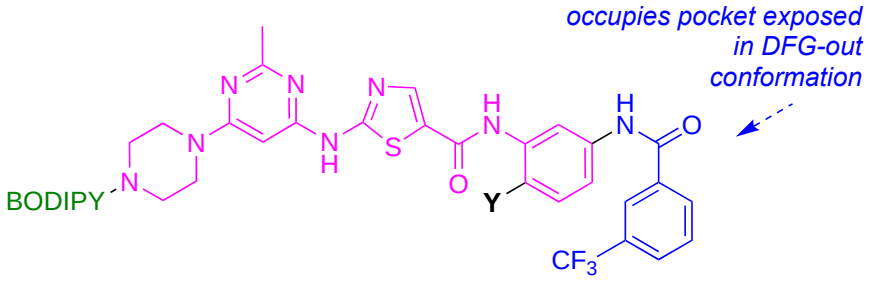

Y = H, **5**-H
= Me, **5**-Me
type II (DFG-out) Src inhibitor

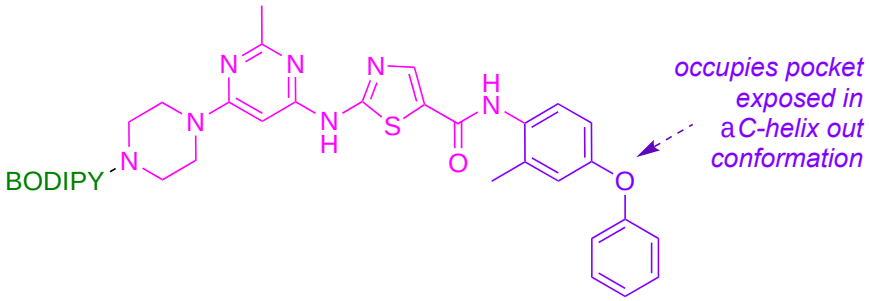

6
type II (aC-helix out) Src inhibitor

The αC-helix-out subset of type II inactive conformations have that helix rotated away from the kinase core. This orientation reorients a key glutamate to point away from active site, breaking the salt bridge between glutamate and catalytic lysine that is critical for the kinase activity (Figure A.3d). Twisting the αC-helix in this way extends the active site and creates a hydrophobic binding pocket which is large enough to favor docking of macrocyclic compounds. An inhibitor of this type featured in this review is ligand **6** bound to Src.

Type II KIs also tend to have longer residence times for kinase binding relative to type I inhibitors. Examples covered later in this review feature KI derivatives for which fluorescence changes can be linked with residence times, and therefore to modes of binding.

Type III (non-ATP competitive), IV (allosteric) and V (covalent) are more unique[114] and cannot be represented by generalized conformations. These types of inhibitors are not illustrated in Figure A.3.

A.3.2 Thermodynamic and Kinetic Parameters via Competitive Binding of Labeled and Unlabeled Kinases

A.3.2.1 Thermodynamic Parameters

In general, early steps in probe-validation for KI-dye conjugates tend to involve measurements or dissociation constants, and/or inhibition of kinase activities.

Dissociation constants for inhibitors bound to kinases can be measured by techniques generally used to track small molecules binding to proteins, *eg* isothermal calorimetry (ITC) or fluorescence polarization (FP, based on changes in fluorescence anisotropies). It should be possible to use FP to deduce K_d values for KI-dye•kinase complexes; this might be called *direct FP*. Direct FP apparently was *not* explored in any papers covered for this review, perhaps because comparative K_d measurements for the parent KIs could not be obtained in the same way (though competitive experiments are possible). Instead, researchers using KI-dye probes have tended to turn to commercial K_d determination methods, like the KINOME*scan*™. KINOME*scan*™ features

combinations of a DNA-tagged kinase, an immobilized, active-site directed ligand; abilities of test samples to compete with immobilized ligand are measured via quantitative PCR of the DNA-tagged kinase.

In any event, IC_{50}'s for enzyme inhibition by KIs are more informative than binding constants because they reveal biochemical effects. For instance, the KI **A** was shown to have IC_{50}'s <25 nM for seven kinases known to adopt DFG-out conformations, but for kinases that appear not to adopt DFG-out conformations the measured IC_{50} values were >1000 nM.[115] The inference of these experiments is **7** binds kinase in the DFG-out conformations, and that could not be surmised from K_d data. However, deconvoluting binding equilibrium constants to k_{on} and k_{off} can be revealing, and sometimes these kinetic parameters can be deduced from fluorescence changes of KI-dye substrates on dissociation from a kinase, as illustrated in the next section.

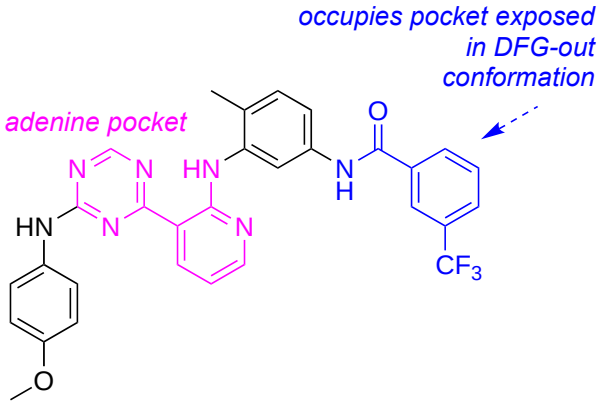

A
type II kinase inhibitor

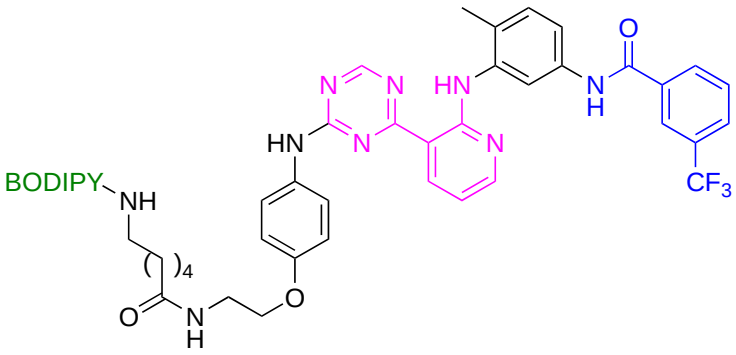

7

A.3.2.2 Kinetic Parameters

Use of fluorescent kinase inhibitor probes in *end point fluorescence assays* to measure kinetic binding parameters is illustrated in Figure A.4. KI **A** has molecular fragments that to bind the hydrophobic pocket exposed in DFG-out conformations and to the ATP binding site. It tends to bind DFG-out conformations of *many* kinases hence can be called a *general type II inhibitor*.[115]

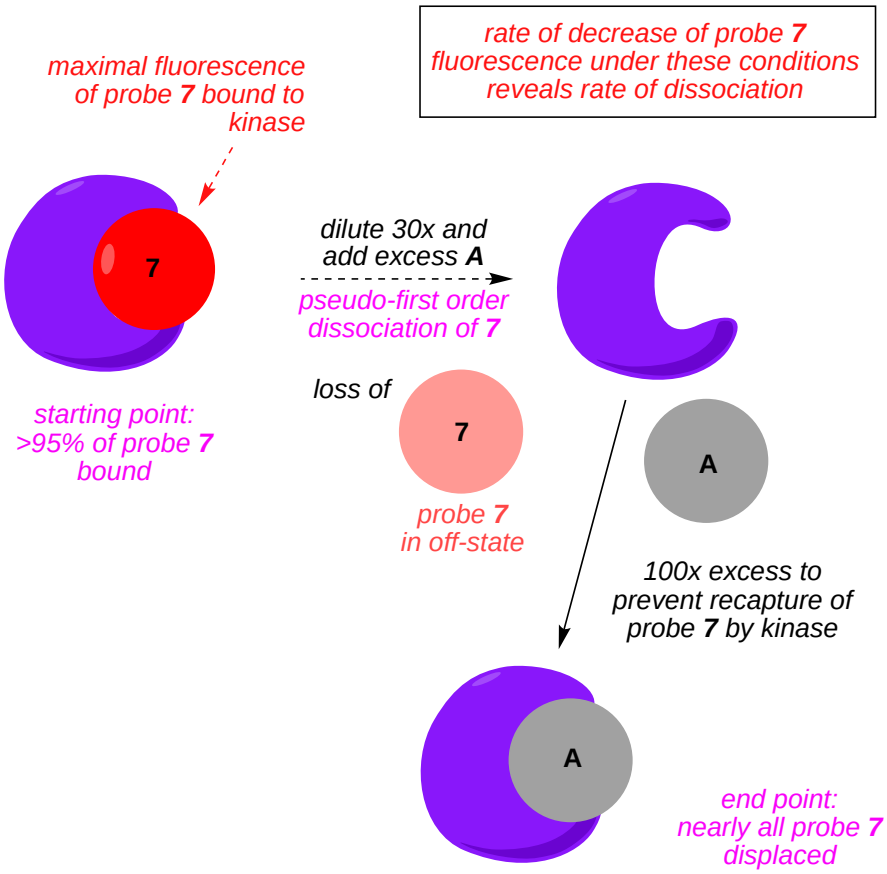

Figure A.4 Principle of end point fluorescence assay applied to kinase inhibitors.

Probe **7** (BODIPY functionalized **A**) binds kinases with similar affinities to the parent inhibitor **A**. The brilliance of **7** increases linearly with probe-to-kinase ratios (provided the kinase is not saturated), and, logically, this increase of fluorescence is competitively suppressed by the parent non-labeled inhibitor **A**. Consequently, when the kinase is pretreated with **A** then **7**, time dependent fluorescence changes of **7** can be used to reveal k_{off} values for **A**. Inhibitors that bind kinases in DFG-out conformations tend to have slow k_{off} rates. Consequently, end point fluorescence assays for probe **7** binding p38 and Abl should give slow off rates because the parent probe **A** is known to bind those

kinases in DFG-out conformations (k_{off} = 1.6 x 10^{-4} and 5.2 x 10^{-5} s^{-1} respectively). Kinases for which DFG-out conformations are unfavorable (*eg* CLK1 and MAP3K5) did not bind this probe with high affinity.

Soellner's group applied Gray's hybridization method (Figure A.5)[116-117] in which fragments that bind the ATP-binding active site are combined with others that bind a complementary hydrophobic pocket on inactive states, thus forcing the kinase into a DFG-out inactive conformation on binding.[25] Thus, this strategy guides modifications of type I inhibitors for transformation into type II. A similar approach can be applied to enforce αC-helix-out inactive conformation. Thus, Soellner's team amalgamated elements of dasatinib (type I) with imatinib (type II, DFG loop out) or a *para*-phenoxy group (known to induce type II αC-helix-out inactive conformers by displacing the ^{310}Glu residue of the helix), as already illustrated in Figure A.3. Consequently, they created inhibitors that bind the ATP binding site in either the DFG-out or αC-helix-out inactive conformers, respectively (Figure A.6a). These inhibitors do not contain a fluorescent label, but they went on to modify them to include one.

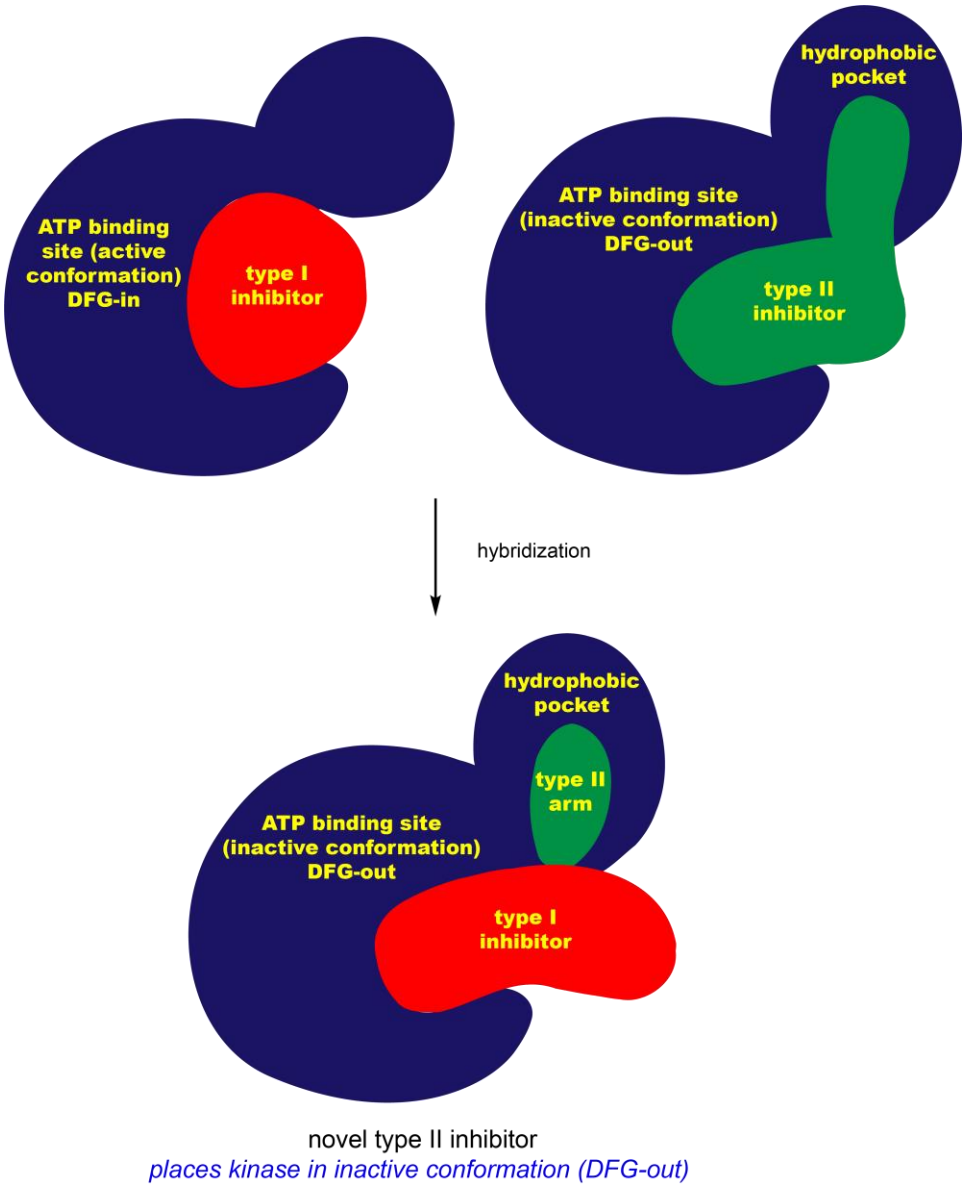

Figure A.5 Gray's hybridization concept.

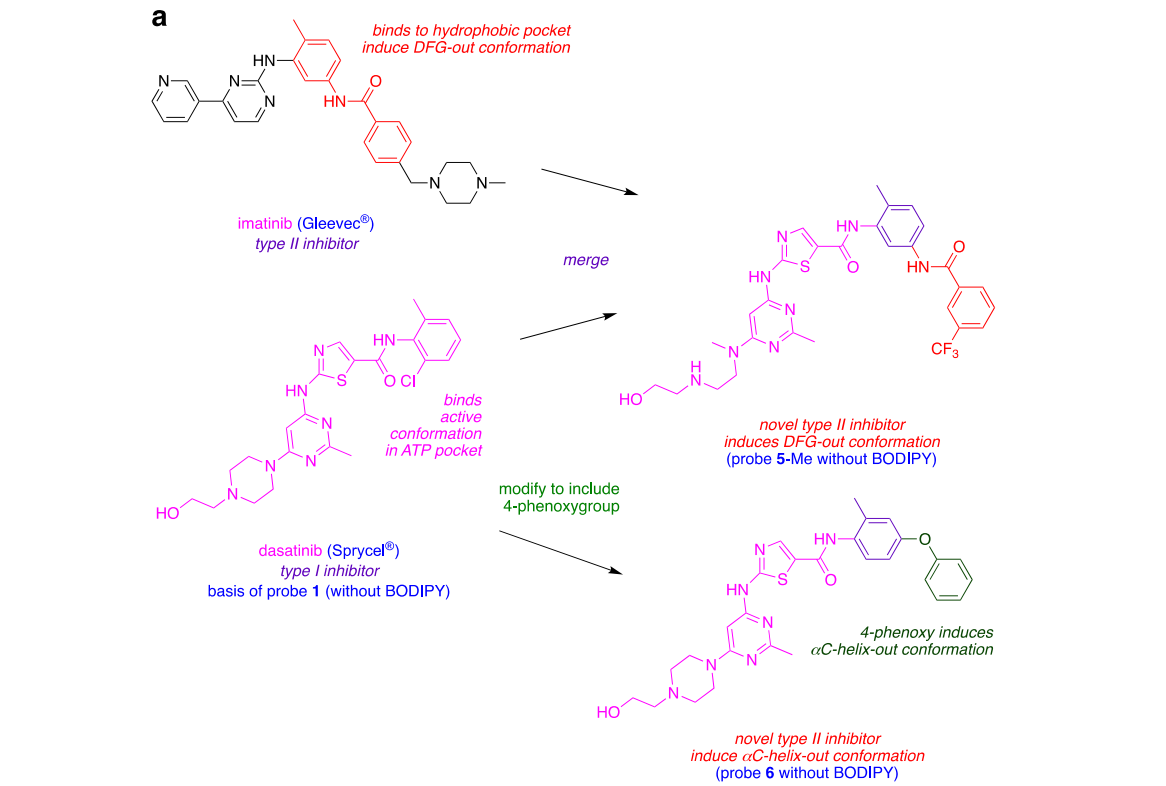

Figure A.6 (**a**) Design of novel type II inhibitors inducing DFG-out and αC-helix-out inactive conformations. Crystal structures of dasatinib (**b**) or its analogs (**c**, **d**) with Src in active (**b**, PDB: 3G5D), DFG-out (**c**, PDB: 4YBJ) and αC-helix-out (**d**, PDB: 4YBK) conformation. **c** Incorporation of trifluoromethyl benzamide group to dasatinib analog II inhibitors lead to DFG-out (dark blue) in contrast to DFG-in (light blue) conformation. **d** Incorporation of para-phenoxy group to dasatinib analog leads to αC-helix-out (orange) in contrast to αC-helix in (red) conformation.

When a BODIPY fragment was joined to the conjugates of dasatinib described above, this resulted in three probes. The first, **1**, binds to Src in its active conformation, the second, **5**, binds the same kinase in the DFG-out inactive conformation, and an αC-helix-out inactive conformation is bound the third, **6**. Dissociation constants with Src and Abl were checked to confirm affinities for the target kinases were acceptable after these modifications, and crystallographic studies confirmed their solid-state bound conformations were consistent with the design expectations (Figure A.6b, 6c and 6d).

Probe **5** (the one giving the type II DFG out conformation) in fluorescent end point assays with Src and Abl showed their off-rates were slower than those expected for binding the type I conformation, so it was inferred that both kinases bound to **5** are in the type II conformation. Conversely, probes **1** and **6** (for the active and αC-helix-out conformations, respectively) had fast, dissociation kinetics, unlike type II DFG-out inhibitors. Off-rates for compounds that bind the αC-helix-out conformation were hitherto largely unknown; the inference of this study is that they are *fast* for this inhibitor bound to the type II αC-helix-out conformation.

Imatinib is a DFG-out type II inhibitor which binds Abl in preference to Src, and the reasons for this had been a subject of conjecture. An interpretation of imatinib preferentially binding Abl is that there may be an energetic penalty for Src to adopt the DFG-out conformation. To test this hypothesis, k_{on}, k_{off}, and K_d parameters were compared for Src bound to probes **1** (binds only active site) and **5**-Me (binds only DFG-out loop inactive conformation, and not the type I active state). Kinase domains of Abl

and Src interacting with each probe (**1** and **5**-Me) showed no significant kinetic or thermodynamic differences. Moreover, no significant difference was observed between Src kinase domain and Src full length construct. There were also no binding differences for probes **1** or **5**-Me to kinase domains of Src and to activation-loop-phosphorylated Src; consequently, these conformation-selective inhibitors did not exhibit an activation state bias. Overall, it appears from this data that there is no energetic penalty for Src to adopt the DFG-out conformation; instead, the implication is that imatinib simply does not bind the Src well.

A.3.3 Environments Elucidated via Solvatochromatic, Intrinsically Fluorescent KIs

A.3.3.1 Xanthine

If a KI is intrinsically fluorescent and solvatochromatic, as distinct from one attached to a solvatochromatic dye, then changes in its electronic spectra on interacting with a protein can be used to infer the environment the target KI. Hong's group at Korea Advanced Institute of Science and Technology developed xanthine derivatives, *eg* **8**,[118-120] that are intrinsically fluorescent and thought to target the ATP binding site. Compound **8** has undesirably short absorption and emission wavelength maxima ($\lambda_{max,abs}$ 338 nm, $\lambda_{max,em}$ 430 nm), but could be observed in cells via confocal microscopy after deconvoluting from cellular autofluorescence. Probe **8** was also observed, albeit extremely faintly, after direct injection into subcutaneous tumors in a murine model.

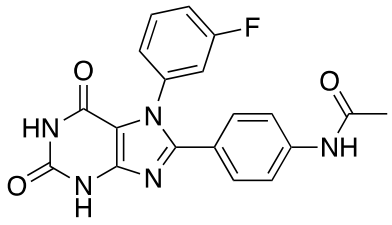

8

intrinsically fluorescent xanthine derivative inhibits PI3Kα

$\lambda_{max,abs}$ 338 nm, $\lambda_{max,em}$ 430 nm

Φ 0.12, IC_{50}(PI3Kα) 68 nM

A.3.3.2 Gefitinib Hybrids

In studying ERBB (human epidermal growth factor receptor) family of kinases, Wilson's group at University of Miami designed hybrids of gefitinib and a fluorescent push-pull stilbene derivative.[121,122] Like probe **8**, derivatives **9** and **10** can be excited at wavelengths used for common nuclear stains like DAPI (4′,6-diamidine-2′-phenylindole), *ie* using excitation wavelengths found on nearly all confocal microscopes. Molar absorbances of the dyes increase with the number of double bonds in conjugation, hence probes **10** tend to be brighter than **9**. Even though probe **10a** absorbs at a relatively short wavelength, it has a large Stokes' shift (absorbs at 391 nm, emits at 561 nm, in chloroform) and this characteristic in intracellular imaging compensates for the short $\lambda_{max\ abs}$.

Probes **9** – **11** have their high "turn-on" ratios. Thus, fluorescence of these probes is greatly enhanced in constrained, hydrophobic pockets of the ERBB receptors. Intracellular turn-on ratios on binding in this way to kinases can be anticipated from fluorescence enhancements measured for the probes in octanol over water ($I_{octanol}/I_{water}$) *in*

vitro. Among these probes, **10a** possesses the highest on/off ratio (> 50-fold); it is highly responsive to changes in the chemical microenvironment.

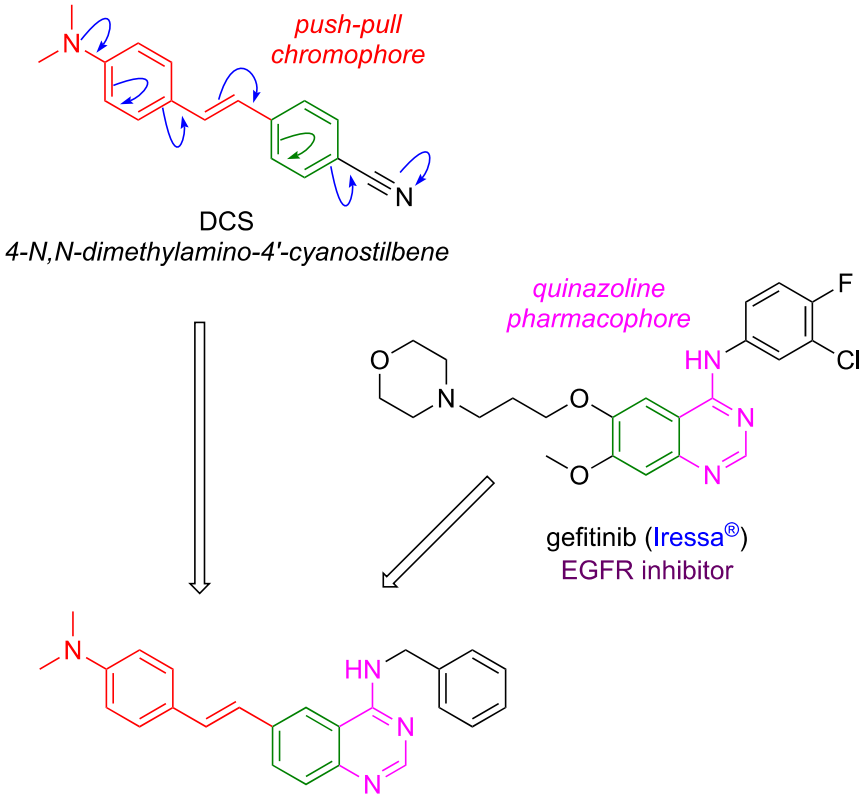

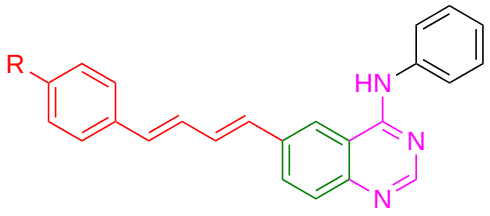

R= NO_2, **10a**, $\lambda_{max,abs}$ 391 nm, $\lambda_{max,em}$ 561 nm
F 0.11, turn-on ratio ~100-fold
R= CN, **10b**, $\lambda_{max,abs}$ 375 nm, $\lambda_{max,em}$ 445 nm
F 0.57, turn-on ratio ~40-fold
EGFR inhibitor

Turn on of fluorescence from probes **9** – **11** bound to the ERBB2 receptors was used to infer their mode of binding.[121] For example, in ERBB2 overexpressing BT474 cells, enhanced fluorescence of **9** correlated with inhibition of ERBB2 autophosphorylation. In a competition experiment, that fluorescent enhancement was quenched in the presence of an inhibitor that binds the ERBB2 active site.

All probes showed inhibition of phosphorylation of ERBB2 *in vitro* at 10 μM. However, in cells the probe with the longest emission maxima, **10b**, did not completely inhibit ERBB2 phosphorylation at concentrations <100 μM. Such inhibition means the probe is vulnerable to alternative modes of interaction with the kinase, binding to other proteins, and to displacement from the kinase via competitive binding of endogenous ATP. We posit it is also possible that electrophilicity of the double bonds in **10** could lead to formation of adducts with nucleophiles like glutathione causing loss of kinase affinity.

Modifications of the kinase inhibitors **9** and **10** led to improved systems **11**[123,124] that incorporate *N*-methyl piperazines in place of aryl amine moieties. These modifications gave more water-soluble probes that aggregate less, and this leads to increased brightness in cells. Secondly, the pharmacophore in **11b** was modified to favor type II inhibition while **11a** only binds the active conformation (type I).

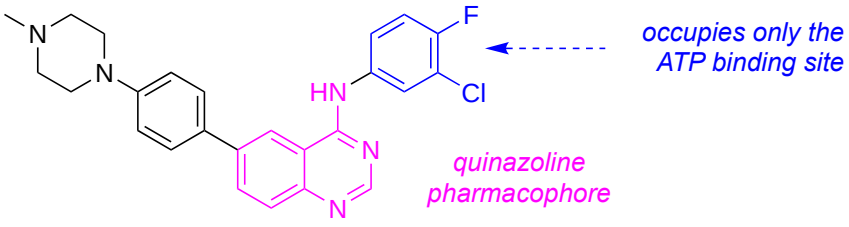

11a

$\lambda_{max,abs}$ 317 nm, $\lambda_{max,em}$ 487 nm, F 0.20

type I ERBB2 inhibitor

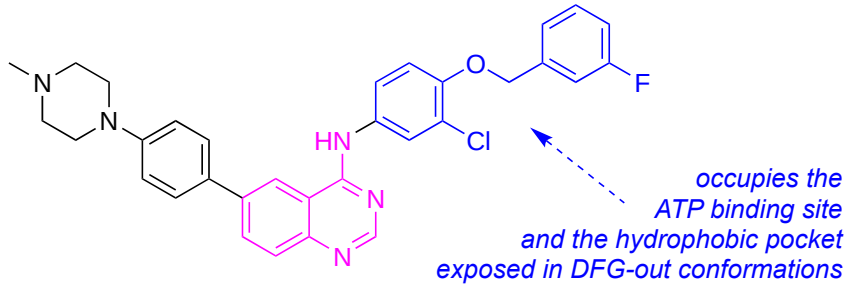

11b

$\lambda_{max,abs}$ 317 nm, $\lambda_{max,em}$ 475 nm, F 0.02

type II ERBB2 inhibitor

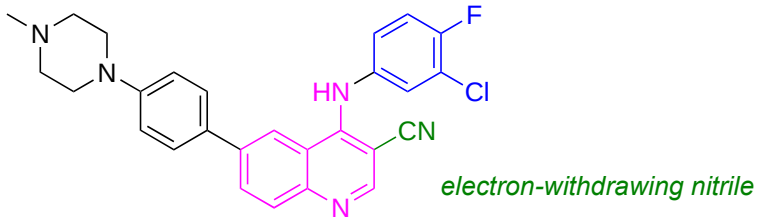

11c

$\lambda_{max,abs}$ 330 nm, $\lambda_{max,em}$ 530 nm, F 0.21

type II ERBB2 inhibitor

Overall, the optimized ligands **11a** (type I) and **11b** (type II) have K_i values comparable to FDA-approved type II inhibitor lapatinib. Both probes afford significant turn-on emission responses in the kinase domain (enhancements: 11x for **11a**, and 4x for

11b) and both were blue-shifted by ~40 nm. However, enhancement was not exclusively due to solvatochromic effects as seen by recording fluorescence intensities as a function of excitation wavelength, *ie* via excitation spectra. These spectra showed a significant emission corresponding to excitation at 280 nm which does *not* correspond to significant absorption by the dye. The authors attribute this observation to energy transfer from Trp and Tyr residues in the enzyme pocket to the probe.

Access to probes **11a** and **11b** facilitated detailed studies of the cancer cell biology of ERBB2 inhibition.[123] For instance, immunohistochemistry with an anti-ERBB2 mAb proved the probe colocalized with the ERBB2 receptor within the complex cell environment. Off rates for **11a** and **11b** in these experiments correlate with expectations for type I (fast) and type II (slow) inhibitors, respectively.

In a co-seeded breast cancer MCF-7(ERBB2-) and BT474(ERBB2+) cell plate treated with **11a**, only BT474 cells were visible in both mAb and probe channels. Heterogeneity between fluorescence levels in the cells was observed in this process, and that could be due to different levels of receptor expression or to fundamental differences in levels of kinase activation. To differentiate between these possibilities, fluorescent activated cell sorting (FACS) was performed to sort BT474 cells into two populations displaying high and low probe signal. After collection of the cells, their ERBB2 receptor phosphorylation levels were allowed to recover for 24 h prior to Western blot analysis. Even after recovery, cells with high probe signal showed 25 % higher phosphorylation signal than the ones with low probe signal, suggesting the fluorescent probes detect *stable* differences in kinase activation states inherent to different cells.

Further modification of structures **11** led to the cyano derivative **11c**.[124] Like **11a**, probe **11c** absorbed at about the same wavelength as the parent inhibitors gefitinib and lapatinib. However, unlike **11a** this compound has a huge (200 nm) Stokes shift giving a longer emission max of 520 nm in the bound form which is easily distinguishable from gefitinib and lapatinib (440 nm). Selectivity for binding ERBB2 was demonstrated by live cell imaging, as outlined above.

Probe **11c** was used in a clever way to differentiate type I and II inhibitors. Briefly, cells were first incubated with **11c** to saturate internal ERBB2, then treated with inhibitors of type I and II states. *Internal* ERBB2 population is reported by probe **11c**, and presumably only the activated extracellular receptors are internalized. Recall that type I inhibitors bind the active conformation, whereas type II's do not. Thus, type I inhibitors (gefitinib, canertinib) induced the *active* ERBB2 conformation, caused dimerization, and *more* ERBB2 to be internalized. Consequently, intracellular **11c** exhibited enhanced shifted emission characteristic of the turned-on probe. Type II inhibitors (lapatinib or neratinib), however, bind in ways that favor inactive conformations of ERBB2, which tend not to dimerize or be internalized. Consistent with this, no change in emission was observed when the **11c** saturated cells were treated with these particular inhibitors. Thus, **11c** reports on the dynamics of internalization ERBB2 activation states, because the probe senses binding modes (in active or inactive, that correlate with endocytosis and also with conformation, type I or II).

A.4 *In Vivo* Localization

A.4.1 Probes Containing Silyl-rhodamines or Aza-BODIPYs

Weissleder's group modified Btk inhibitors, ibrutinib (FDA approved) and AVL-292 (in clinical trials) to incorporate an amine handle for conjugating with fluorescent dyes.[125] Subsequently, four different dye cores (silyl rhodamine, rhodamine, fluorescein and BODIPY) were used to prepare six different conjugates of ibrutinib and AVL-292. Colocalization studies of these probes with Btk-mCherry (expressed in HT1080 cells) showed the silicon rhodamine carboxylate conjugates **12** and **13** were most closely associated with the kinase. This could mean that the physiochemical properties of that particular dye endowed it with favorable PK characteristics and/or, the fluor was most suitable for synergistic binding between the inhibitor and the kinase; it is hard to tell which without comparative *in vitro* experiments, and even with these it is unclear that the answer would be definitive.

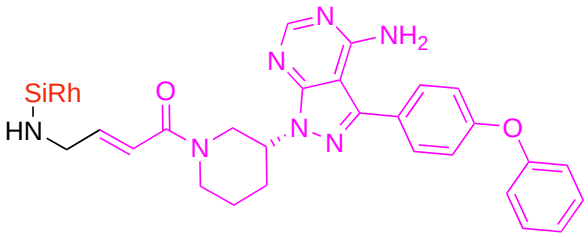

12
ibrutinib (Imbruvica®)
Btk inhibitor

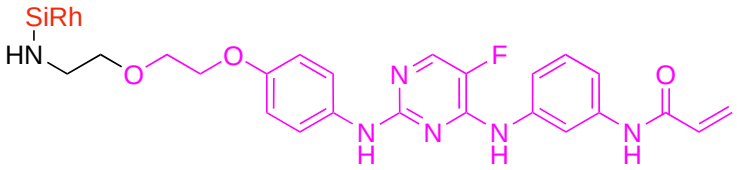

13
spebrutinib (AVL-292)
Btk inhibitor

Silyl-rhodamines in **12** and **13** have good photophysical properties; they are, zwitterionic, with red-shifted absorbance wavelength and emission maxima relative to rhodamines (but still shorter than cyanine-7 dyes), and they have high extinction coefficients and quantum yields. Conjugates **12** and **13** formed from these dyes were shown to have good cellular uptake, binding selectivities, and they inhibited the kinase activity of Btk. Fluorescent gel scanning confirmed **12** acted like ibrutinib insofar as it covalently and selectively bound Btk in Btk^+ {B lymphocytes, specifically Toledo} but not in Btk^- {T lymphocytes, *ie* Jurkat} cells. Compound **12** was further tested in mice implanted with a mixed population of two cell types: HT1080 expressing Btk-mCherry, and HT1080-H2B-GFP Btk^-; it localized selectively with the m-Cherry label in Btk^+ cells with a vascular $t_{1/2}$ of ~18 min.

In another application of this kind of fluorescent KI-probes, the Weissleder group examined BODIPY and silicon rhodamine derivatives of vemurafenib.[126] Vemurafenib is a non-covalent serine/threonine kinase inhibitor directed to the $BRAF^{V600E}$ mutation. $BRAF^{V600E}$ is an oncogenic driver of several cancer types, particularly melanoma.[127] Structural analyses show the *p*-chlorophenyl substituent of vemurafenib points into solvent and away from the kinase binding pocket, hence modifications at that position

should be relatively unlikely to compromise the KI's binding. Six fluorescent conjugates were synthesized based on the BODIPY and silicon rhodamine cores, and the top three based on their EC_{50}'s and binding affinities to $BRAF^{V600E}$ were selected for further studies. Those three compounds were screened for penetration and retention in melanoma cancer cells (A375 and SK-MEL-28), which revealed **14** seemed to have the most favorable pharmacological properties.

Confocal imaging showed **14** localized in cellular cytoplasm, the putative site for accumulation of $BRAF^{V600E}$, and the fluorescent signal lingered there for an extended period. *In vivo* imaging on vemurafenib-sensitive and -resistant cancer cell lines (A375 and A375R respectively) revealed **14** localized in tumor, and its fluorescence was retained there even after 24 h.

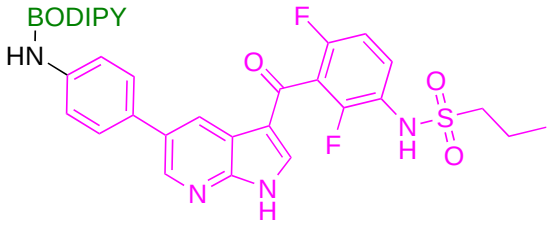

14
vemurafenib (Zelboraf®)
$BRAF^{V600E}$ inhibitor

Weissleder and co-workers also studied fluorescent conjugate of UNC2025, a preclinical inhibitor of receptor tyrosine Mer (MERTK).[128] MERTK is a transmembrane protein implicated in variety of cancers, wherein it plays a role in metastatic spread.[129]

Crystallographic analyses of Mer complexed with UNC2025 and with a closely related structure (UNC569; PDB ID: 3TCP) indicate modifications to the methyl piperazine of the KI should not significantly impact complexation, so the methyl piperazine was modified to a piperazine fragment then conjugated to a zwitterionic silicon rhodamine carboxylate to give **15**.[130]

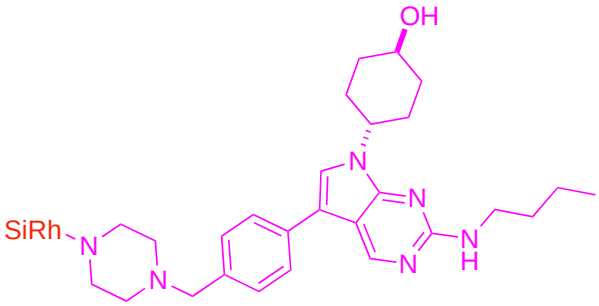

15
UNC2025
Mer inhibitor

In vitro imaging of **15** on cells which overexpress Mer (SK-MEL-3 melanoma), revealed the conjugate accumulates in the cytoplasm near the nucleus. In blocking experiments, uptake of **15** was suppressed by excess UNC2025, and also in SK-MEL-3 cells in which Mer had been knocked down via SiRNA; both experiments indicate uptake of **15** is mediated by that kinase. Conjugate **15** was inferior to the parent kinase inhibitor with respect to cytotoxicity and phosphorylation activity. Nevertheless, **15** co-localized with Mer *in vivo*, as shown using a mouse model in which the endogenous expression of the kinase was engineered to be coupled with GFP expression. Surprisingly, **15** was uptaken more in tumor-associated macrophages than in tumor cells.

Changjun Lv and coworkers at University of Chinese Academy of Sciences, applied a targeted prodrug approach to deliver gefitinib to non-small-cell lung cancer (NSCLC).[131] Their prodrug **16a** consists of three fragments: targeting ligand, cleavable linker, and gefitinib. For the targeting ligand they chose a polyamine which is endocytosed through polyamine uptake system (PUS);[132] that PUS-system is overexpressed in NSCLC.[133] A cleavable disulfide linker was used to release gefitinib via disulfide-thiol exchanges in the intracellular tumor environment where glutathione is abundant.

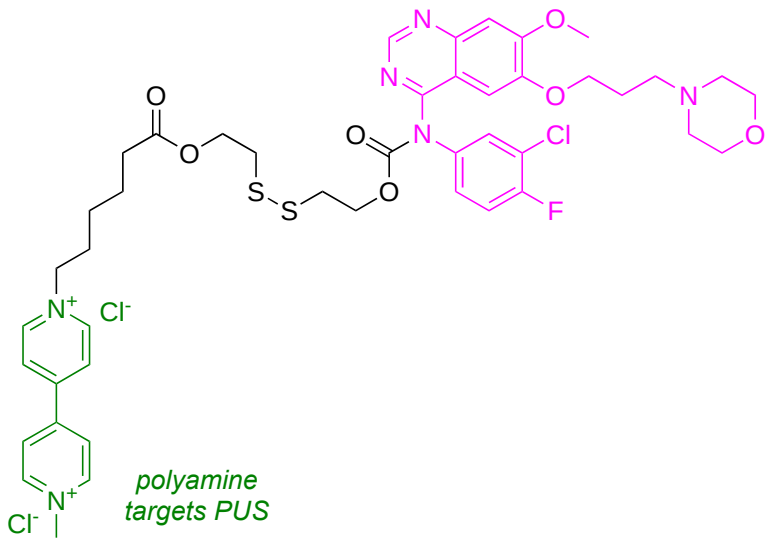

16a
gefitinib (Iressa®)
EGFR inhibitor

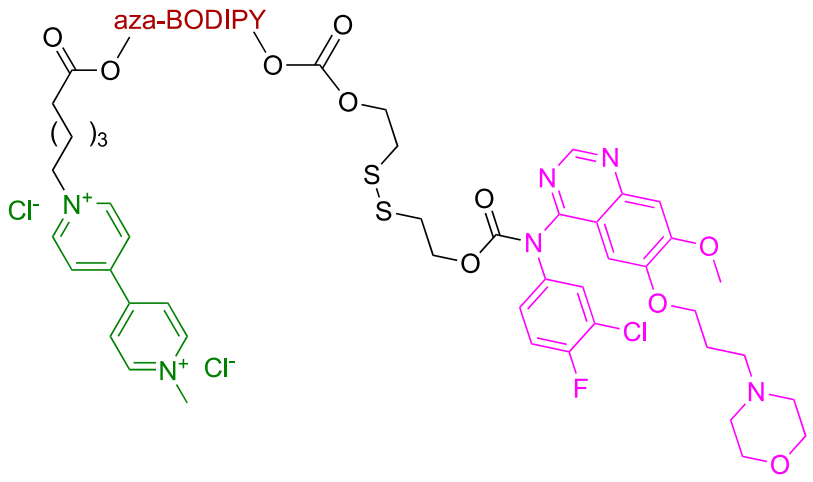

16b
gefitinib (Iressa®)
EGFR inhibitor

The structure of **16a** was modified for tumor imaging, by incorporating an aza-BODIPY. Both the non-fluorescent (**a**) and fluorescent (**b**) forms of **16** were tested in two NSCLC cell lines: one sensitive (PC9) and the other resistant (H1650) to gefitinib. Both conjugates were more toxic to cells than the parent kinase inhibitor, possibly due to polyamine inhibition of pAkt,[134] an important signaling pathway downstream to EGFR (Epidermal Growth Factor Receptor). Annexin V/PI staining in flow cytometry indicated compounds **16** had higher tendency to kill cells by apoptosis than necrosis, implying cytotoxicity was induced by disruption of cell signaling pathways by the KI.

In two parallel experiments, probe **16b** was administered *iv* via the tail of mice with impregnated with subcutaneous tumors grown from PC9, and from H1650 cells. In both cases it selectively localized in tumors, and a robust fluorescence signal persisted there for up to 24 h post injection. An attribute of **16b** is that it *gains* fluorescence after the disulfide bond is cleaved inside the tumor microenvironment. In the tumor burden part of the study, **16b** and gefitinib inhibited the growth of tumors from gefitinib-sensitive

cells (PC9) to about the same degree. However, the impact of **16b** on gefitinib-resistant H1650 cells was greater that observed for gefitinib, demonstrating the effect of the PUS targeting group. Encouragingly, the conjugate **16b** performed better in detecting samples from patient derived NSCLC than commercially available serum biomarkers (carcinoembryonic antigen and cytokeratin 19).

A.4.2 Probes Containing "Tumor-seeking Cyanines"

Recent work from our laboratories has exposed some fluorophore-kinase conjugates that limit cell proliferation *more* effectively than the parent kinase.[69] All these conjugates feature a "tumor-seeking dye" like the cyanine-7 dye MHI-148 **A** (Figure A.7). The special characteristics of MHI-148 **A** are first that it accumulates in tumor tissues *in vivo* after *iv* injection, and second that it is retained there for several days.[135-136] Amazingly, this characteristic is independent of the type the type of solid tumor implanted into the mouse.

We reasoned that conjugates of KIs with MHI-148 could be used to target solid tumors, and cause the kinase to accumulate there. Unfortunately, but as expected, probe **17**, from dasatinib with MHI-148, binds *less* well to two illustrative kinases than the parent KI (K_d for **17**: 2.4 nM with Src, and 17 nM with Lyn; literature K_d values for dasatinib are 0.07 nM with Src[113] and 0.57 nM with Lyn[113]). Moreover, in assays to gauge enzyme activity the conjugate was also *less* active than the parent KI (18.4 nM to Src, and 55.6 nM to Lyn: while the corresponding IC_{50} values for dasatinib were 1.2 nM for Src, and 1.8 nM for Lyn). However, **17** is cell permeable (localizes in the mitochondria and

lysosome), and has a greater effect on cell proliferation than the parent KI and MHI mixed at equimolar concentrations.

In other work we have established than thiols (but not amines, alcohols or phenols) react with **A** via displacement of its *meso*-chloride under physiological conditions.[137] The only free thiol in albumin is ^{34}Cys. It transpired that the ^{34}Cys of albumin forms a covalent conjugate via binding to the cyanine at the *meso*-position.[138] Independent studies by Goncalves and co-workers were published almost simultaneously, and confirmed these observations.[139]

The inference of the observations above is that the effects of KIs on cell viability sometimes can be increased by binding to albumin. Consistent with this, it has been reported that erlotinib analogues conjugated to albumin slowed proliferation of A549 and H1975 (NSCLC) cell lines more than erlotinib itself.[140]

a

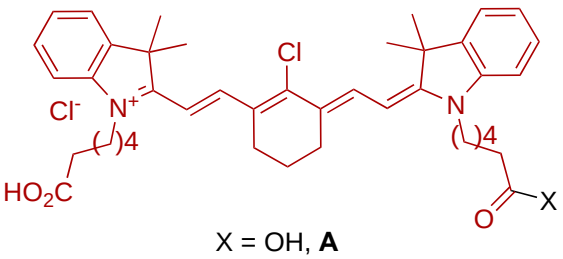

X = OH, **A**
X = *dasatinib*, **17**

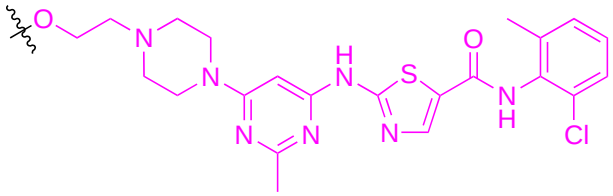

dasatinib (Sprycel®)
Src inhibitor

b

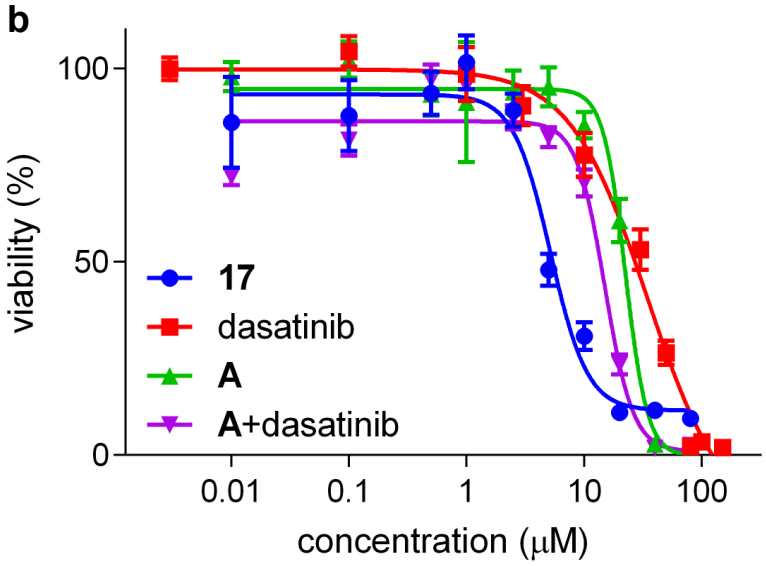

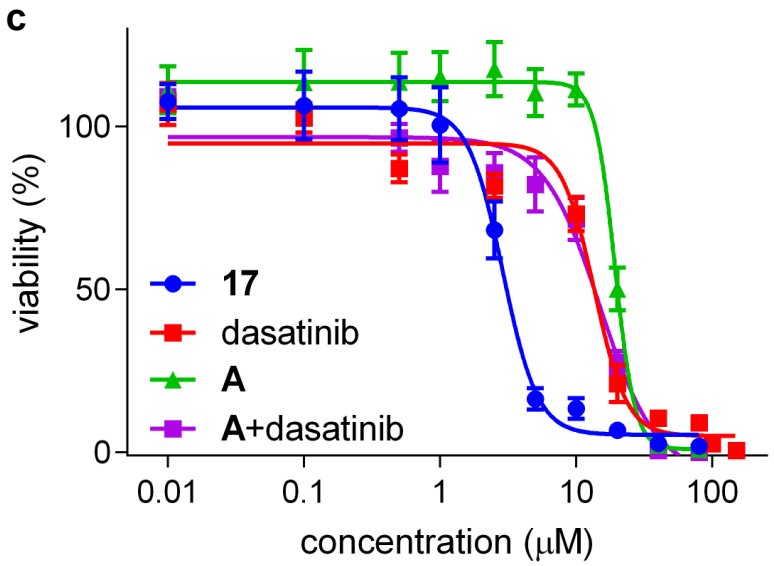

Figure A.7 (**a**) Conjugate **17**, from a tumor-seeking near-IR dye and dasatinib, gives enhanced impact on the viability of: (**b**) HepG2 liver cancer cells; and, (**c**) U87-MG glioblastoma cancer cells.

Cell studies had consistently been reported showing MHI-148 **A** (and related dyes) were transported into cells via Organic Anion Transporter Polypeptides (OATPs). However, we showed the evidence for OATP transport in those cell studies is only seen if serum free media are used, *ie* an environment without albumin.[141] Subsequently, we showed MHI-148 **A** binds albumin non-covalently then slowly transforms to the covalent adduct. Both the covalent and the non-covalent adduct were uptaken into tumor cells selectively over non-tumorigenic cells. Moreover, MHI-148 **A** non-covalently bound to albumin covalently labelled with fluorescein (albumin-FITC) was uptaken into tumor cells and the two labels colocalized. On the basis of these experiments it would appear MHI-

148 **A** is uptaken into cancer cells via albumin receptors. There are several albumin receptors, and they tend to be over-expressed on cancer cells,[142] probably because of their enhanced rates of metabolism. On the basis of those data, *based exclusively on cellular assays*, one might conclude that uptake into tumors were mediated exclusively by albumin interacting with its receptor. However, if the uptake into cancer cells could be mediated via both non-covalent and covalent binding to albumin, then covalent binding might not be necessary for persistence of the dye in tumor *tissue* over several days. There now follows a lengthy digression to answer this question for the case of tumor seeking cyanine dyes without KIs conjugated to them, which presumably can be extrapolated to their KI conjugates.

A series of *in vivo* experiments were planned since *accumulation* of MHI-148 **A** into tumor tissue could be explained via uptake via albumin receptors, but reasons for *persistence* of the fluorescence in tumors were unclear. These *in vivo* studies featured four dyes with complementary properties which include **A**. Fluor **A**-Ph forms a non-covalent adduct with albumin and cannot form a covalent one. "QuatCy" **B** does not form a non-covalent albumin adduct, and only slowly forms a covalent one. Finally, **B**-Ph does not form a non-covalent albumin adduct, and cannot form a covalent one.

Complimentary characteristics **A**, **A**-Ph, **B**, and **B**-Ph) facilitated deduction of structural features that determine *in vivo* accumulation and persistence. They were injected *iv* into healthy mice, and into others implanted with subcutaneous triple negative breast tumors (E0771); the passage of fluors were monitored via near-IR fluorescence in the living animals, and in their organs *post mortem*.[141]

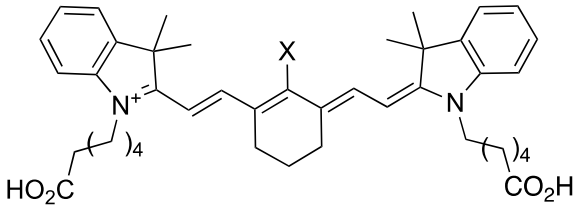

X = Cl, MHI-148, **A**, *reacts quickly with albumin*, logP= 6.57, logD= 3.82
= Ph, **A**-Ph, *cannot react with albumin*, 7.85, 5.09

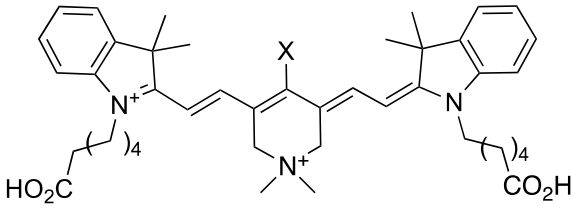

X = Cl, QuatCy, **B**, *reacts slowly with albumin*,1.10, 2.64
= Ph, **B**-Ph, *cannot react with albumin*, 2.38, 3.92

Experiments with the healthy mice revealed **A** was predominantly cleared via the liver, while **B** cleared more quickly via both renal and hepatic pathways. Fluor **B** was detected in the gastrointestinal tract from 1 h post-injection, indicating fast excretion from liver and bile duct, while **A** gave signal in the liver and duodenum even after 4 h post-injection. Insignificant urinary excretion was observed for **A**, and this dye had a blood plasma fluorescence half-life of 195.2 min. Compound **B** at 25 nmol *iv* had a plasma elimination half-life of 100 min and 32% of injected dose was excreted through the urine.

For the tumor-bearing mice, the blocked compounds **A**-Ph and **B**-Ph had poor preferential tumor accumulation and no significant persistence, hence tumor-to-background ratios (TBRs) did not deviate significantly from unity, *i.e.* there was little

contrast between the tumor and the background. Conversely, the fluors that can form albumin adducts, **A** and **B**, displayed high tumor accumulation and prolonged retention (TBR was 3.5 and 10, respectively,48 h post-injection). Accumulation of **A** and **B** into the tumor and background tissues was rapid, but **B** cleared faster from the healthy tissue, giving comparatively high TBR values for each time point at which the tumor could be discerned; high contrast was observed 4 h post-injection of **B** while 48 h was needed for **A**. At 48 h post-injection, when the *meso*-phenyl dyes (**A**-Ph and **B**-Ph) were almost completely cleared from the body, but the *meso*-chloride dyes (**A** and **B**) could be clearly seen in the tumor tissue.[141]

The studies outlined above indicate non-covalent binding is insufficient for retention of tumor seeking dyes. Moreover, over a relatively short time (4 - 6 h) in the body, the dyes that could not form covalent adducts did not appear to accumulate in tumors selectively over healthy tissue, and after that they were mostly excreted. This observation is unexpected from the cell data where, recall, non-covalent adduct formation did result in dye uptake. *In vivo*, only covalent adduct formation resulted in accumulation and persistence in tumors.[141]

Overall, the studies described above teach it is unwise to extrapolate too much from cellular assays to predict *in vivo* behavior. Cellular data alone might lead to the prediction that uptake into tumor tissues *in vivo* was due to uptake via albumin receptors, but the *in vivo* studies indicate this is not necessarily the sole mechanism, and the EPR effect, originally postulated based on labeled-albumin in tumors,[143-147] may play a role also, and might even be the predominant reason for persistence. In either case, it seems

the root cause of accumulation and persistence of tumor seeking dyes is the extremely long residence time of albumin in the body coupled with the high abundance of that carrier-protein (in human blood, turn-over >20 d and concentration 0.53-0.73 mM[148]).

The focus of this review is dye-KI conjugates, not tumor seeking dyes. However, the digression above is necessary to convey an important point about accumulation and persistence of tumor seeking dye KI *conjugates* in tumors, at least when the KI cannot covalently bind the target kinase. Specifically, accumulation and persistence probably require a leaving group, typically a *meso*-chloride, on the Cy7 system. Dye-KI conjugates formed by displacing the *meso*-chloride, or from dyes where this is blocked (*eg* via a phenyl group as in the control studies above) will not endow the KI with preferential accumulation and persistence. Beyond that, the PK behavior of **A** and **B** brings to the fore a variety of important questions that are being investigated, but have not yet been published. Prevalent among these questions are the unresolved impacts of dye-KI adducts on tumors *in vivo*. There is only a preliminary report of this at the moment.[149]

That preliminary report, to show localization of compound **17** in tumors *in vivo*, has shown promising results (Figure A.8).[149] Fluorescence from compound **17** localized and persisted for 72 h in mice impregnated with subcutaneous U87-MG tumors. This observation does not mean the *intact* dye-KIs accumulated and persisted in the tumors, but it leaves open the possibility that these conjugates may drastically increase the residence time of a KI in a tumor, and, simultaneously, provide a near IR-probe for optical imaging *in vivo*.

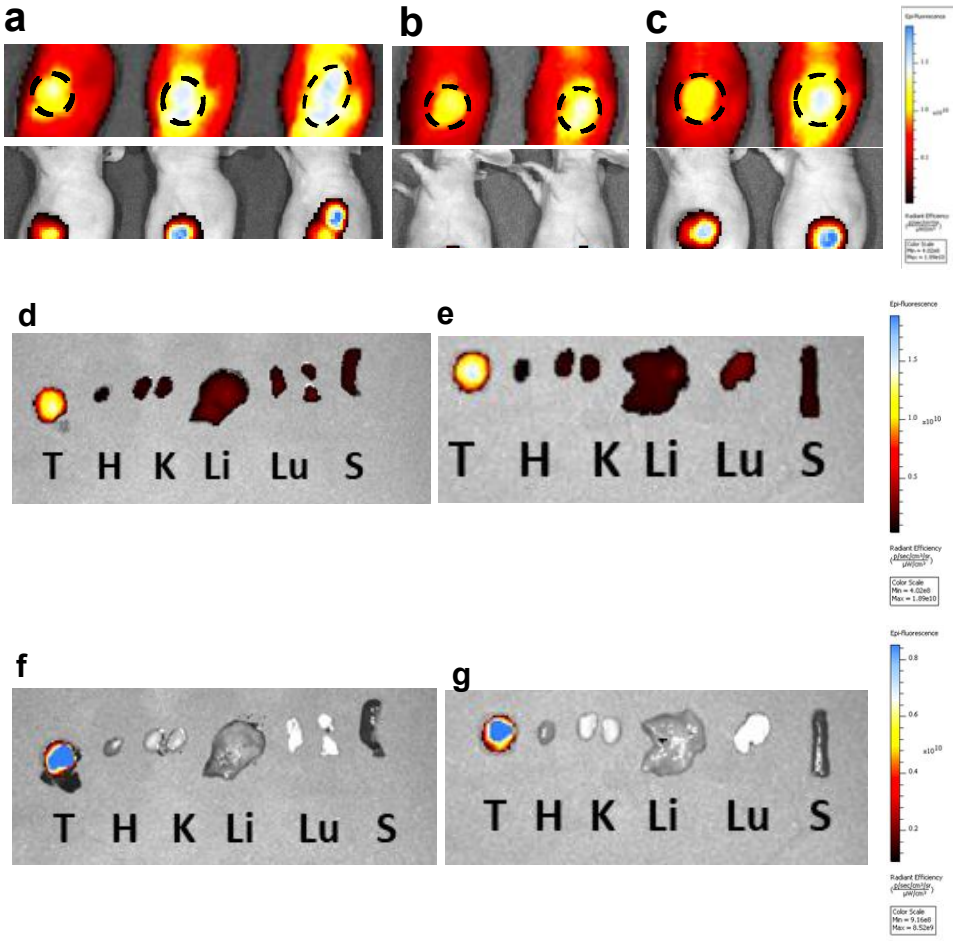

Figure A.8 Localization of **17** and fluorescence of RFP in the tumor tissue showing the region of interest after retroorbital *iv* injections at 10 mg/Kg, at: (**a**) 24; (**b**) 48; and, (**c**) 72 h. *Post mortem* fluorescence of organs after sacrifice at 72 h: (**d**) near-IR for mouse 1; (**e**) near-IR for mouse 2; (**f**) RFP mouse 1; and, (**g**) RFP mouse 2.

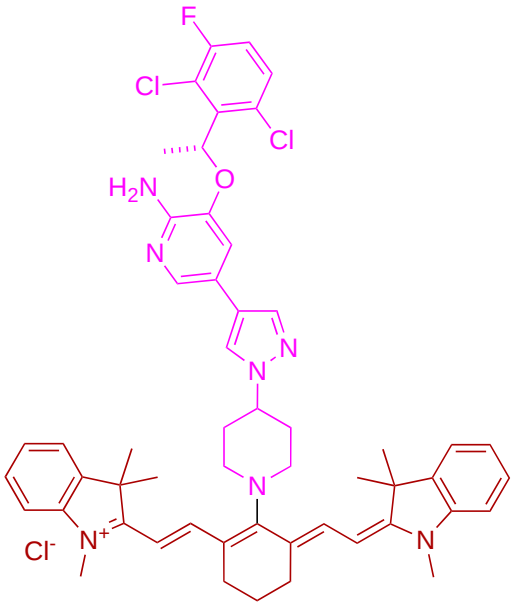

18
crizotinib (Xalkori®)
ALK inhibitor

Following our work, recently there has been a publication by Jose and co-workers at University of Auckland on crizotinib, an anaplastic lymphoma kinase (ALK) inhibitor, with a NIR cyanine dye (IR-786).[150] They exploited piperazine of crizotinib that points outside from the binding pocket of the kinase inhibitor and displaced the *meso*-Cl IR-786, conjugate **18**. Apart from targeting ALK, that is overexpressed in GBM, crizotinib also targets kinases in Met and ROS1 pathways. Hence, it is an ideal candidate to target GBM tumors.[151-152] Crizotinib, free dye and conjugate **18** were tested against three patient-derived GBM cell lines. Remarkably, the cytotoxicity of **18** was 100x more than the free dye or kinase inhibitor. All three patient-derived cells were resistant to temozolomide (TMZ; FDA approved chemotherapeutic for glioblastoma), but synergistic effects were observed when equimolar concentrations of TMZ and **18** were added to the cells.

A.4.3 Probes Containing Other Cyanines

Discussion of probe **19** in the introduction noted this featured afatinib split to incorporate glycine between the active site-binding fragment and an electrophilic double bond in the parent KI; either Cy3 or Cy5 dyes were bound at the other terminus.[153] These modifications profoundly changed the chemistry of the kinase interaction insofar as the Michael receptor of afatinib combines with the cysteine residue near the enzyme active site to irreversibly form a covalent adduct, but there was no evidence of this for **19**. Specifically, flow cytometry of cells treated with **19** then with afatinib showed decreased signal intensity indicative of reversible binding to the kinase. It appears that **19** is regiochemically unable to undergo a similar Michael addition. It is unclear if loss of covalent binding was intended at the onset of this study.

The Cy3-functionalized version of probe **19** was administered *iv* in an immune compromised murine model featuring subcutaneous tumors xenografted with A549 lung cancer cells. Fluorescence in the tumor was clearly discerned from 12 - 48 h post injection in live mice, and this was confirmed via *ex vivo* imaging *post mortem*. We are unsure why the Cy5 modification was not used in this experiment; it should be more conspicuous *in vivo.*

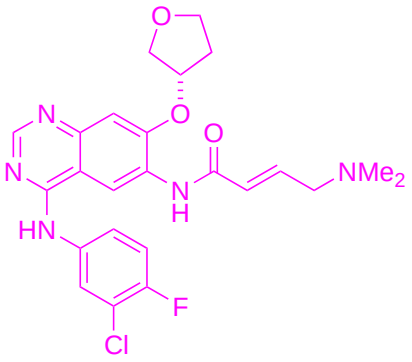

afatinib (Gilotrif®)
EGFR/HER2 inhibitor

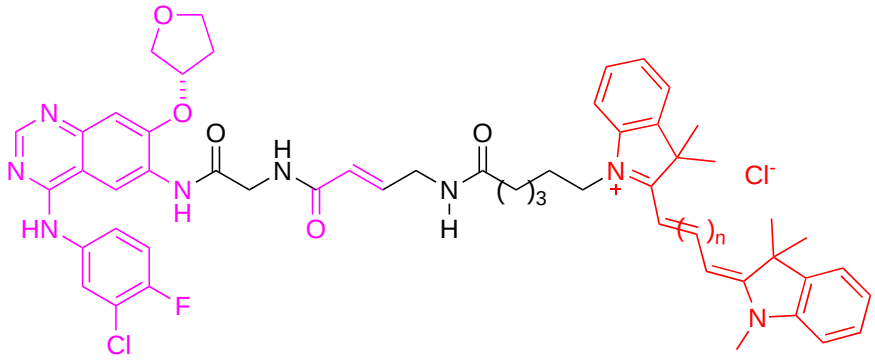

19
n=1, Cy3; n=3, Cy5
afatinib (Gilotrif®)
EGFR/HER2 inhibitor

A.5 Multimodal Probes

As already indicated in this review, optical imaging *in vivo* is constrained by penetration of light through tissue, thus it is critically dependent upon the λ_{max} values of the dyes involved. However, even if the dye is not ideal for *in vivo* imaging, in research studies combination of optical images with signals from other diagnostic probes (*eg* ones for PET, CT, MRI) can provide holistic visualizations of tumor microenvironments

relative to those obtained using one technique alone. This strategy is most conveniently reduced to practice using nanoparticles wherein components can be added to inert matrices giving a distribution of molecular compositions and particle sizes. This process is convenient for nanoparticles because the components do not have to be covalent connected in small molecules, which require more extensive characterization. Unfortunately, batch-to-batch variability of nanoparticles which has become acceptable in research studies, is their weakness with regards to clinical studies that necessitate reproducibility. Consequently, this review is restricted to discrete small molecules of defined structures throughout, and that focus has the effect of excluding most multimodal probes. Indeed, adopting that focus means there are currently only two studies that need to be discussed.

Ting, Souweidance, and co-workers [154]used multimodality to explore Convection Enhanced Delivery (CED), an invasive method in which catheters are inserted in and around the tumor to bypass the blood brain barrier (Figure A.9).[155] Optical imaging and PET complement each other because fluorescence spectroscopy provides higher resolution, whereas radiolabel-based tomography can image deep tissue environments. A multimodality probe was formed by conjugating dasatinib (promiscuous kinase inhibitor), a Cy3 dye (useful, but not the best cyanine for near-IR imaging) and a Perrin ^{18}F capture agent in the small molecule "package" **20**.[156-157] Conjugate **20** proved to be less potent than the parent kinase inhibitor in cellular assays, but still effective at nanomolar concentration doses. Delivery to tumor region was shown to be more effective via CED than with *iv* in an orthotopic glioma mouse model.

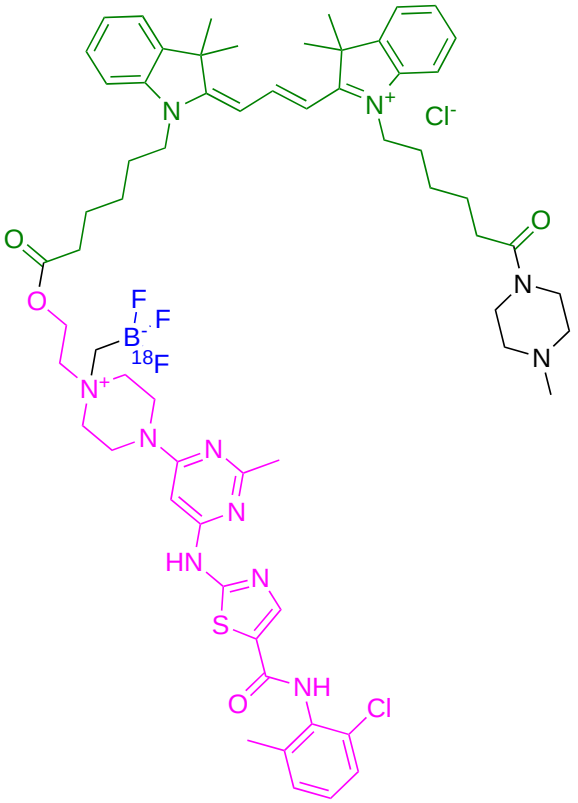

20

dasatinib (Sprycel®)

Src inhibitor

targeted therapeutic strategy
to deliver drugs directly
to region of interest in brain

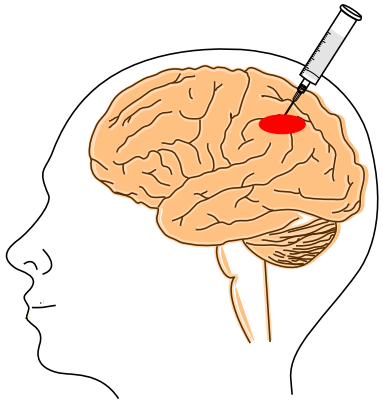

Figure A.9 Convention Enhanced Delivery (CED) in which thin tubes penetrate the brain directly and bypass the BBB.

Stimulation of EGFR, a tyrosine receptor overexpressed in many different cancers,[158] results in cellular proliferation, inhibition of apoptosis, metastases and angiogenesis.[159] For one report, [160] Pandey and co-workers synthesized several theranostic molecules combining PET, PDT and fluorescence imaging agents. Erlotinib, a specific inhibitor of EGFR was conjugated with chlorin (a porphyrin-based imaging and PDT moiety) and ^{124}I for PET was introduced at two different positions, 3 and 17, giving conjugates **21** and **22**. Their choice of conjugation was surprising because the erlotinib the alkyne position points *inside* the binding pocket, *ie* when erlotinib binds EGFR, crystallography indicates only the other end of the molecule, the ethylene glycol fragment, protrudes into solvents-space.[161] Chlorins are hydrophobic, consequently surfactants (Tween 20 and Pluronic F-127) were required to solubilize **21** and **22**, and this must effect their cellular localization and PDT properties. PET imaging using ^{124}I agents is interesting; this radionuclide is harder to produce than ^{19}F but its long half-life (4 d) facilitates shipped to regions where there is no suitable cyclotron locally. Both conjugates showed good tumor-to-background ratios for $EGFR^+$ tissue (from UMUC3 cells) over $EGFR^-$ (T24 cells) hence they could serve as imaging agents. Only conjugate **22** showed much better singlet oxygen generation compared to chlorin structure, and it is therefore the better theranostic candidate of the two choices.

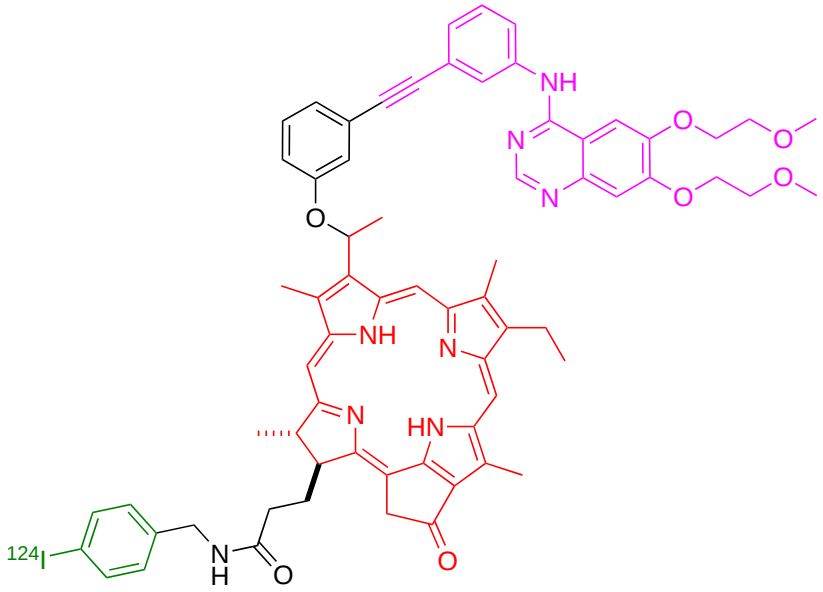

21
erlotinib (Tarceva®)
EGFR inhibitor

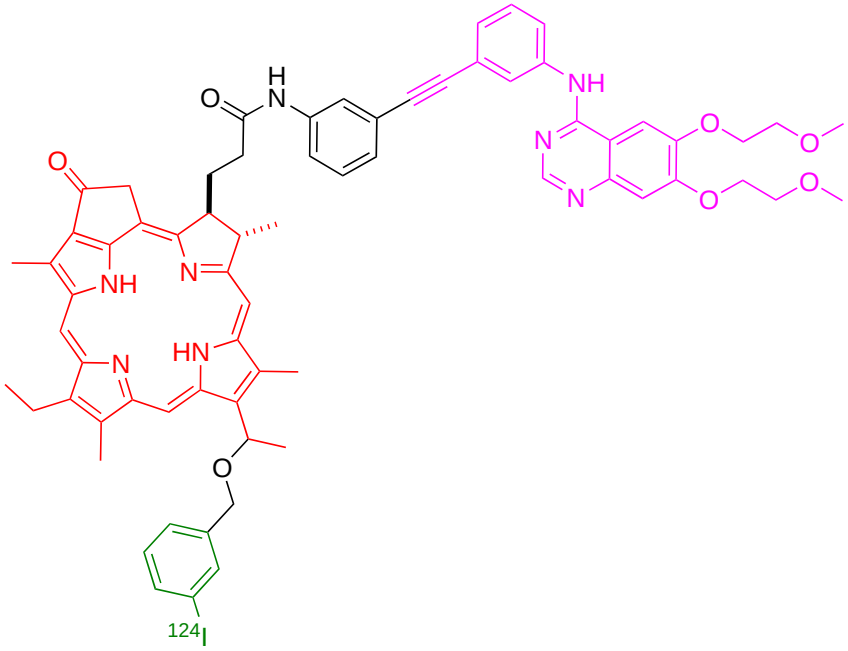

22
erlotinib (Tarceva®)
EGFR inhibitor

A.6 Conclusions

Figure A.1 reveals surprisingly few fluorophores have been used fluorophore-KI probes; specifically, a commercially available BODIPY, an aza-BODIPY, a silyl rhodamine, a porphyrin, and a few cyanine dyes. However, the dyes that have been incorporated cover a broad spectrum of photophysical properties, from short (<400 nm) to relatively long (780 nm or more) wavelength absorption and fluorescence maxima. It is dye properties that should dictate the applications of KI-probes though the fluor that has been used is not ideal for the application reported in some cases described above.

Table A-1 lists all the probes reviewed here, their primary kinase targets, the dyes used (approximately from shorter to longer wavelength absorption maxima), binding and kinase inhibition properties (where available), and potencies relative to the parent KIs.

A.6.1 Probes Containing Blue-fluors

Simple BODIPY dyes tend to absorb UV and fluoresce in the 500 – 550 nm range, ideal for many *in vitro* assays. This spectral window overlaps with background intracellular autofluorescence, nevertheless, BODIPY fluors are so brilliant that many intracellular imaging experiments using them are highly informative. All the BODIPY-KI probes reported to date, **1** – **7** and **14**, feature the same BODIPY. This molecular fragment probably dominates because it is commercially available ("BODIPY-FL" from Thermofisher). This reflects the fact that practitioners studying KIs are, understandably, reluctant to spend time preparing custom BODIPY-dyes. However, the unintended

consequence of this is that all these types of probes, **1** – **7** and **14**, are considerably more hydrophobic than the parent KIs because of the lipophilic BODIPY attached.

Table A-1. Fluor-KI conjugates in this review, their targets, specificities and potencies.

conjugate	KI	target	dye	binding and kinase inhibition (cell-free, nM, unless otherwise noted)	potencies relative to parent KI
1[25]	dasatinib	Src, Abl	BODIPY	K_d: Src 0.5; Abl 0.15	N/A
2a[108], **2b**[109]	ibrutinib	Btk		IC_{50}: **5a** N/A: **5b** ~200	100x inferior
3[107]	BI2536	PLK1-3		IC_{50}: PLK1 5.01; PLK2 19.4; PLK3 9.37	comparable
4[111]	nilotinib	BCR-Abl		N/A	inferior
5[25]	dasatinib (DFG-out)	Src, Abl		K_d: Src 2.8; Abl 0.75	ligand induced different binding conformation
6[25]	dasatinib (αC-helix-out)			K_d: Src 4.6; Abl 0.58.	
7[115]	a type II KI	Src, p38		IC_{50}: Src 25.4; p38 25.5	N/A
8[29]	HS-133	PI3Kα	intrinsically fluorescent	IC_{50}: 68 nM	N/A
9[121]	gefitinib	ERBB2		K_i (in cell): 3,100	N/A
10a-b[122]				K_i (in cell): **11a** N/A, **11b** 9 μM	reporter of type I or II binding mode

11a[123], **11c**[124]				K_i (in cell): **11a** 71; **11c** N/A	
11b[123]	lapatinib			K_i (in cell): 27	
12[125]	ibrutinib	Btk	SiRh	IC_{50}: 122	200~300x inferior
13[125]		Btk	SiRh	IC_{50}: 283	
14[126]	vemurafenib	$BRAF^{V600E}$	BODIPY	EC_{50}: 380	3x inferior
15[128]	UNC2025	MERTK	SiRh	IC_{50} (in cell): 19.7 μM	inferior
16[131]	gefitinib	EGFR	aza-BODIPY	IC_{50} (in cell): PC9, 50 H1650, 780	superior
17[69]	dasatinib	Src, Lyn	near-IR cyanine (MHI-148)	IC_{50} (Src, cell-free): 184 IC_{50} (in cell): 5380	less potent in cell-free than in cell-based assays
18[150]	crizotinib	ALK	near-IR Cy (IR-786)	EC_{50}: (average of 3 GBM cell lines): 50 ± 20	100x superior
19[153]	afatinib	EGFR, HER2	Cy3 and Cy5	IC_{50} (three cell lines average): Cy3-AFTN 1480 Cy5-AFTN 2460	inferior
20[154]	dasatinib	Src	Cy5	IC_{50} (in cell): 46 ± 30 nM	similar but inferior (used for PET)
21[160]	erlotinib	EGFR	porphyrin	N/A	used as PDT photosensitizer
22[160]					

Most KIs are not fluors, only KI **8** in this review is intrinsically fluorescent without modification. If the fluorescence is not seamlessly intrinsic to the KI then tension in molecular designs is inevitable; changes to produce rigid, extended, chromophores with large cross sections (to enhance quantum yields, wavelengths, and extinction coefficients, respectively) alter the KIs-heterocyclic core and invariably result in diminished binding affinities and kinase inhibition activities. The KIs in this category that have been reported so far are structurally modified so that their aromatic systems become part of "push-pull" chromophores loosely based on DCS (4-*N*,*N*-dimethylamino-4'-cyanostilbene). More specifically, modifications that conjugate an aryl alkene to the KI core (*eg* **9** – **11**) are the only ones tested so far, and if there is another good way to modify KIs so that they become part of a fluorescent chromophore with minimal structural perturbation, we do not see it. Certainly, to modify KIs to become fluorescent and retain their binding is a molecular design challenge.

We do, however, see a way of exploiting fluorescent push pull KIs that has not been reported so far. Modifying a KI to become part of a push-pull system tends to introduce alkenes. It could be an objective to these alkenes electrophilic enough to covalently bind kinases. Screening these self-indicating KIs for binding to different kinases would be fast and informative, and it would be especially when paired with counter-screens to measured degree of inhibition independent of covalent binding.

When considering kinase inhibition assays, readers might look up the recent *Science* paper that forcefully illustrates how binding affinities and inhibition IC_{50} values for *isolated kinases in vitro*, may not represent the course of events in cells and *in vivo.*[162]

This is because many kinases in cells function as quaternary complexes *with other proteins*; assays in which those cooperative proteins are absent are over-simplistic. This cloud of uncertainty looms above much of the data presented in the Table. In cases where this is a concern, modifying KIs to include fluorescent dyes is more likely to impact interactions with quaternary protein complexes than with isolated kinases because inclusion of large dyes may disrupt, or even synergistically bind to, oligoprotein complexes. This issue is unlikely to influence all *in vitro* data, and it could be that the cyclin dependent kinases, CDKs 4 and 6, studied in that *Science* paper[162] are exceptional insofar as their cell signaling biology involves more protein-protein interactions than average. However, the issue is one to consider when interpreting dye-KI characteristics.

A.6.2 Probes Containing Dyes That Absorb 600 - 700 nm

The silyl rhodamine featured in this review (SiRh) has an absorbance wavelength significantly above the cell autofluorescence region, but shorter than ideal for imaging through tissue. Probes containing this dye are larger than necessary for *in vitro* assays, but not large enough for maximal contrast *in vivo*. However, they are just as good, if not better, than BODIPYs for intracellular imaging, and the SiRh-probes **12**, **13** and **15** have better water solubility too.

In contrast to SiRh fluors, aza-BODIPYs, as in **16**, are so poorly soluble in aqueous media that they tend to aggregate. This probably accounts for the literature bias towards SiRh dyes in this wavelength range for forming dye-KI conjugates. In fact, the sole aza-BODIPY probe featured in this review, **16**, has a polyamine group for PUS uptake[163-164]

conveniently enhances the water solubility of the system overall. However, it would be interesting to check the UV/fluorescence properties of this dye-KI probe change with concentration over the assayed range; if they do, that would indicate kinase inhibition might be influenced by formation of particles or micelles in solution.

Probe **19** is the unique one in which the key structural features of afatinib were split then recombined with a spacer (Gly) in between. Compounds **19** feature Cy5 (absorbs and emits above 600 nm) or Cy3 (absorbs at 554 nm and emits at 570 nm) fluors.[153] It is hard to explain why SiRh dyes have been used more than Cy3 and Cy5 fluors in this area, but the number of examples are probably too few to classify this bias as a trend.

A.6.3 Probes Containing Tumor-seeking Dyes

Tumor-seeking characteristics of some Cy7 dyes are associated with leaving groups at the *meso*-position. If the dye covalently binds albumin *in vivo* (and in some cell assays, depending on the conditions), then the dye-KI adduct will assume the PK properties of albumin.

Probe **17** (and the parent dyes MHI-148 **A** and QuatCy **B**) can form albumin adducts by displacement of their *meso*-Cl functionalities with the free ^{34}Cys of albumin, but the other dye-KI in this class, **18**, cannot. Consequently, we predict the behavior of **17** and **18** will be different *in vivo*; contrasting PK has been demonstrated in similar systems that do not contain KIs,[165] but the experiments have not yet been reported for dye-

KI conjugates like **17** and **18**. In general, probes that do and do not bind albumin may be complement each other for different applications.

A.6.4 Multimodular Probes

Three multimodal dyes are featured in this review. One of them, **20**, contains a trimethine cyanine dye (Cy3) attached to one of Perrin's ^{18}F-capture agents,[156, 166-170] while the other two have porphyrin derivatives with a radioactive iodine isomer, ^{124}I. Probes **20** – **22** are designed to combine fluorescence indicators with labels for positron emission tomography (PET).[171-172] Porphyrin rings in structures **21** and **22** endow them with fluorescence and singlet-oxygen generation properties, hence they can be used in experimental approaches to photodynamic therapy (PDT).[173-174] Combined near-IR fluorescence, PET, MRI, photodynamic or photothermal characteristics are probably the destiny of probes of this kind. Discrete molecular systems are generally more likely to reach clinical trials than ones based on nanoparticles that cannot be reproducibly prepared to the high level of consistency required for clinical work.

A.6.5 Generalities Regarding Dye-KI Conjugates as Research Probes

This review focuses on dye-KI conjugates as research tools, *eg* for studying modes of binding to kinases, non-covalent *vs* covalent interactions, intracellular and *in vivo* localization. For intracellular imaging and some animal studies, KI-dyes probes could complement strategies featuring genetically engineered fusions between fluorescent and target proteins, and immunofluorescence techniques. They are useful provided the

fluorophore does not interfere prohibitively with kinase binding, or non-selectively bind proteins in general. Thus, the dyes used matters, and there is much room for improvement because so few dyes have been explored in this context (see above). For instance, one virgin area for future exploration involves pH- or metal-sensitive-fluors attached to KIs.

In vivo studies of KI-fluorophore probes are limited by the fluorophore. None of the studies featured above, except those with conjugates **17** and **18**, involve fluors truly suitable for observation in tissue without physically implanting a "window" into the animal. Development of near-IR dye-KI conjugates is definitely an area with a research future; for instance, we do not yet know how tumor-seeking dye-KIs impact tumor growth in animal models, but that is an area that needs to be explored. Near-IR dyes are necessarily larger than probes that function at shorter wavelengths, conjugates of these must have significantly different kinase binding properties, physiochemical and PK characteristics relative to the parent KIs; in many cases these properties will compromise the activity of the KI, but in rare cases, like for tumor seeking dyes, they might enhance it because of PK factors. Almost invariably, the behavior of these systems will depart more from the properties of the KI than labelling strategies featuring small blue fluors.

A flow of routine validation steps in development of fluorescent-KI probes is emerging, as summarized in Figure A.10.

A.6.6 Outlook for Practical Applications of Dye-KI Conjugates

Kinase inhibitor fluorophore conjugates have the potential for practical applications beyond research probes. This potential is discussed below, even though dye-KI probes have yet to find a widespread practical application.

We believe the most imminent real-world, practical application of dye-KI conjugates is as diagnostic markers, for instance, in flow cytometry to track certain kinases in diseased cells like in cancers of the blood, or macrophages during infection. Other diagnostic applications might encompass histological fixed tissue imaging. Labelled KIs that become *covalently* bound to their targets should be particularly informative and easy to apply in these situations because they are impervious to wash out.

It is possible that dyes which actively target tumor tissue (tumor-seeking dyes) may be used in theranostics that deliver KIs to tumor tissue, and simultaneously for near-IR imaging of tumor tissue in surgeries. It is more likely that tumor-seeking dyes without KI cargoes will be pursued as surgical staining agents, and KI's attached to albumin will be explored separately as potential therapeutics, but these two applications would be guided or even inspired by research on dye-KI probes.

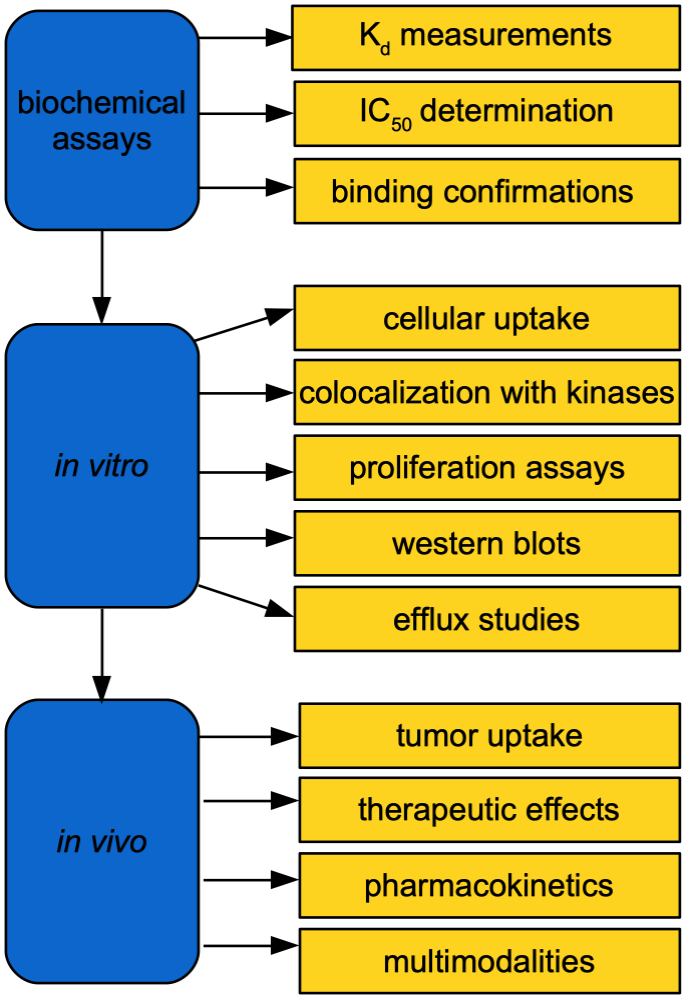

Figure A.10 Ordering of validation steps in development of fluorescent dye-KI probes.

APPENDIX B

PROTACS APPROACH TO SELECTIVE INHIBITION OF CDK2

B.1 Introduction

Pancreatic ductal adenocarcinoma (PDAC) has a dismal prognosis with a 5-year survival of approximately 8-10%.[175-179] The approved systemic therapies have a relatively modest impact, hence PDAC is considered therapy recalcitrant.[177-178, 180] Interestingly, treatment of PDAC remains largely centered on chemotherapy,[181] with few approaches that exploit its genetic features. This is partly because PDAC is driven by multiple oncogenic events (*eg* KRAS), which are considered non-actionable from a therapeutic perspective.[175] Additionally, most PDAC tumors contain multiple oncogenic events (*eg* TP53, SMAD4 and CDKN2A dysfunction) that further contribute to its aggressive nature.

PROTACs can suppress protein expression, therefore provide an alternative method for regulating protein activities, as described in Chapter IV for CDK4/6. However, there are some drug-resistant issues emerging during the clinical trial of CDK4/6 inhibitors, and a key mechanism driving resistance is cell cycle plasticity. In cell cycle mechanism, retinoblastoma protein (Rb) potently suppresses many genes critical for cell cycle, whereas CDK4/6 regulates the phosphorylation of Rb, leading to the expression of Cyclin E. Cyclin E can active CDK2 by forming a complex with it and this can hyperphosphorylate Rb and lead to cell cycle progression (Figure B.1). Comparison of some PDAC models with breast cancer models cultured in both 2D and 3D culture (Figure B.2) shows these PDAC samples were far less perturbed by palbociclib treatment,

compared to breast cancers. CDK2 activities were upregulated in these PDAC models, and most importantly, palbociclib became effective on PDAC cells if CDK2 was knocked down (Figure B.3), indicating CDK2 activity was crucial for resistance. It is emerging that CDK4/6 and CDK2 inhibition have to be combined to potently inhibit the cell cycle.[38, 42, 99-100]

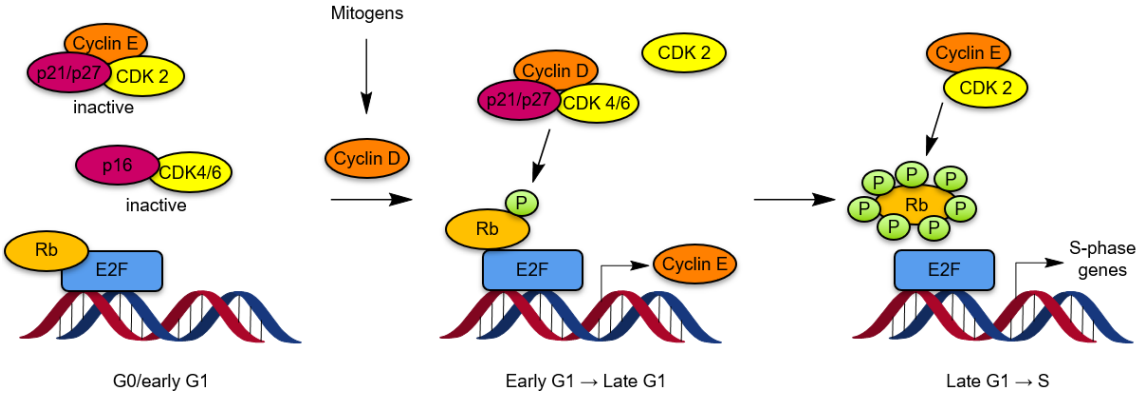

Figure B.1 Illustration for roles of CDK2, 4, 6 and cyclins in cell cycle G1-S transition.

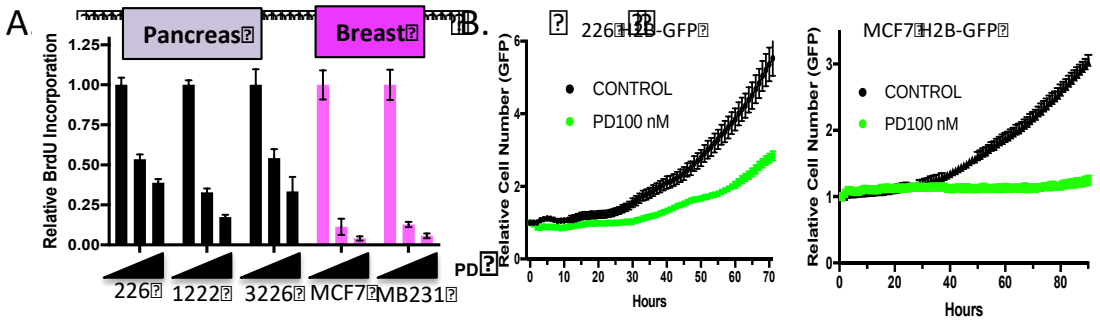

Figure B.2 (**a**) Relative BrdU incorporation between PDAC and breast cancer cell lines treated with palbociclib (PD). The pancreatic cancer models are more resistant (PD-dose escalation 0, 100, 250 nM). (**b**) Live cell count of H2B-GFP labeled PDAC (left) or breast (right) cells treated with 100 nM palbociclib (PD). Breast cancer models are

completely arrested, while data for the pancreatic cancer model 226 is representative of resistance present in most pancreatic models studied.

Selective inhibitors of CDKs are highly desired to minimize off-target effects. CDK1 performs essential processes for healthy cells, so selective inhibitors of CDK2 are required with respect to CDK1.[42, 182] Unfortunately, there are no FDA-approved selective CDK2 inhibitors, and most of the experimental ones show sub-optimal selectivity, despite extensive efforts in this field.[182-184] However, PROTACs derivatized from current CDK2 KIs can be made more selective for CDK2 over other CDKs than parent KIs by exploiting the fact that the effectiveness of PROTACs, and therefore its selectivity, are highly sensitive to linker structure, and E3 ligase ligand. Thus, PROTACs modifications may provide opportunities for selectivity optimization that are not available to the parent KIs.

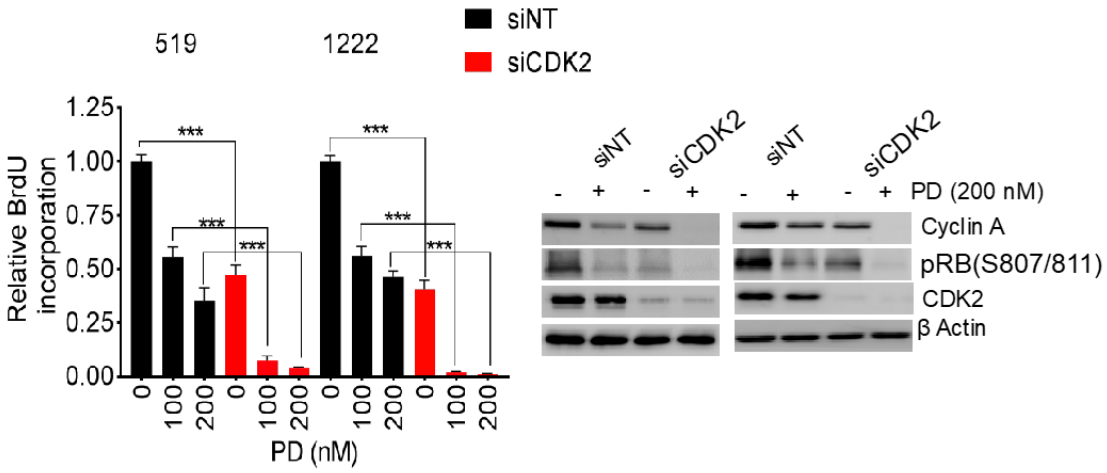

Figure B.3 RNAi-mediated depletion of CDK2 was evaluated for its cooperative effects with palbociclib (PD). Representative immune blots and BrdU incorporation is shown (***p<0.001).

B.2 Materials and methods

B.2.1 Materials and instrumentation

All reactions were carried out under an inert atmosphere (nitrogen or argon where stated) with dry solvents under anhydrous conditions. Glassware for anhydrous reactions was dried in an oven at 140 ºC for minimum 6 h prior to use. Dry solvents were obtained by passing the previously degassed solvents through activated alumina columns. Yields refer to chromatographically and spectroscopically (^{1}H-NMR) homogeneous materials, unless otherwise stated. Reagents were purchased at a high commercial quality (typically 97 % or higher) and used without further purification, unless otherwise stated. Analytical thin layer chromatography (TLC) was carried out on Merck silica gel plates with QF-254 indicator and visualized by UV. Flash column chromatography was performed using silica gel 60 (Silicycle, 230-400 mesh). ^{1}H and ^{13}C spectra were recorded on a 400 MHz spectrometer and were calibrated using residual non-deuterated solvent as an internal reference. The following abbreviations or combinations thereof were used to explain the multiplicities: s = singlet, d = doublet, t = triplet, q = quartet, m = multiplet, dd = doublet of doublet, ddd = doublet of doublet of doublets.

MDA-MB-231 cells (from American Type Culture Collection) were cultured on 75 cm^2 culture flasks in Dulbecco's Modified Eagle Medium/nutrient mixture F-12 (DMEM/F12, Sigma Chemical, St. Louis, MO) supplemented with 10 % FBS. CDK1, CDK2 mAb and BrdU cell proliferation ELISA kit was purchased from Abcam. CDK4, CDK6, CDK9 and Phospho-Rb (Ser780) mAb were purchased from Cell Signaling Technology. Goat anti-rabbit (H+L) secondary antibody (HRP conjugated) were

purchased from ThermoFisher Scientific. SuperSignal West Dura Substrate (ThermoFisher Scientific) was used as Western blot substrate.

B.2.2 Experimental procedures

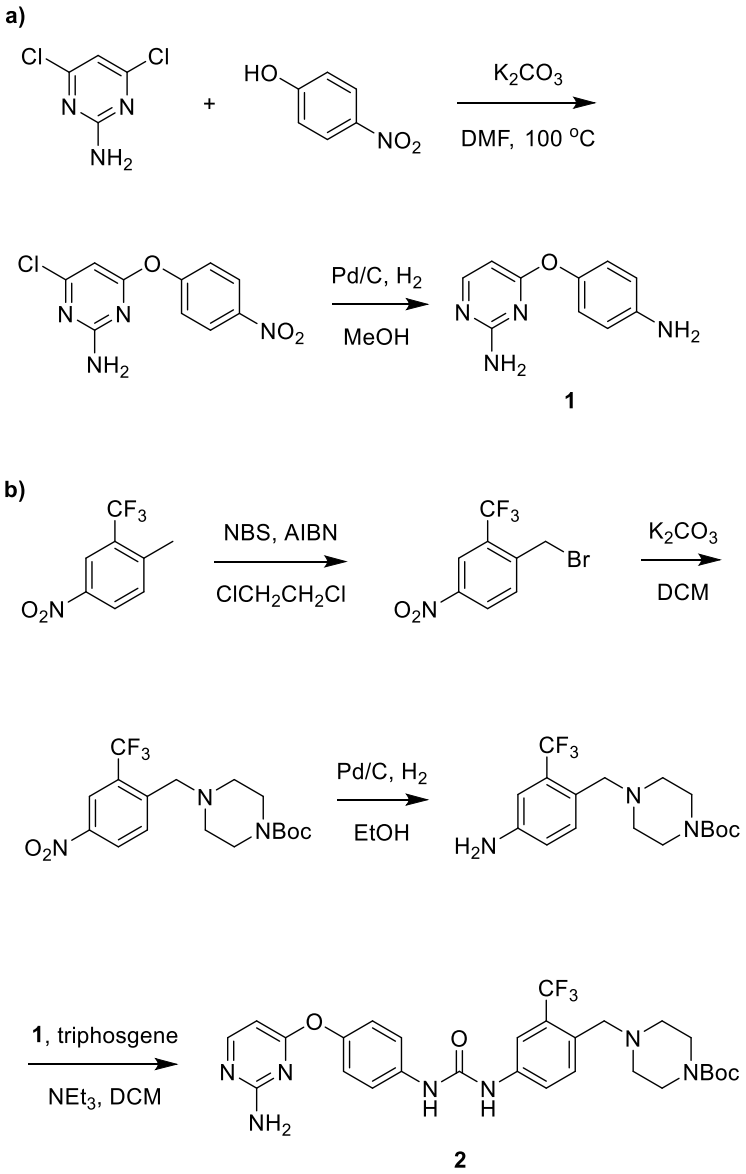

Figure B.4 Synthetic scheme of (**a**) precursor **1** and (**b**) K03861 analog **2**.

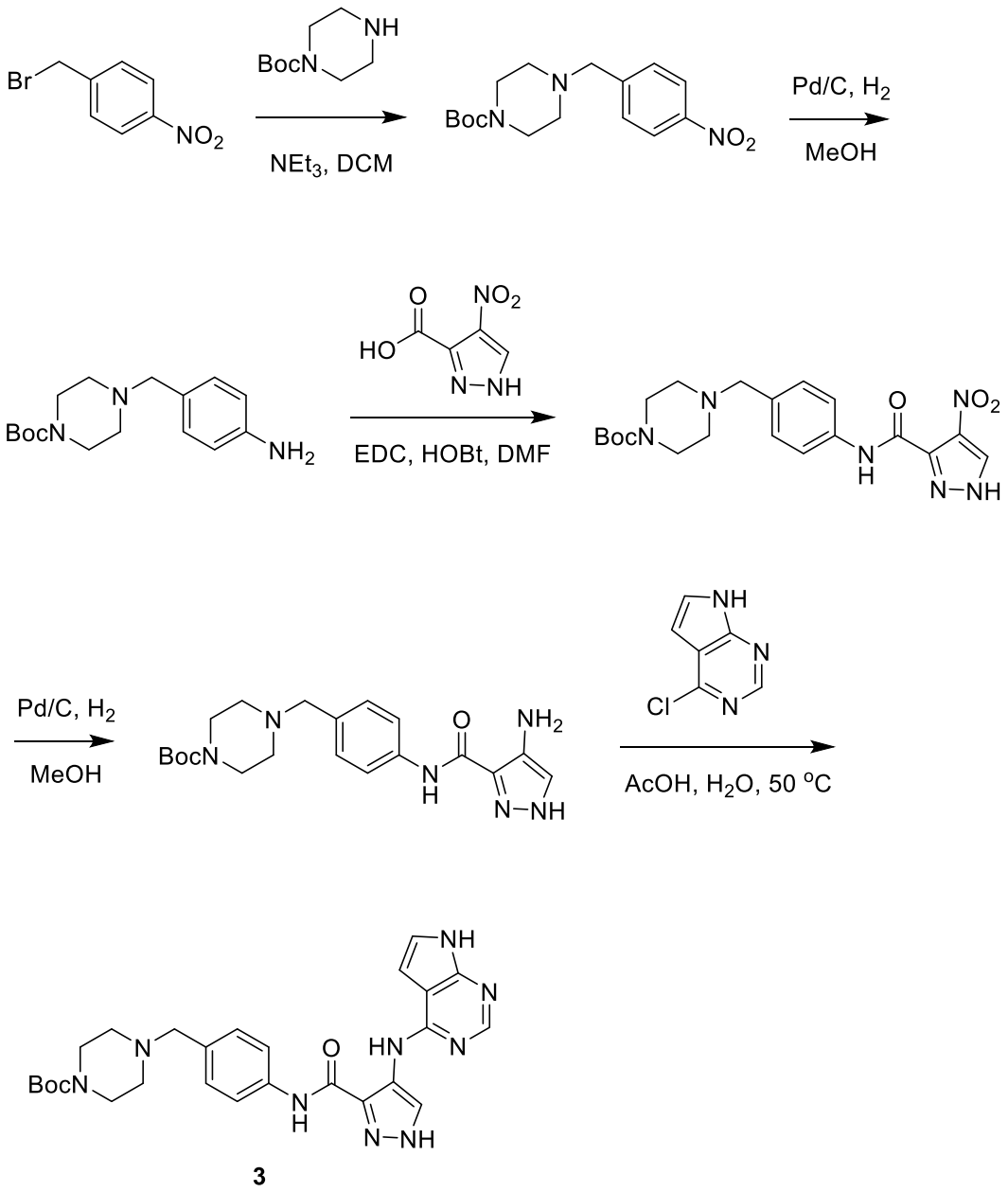

3

Figure B.5 Synthetic scheme of FN-1501 analog **3**.

N-Boc analog of K03861, **2**, was synthesized according to literature[185] (Figure B.4). *N*-Boc analog of FN-1501, **3**, was synthesized according to literature[186] (Figure B.5).

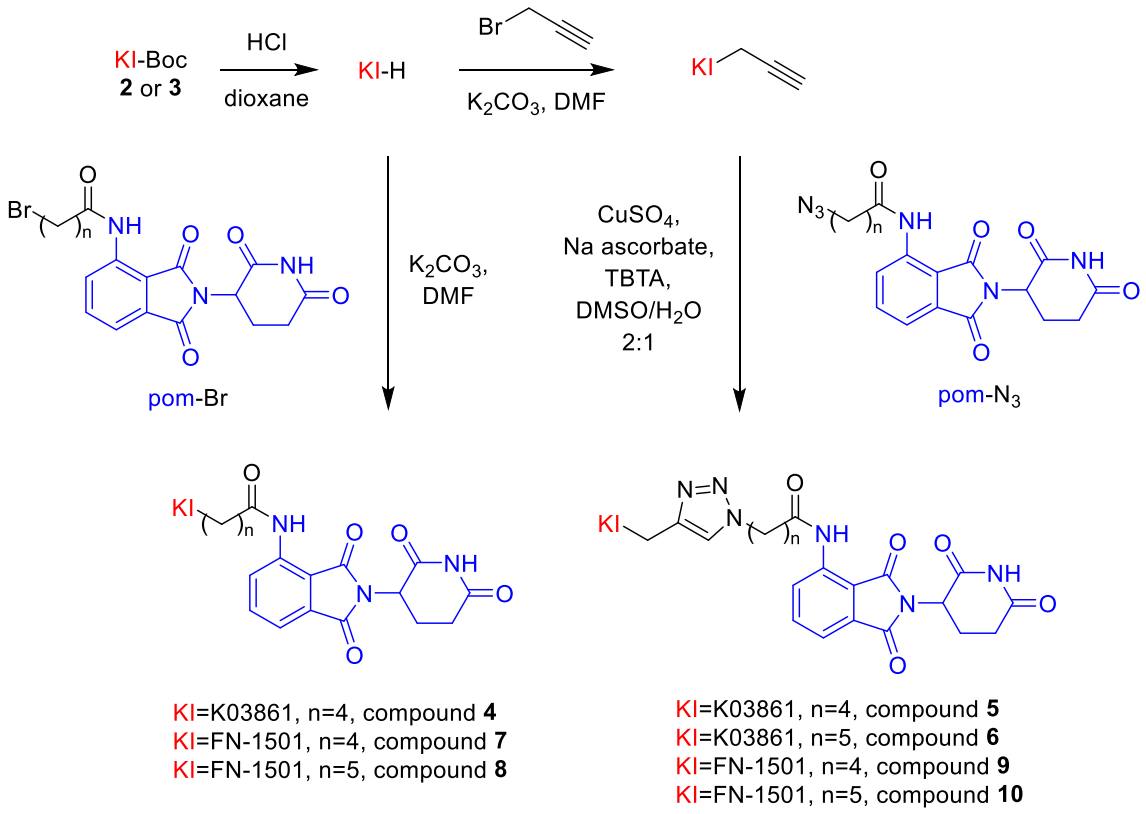

Figure B.6 Synthetic scheme of CDK2 PROTACs starting from kinase inhibitors (KIs) K03861 and FN-1501 analog **2** and **3**.

General Procedure I (Syntheses of Compounds 4, 7 and 8) (Figure B.6)

To a solution of *N-Boc* analog of CDK2 kinase inhibitors (K03861 or FN-1501, 0.05 mmol) was added 4M HCl (1 mL) in dioxane. The mixture was stirred for 1 h at room temperature. Solvent was removed, pom-Br[71] (0.06 mmol), K_2CO_3 (0.15 mmol) and 0.8 mL DMF was added. The mixture was heated to 80 °C and stirred for 20 h. Solvent was removed and the crude material was purified by prep-HPLC to obtain the product.

General Procedure II (Syntheses of Compounds 5, 6, 9 and 10)

To a solution of *N-Boc* analog of CDK2 kinase inhibitors (K03861 or FN-1501, 0.05 mmol) was added 4M HCl (1 mL) in dioxane. The mixture was stirred for 1 h at room temperature. Solvent was removed, propargyl bromide (0.06 mmol), K_2CO_3 (0.15 mmol) and 0.8 mL DMF was added. The mixture was heated to 80 °C and stirred for 7 h. Solvent was removed and the crude material was purified by prep-HPLC to obtain the propargyl KI intermediates.

To a solution of obtain the propargyl KI intermediates and pom-N_3[71] (0.024 mmol) in DMSO was added solution of $CuSO_4$ (0.006 mmol) and sodium ascorbate (0.024 mmol) in water (0.25 mL) and TBTA (0.006 mmol) in DMSO (0.5 mL). The mixture was stirred at room temperature for 18 h. Solvent was removed and the crude material was purified by prep-HPLC to obtain the product.

Protein Degradation (Western Blot)

Cells were seeded in 24-well plate (100,000 cells/well) and allowed to adhere overnight. Culturing media were replaced by fresh media with PROTACs (DMSO < 0.5%). Cells were incubated for certain time (varies according to different experiments, see below) before lysed by RIPA buffer (Pierce) according to manufacturer's instructions. Total protein concentrations were determined and calibrated by BCA protein assay (Pierce). Whole cell lysates were either subjected to traditional Western blot or analyzed by Jess (ProteinSimple).

For time course study, MDA-MB-231 cells were treated with PROTACs or 0.3% DMSO for different time period before cell lysis. For blocking experiments, cells were pretreated with FN-1501, pomalidomide, MLN4924, MG-132 or 0.1% DMSO for 2 h before treated with PROTACs or 0.3% DMSO for 24 h and cell lysis.

BrdU Cell proliferation Assay

MDA-MB-231 cells were seeded in 96-well plate (8,000 cells/well) in 0.5 mL DMEM/F12 media with 10% FBS and allowed to adhere overnight. Compounds were added and incubated at 37 ^{o}C for 48 h. BrdU solution was added to each well 24 h prior to the end of incubation. Culture media were aspirated from wells. Fixing Solution was added and incubated for 30 min at room temperature. Solution was aspirated and washed three times with Wash Buffer. Anti-BrdU monoclonal Detector Antibody solution was added and incubated for 1 h at room temperature. Solution was aspirated and washed three times with Wash Buffer. Peroxidase Goat Anti-Mouse IgG Conjugate was added and incubate for 30 min at room temperature. Solution was aspirated and washed three times with Wash Buffer. Finally, TMB Peroxidase substrate was added and incubated 30 mins at room temperature in the dark. Stop Solution was added and the color of positive wells will change from blue to bright yellow. Results were read by a plate reader set at a dual wavelength of 450/550 nm.

B.3 Results and discussion

Two kinase inhibitors (KIs) were selected for the development of CDK2 PROTACs: K03861 and FN-1501 (Figure B.7). CDK2 is inhibited by K03861 via a type II mechanism.[184] Type II KIs often have better selectivities than the first generation, type I.[113-114] In the structure of K03861 co-crystallized CDK4, the *N-Me* group points into solvent (Figure B.7); this is ideal for derivatization.

While CDK2 is the primary target, there are obvious benefits if CDK4 and CDK6 can be targeted simultaneously. FN-1501 is one of two CDK2/4/6 inhibitors we have identified so far (the other one is PF-06873600); it has IC_{50} values of 2.47, 0.85 and 1.96 nM for CDK2/cyclin A, CDK4/cyclin D1 and CDK6/cyclin D1, respectively.[186]

To develop the potential candidates as CDK2 PROTACs, the *N-H* analog of K03861 and FN-1501 was prepared according to the literature[185-186] and conjugated with pomalidomide derivatives via hydrocarbon or triazole linkers, to afford PROTACs **4**-**10** (Figure B.6, B.8).

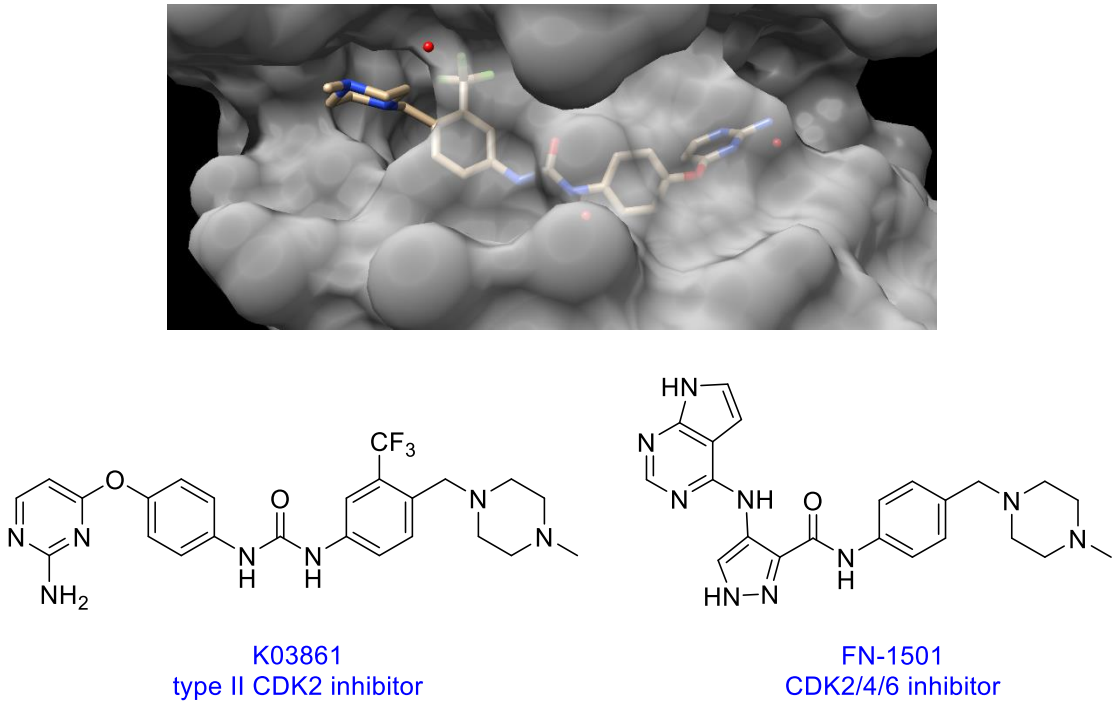

Figure B.7 Top: CDK4 complexed with kinase inhibitor K03861 (PDB: 5A14) showing *NMe* projecting into solvent. Bottom: structures of K03861 and FN-1501.

PROTAC candidates (**4**-**10**) were first examined in MDA-MB-231, a triple negative breast cancer cells line, for the regulation of cellular CDK2 level. Selective suppression of CDK2 are highly desired with respect to CDK1, so CDK1 level was also checked. PROTACs based on K03861 (**4**-**6**) had little or no effect on either CDK1 or CDK2 levels, while those derivatized from FN-1501 (**7**-**10**) could degrade CDK2 without significant suppression of CDK1 level (Figure B.9). PROTAC **8** was the most efficient degrader of CDK2, at a concentration of 2 μM, therefore will be the focus in the rest of the study.

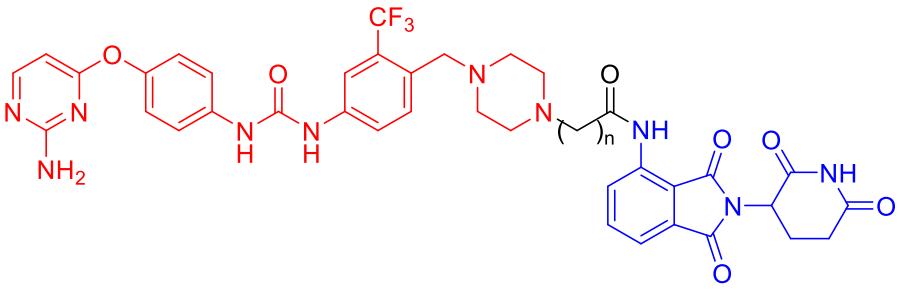

n=4, **4**

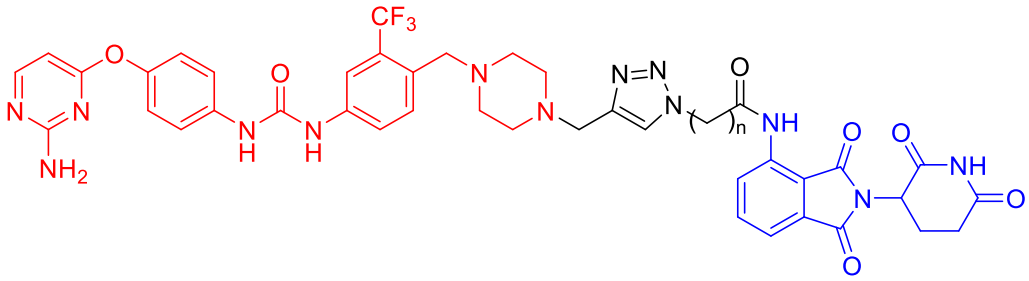

n=4, **5**; n=5, **6**

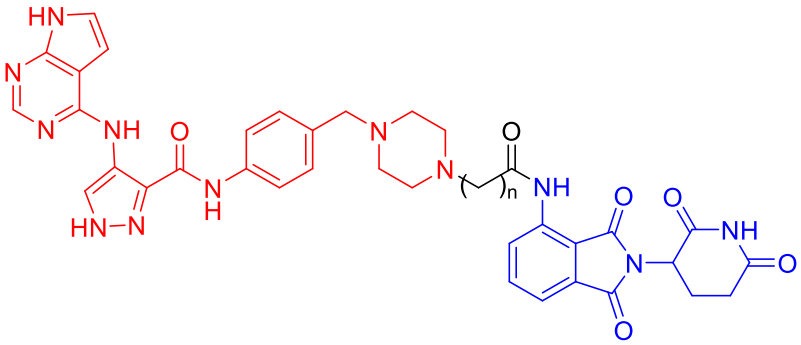

n=4, **7**; n=5, **8**

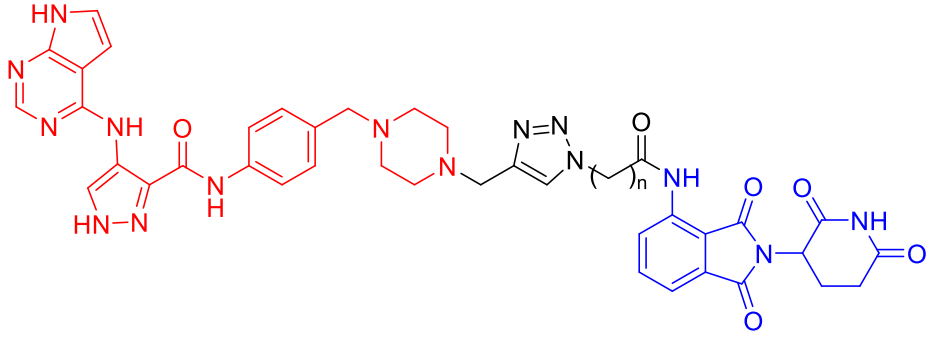

n=4, **9**; n=5, **10**

Figure B.8 Summary of PROTACs (**4**-**10**) investigated in this study.

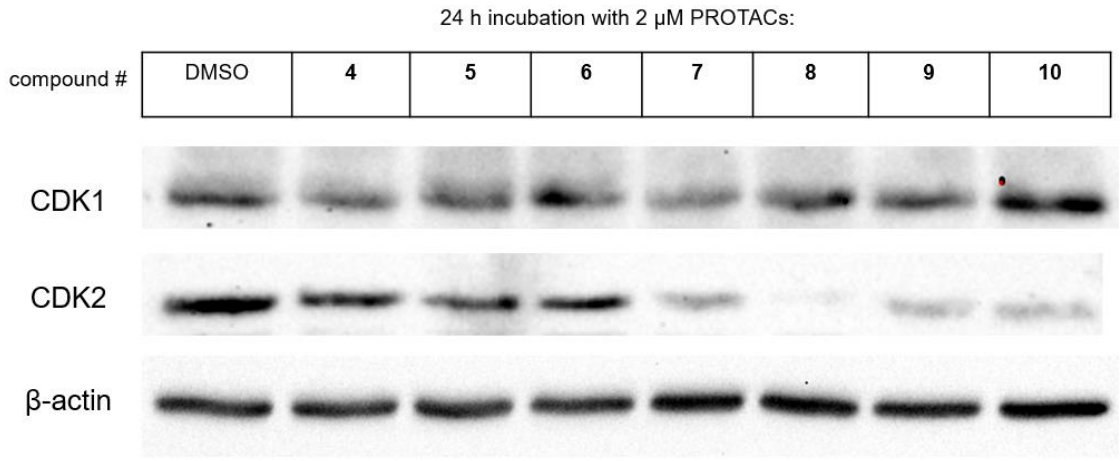

Figure B.9 Cellular level of CDK1 and CDK2 after 24 h incubation of 2 μM PROTACs (**4**-**10**) in MDA-MB-231.

To further investigate the efficacy and selectivity of degradation, PROTAC **8** was tested in a range of concentrations against several CDKs (Figure B.10). Consistently with previous result, **8** exhibited potent CDK2 degradation (DC_{50} = 12.9 nM) without significant effect on CDK1 level. It is worth noting that **8** did not induce dose-dependent degradation of CDK4, and the maximal degradation (D_{max}) is only around 50%. This observation validates the hypothesis that selective suppression of CDK2 can be realized by recruiting a pan-CDK inhibitor FN-1501. Surprisingly, CDK9 was degraded by **8** (DC_{50} = 3.7 nM) even more effectively than CDK2, although the parent inhibitor FN-1501 was not reported as an inhibitor of CDK9.[186] In fact, this finding is consistent with a recent report, but **8** is more effective than the reported PROTAC.[187]

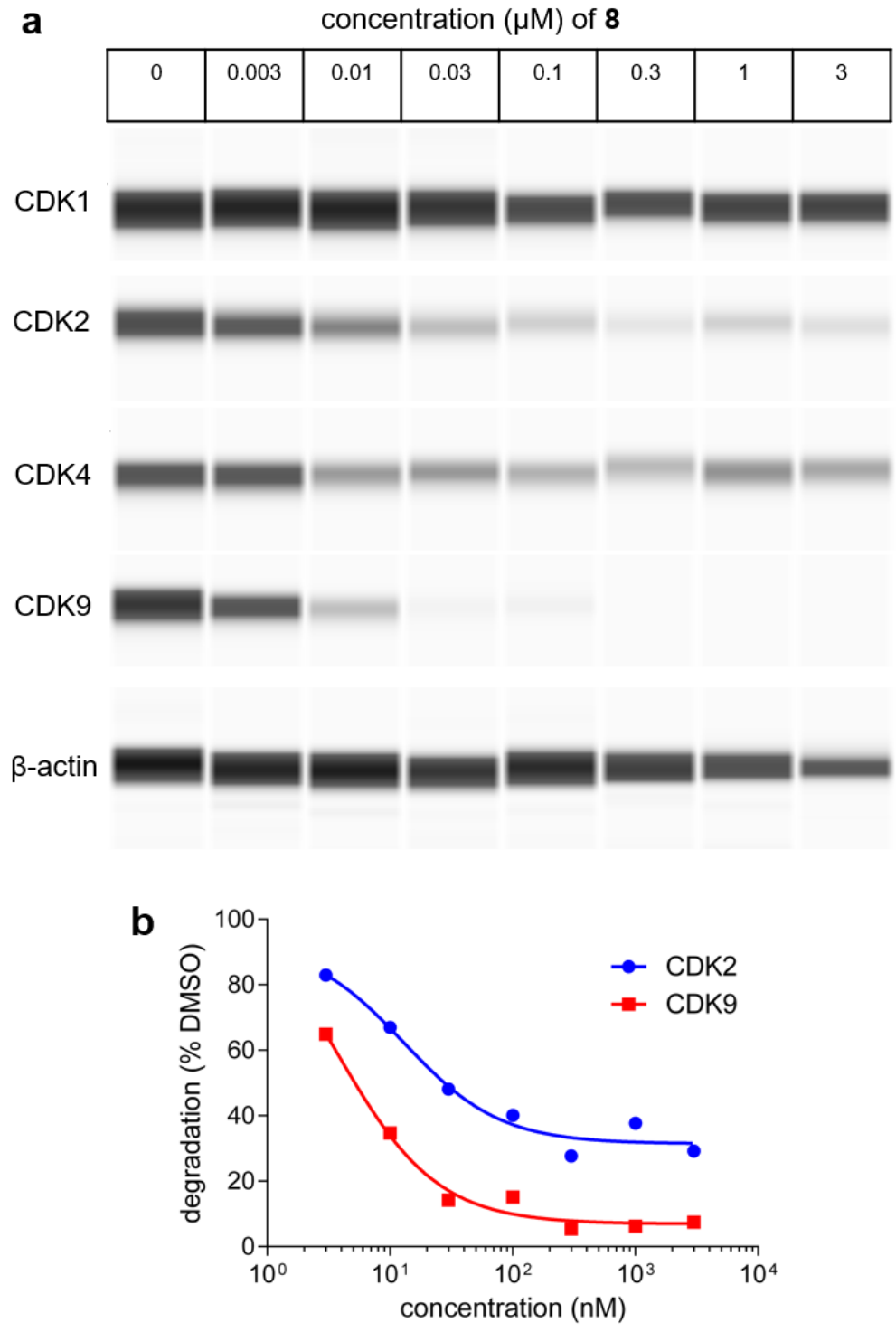

Figure B.10 (**a**) Western blot analysis on CDK levels in MDA-MB-231 cells upon 24 h treatment with CDK2 PROTACs **8**. (**b**) Quantitated data for CDK2/9 degradation level.

A time course study demonstrated that CDK2 degradation by 300 nM **8** was observable after 2 h, and reached the maximum after 6 – 24 h (Figure B.11a). Additionally, a series of blocking experiments with negative controls were performed to confirm the mechanism of the observed CDK2 degradation by **8** (Figure B.11b). Preincubation with excess of either FN-1501 (10 μM) or pomalidomide (10 μM) to compete with **8** for CDK2 or cereblon binding, as expected, rescued the CDK2 from decomposition. Pretreatment with neddylation inhibitor MLN4924 (1 μM) also blocked the CDK2 degradation effectively, because MLN4924 inhibits NEDD8-activating enzyme (NAE) and therefore prevents activation of cullin-RING ligases, which are critical for proteasome-mediated protein degradation.[84] Another blocking experiment by preincubation of 20 μM of the proteasome inhibitor MG-132[85] could prevent CDK2 from decomposition. All blocking experiments stated above suggests that mechanism of CDK2 degradation by **8** involves binding to CDK2 and E3 ligase cereblon, ubiquitin-dependent and proteasome-mediated degradation. Finally, effects of monovalent ligand FN-1501 (3 μM) and pomalidomide (3 μM) on CDK2 were also studied. Incidentally, some extent of CDK2 degradation was observed after 24 h incubation with 3 μM FN-1501, and this is in accordance with the previous blocking experiment by 10 μM FN-1501, where CDK2 was only partially rescued, indicating a possible indirect CDK2 regulation by FN-1501 alone. No substantial effect on CDK2 was observed when treated with 3 μM pomalidomide.

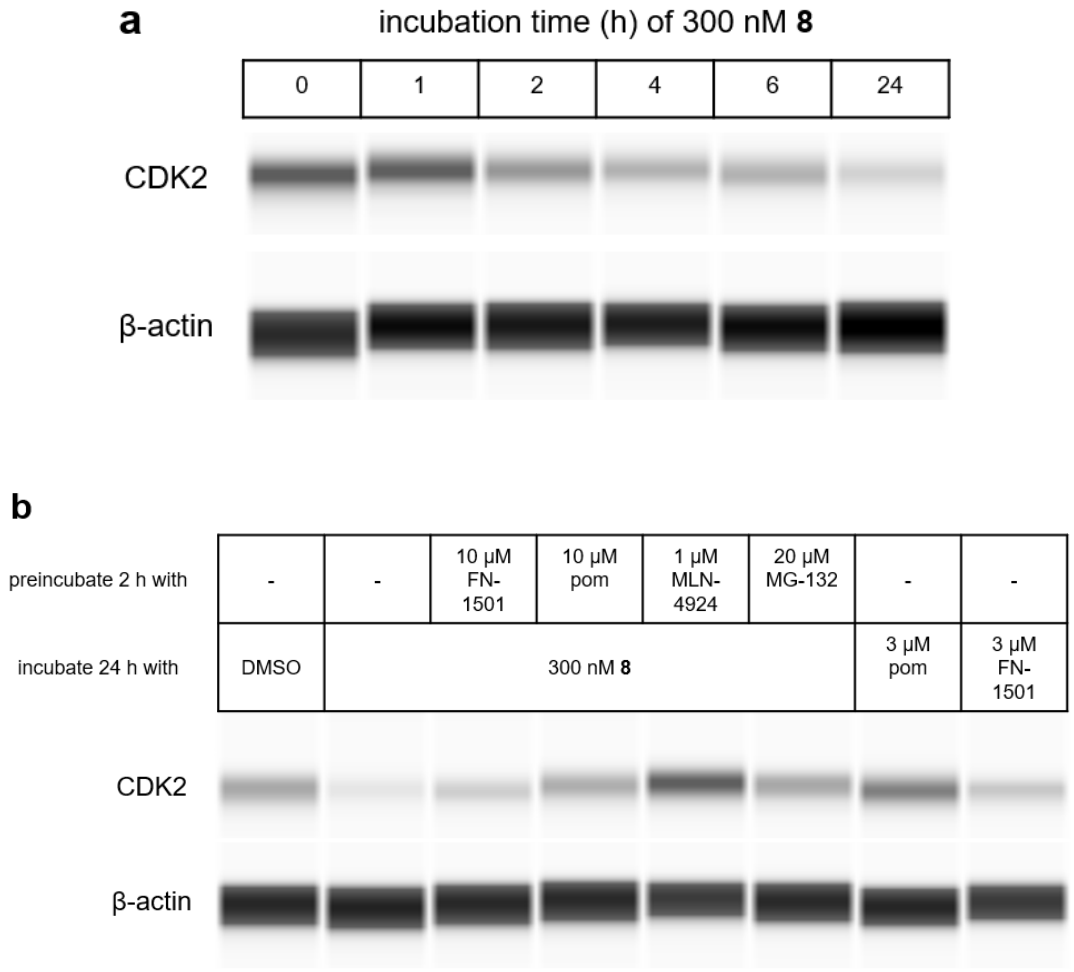

Figure B.11 (**a**) Time course study on CDK2 degradation by PROTAC **8** in MDA-MB-231 cells. (**b**) Blocking experiments to study the mechanism of CDK2 degradation by **8**. MDA-MB-231 cells were pretreated with 10 μM FN-1501, 10 μM pomalidomide (pom), 1 μM MLN-4924 or 20 μM MG-132 for 2 h before 24 h incubation with 300 nM PROTAC **8**.

CDK2, 4 and 6 are critical regulators of cell cycle, therefore CDK inhibitors should induce cell cycle arrest which leads to less bromodeoxyuridine (BrdU, an analog of the nucleoside thymidine) incorporation into cells. In the BrdU cell proliferation assay, both **8** and FN-1501 induced cell cycle arrest after 48 h, and surprisingly, **8** is significantly

more potent (Figure B.12). This observation may imply some indirect regulation of cell cycle mediated by CDK9 decomposition, which is unique for PROTAC **8**.

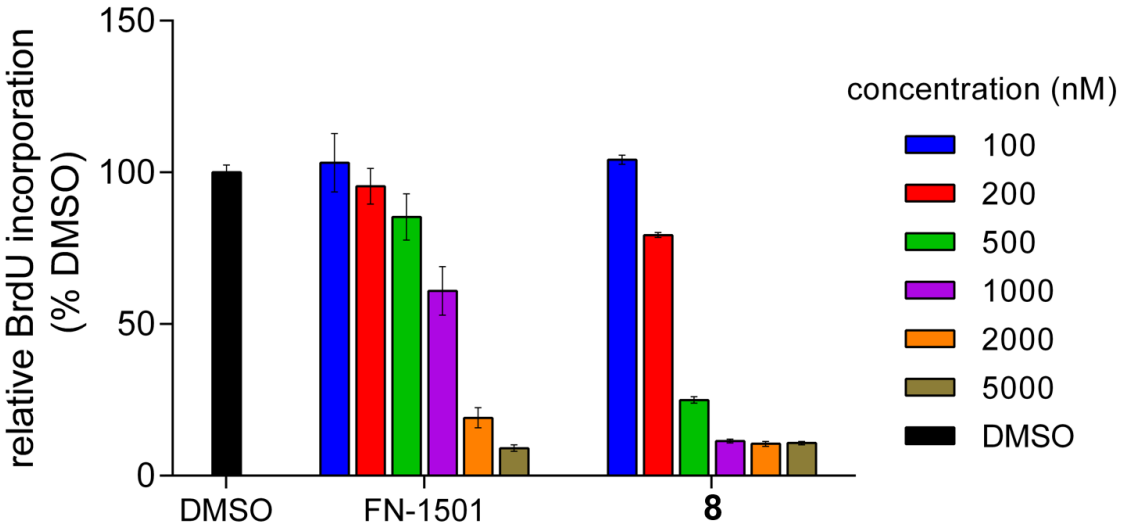

Figure B.12 BrdU cell proliferation assay on MDA-MB-231 cells treated (48 h) with **8** and parent kinase inhibitor FN-1501.

All of the above experiments were performed in MDA-MB-231, a triple negative breast cancer cell line, to validate the hypothesis of selective CDK2 degradation. Next, PROTAC **8** was examined in a palbociclib-resistant pancreatic ductal adenocarcinoma (PDAC) model, 1222 cell line, to study if the resistance could be overcome by CDK2 decomposition.

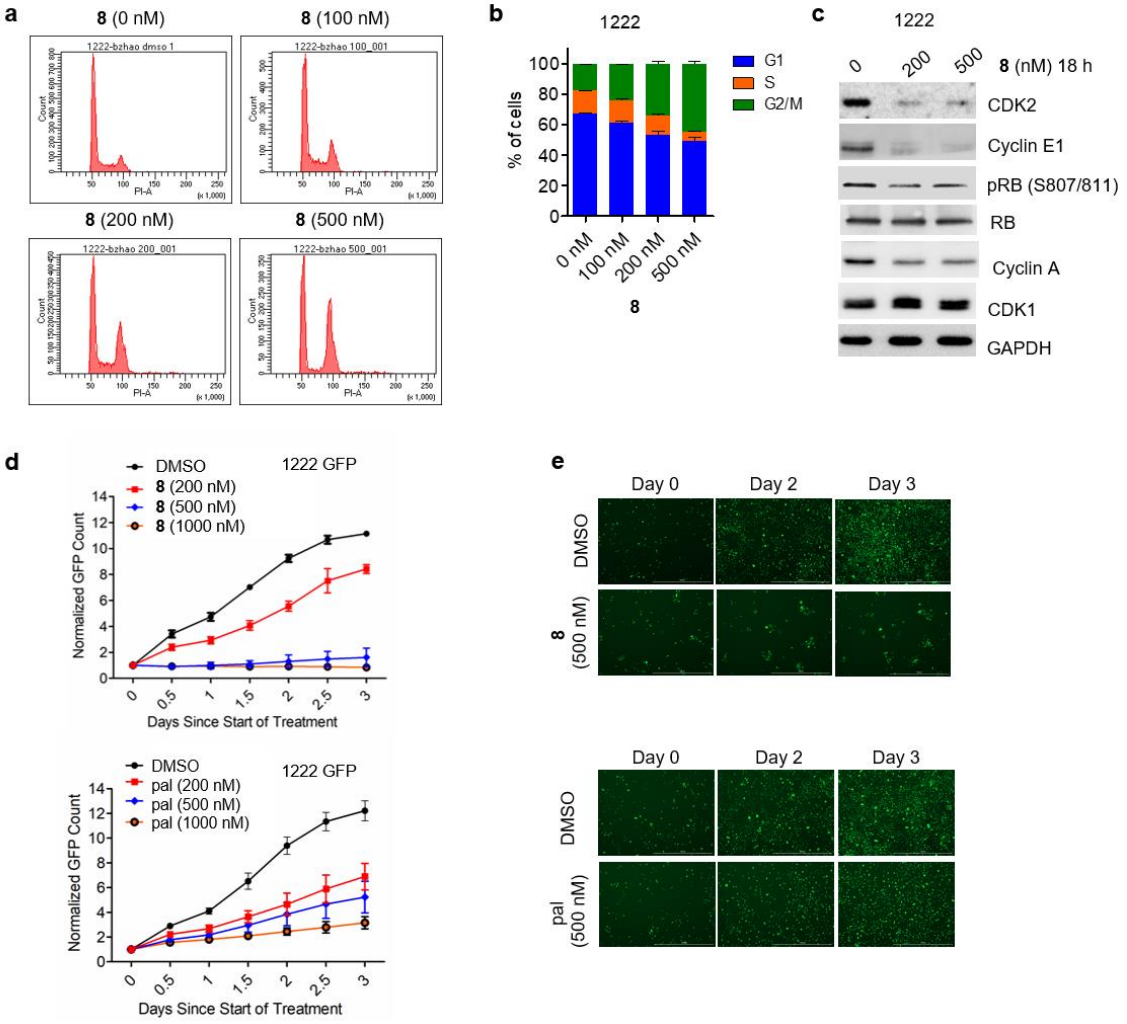

Figure B.13 (**a**) Flow cytometry on the cell cycle phase distribution of 1222 cells treated with PROTAC **8**. (**b**) Quantitated result for (**a**). (**c**) Western blot analysis on 1222 cells treated with PROTAC 8. (**d**) Effect of **8** and pal on cell proliferation of 1222-GFP cells in a 3-day period. (**e**) Fluorescent microscopic imaging of 1222-GFP cells in (**d**).

In an experiment of cell cycle analysis by flow cytometry, **8** was shown to induce potent cell cycle arrest at G2/M phase, at a concentration of 200 - 500 nM (Figure B.13a and B.13b). Similar to the result from MDA-MB-231 cell line, cellular level of CDK2 was diminished after 18 h. Interestingly, Cyclin E1, the binding partner of CDK2 in the bioactive CDK-Cyclin complex, was also degraded as efficiently as CDK2. This

unexpected Cyclin E1 degradation might proceed via the interaction of **8** with the whole CDK-Cyclin complex, or some unknown indirect signaling pathways (Figure B.13c). As another binder of CDK2, Cyclin A was not significantly degraded, which implies that the degradation majorly happens in certain cell cycle phases (Figure B.13c). Surprisingly, p-Rb level remained nearly the same throughout (Figure B.13c). Cell proliferation assay was carried out in a 3-day period and quantitated by live cell counting using an engineered 1222-GFP cells (Figure B.13d and B.13e). In a comparison experiment between **8** and palbociclib, while similar profile was observed at 200 nM, **8** inhibited the cell proliferation more potently than palbociclib at 500 and 1000 nM, suggesting **8** as a promising lead in the treatment of palbociclib-resistant PDAC cell line.

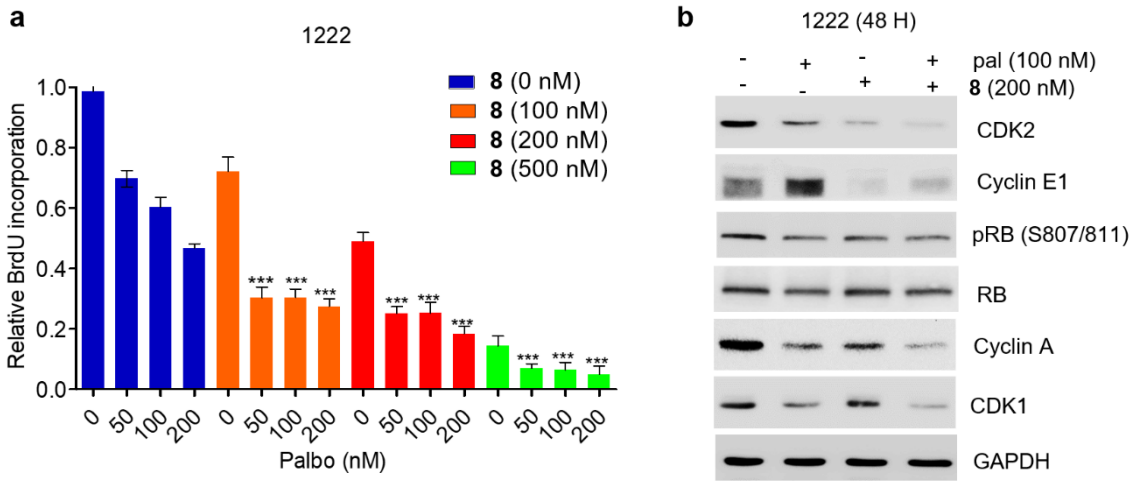

Figure B.14 (**a**) BrdU cell proliferation assay on **8** in combination with palbociclib (pal) in 1222 cells. (**b**) Western blot analysis on 1222 cells treated with 100 nM pal, 200 nM **8**, or the combination.

Next, a combination of **8** and palbociclib was tested against 1222 cell line to see if any synergistic effect could be observed. In the BrdU assay, the combinatory treatment showed a dose-dependent and cooperative inhibition of cell proliferation (Figure B.14a), and interestingly, induced even more CDK2 and Cyclin A degradation than single treatment of **8** while having less effect on Cyclin E1 (Figure B.14b). Additionally, the combination could also downregulate CDK1 level in a greater extent (Figure B.14b), which could be explained by the intrinsic binding of CDK1 with Cyclin A.

B.4 Conclusions

In summary, this study features a potent PROTAC (**8**) on CDK2/9, which was optimized from a combination of seven PROTACs with different linkage between two non-selective CDK2 inhibitors and E3 ligand pomalidomide. Efficacy of CDK2/9 degradation by **8** was quantitated (DC_{50} = 12.9 nM and 3.7 nM, respectively) by a dose-dependent study. Time course study was performed and degradation mechanism was confirmed to be ligand-specific, ubiquitin-dependent and proteasome-mediated. Besides, **8** induced cell cycle arrest more efficiently than the parent KI FN-1501, possibly because of the unexpected suppression of CDK9 or Cyclin E1. Most importantly, **8** was more effective in inhibiting cell proliferation than the approved drug palbociclib in a PDAC model, validating the importance of CDK2 downregulation in the palbociclib-resistant cell line. Additionally, combinatory treatment with **8** and palbociclib had a more profound effect in the same cell line, suggesting an alternative approach in the clinical trial of palbociclib-resistant model. However, an insightful view of the downregulation of CDK9

and Cyclin E1 by **8**, needs to be given to fully understand the mechanism of action of this CDK2 PROTAC.

APPENDIX C

CDK4/6 PROTACS WITH FLUORESCENT LINKERS

C.1 Introduction

Recent work from our laboratories has exposed some fluorophore-kinase conjugates that limit cell proliferation more effectively than the parent kinase.[69] All these conjugates feature a "tumor-seeking dye" like the cyanine-7 dye MHI-148. This water-soluble fluorophore absorbs at around 780 nm and fluoresces at around 800 nm. Cellular and *in vivo* studies indicate this dye localizes in many types of cancer and in solid tumors but not in normal cells and tissue.[135, 188-191] Preferential uptake of MHI-148 in cancer is mediated by Organic Anion Transporting Polypeptides (OATPs)[192-193] and possibly via albumin in the growth media.[138] The special characteristics of MHI-148 **A** are first that it accumulates in tumor tissues *in vivo* after *iv* injection, and second that it is retained there for several days.[135-136]

In other work we have established than thiols (but not amines, alcohols or phenols) react with **A** via displacement of its *meso*-chloride under physiological conditions.[137] The only free thiol in albumin is ^{34}Cys. It transpired that the ^{34}Cys of albumin forms a covalent conjugate via binding to the cyanine at the *meso*-position.[138] Independent studies by Goncalves and co-workers also confirmed these observations.[139]

Therefore, there is potential of incorporating cyanine dyes like MHI-148 as linkers into the design of PROTACs. As far as we are concerned, there is no report of PROTACs with fluorescent property. Therefore, these PROTACs might be preferentially delivered

into cancer over normal cells, and their fluorescence properties would facilitate intracellular imaging so uptake of the PROTACs could be tracked.

C.2 Materials and methods

C.2.1 Materials and instrumentation

All reactions were carried out under an inert atmosphere (nitrogen or argon where stated) with dry solvents under anhydrous conditions. Glassware for anhydrous reactions was dried in an oven at 140 ºC for minimum 6 h prior to use. Dry solvents were obtained by passing the previously degassed solvents through activated alumina columns. Yields refer to chromatographically and spectroscopically (^{1}H-NMR) homogeneous materials, unless otherwise stated. Reagents were purchased at a high commercial quality (typically 97 % or higher) and used without further purification, unless otherwise stated. Analytical thin layer chromatography (TLC) was carried out on Merck silica gel plates with QF-254 indicator and visualized by UV. Flash column chromatography was performed using silica gel 60 (Silicycle, 230-400 mesh). ^{1}H and ^{13}C spectra were recorded on a 400 MHz spectrometer and were calibrated using residual non-deuterated solvent as an internal reference. The following abbreviations or combinations thereof were used to explain the multiplicities: s = singlet, d = doublet, t = triplet, q = quartet, m = multiplet, dd = doublet of doublet, ddd = doublet of doublet of doublets.

MDA-MB-231 cells (from American Type Culture Collection) were cultured on 75 cm^2 culture flasks in Dulbecco's Modified Eagle Medium/nutrient mixture F-12 (DMEM/F12, Sigma Chemical, St. Louis, MO) supplemented with 10 % FBS. BrdU cell

proliferation ELISA kit was purchased from Abcam. CDK4, CDK6 and Phospho-Rb (Ser780) mAb were purchased from Cell Signaling Technology. Goat anti-rabbit (H+L) secondary antibody (HRP conjugated) were purchased from ThermoFisher Scientific. SuperSignal West Dura Substrate (ThermoFisher Scientific) was used as Western blot substrate.

C.2.2 Experimental procedures

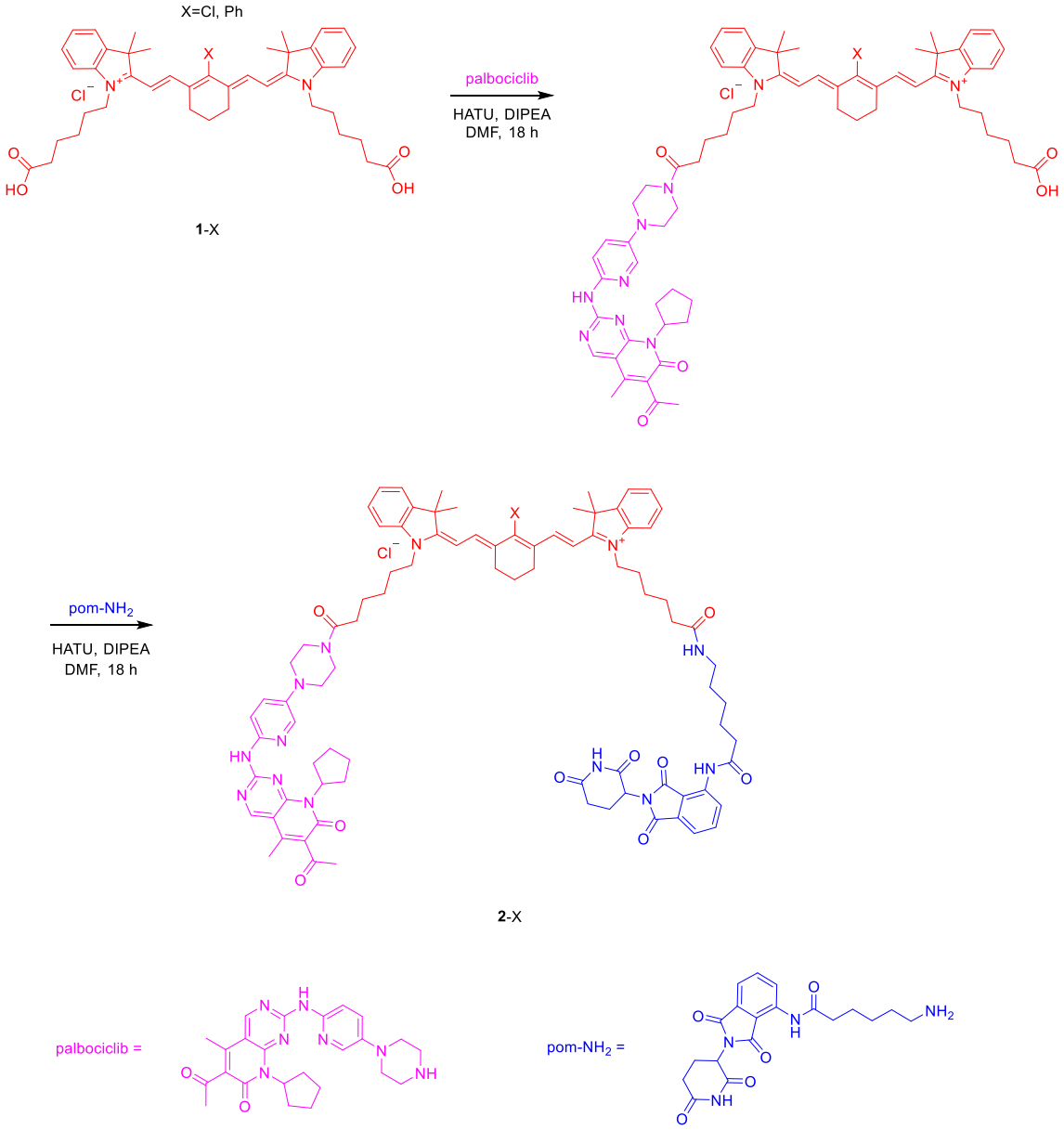

Figure C.1 Synthetic scheme of fluorescent PROTACs **2** with a core of heptamethine cyanine dye MHI-148.

Heptamethine cyanine dye **1** and ICG were made according to literature.[138] Palbociclib was purchased from LC Laborotaries. Pom-NH_2 was made according to literature.[71]

Synthesis of Fluorescent PROTACs 2 (Figure C.1)

To a solution of cyanine dye (X=Cl, MHI-148) **1** (1 eq) and palbociclib (1.1 eq) in DMF was added DIPEA (1.2 eq) and HATU (1 eq). The mixture was stirred at room temperature for 18 h. DMF was removed and the crude product was purified by prep-HPLC. Mono-substituted product was concentrated and subjected to next step.

To a solution of mono palbociclib-substituted cyanine from last step (1 eq) and pom-NH_2 (1.1 eq) in DMF was added DIPEA (1.2 eq) and HATU (1 eq). The mixture was stirred at room temperature for 18 h. DMF was removed and the crude product was purified by prep-HPLC to afford the final product **2** as a white powder.

Synthesis of Fluorescent PROTAC 3

Fluorescent PROTAC **3** (Figure C.2) was made in a similar way as PROTACs **2** starting with a different commercial cyanine dye (ICG).

Synthesis of Fluorescent PROTACs 4-6

Fluorescent PROTAC **4-6** was made in a similar way as PROTACs **2** (Figure C.3). In the first step, three palbociclib derivatives with PEG linker were used instead of palbociclib.

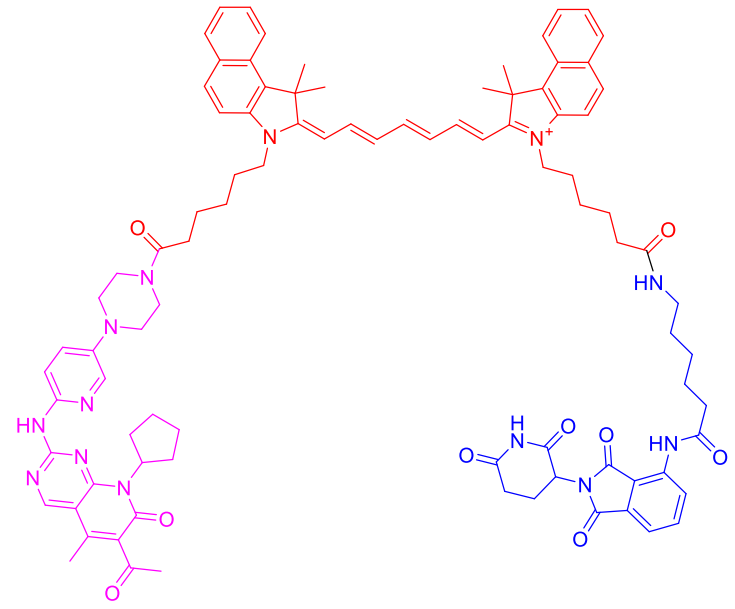

3

Figure C.2 Structure of fluorescent PROTACs **3** with a core of heptamethine cyanine dye ICG.

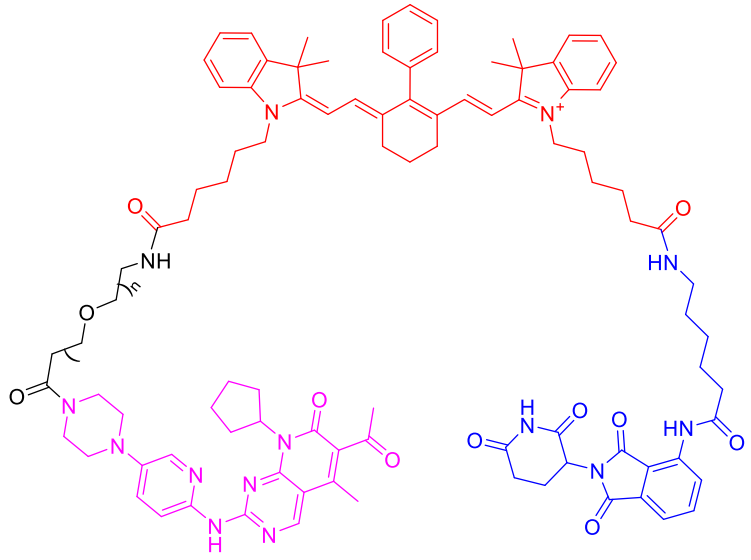

n=1, **4**
n=2, **5**
n=3, **6**

Figure C.3 Structure of fluorescent PROTACs **4-6** with PEG linkers between MHI-148 dye and palbociclib.

Protein Degradation (Western Blot)

Cells were seeded in 24-well plate (100,000 cells/well) and allowed to adhere overnight. Culturing media were replaced by fresh media with PROTACs (DMSO < 0.5%). Cells were incubated for 18-24 h before lysed by RIPA buffer (Pierce) according to manufacturer's instructions. Total protein concentrations were determined and calibrated by BCA protein assay (Pierce). Whole cell lysates were either subjected to Western blot protocol.

BrdU Cell proliferation Assay

MDA-MB-231 cells were seeded in 96-well plate (8,000 cells/well) in 0.5 mL DMEM/F12 media with 10% FBS and allowed to adhere overnight. Compounds were added and incubated at 37 ^{o}C for 48 h. BrdU solution was added to each well 24 h prior to the end of incubation. Culture media were aspirated from wells. Fixing Solution was added and incubated for 30 min at room temperature. Solution was aspirated and washed three times with Wash Buffer. Anti-BrdU monoclonal Detector Antibody solution was added and incubated for 1 h at room temperature. Solution was aspirated and washed three times with Wash Buffer. Peroxidase Goat Anti-Mouse IgG Conjugate was added and incubate for 30 min at room temperature. Solution was aspirated and washed three times with Wash Buffer. Finally, TMB Peroxidase substrate was added and incubated 30 mins at room temperature in the dark. Stop Solution was added and the color of positive wells will change from blue to bright yellow. Results were read by a plate reader set at a dual wavelength of 450/550 nm.

C.3 Results and discussion

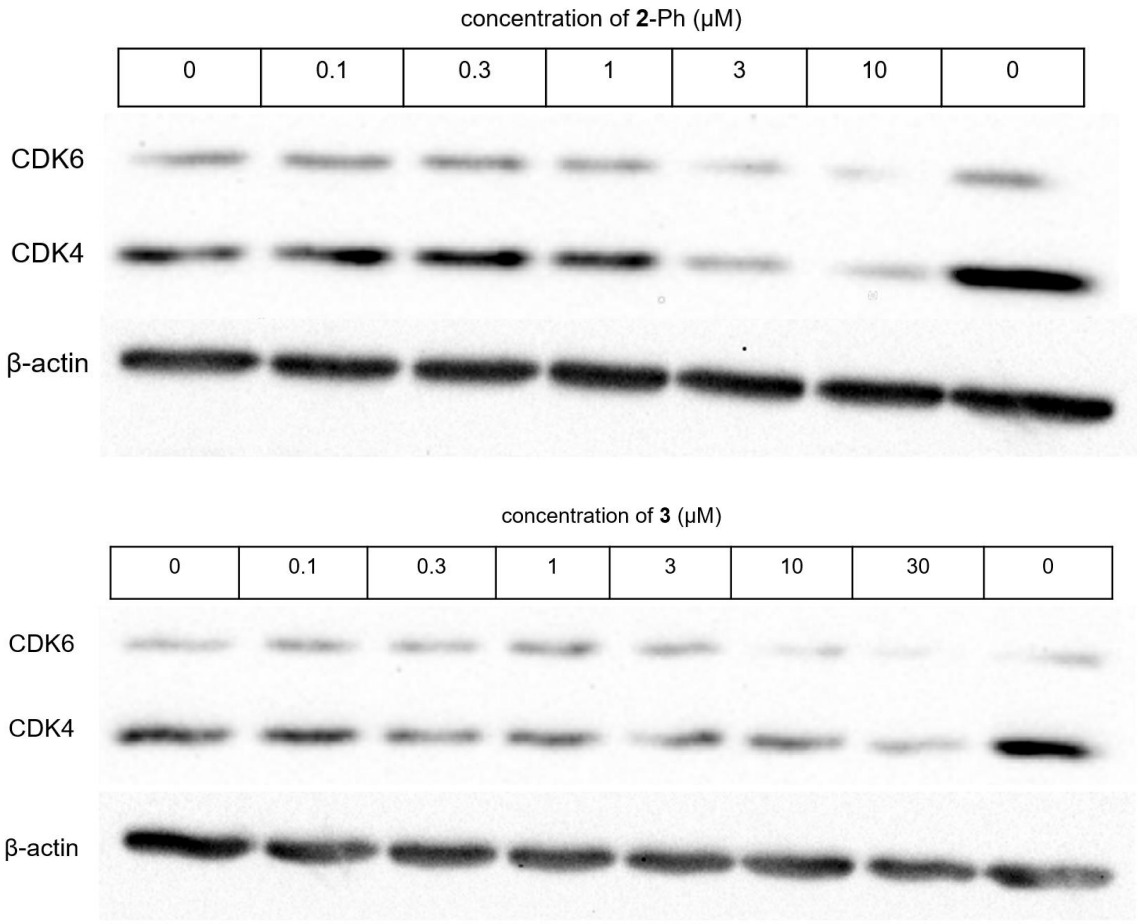

Figure C.4 Cellular level of CDK4/6 after 18 h incubation of PROTACs **2**-Ph and **3**. 30 μM of **2** was also tested but most cells were died at the end of incubation.

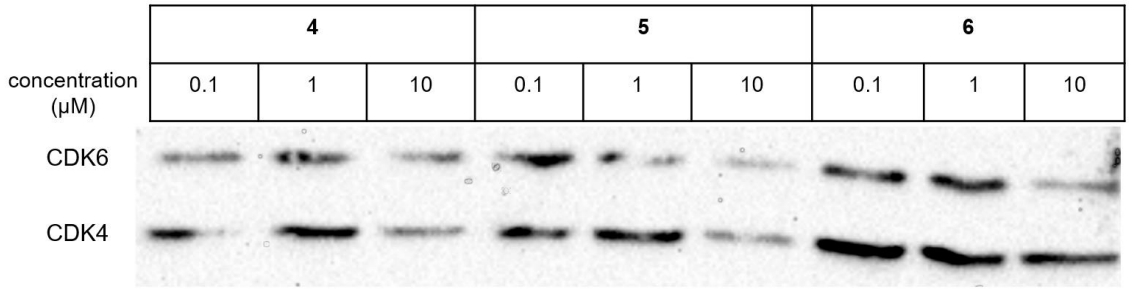

Figure C.5 Cellular level of CDK4/6 after 18 h incubation of PROTACs **4**-**6**.

A series of PROTACs (**2**-**6**) with heptamethine cyanine dye linkers were synthesized by two amide coupling reactions with the amino derivatives of palbociclib and pomalidomide. Importantly, the -Cl group in the *meso* position of the cyanine dye MHI-148 was replaced by a phenyl group, because the formation of a covalent adduct of MHI-148 with albumin in the cell culture media[138] would render the PROTAC to be inactive. These PROTACs were first examined in MDA-MB-231, a triple negative breast cancer cells line. Substantial degradation of CDK4 and CDK6 were observed after 18 h incubation with **2**-Ph at a concentration of 3 μM or higher, and most cells were died at 30 μM (Figure C.4). PROTAC **3** also induced partial decomposition of CDK6 at 10 μM or higher, and of CDK4 at 30 μM (Figure C.4). Linker length in PROTACs could be important for the stability of ternary complex and therefore the efficiency of degradation[34] Analogs of **2**-Ph, specifically **4**-**6**, were also tested in the same conditions as **2**-Ph (Figure C.5). However, Western blot analysis on CDK4/6 levels showed they are less potent in target degradation compared to **2**-Ph. In conclusion, **2**-Ph showed the best activity among all PROTAC prepared in term of protein degradation, therefore will be the focus in the rest of the study.

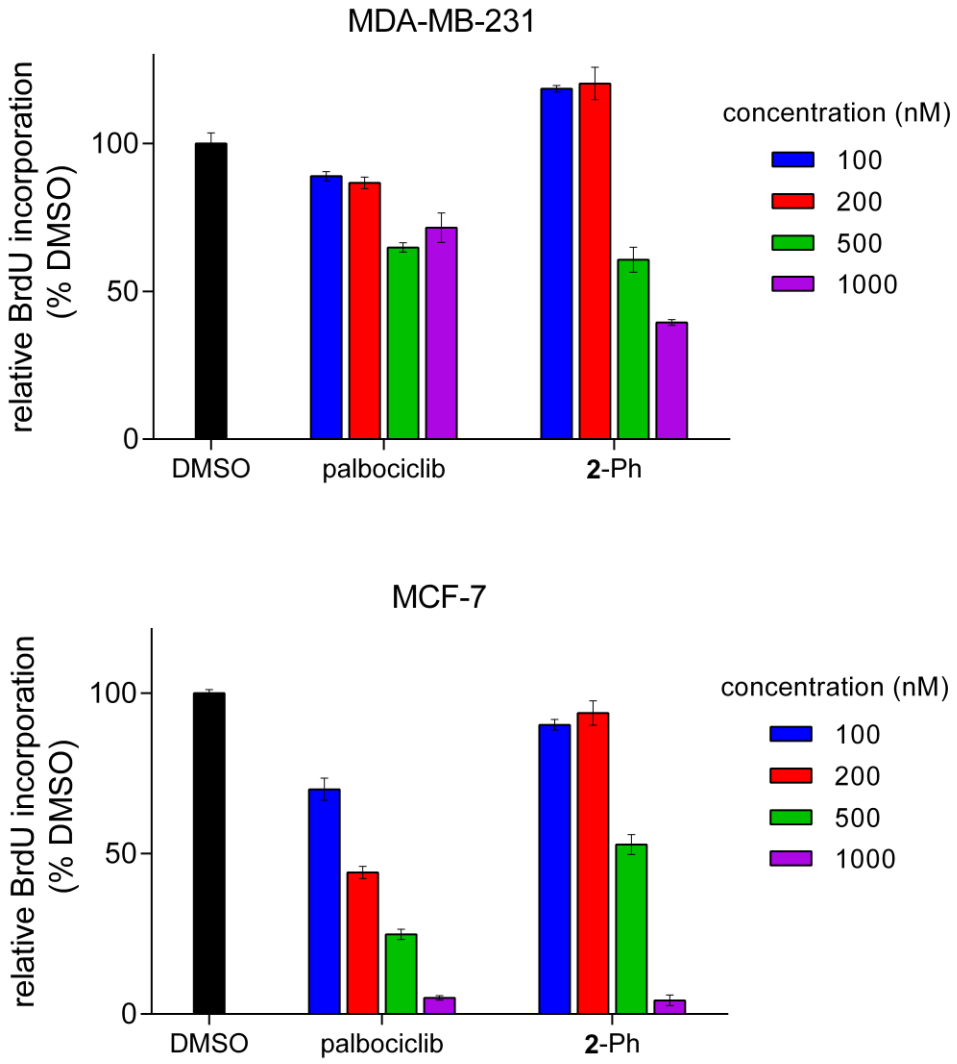

Figure C.6 BrdU cell proliferation assay of palbociclib and **2**-Ph on MDA-MB-231 and MCF-7 cells (72 h incubation).

Next, several cellular assays were performed to examine the overall effect of **2**-Ph compared to the parent drug palbociclib. CDK4 and 6 are crucial regulators of G1-S transition in the cell cycle, therefore suppression on CDK4/6 should lead to cell cycle arrest which can be reflected and quantitated by bromodeoxyuridine (BrdU, an analog of the nucleoside thymidine) incorporation into cells. In BrdU assay, both **2**-Ph and

palbociclib induced cell cycle arrest after 72 h (Figure C.6). Though **2**-Ph is not as effective as palbociclib at concentration of 500 nM or below, it is comparable with palbociclib at 1 μM in MCF-7 (ER^+, $HER2^-$ breast cancer) and even more potent in MDA-MB-231 (triple negative breast cancer) where cells show some resistance to palbociclib.

In cytotoxicity assay, **2**-Ph gives the best IC_{50} (~ 1.0 μM) compared to the ICG-linked PROTAC **3** and palbociclib, in MDA-MB-231 cell line (Figure C.7). Since palbociclib, as a CDK4/6 inhibitor, induce cell cycle arrest and therefore drives cell into senescence, it is not expected to be cytotoxic and this is in accordance with the trend we observed (Figure C.7, green curve). Hence, cytotoxicity of PROTAC **2**-Ph might be a result of the dye core, **1**-Ph (MHI-148 with *meso*-phenyl modification). PROTAC **3**, with a different dye core ICG, is less toxic than **2**-Ph (Figure C.7, red curve), which supports this hypothesis. Besides, similar cytotoxicity profile was observed in MCF-7 and MCF-10A (breast epithelial) cells (Figure C.8), further suggesting the sudden drop of viability at ~ 1 μM might be inherent to the parent dye **1**-Ph.

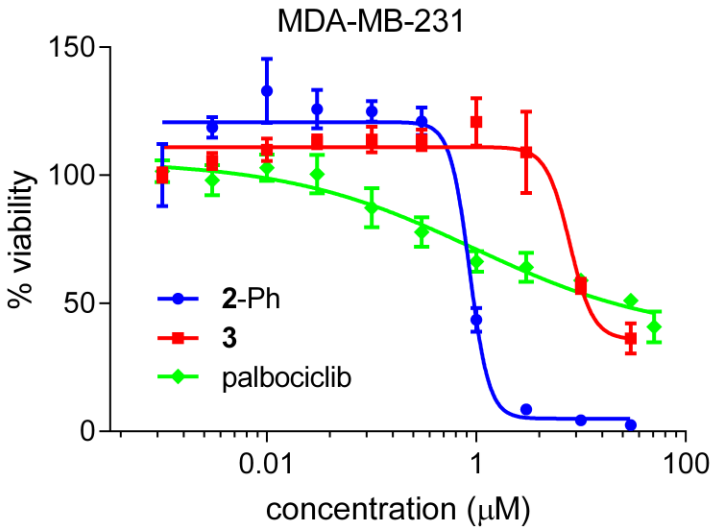

Figure C.7 Cytotoxicity assay of **2**-Ph, **3** and palbociclib on MDA-MB-231 cells.

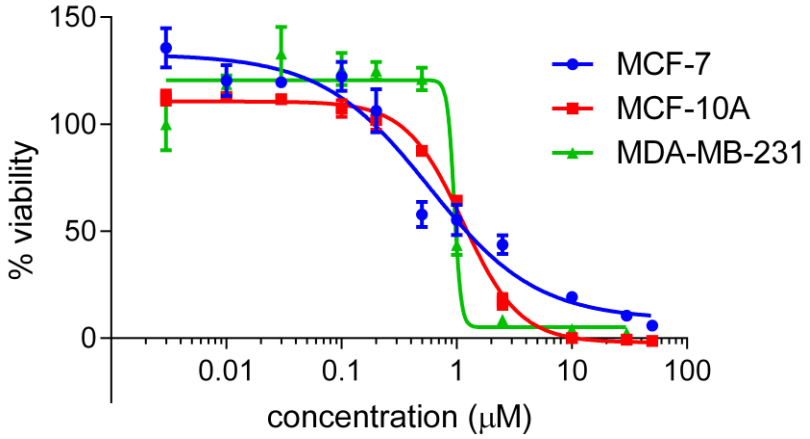

Figure C.8 Comparison of cytotoxicity of **2**-Ph in MDA-MB-231, MCF-7 and MCF-10A cells.

C.4 Conclusions

In summary, this study features fluorescent PROTACs (**2-6**) with MHI-148 and ICG cyanine dye core which acts on CDK4/6. Efficacy of CDK4/6 degradation by these PROTACs was assessed by Western blot and **2**-Ph had the best performance. In the structure of **2**-Ph, *meso*-Cl of dye core MHI-148 was replaced by a phenyl group to avoid the formation of covalent adduct with protein with free cysteine. PROTAC **2**-Ph was further tested in BrdU cell proliferation assay, and showed a comparable effect with parent drug palbociclib in cell cycle arrest at the concentration where substantial degradations of CDK4/6 were observed. Besides, **2**-Ph was more cytotoxic than palbociclib in MDA-MB-231 cells line, and this is likely because of the inherent toxicity of the MHI-148 with *meso*-phenyl modification. This is the first report of a PROTAC with fluorescent linker. In the near future, *in vivo* study on **2**-Ph would be interesting in two aspects: the ability to retain the "tumor-seeking" property of MHI-148 and the possibility of a combination therapy with regards to the cytotoxicity of the dye core and the cytostatic effect of CDK4/6 knockdown by PROTACs.